NASA/CR—2001-210881

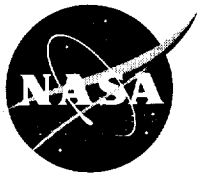

Science Data Report for the Optical Properties Monitor (OPM) Experiment

D.R. Wilkes and J.M. Zwiener
AZ Technology, Inc., Huntsville, AL 35806

National Aeronautics
and Space Adminstration

Prepared for Marshall Space Flight Center•MSFC, Alabama 35812

March 2001

TABLE OF CONTENTS

TABLE OF CONTENTS

TABLE OF CONTENTS

LIST OF FIGURES

LIST OF FIGURES

LIST OF FIGURES

LIST OF FIGURES

LIST OF FIGURES

LIST OF FIGURES

LIST OF TABLES

ACRONYMS AND ABBREVIATIONS

α	Absorptance
α_s	Solar Absorptance
Å	Angstroms
A-D	Analog to Digital Converter
AF	Air Force
AFM	Atomic Force Microscopes
Ag	Silver
Al	Aluminum
AO	Atomic Oxygen/Announcement of Opportunity
Au	Gold
BFO	Beat Frequency Oscillator
BSA	Boric Sulfuric Anodize
C	Carbon
CCW	Counter Clockwise
cm3	Cubic Centimeter
CMOS	Complementary metal Oxide Semiconductor
CN	Carbon Nitride
C°	Degrees Centigrade or Celsius
COR	Clear Oxygen Resistant
CPU	Central Processing Unit
CVD	Chemical Vapor Deposition
CW	Clockwise
DACS	Data Acquisition and Control system
DM	Docking Module
DMT	Decreed Moscow Time
DoD	Department of Defense
EDAC	Error Detection and Correction
EDAX	Electron Dispersive X-Ray Analysis
ESCA	Electron Spectroscopy for chemical Analysis
ESH	Equivalent Sun Hours
EV	Electron Volts
EVA	Extra Vehicular Assembly
FEP	Fluoroethyleneproplyene
FOV	Field-of-View
G	Grams
GSFC	Goddard Space Flight Center
Hz	Hertz (unit of frequency)
IITRI	Illinois Institute of Technology Research Institute
INSTEP	In Space Technologies Experiment Program
IR	Irradiance
ISS	International Space Station

ACRONYMS AND ABBREVIATIONS

IVA	Intra Vehicle Activity
K	Potassium
K°	Degrees Kelvin
KSC	John F. Kennedy Space Center
LaRC	Langley Research Center
LDEF	Long Duration Exposure Facility
LEO	Low Earth Orbit
LeRC	Lewis Research Center (now John Glenn Research Center)
LPSR	Laboratory Portable SpectroReflectometer
MgF2	Magnesium Fluoride
μ	Micron
μm	Micrometer
MIPS	Mir Interface to payload System
MLI	
MSFC	George C. Marshall Space Flight Center
MT	Moscow Time
NAR	Non-Advocate Review
NASA	National Aeronautics and Space Administration
$NaSiO_4$	Sodium Silicate
NAWC	Naval Air Warfare Center
Nb	Niobium
Nb2O5	Niobia Oxide
nm	Nanometers
°	Degrees
O	Oxygen
OAST	Office of Aeronautics and Space Technology
OPM	Optical Properties Monitor
PAC	Power Amplifier Center
PAS	Power Amplifier System
PbS	Lead Sulfide
PFA	Copolymer of Tetrafluoroethylene-Perfluoroalkoxy
PI	Principal Investigator
POSA-I	Passive Optical Sample Assembly number One
PRT	Platinum Resistance Thermister
PSC	Power Supply Center
PSD	Phase Sensitive Detector
Pt	Platinum
PTFE	Polytetra Fluorinated Ethylene
RE	Reaction Efficiency
rms	Route mean square
RSA	Russian Space Agency
RSC-E	Russian Space Company - Energia

ACRONYMS AND ABBREVIATIONS

SAA	Sulfuric Acid Anodize
SEE	Space Environmental Effects
SEM	Scanning Electron Microscope
Si	Silicon
SiO2	Silicon Dioxide
SSAC	Sample Selection Advisory Committee
SSO	Sample Selection Officials
TCSE	Thermal Control Survaces Experiment
TE	Thermo-Electrically
TED	Thermo-Electric Device
TFLC	Tuning Fork Light Chopper
TFLC	Tuning Fork Light Chopper
ε_T	Thermal Emittance
TiN	Titanium Nitride
TIS	Total Integrated Scatter
$Ti_xB_yN_z$	Titanium Boron Nitride
$Ti_xB_yO_z$	Titanium Diboride
TQCM	Temperature Controlled Quartz Crystal Microbalance
ε_T	Total Emittance
UAH	University of Alabama in Huntsville
Ultem	Polyetherimide film
UV	Ultra-Violet
V	Voltage
VDA	Vacuum Deposited Aluminum
VDC	Volts Direct Current
VUV	Vacuum UltraViolet
WPAFB	Wright Patterson Air Force Base
XPS	X-ray Photoelectron Spectroscopy
Yb	Ytterbium
Zn	Zinc
ZnO	Zinc Oxide
ZrO2	Zirconium Dioxide
$Zr_xB_yN_z$	Zirconium Diboride

1.0 INTRODUCTION

Long term stability of spacecraft materials when exposed to the space environment continues to be a major area of investigation. The natural and induced environment surrounding a spacecraft can decrease material performance and limit useful lifetimes. Materials must be thoroughly tested prior to critical applications. The Optical Properties Monitor (OPM) experiment provides the capability to perform the important flight testing of materials and was flown on the Russian Mir Station to study the long term effects of the natural and induced space environment on materials. The core of the OPM in-flight analysis was three independent optical instruments. These instruments included an integrating sphere spectral reflectometer, vacuum ultraviolet spectrometer, and a Total Integrated Scatter instrument. The OPM also monitored selected components of the environment including molecular contamination. The OPM was exposed on the exterior of the Mir Docking Module for approximately 8-1/2 months. In-flight OPM data measured a low, but significant, level of contamination compared to findings on other experiments deployed on Mir. Degradation of some materials was greater than expected including aluminum conversion coatings and Beta Cloth. Also, significant particulate contamination was detected by the TIS instrument from the return trip from Mir to the ground laboratory.

The OPM development and the OPM mission to Mir was carried out under Contract NAS8-39237 which was managed by the NASA George C. Marshall Space Flight Center (MSFC). This Science Data Report serves as the final report for this contract. This report describes the OPM experiment, a brief background of its development, program organization, experiment description, mission overview including space environment definition, performance overview, materials data including flight and ground data, in-depth post flight analysis and a summary discussion of the findings and results. The OPM Systems Report, AZ Technology Report No. 91-1-118-164, provides more detail on the design, implementation, testing and performance of the OPM core systems, instruments and monitors. There are a number of other OPM reports available. The OPM Bibliography is listed in Section 6.

1.1 Background

In 1986, the National Aeronautics and Space Administration (NASA) Office of Aeronautics and Space Technology (OAST) released an Announcement of Opportunity (AO) under the In-Space Technologies Experiment Program (IN-STEP). The objective of the IN-STEP program was to demonstrate newly developed in-space technology experiments. In response to this AO, the OPM experiment was proposed as an in-space materials laboratory to measure in-situ the effects of the space environment on thermal control materials, optical materials, and other materials of interest to the aerospace community. The OPM was selected for a Phase A study to determine technical feasibility of the experiment, technical approach, and the estimated cost. The MSFC in Huntsville, Alabama was selected by the NASA/OAST to manage the project. A second AO was issued by NASA/OAST for the development phase of the IN-STEP experiments. OPM was selected under this solicitation for development and flight. Phase B (Preliminary Design) was funded to develop the OPM design and cost parameters, and consider available payload carriers suitable for an OPM mission. In late 1992, a peer review,

consider available payload carriers suitable for an OPM mission. In late 1992, a peer review, called the Non-Advocate Review (NAR), was held to verify the need and worth of the experiment prior to further funding. The OPM was subsequently approved for further development, and the final Phase C/D (Final Design through Mission Support/Data Analyses) funded in April 1993. Between April 1993 and September 1996, the OPM design was completed, fabricated, integrated, tested, and delivered to MSFC.

The OPM was launched on STS-81 on January 12, 1997, mounted in the SpaceHab. The OPM was Intravehicular Activity (IVA) transferred into the Mir Space Station on January 16, 1997. It was stowed for two and one-half months before deployment and being powered up on the Mir Docking Module by the first joint Russian-American Extravehicular Activity (EVA) on April 29, 1997. On June 25, 1997, the OPM lost power because of the Progress collision into Mir's Spektr module and did not regain operational status until September 12, 1997. The OPM continued operation until January 2, 1998 when the OPM was powered down in preparation of the January 8, 1998 EVA to retrieve the OPM. After a successful Russian EVA retrieval, the OPM was later transferred IVA into the Shuttle (STS-89) and returned to Kennedy Space Center (KSC) on January 31, 1998.

1.2 Organization and Participants

The Russian Mir Station provided a unique opportunity to study the behavior of materials in the space environment around a complex space station. The OPM experiment was exposed on the Mir Station as part of the International Space Station (ISS) Phase 1 program. The OPM flight hardware was developed under the NASA Crosscutting Technology Program managed by the Office of Space Science. The ISS Phase 1 program provided joint funding and support for the OPM mission to Mir. The OPM program was managed by the MSFC and members of the Science Team are listed in Table 1-1.

Table 1-1. Science Team for OPM

Principal Investigator	D.R. Wilkes, AZ Technology
Project Scientist	J.M. Zwiener, NASA Marshall Space Flight Center
Program Manager/s	D. W. Cockrell, NASA Marshall Space Flight Center R. M. Baggett, NASA Marshall Space Flight Center S.R. Davis, NASA Marshall Space Flight Center G. E. Thomas, NASA Marshall Space Flight Center
Co-Investigators	J.M. Bennett, AZ Technology E. R. Miller, AZ Technology

Science Team	J.B. Hadaway, University of Alabama at Huntsville, Center for Applied Optics R.R. Kamenetzky, NASA/Marshall Space Flight Center J. C. Gregory, University of Alabama at Huntsville J.S. Harchanko, AZ Technology D. Crandall, AZ Technology R.M. Mell, AZ Technology
Chief Engineer	L.L. Hummer, AZ Technology

1.3 Mission Summary and Objectives

It has been demonstrated that the natural and induced space environment can cause optical, mechanical, and thermal damage to exposed surfaces. This materials damage can, and has, seriously affected the performance of critical spacecraft systems, including solar arrays, optical instruments, and thermal control systems. The stability of materials in the space environment is not well understood. To compensate for this uncertainty, spacecraft and instrument designers frequently overdesign systems at greater cost and weight—sometimes with reduced performance. For the large, long-duration missions of the future such as the Space Station, overdesign of systems and instruments is extremely undesirable, and in many cases, impossible.

The space environment is a complex combination of mostly independent constituents, including atomic oxygen (AO), particle radiation (electrons, protons, etc.), electromagnetic radiation, thermal vacuum, micrometeoroids, orbital debris and contamination (molecular and particulate). These constituents vary in composition and magnitude with orbital parameters, solar activity, seasons of the year, and time of day. The complex nature of the space environment makes it difficult—if not impossible—to simulate an individual constituent accurately, and certainly not the combined environment nor the synergistic effects of this environment.

Much effort has gone into the development of environmental effects lifetime prediction models and ground simulation testing techniques. These models and techniques must be validated using in-space, time referenced measurements of environmental effects versus the exposure environment. The in-situ or in-vacuum measurement of materials optical properties is particularly important because environmental damage for many materials is reversible to some degree when the test material is returned to the laboratory environment. Oxygen bleaching of surface damage of ZnO pigment based thermal control paints is a prime example.[1-3]

The OPM, which was derived from the Thermal Control Surfaces Experiment (TCSE)[4,5], flown on the Long Duration Exposure Facility (LDEF)[6-9] was developed to address these needs to better understand and predict the effects of the space environment on the surface properties of materials. The OPM is a multifunctional, reusable in-flight laboratory for the in-situ study of the surface optical properties of materials[10]. Selected materials were exposed to the low earth orbit

space and Mir induced environment and their effects measured through in-situ measurements and post-flight analyses.

Optical and thermal properties were measured by the OPM in-situ measurement subsystems: spectral total hemispherical reflectance, Total Integrated Scatter (TIS), Vacuum UltraViolet (VUV) reflectance/transmittance, and total emittance. Environmental monitors measured selected components of the space environment (solar/earth irradiance, molecular contamination, and atomic oxygen) to which the test samples were exposed. Detailed optical and thermal properties, surface degradation, and contamination are being determined by post-flight analyses.

The overall OPM experiment objective was to study the effects of the Mir space environment, both natural and induced on optical, thermal control, solar array, and other materials. Specific objectives were:

- Determination of the effects and damage mechanisms of the Mir space environment on materials.
  - * Planned use of Mir II as an element of the ISS dictates that its environment be characterized and understood prior to its use on ISS.
  - * Mir was the only opportunity to study the environment around a large space platform for an extended period and its effects on materials and systems.
  - * The high inclination orbit of the Mir results in a different mix of environmental constituents than that observed on other long duration missions such as the LDEF. The OPM mission on Mir offered the opportunity to study this environment.
  - * Quantitative in-flight data are needed to determine the effects of this environment on optical, thermal control, and power system materials and on operational systems and payloads.
  - * In-situ optical property measurements of test materials due to the bleaching effects when test samples are returned to the terrestrial environment.
- Provide space flight testing of spacecraft and optical materials.
  - * Critical materials will be required to operate in the environment around a large space platform. Candidate materials for the ISS payloads and other future missions were exposed to the Mir environment and the effects measured by pre-flight, in-situ, and post-flight tests.
- Provide data to validate ground test facilities and prediction models.
  - * All candidate materials for use in space cannot be flight tested in the exact environment where they will be used or for the complete mission duration.
  - * Accelerated ground based testing and lifetime prediction models will remain the basis for space system design and mission planning. These tests and models require time dependent flight data for validation.
  - * The OPM is designed to provide in-space time dependent optical measurements of materials as they are normally measured during ground testing.
- Development and test of a multifunctional, reusable flight instrument for the in-situ study of the behavior of materials in the space environment.

* The OPM is the most comprehensive instrument system ever developed to study the behavior of materials in space.
* The OPM is designed to be easily accommodated on different payload carriers and be reprogrammed to meet varied mission requirements.

1.4 Sample Selection Process

The OPM is multifunctional in-space optical laboratory for the study of the behavior of materials in the space environment. Many different materials can be tested and investigations carried out on an OPM mission. The purpose of the sample selection process was to choose and optimum set of test materials and investigations to be flown on the OPM mission to Mir.

Proposals for samples to fly on the OPM were solicited from all sources, including NASA, the DoD, industry, Universities and ISS international partners. The OPM sample selection process accommodated a wide range of interest and participation. A total of 228 sample proposals were received from 17 US organizations and two ISS international partners. An OPM Sample Selection Advisory Committee (SSAC) was formed and reviewed all submitted sample proposals and provided their evaluations to the OPM Sample Selection Officials. The OPM SSAC and Sample Selection Officials (SSO) are shown in Table 1-2. The SSO considered mission objectives, sample proposals and reviewed evaluations from the SSAC in making the final selections. Samples were selected to fly on the OPM from four NASA centers, five ISS Contractors, one University, two Department of Defense (DoD) organizations and the Russian Space Company-Energia (RSC-E). A listing of the samples flown on OPM are shown in Appendix A, along with the sponsoring organization and technical contact.

Table 1-2. OPM Sample Selection Officials/Advisory Committee.

Sample Selection Officials	
D. Wilkes - OPM Principal Investigator	
S. Pearson - Space Environmental Effects (SEE) Program Manager	
R. Suggs - ISS Environments	
Sample Selection Advisory Committee	
NASA/MSFC:	J. Zwiener, S. Clifton, A. Shapiro
NASA/LaRC:	D. Stoakley
NASA/GSFC:	L. Kauder, P. Chen, R. Keski-Kuha
NASA/JSC:	S. Koontz
NASA/LeRC:	B. Banks
NASA/JPL:	T. O'Donnell
NASA/ISS:	T. May
MacDac/ISS:	H. Babel
Boeing/ISS:	J. Golden, N. Lowrey
Rocketdyne/ISS:	K. Wefers
DoD/Aerospace:	M. Meshishnek
DoD/AF	P. Carlin (WPAFB)
OPM/AZ Tech:	J. Bennett, E. Miller

2.0 OPM HARDWARE DESCRIPTION

2.1 System Overview

The OPM is a fully integrated package including three optical instruments, three environmental monitors, a data acquisition and control system (DACS), a power supply center (PSC), a power amplifier system (PAS), a sample carrousel, and the OPM structure (see Figure 2-1). Optical and thermal properties were measured by the OPM utilizing three in-situ measurement subsystems (as shown in Figure 2-1) spectral total hemispherical reflectance, TIS, and VUV reflectance/transmittance. Thermal emittance was measured using calorimetric techniques. Major constituents of the space environment were also measured (solar/earth irradiance, molecular contamination, and atomic oxygen) to document the natural and induced space environment to which the test samples were exposed. It should be noted that the OPM was designed to accommodate different measurement sub-systems. OPM provides a common mounting structure, common multi-sample carousel, command and control software, passive system thermal control, power, data acquisition and limited on board analysis to support individual investigators unique requirements. Test samples were arranged on half of the circular sample carousel in four concentric circular rows. Additional irregularly shaped samples were accommodated inside of the four rows of samples. Samples in the three outer rows were called "active" samples because they were measured by the on board optical instruments. The inner samples are called "passive" because they are not measured in-flight and are evaluated in pre- and post-flight analyses.

A summary listing of the basic properties of the OPM experiment is provided in Table 2-1.

In the following sections, the design and performance of the on board optical instruments and environmental monitors are discussed. Details on the OPM support systems and additional design information of the science instruments are provided in the *OPM Systems Report, AZ Technology Report No. 91-1-118-164.*

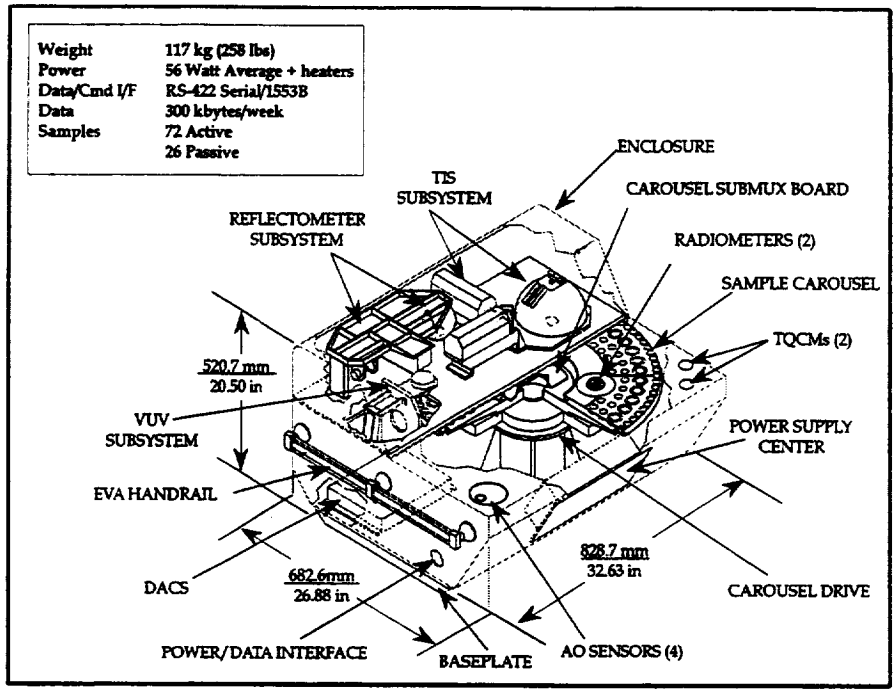

Figure 2-1. OPM Schematic

Table 2-1. Basic OPM Specifications.

Size (LxWxH) includes MLI	82.9 x 68.3 x 52.1 cm (32.6" x 26.9" x 20.5")
Weight OPM w/MLI, EVA handrails, sample cover & flight bag Deployed weight with Interface Plate and Latch	 117.3 kg (258 lbs) 146.8 kg (323 lbs)
Power Source Average Peak	 Spacecraft 27 VDC 56 Watts (+39 Watts for Heaters) 196 Watts
Spacecraft Command/Data I/F Type Data Rate	 RS-422 Serial 300 Kbytes/week
Thermal Control System	Passive - Ext. Radiator w/Heaters
Test Sample Capacity	72 Active Samples 26 Passive Samples

2.2 Sample Carousel and Flight Samples

The sample carousel housed all ninety-eight flight samples. There were seventy-two "active" samples; meaning these were measured in flight. These samples were further categorized by instrument: the reflectometer contained twenty samples, the VUV had thirty-two

samples (at forty-one sample positions), and the TIS had twenty samples. The VUV contained forty-one sample positions. There were nine calibration positions, one VUV calibration hole at every fifth VUV sample position (reference Figure 2-2). There were twenty-six "passive" samples. Passive meant the samples were measured only by pre- and post-flight analyses. A listing of all flight samples is provided in Appendix A, including location number, description, supplier, and main technical contact.

The samples were spaced around the carousel in a polar configuration with the VUV samples on the outer row, followed by the reflectometer, TIS, and passive samples respectively on the inner rows. Figure 2-2 illustrates the placement of the samples on the sample carousel. The samples were spaced at 9° increments, except for the VUV samples, which were spaced at 4.5° increments because of the increased area available on the outer row.

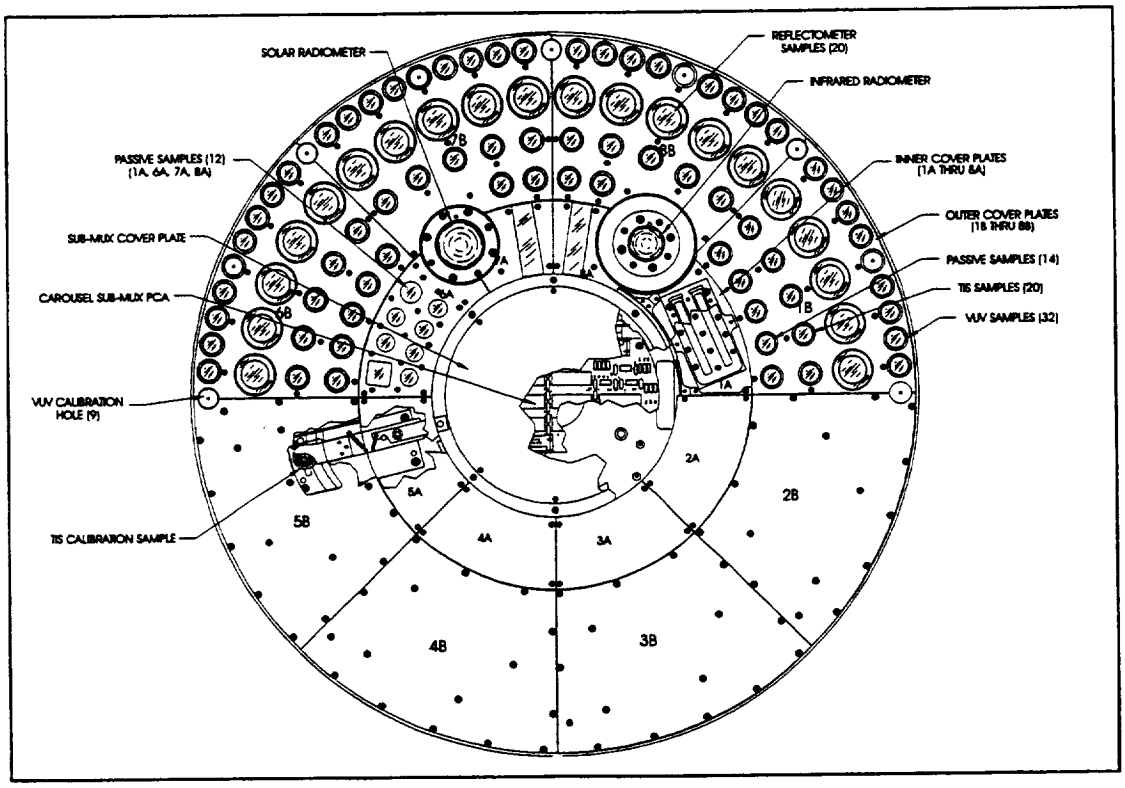

Figure 2-2. Sample Carousel

The flight samples were installed in sample holders to accommodate the various thickness of flight samples, to mechanically hold them in place during the launch environment, and to enable ease of installation/removal in the Sample Carousel. These sample holders were customized for the reflectometer, TIS, VUV, and the passive samples. Figure 2-3 illustrates the three basic sample holders used in the Sample Carousel. The VUV and TIS/passive samples were identical except the outer circumference was machined to permit closer spacing around the carousel perimeter.

The reflectometer sample holders were calorimeters that provided a simple method to determine solar absorptance (α_s) and thermal emittance (ε_T) of test samples. The calorimetric technique measured the inputs to the heat balance equation and calculated solar absorptance and total emittance. The design of the calorimeters isolated the test sample thermally from the OPM to minimize errors caused by radiative and conductive losses. The OPM calorimeter design was based on the design that was used on the LDEF TCSE [4,5] and that was developed originally by the GSFC [11].

The calorimetric measurement procedure was an improvement over past experiments for determining ε_T. Previous experiments determined ε_T when the calorimeter viewed deep space only (i.e., no view of the sun or earth). This orientation was difficult to insure, and the time spent in this orientation was, at times, too short to provide accurate measurements. The OPM procedure, however, rotated the samples inside the instrument, eliminating any view of the sun or earth.

The calorimeter consisted of three major parts: the sample disk, the inner cup, and the outer cup (see Figure 2-4). The concept for the three-part calorimeter was for the inner cup to act as a thermal guard for the sample disk. This design featured virtually zero conduction back through the sample holder, and low measurable radiative heat transfer to the sides. The inner cup, or "guard", had the same exposed area and coating as the sample disk to maintain the inner cup temperature close to the temperature of the sample. The thermal capacitance of the inner cup was also as close as possible to that of the sample disk to ensure the guard was effective - even during transient sample temperatures. Kapton films, formed into cylinders, were used to fasten the sample disk to the inner cup and to fasten the inner cup to the outer cup. Crimped double-faced aluminized Mylar sheets were placed inside each cylinder to reduce the radiative heat losses. Vent holes were put in the cylinders and bases of the inner and outer cups, enabling the interior of these cups to vent to the vacuum environment. A solar absorber material was applied to the inner sides of both the inner cup and the outer cup to minimize errors caused by light leaks through the gaps between the sample, inner cup, and outer cup. A Platinum Resistance Therometer (PRT) was attached to the underside of each sample disk with thermally conducting silver epoxy to assure good thermal contact with the sample substrate. The OPM DACS monitored the PRT to measure the temperature of the sample disk. The calorimeter was mechanically clamped onto the carousel by the carousel mounting cover. The top of the calorimeter was flush with the top of the carousel.

The sample carousel total rotation was fixed at 535, (525° nominal) to enable the samples to be rotated under the measurement instruments aperture. From the nominally exposed position ("Home" position or 0°), the carousel rotated 205° Counter Clockwise (CCW) and 330° Clock Wise (CW). These rotation limits were devised for the singular operation of each instrument to optimize instantaneous power as well as the carousel motor operation time.

The sample field-of-view (FOV) from the carousel plane was 123° minimum in one direction (towards the Top Cover), and 180° in the other directions (see Figure 2-5). The restricted view was towards the OPM cover that enclosed the three measurement instruments. Only those samples immediately adjacent to the Top Cover had the limited 123° FOV, all other samples had a FOV greater than 123° toward the Top Cover.

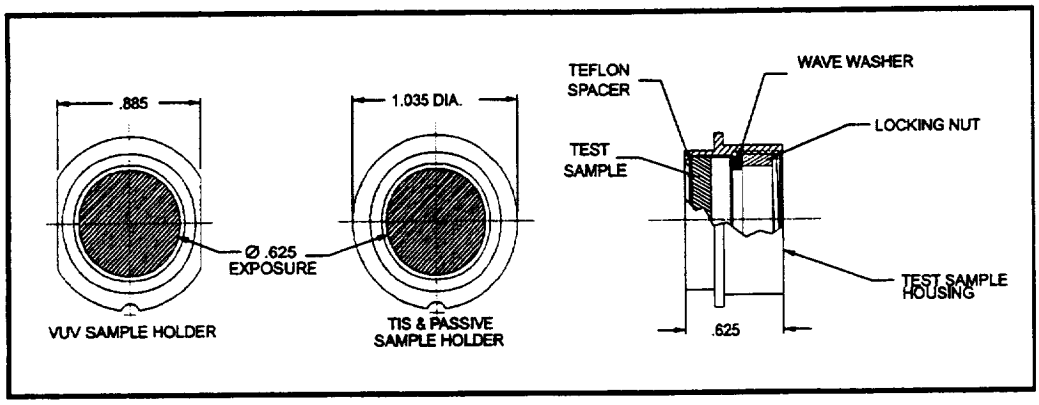

Figure 2-3. Test Sample VUV, TIS, and Passive Sample

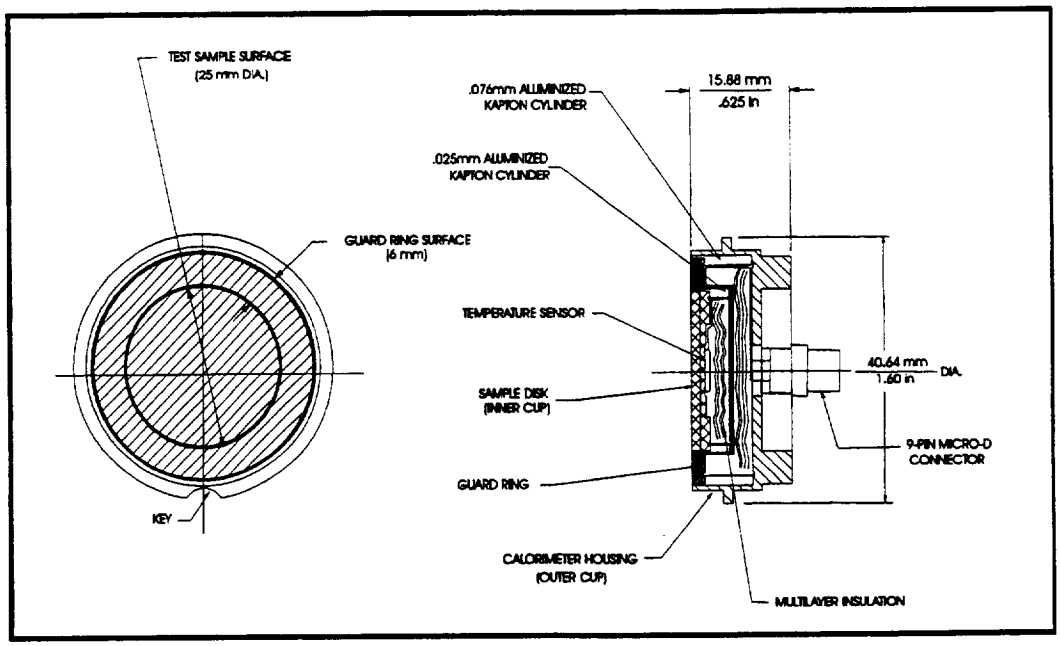

Figure 2-4. Calorimeter Sample Holder (Reflectometer Sample)

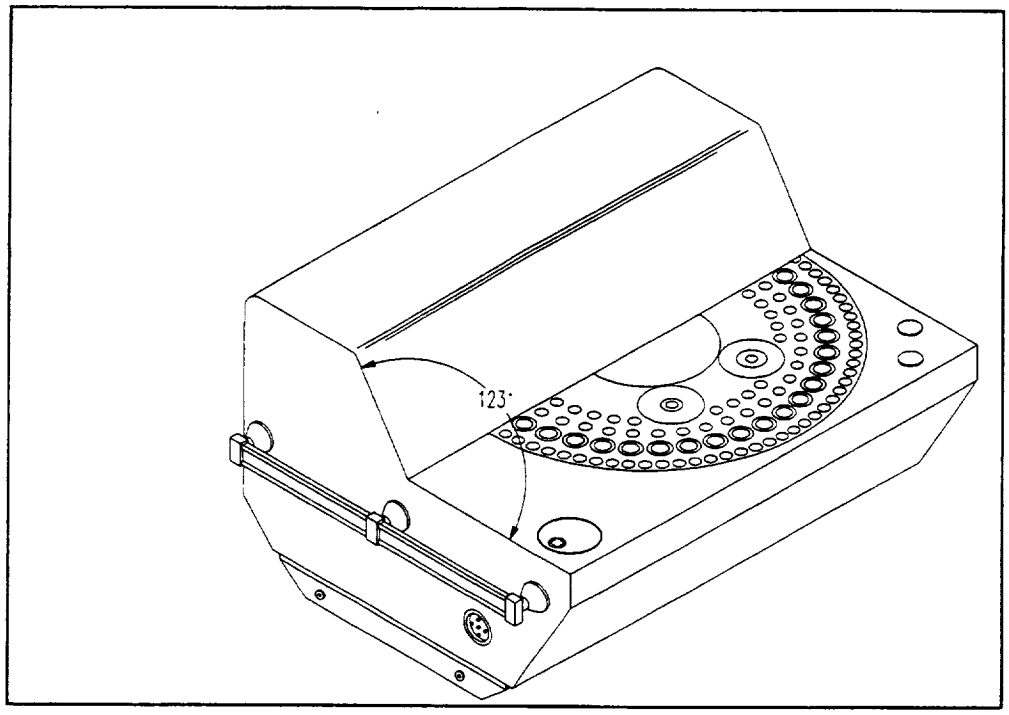

Figure 2-5. Sample Field-of-View

2.3 Reflectometer Subsystem

The OPM reflectometer measured the spectral total hemispherical reflectance of test materials over the spectral range of 250nm to 2500nm. This instrument is of conventional laboratory design that used an integrating sphere, a prism monochromator, two light sources, and two detectors to perform the required measurements. The measurement specifications for this instrument were:

- Spectral Range: 250nm to 2500nm
- Accuracy: ± 3%
- Repeatability: ± 1%
- Spectral Resolution: ± 5% of wavelength

The OPM reflectometer was designed and built by the prime contractor, AZ Technology. This instrument was based on AZ Technology's commercial instrument, the Laboratory Portable SpectroReflectometer (LPSR).

2.3.1 Optical Design

The reflectometer optical system is shown in Figure 2.6. Two light sources were used to span the spectral range of the instrument. The instrument measurement scan was from 2500nm (starting point) to 250nm (ending point). This scan order was chosen to allow the deuterium lamp to stabilize prior to the scan entering the region where this lamp was used. A Tungsten filament source was used from 2500nm to 420nm. The tungsten lamp was powered by a

programmable constant current source that allowed the lamp intensity to be varied during the scan to optimize detector signal level. The deuterium arc lamp was used to cover the 410nm to 250nm portion of the wavelength scan. The intensity of the deuterium source was not varied during the scan. The collection optics (see Figure 2-6) included a 400nm to 2500nm high pass dichroic filter. The dichroic filter passed the longer wavelength tungsten lamp energy but reflected the Ultra-violet (UV) energy from the deuterium lamp.

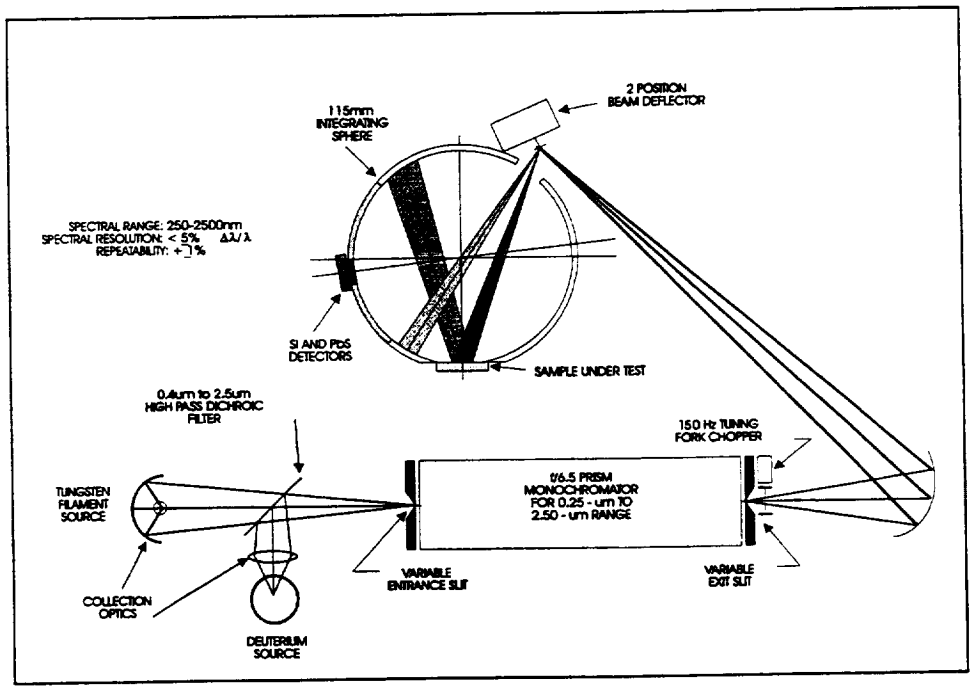

Figure 2-6. Reflectometer Optical Schematic

Next in the optical path was a f/6.5 prism monochromator. This monochromator used two space qualified stepper motors to control wavelength and slit width. The wavelength motor drove a worm gear/cam mechanism that moved a Littrow mirror behind the prism inside the monochromator to select the wavelength of light output. The second motor drove a worm gear/cam mechanism that opened and closed the entrance and exit slits of the monochromator. The variable entrance and exit slits allowed the output intensity of the monochromator to be controlled to optimize signal level and to control spectral resolution. Figure 2-7 shows the actual wavelength resolution for the OPM reflectometer. Position sensors were coupled to both the wavelength and slit width mechanisms to provide position feedback to the control system in the DACS.

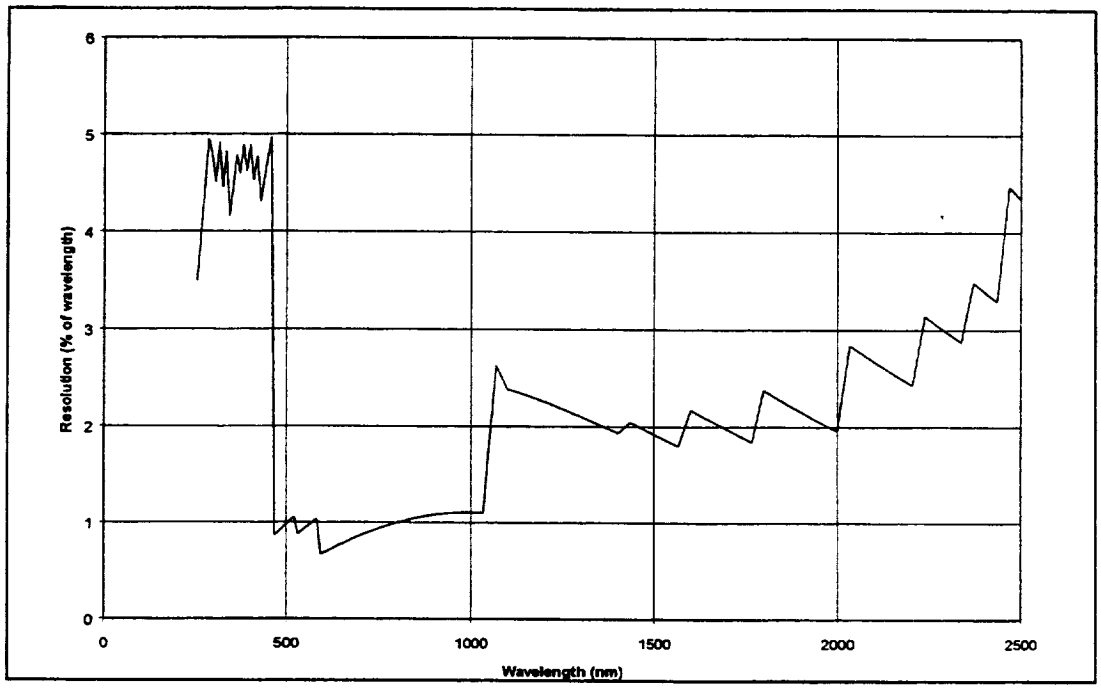

Figure 2-7. Reflectometer Wavelength Resolution

The output of the monochromator was then chopped or modulated by a 150Hz Tuning Fork Light Chopper (TFLC). The chopped optical system was used to achieve increased signal to noise performance of the instrument. This will be discussed in more detail in the next section.

The optical beam is then focused onto the beam deflector mirror. This mirror had two positions and was moved by a third stepper motor. In one position the beam was directed through the integrating sphere onto the sample being measured. In the other position the beam was directed to the integrating sphere wall for a 100% reference. The ratio between these two measurements is the reflectance at that wavelength.

A specially designed 115mm integrating sphere was used to collect and integrate incident light energy. The heart of the reflectometer optical design is the integrating sphere. The monochromatic beam enters the integrating sphere by reflecting from the common path beam deflector mirror. The beam is directed alternately onto the sample and the sphere wall. Integrating sphere theory states that, for an integrating sphere with no hole losses, a perfectly reflecting diffuse coating, and an ideal detector, the detector output is directly proportional to the radiance entering the sphere. When the beam is directed alternately to the sphere wall and the test sample, the geometry of the two beams is identical--except for the absorptance of the sample material. The ratio of the detector readings for the sample and the sphere wall positions is the total hemispherical reflectance of the sample. The properties of the sphere cancel out, resulting in an absolute-type measurement.

In practice, sphere coatings are not perfect, diffuse reflectors. Detectors are spatially and directionally nonuniform, and integrating spheres have hole losses. These factors determine the

accuracy of the reflectance measurement. This is particularly important when measuring samples ranging from specular to diffuse. The most critical feature for non-ideal integrating sphere design is to maximize the detector FOV of the sphere wall while not permitting the detector to view the sample, the first specular reflection onto the sphere wall, nor the direct illumination of sphere wall by the incident beam. The design of the integrating sphere for the OPM and the commercial LPSR instruments eliminates the major errors in the measurement of either specular or non-specular samples. This is accomplished by employing unique detector optics with integral baffles. In addition to the integrating sphere geometry, the internal sphere coating is critical. The OPM sphere coating was a 6mm thick liner of Spectralon™ by Labsphere, Inc.

Two detectors were used to span the spectral range of the instrument. A Thermo-Electrically (TE) cooled lead sulfide (PbS) detector was used from 2500nm to 1100nm. The second detector was a Silicon (Si) photodiode with a built-in pre-amplifier that was used from 1067nm to 250nm.

2.3.2 Electronics Design

Figure 2-8 shows the basic block diagram of the reflectometer system. All aspects of reflectometer operation were controlled by the OPM DACS. The PAC provided power and control for the following functions:

- Deuterium Lamp Heater control circuit,
- Deuterium Lamp Strike circuit,
- Deuterium Lamp constant current source,
- Tungsten Lamp programmable current source,
- PbS TE Cooler drive constant current source, and
- Motor drivers (Beam Deflector, Monochromator slit and wavelength drive motors).

The Deuterium lamp heater control circuit provided a constant 10V to the deuterium lamp during warm-up. The heater filament inside the lamp heated the lamp's cathode. After the lamp struck, the heater voltage dropped to 7V during operation. The heater was turned off when the lamp was not in operation. The deuterium lamp required a large discharge voltage in order to initialize the arc. The strike circuit discharged a capacitor into an auto-transformer in order to generate the 600 to 800V required to strike the lamp. Once the deuterium lamp struck, it required a constant 300mA current flow through the arc in order to maintain stability. The PAC contained a 300mA constant current source which powered the lamp after the lamp struck. This circuit also provided the OPM DACS with a feedback signal so the software would know the lamp had struck

The Tungsten lamp current source was used to drive and control the intensity of the Tungsten lamp under DACS software control. The PbS TE Cooler drive was a constant current source which powered the TE cooler mounted inside the PbS photoconductor. The TE Cooler was turned off when the reflectometer was not in use.

The signal conditioning electronics for the detector signal began with a CMOS switch which selected between the two photodetectors, depending on the point in the scan. Figure 2-9 shows additional detail of the signal conditioning electronics. The selected detector signal was first fed through a 150Hz band-pass filter to remove much of the out-of-band noise. A programmable gain amplifier under DACS control was used to adjust the signal level before the synchronous detection stage.

A lock-in amplifier, sometimes called a phase or synchronous demodulator, was used to further condition the analog signal. The band-pass filter/lock-in amplifier combination was extremely effective in rejecting out-of-band noise from both external and internal sources. This chopped optical/electrical system also minimized effects of stray light.

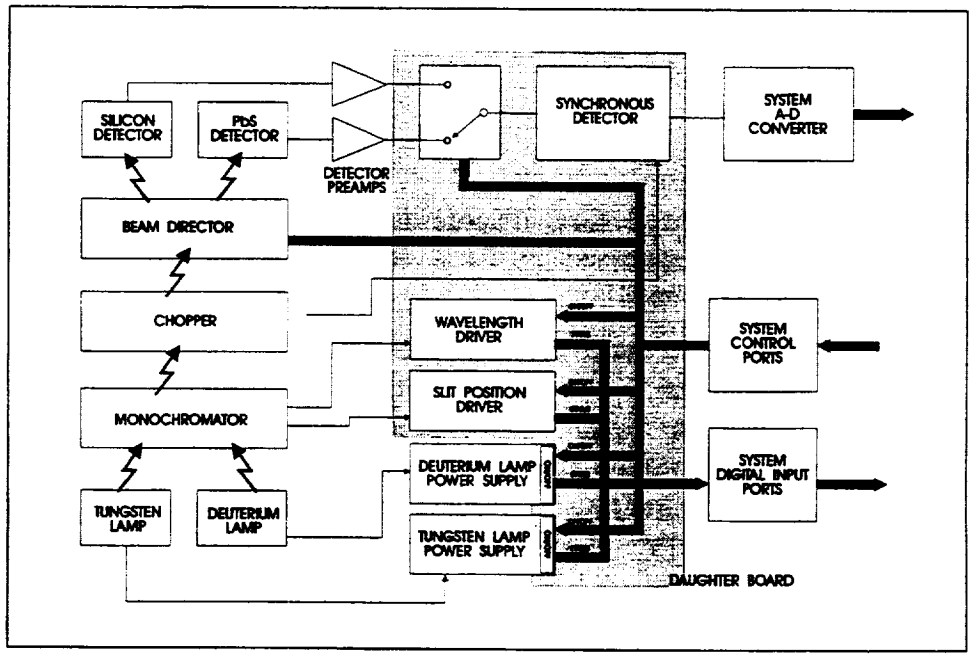

Figure 2-8. Integrating Sphere Reflectometer Subsystem

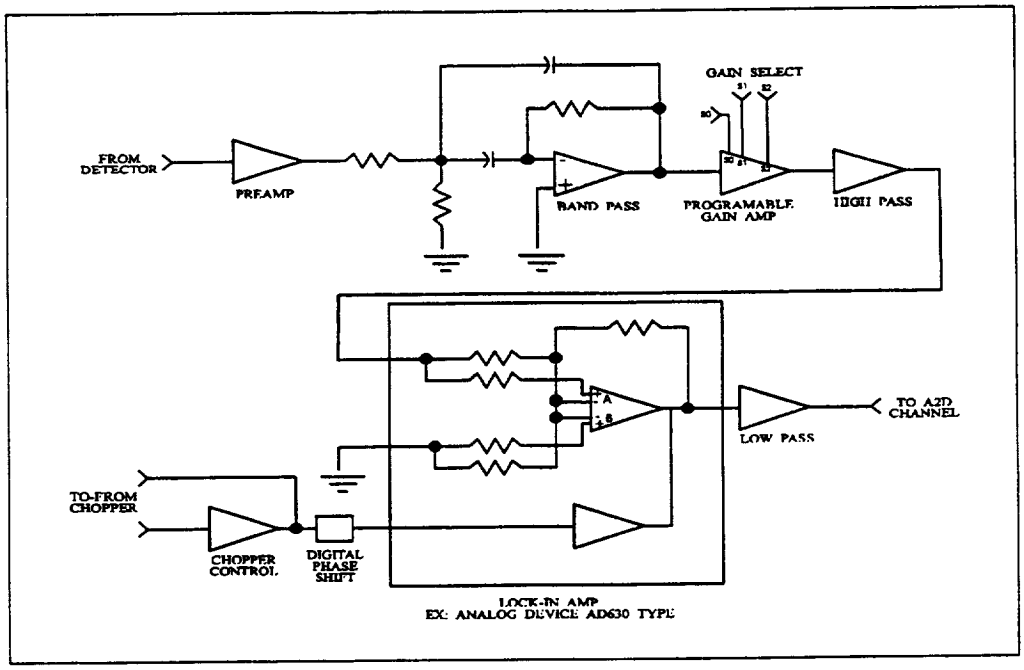

Figure 2-9. Signal Conditioning Circuitry

2.3.4 Mechanical Design

The reflectometer optical/mechanical system was developed as a stand-alone module that allowed the unit to be built and tested as a separate unit. This allowed for ease in optical alignment, calibration, testing and verification of the reflectometer unit. The reflectometer was built on a base-plate assembly that served as an optical bench providing the necessary rigidity to maintain optical alignment. The base-plate provided mounting for the two light sources, monochromator, beam deflector, all optics, PbS pre-amp, and the integrating sphere. During OPM integration, this assembly was placed "upside down" and mounted to the OPM emissivity plate. The emissivity plate had a cutout to allow the sphere to fit into proper position for measuring the samples on the carousel. Figure 2-10 shows a photograph of the reflectometer assembly. Figure 2-11 is a drawing showing the reflectometer assembly, both plan and elevation views. Figure 2-12 shows a photograph of the assembly integrated into OPM. The TIS assembly is in the foreground.

To further increase mechanical rigidity, the body of the monochromator was machined out of a solid block of aluminum. The solid-body monochromator exhibited less flexing when bolted down to the base. Additionally, the solid body monochromator had less of a thermal-gradient -- providing increased wavelength stability. Dimensions of the reflectometer were 8.1-inches at the widest point, 14.3-inches long, and 6.4-inches high. The approximate weight of the reflectometer assembly was 12.2 pounds.

2.3.5 Measurement Sequence

As with all the OPM instruments, the reflectometer was controlled by the software in the DACS. When a reflectometer measurement sequence was initiated, the first reflectometer sample was rotated into measurement position by the carousel and the reflectometer system was powered up. Before the lamps were turned on, a set of "zero" readings were taken on the detector circuitry. These data were used in post-flight data reduction to remove any residual detector offset. The lamps were then powered on and allowed to stabilize. Internal calibration tables were used by the software to position the monochromator wavelength and slit width, to set the lamp intensity, and to select the proper detector and circuit gain. Detector readings were taken and stored for the sample and reference positions of the beam deflector. The sample reflectance at that wavelength is the ratio of the detector readings.

This process was repeated for each of the 100 wavelengths for the 2500nm to 250nm range. Lamps and detectors were switched as appropriate for the selected wavelength. This process was repeated for each of the twenty Reflectometer samples. Twenty-seven sets of reflectometer measurements were performed during the OPM mission to Mir.

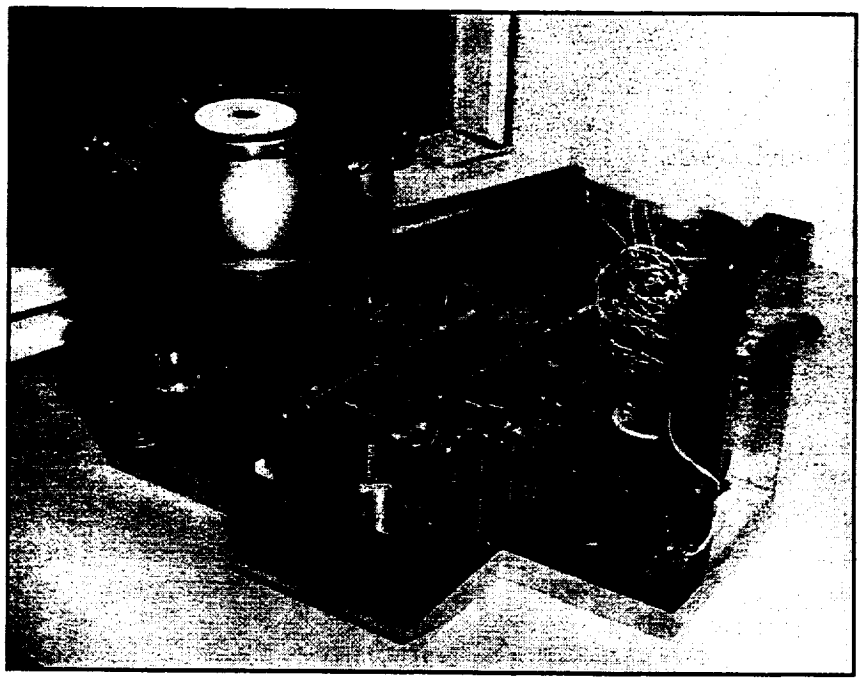

Figure 2-10. Photograph of the Reflectometer Assembly

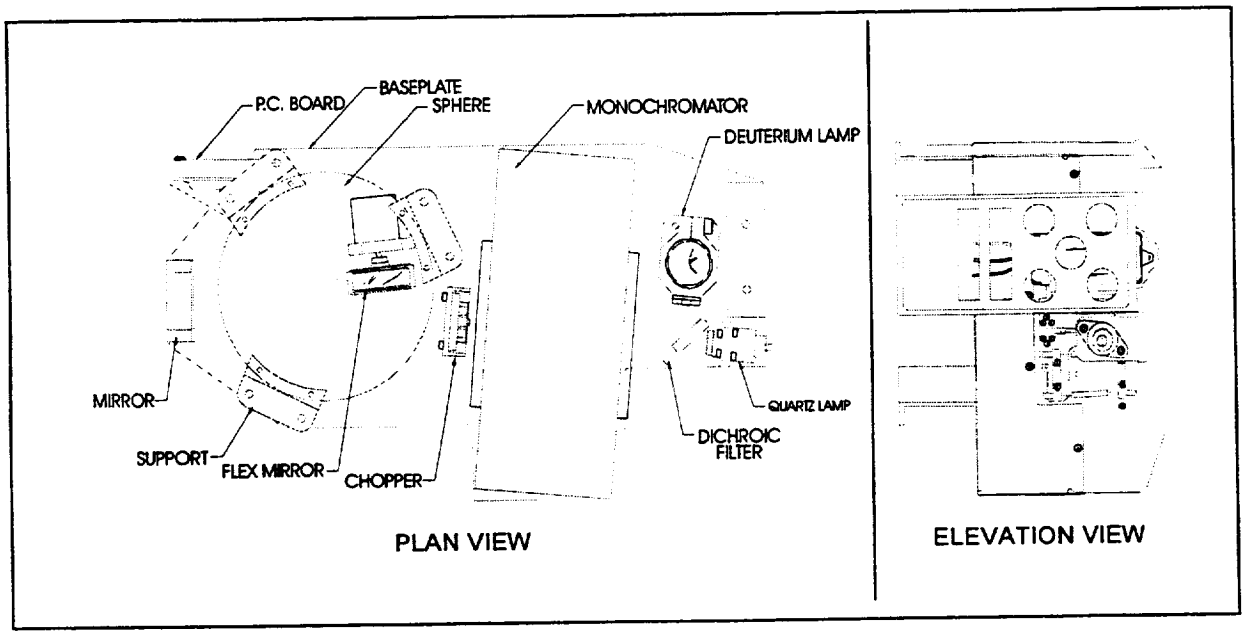

Figure 2-11. Drawing of the Reflectometer Assembly

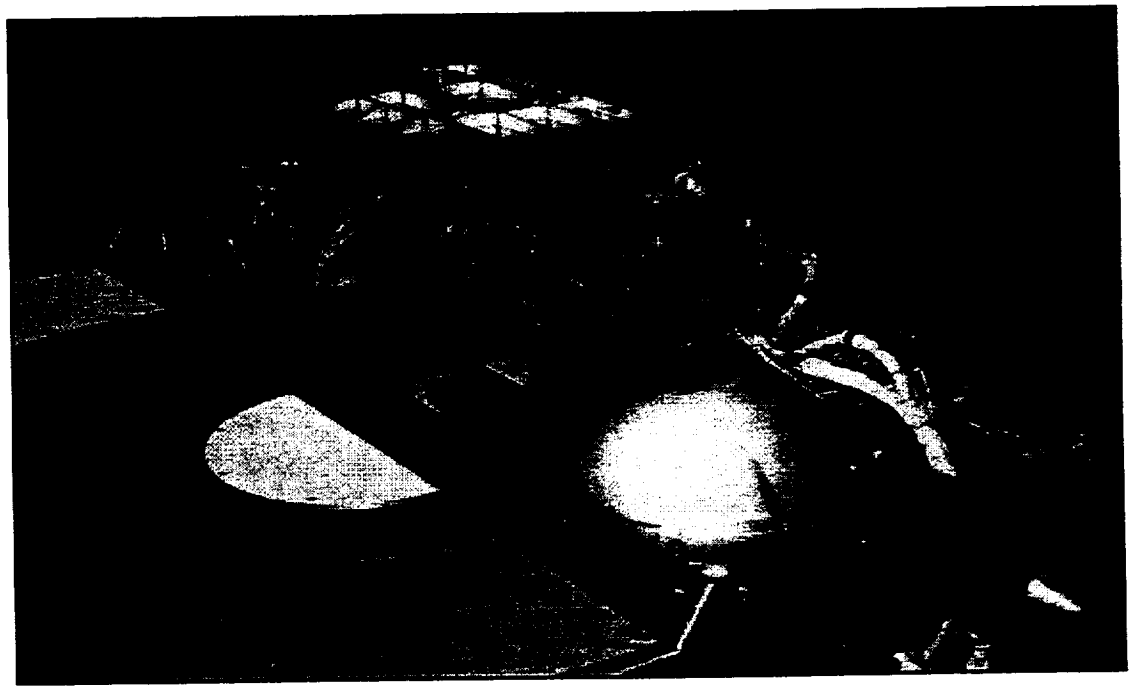

Figure 2-12. Instrument Assembly integrated into OPM

2.4 Total Integrated Scatter (TIS) Subsystem

The TIS Scatterometer measurements augment the data taken by the reflectometer and VUV OPM instruments. The OPM reflectometer and VUV instrument measured transmittance and/or reflectance of selected samples, but cannot identify other effects that can impact surface transmittance/reflectance, such as, surface roughening and surface particulate contamination. Roughening, erosion, and/or surface conversion of various materials by Low Earth Orbit (LEO) AO can have significant effects on optical performance. Further, particulate surface contamination from the natural or spacecraft induced environment can adversely impact optical properties. The most common surface inspection methods used in ground laboratories include profilometers and microscopes - both difficult to accomplish on-orbit. An alternative technology, the TIS can be used to monitor both effects of surface roughening and particulate contamination. The design and verification specifications for this instrument are listed in Table 2-2.

Table 2-2. Basic TIS Specifications

Measurement wavelengths:	532nm and 1064nm
Minimum angular extend of scatter collection:	2.5° to 80° from specular
TIS measurement range:	1×10^{-4} minimum TIS value (5 to 500Å rms roughness)
Accuracy:	±10%
Repeatability:	±2%

The TIS provided laboratory grade measurements on exposed materials while exposed to the space environment. This was the first time this type of instrument had been flown.

The significance of the TIS measurement was in-situ monitoring of surface damage (roughness) and/or contamination of optical and thermal control surfaces caused by the space environment. A two color system operating at 532nm and 1064nm, differentiated the changes in TIS values between surface damage and/or particulate contamination respectively. These data are needed by spacecraft designers to select materials that exhibit minimal changes in the surface properties of materials due to the space environment.

The TIS of a surface (in reflectance) is defined as the ratio of the scattered power to the total reflected power of a light beam incident on the surface, or

$$TIS = scatter/(scatter + specular) \quad (1)$$

A schematic representation of an instrument to measure TIS is shown in Figure 2-13. A narrow beam of light (usually from a laser) is incident on the sample at a slight angle to the normal. The specular reflected beam travels back to one detector while the scattered light is collected by a hemispherical mirror (called a Coblentz sphere) onto another detector. The optical powers measured by these two detectors are then used to calculate the TIS of the sample. The beam is usually chopped and synchronous detection employed to improve the signal-to-noise ratio. Since the hemispherical mirror can not collect all of the scattered light, a correction factor

is determined by measuring a highly-Lambertian surface. The TIS of a perfectly Lambertian surface is equal to 1, which leads to a correction factor of

$$C = V_{INC} * R_{LAMB} / V_{SCATT} \quad (2)$$

Where V_{INC} is the power incident on the Lambertian sample (measured by moving the scatter detector into the incident beam), R_{LAMB} is the certified total hemispherical reflectance of the Lambertian, and V_{SCATT} is the measured scattered power from the Lambertian. All subsequent scatter readings are then multiplied by the correction factor which is usually in the range of 1.3 to 1.5.

For randomly rough surfaces, the rms roughness (within a certain band of spatial frequencies defined by the angular extent of the collected scattered light) can be calculated using the following equation:

$$\delta_{RMS} = (\lambda/4\pi) [-\ln(1 - TIS)]^{1/2}. \quad (3)$$

This equation assumes that all of the reflected light comes from the first surface and that the rms roughness is much less than the wavelength of the light. These assumptions are valid from 5 to 500Å rms surface roughness.

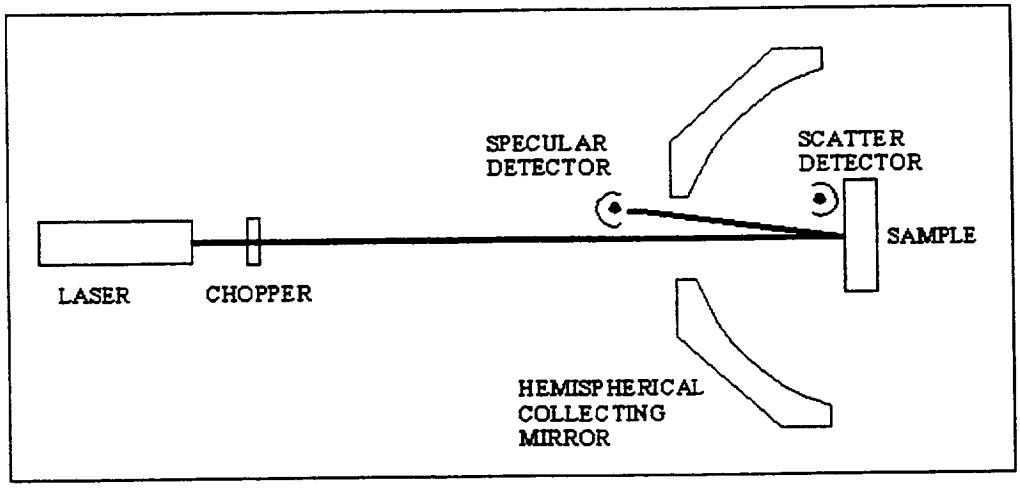

Figure 2-13. Schematic of a TIS Instrument

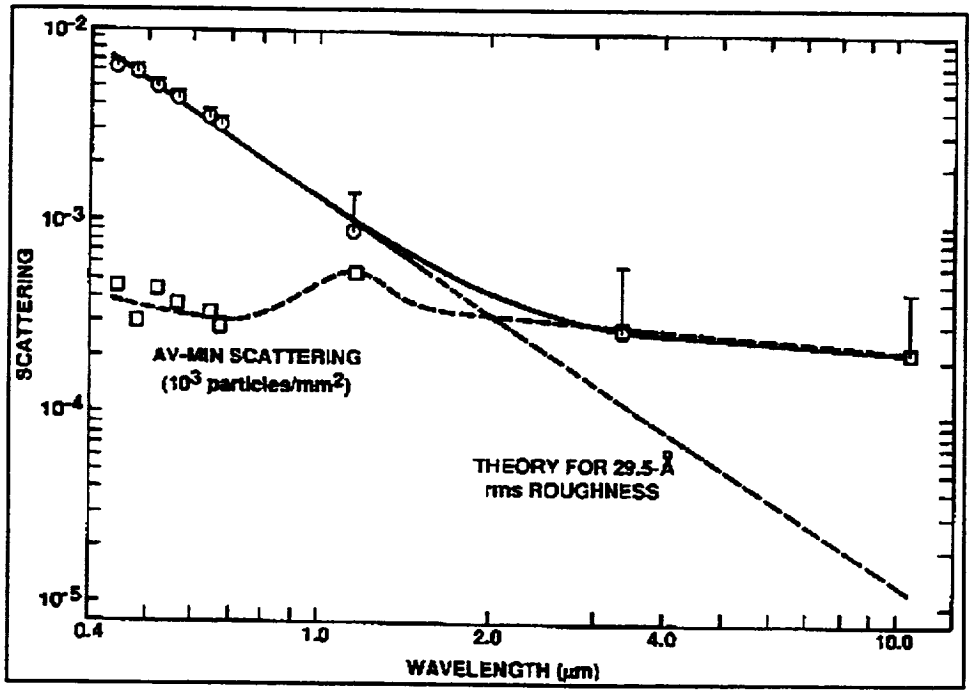

Figure 2-14. Relationship between TIS and Wavelength

Figure 2-14 shows the TIS of a sample (rms roughness of 2.95nm) as function of wavelength.[12] Theory predicts a linear relation on a log-log scale. Actual measurements obey this relation out to about 2μm. At this point, the contribution from particulate scatter begins to dominate. The particulate scatter is roughly constant for all wavelengths, except at wavelengths close to the particle size (notice the slight peak at 1μm). Thus, if one uses two wavelengths, one short and one long, then the effects of surface roughening and particulate contamination can be distinguished. As a surface gets rougher, the two TIS readings will increase together as predicted by Equation (3). As particulate contamination increases, the ratio of the short-to-long TIS readings will decrease. Laboratory experiments on a breadboard TIS instrument have proven the validity of this method.[13] Thus, a two-wavelength measurement of the TIS of the exposed samples can provide both the surface roughness and the particulate contamination in a relatively simple instrument.

2.4.1 Optical Design

2.4.1.1 Total Integrated Scatter (TIS) Subsystem

The TIS instrument measures the total integrated scatter at 532 nm and 1064 nm (See Figure 2-15.[12-14]) The basis of the TIS instrument is a the hemispherical collecting mirror (Coblentz sphere) which collects scattered light from the sample and focuses this onto the main detector. The illuminated spot on the sample surface and the scattered light detector are located at conjugate foci of the collecting mirror. Light from two laser sources is chopped before striking the sample surface at a near normal angle. The specular beam returns at a small angle to

the incident beam direction and is measured by the specular detector. A certified Lambertian surface and a low scatter mirror are used to calibrate the system periodically. These calibration samples are protected from space exposure by a special mechanism that only uncovers the samples while they are being measured. These samples were measured before each set of sample measurements to re-calibrate the system.

Total integrated scatter values down to $1x10^{-4}$ can be measured by this instrument. The accuracy of the measurements is 10%, which is comparable to the best laboratory instruments. More importantly for the OPM, the repeatability is within 2%. This gives the instrument the required ability to measure small changes in the surface characteristics of the test samples caused by exposure to the space environment.

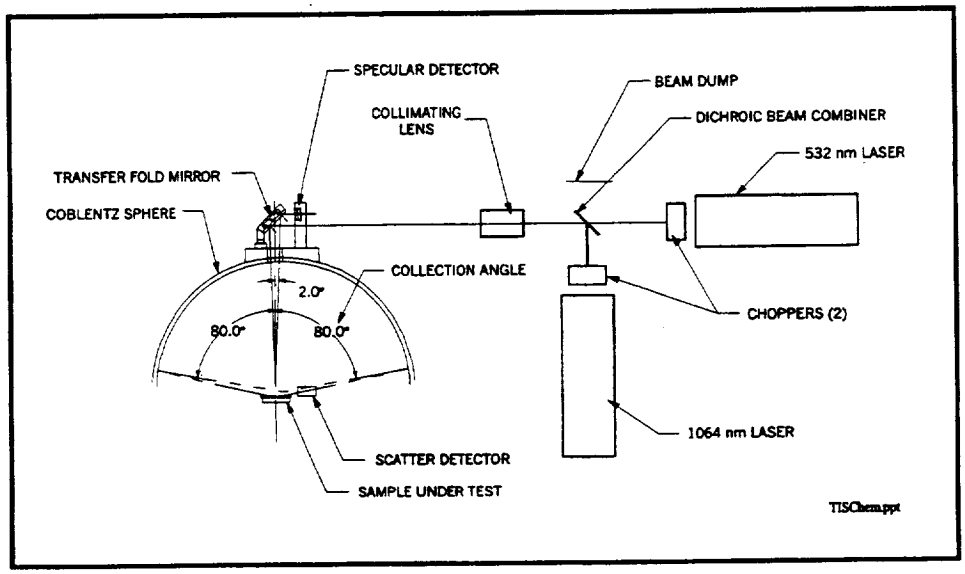

Figure 2-15. TIS Optical Schematic

Two diode-pumped Nd:YAG lasers, manufactured by ATx Telecom and modified by AZ Technology for flight, were used to provide the two color wavelengths of 532nm and 1064nm. Both lasers produced vertically-polarized, CW output within the stability requirement of ±2%. The output powers were nominally 5 and 50mW for the 532nm and 1064nm units respectively. Reference Figure 2-16, TIS instrument layout, for the flight unit assembly. Space-qualified tuning-fork choppers (from TFR Labs), located directly in front of each laser, were used to modulate the beams and shutter them when necessary.

Following the choppers, a fused silica window at 45° was used to combine the beams. Fresnel reflection resulted in equal power beams after the combiner. A beam dump collected the unused beams. Next, a collimating lens, also from ATx telecom, was used on the combined beams to insure that the beam size at the sample was less than 1mm in diameter and had a Raleigh range of at least 13-inches. The total path length from the laser to the sample was about 12-inches, so no other beam focusing optics were required. An aluminum/MgF_2-coated, Zerodur

fold mirror sat atop the Coblentz sphere to reflect the beams down to the sample location (at an incidence angle of 2°) and to reflect the returning specular beams onto the specular detector.

The 7-inch diameter sphere, made of electro-formed nickel with a rhodium coating (Opti-forms, Inc), had a 0.4-inch diameter hole near the vertex (5mm to the side of the optical axis). The hole was located off center so that the beam entered the sphere at an angle of 2° to the sample normal and struck the sample at a point 5mm to one side of and 4mm outside the center a curvature of the sphere. This gave the optimum horizontal separation of the beam and detector as well as vertical separation of the sample and detector. The specular reflected beam exited the sphere at a small angle from the incoming beam so that it was measured by a detector. Since aberrations did not allow efficient collection of light beyond 80°, the sphere was masked to collect from 2.5° to 80° from the specular direction.

The detectors were off-the-shelf Si photodiodes from Hamamatsu (S2386-45K) with 3.9mm x 4.6mm active areas. They possessed a linear dynamic range of more than six decades. Custom pre-amplifiers were designed and built with the proper gain to handle the expected signals. A synchronous detection circuit located in the main OPM DACS provided further gain up to a factor of 16. The analog signal processing for the TIS was identical to that used on the reflectometer as described in Section 2.3 and to TIS detailed block diagram in Figure 2-17.

2.4.2 Mechanical Design

The TIS was designed for mounting all components to a solid, single-piece, aluminum baseplate for structural integrity. The lasers and Coblentz sphere were accurately located using dowel pins. The other components were attached in ways that allowed for rotation, tilt (with shims), and lateral adjustment for alignment. A boss on the underside of the baseplate was designed to fit very closely into a pilot hole in the OPM emissivity plate to accurately place the TIS instrument relative to the samples in the carousel. In this configuration, the illuminated spot on the sample was located 5mm to one side and 4mm outside the center of curvature of the Coblentz sphere. The center of the scatter detector was then located at the conjugate point 5mm to the other side and 4mm inside the center of curvature. The aluminum surfaces of the instrument were either alodined (for corrosion resistance) or painted with a low-reflectance black coating developed by AZ Technology (for stray light control). Eight easily-accessed bolts were used to fasten the TIS to the OPM. Two power cables connected the lasers to the OPM PSC. Two other connectors interfaced the choppers, detectors, and thermistors (one on each laser) to the OPM DACS.

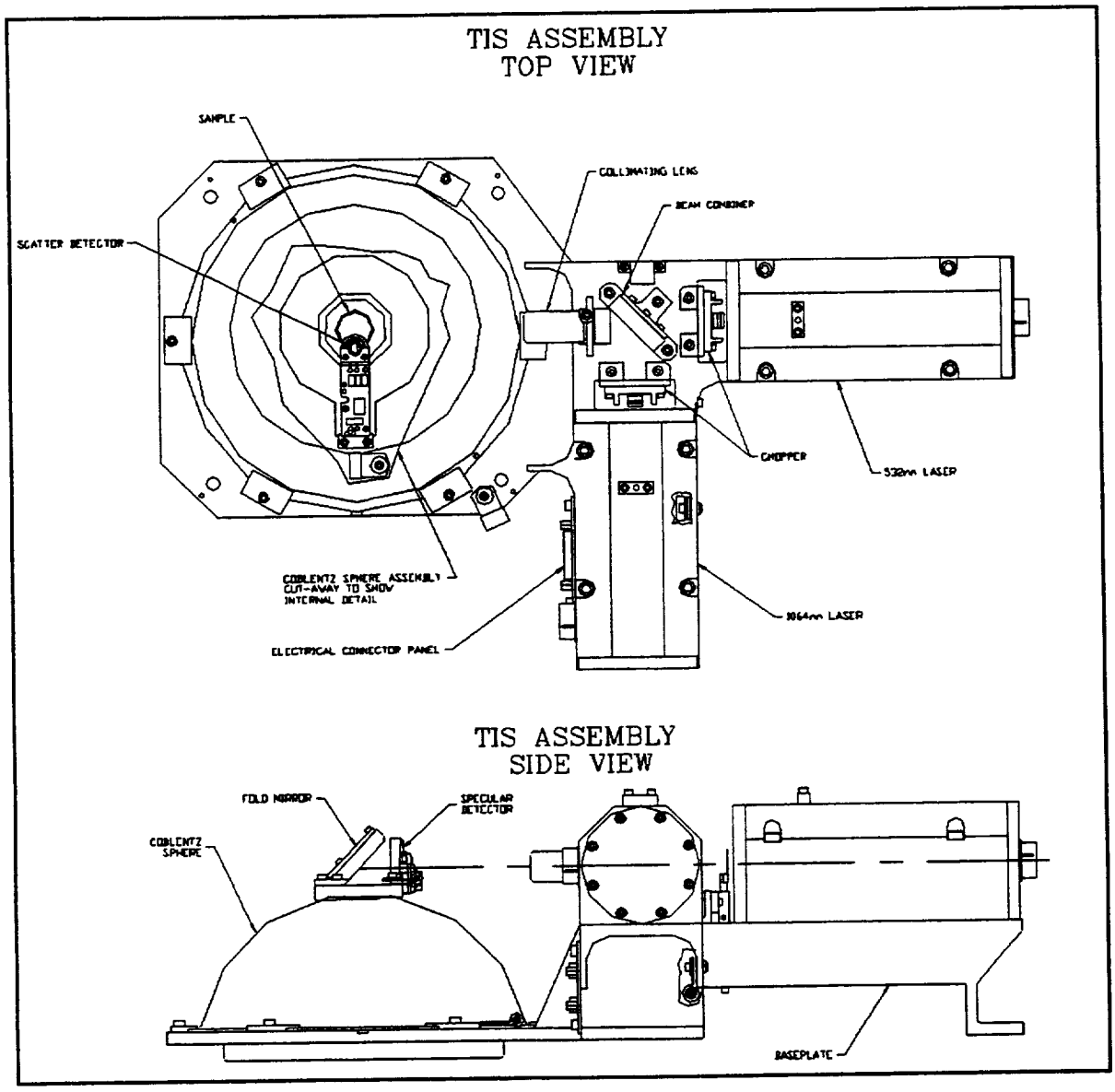

Figure 2-16. TIS Flight Assembly

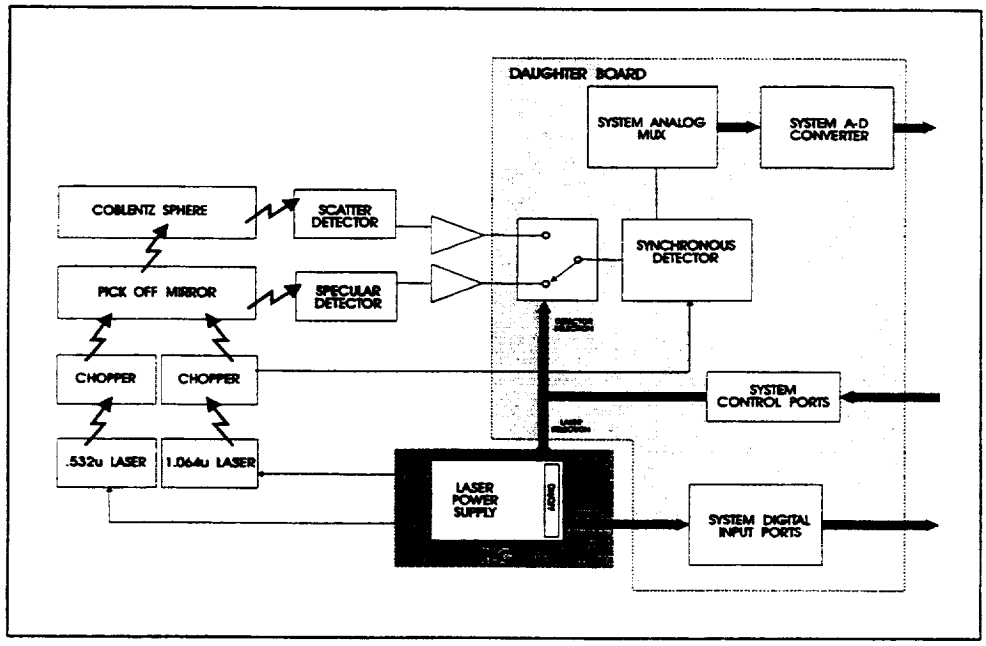

Figure 2-17. Detailed Block Diagram

The most challenging components for the flight instrument were the lasers. No space-qualified lasers were found that were suitably compact, low power, nor of the desired wavelengths for the TIS. The only space-qualified lasers identified at the time were extremely expensive, bulky, and designed as one-of-a-kind components for specific flight programs. Small diode-pumped Nd:YAG lasers made by ATx Telecom were used in the conceptual breadboard TIS instrument. With their small size and ruggedness (developed for field use in the telecommunications industry), these lasers seemed to be the best choice for flight. A sealed, aluminum housing was designed to make the lasers vacuum-compatible. The standard ATx laser cores (one 532nm and one at 1064nm) were put into the housings and sealed with Viton o-rings. The resulting lasers were roughly 5.5-inches long x 2.5-inches wide x 2.5-inches tall and weighed about 1.2kg (2.7lbs) each (the 532nm laser is slightly bigger than the 1064nm laser). Sealed connectors were mounted to the housing for power/feedback control cabling.

The final configuration of the TIS envelope was 18-inches wide x 11-inches deep x 6-inches high. The TIS flight weight was approximately 14lbs.

2.4.3 Measurement Sequence

TIS was the first instrument operated during the weekly optical measurement run. During initialization processing, the instrument relays were enabled, a "zero offset" reading was made of the detectors. The 532nm and 1064nm lasers were struck and allowed to warm up/stabilize for 30 minutes. Next a calibration was performed prior to test sample measurement to account for any changes in the system, such as a change in Coblentz sphere reflectance. A special calibration sample was developed consisting of a Lambertian material surrounding a

high-quality mirror (Figure 2-18). The Lambertian material was a space-grade Spectralon™ (PTFE) which has been shown to be, with proper handling, a clean, stable sensor calibration material for LEO. The total hemispherical reflectance of the Spectralon™ at both TIS wavelengths is 0.99. The mirror was required since the scatter detector can not be moved into the incident beam to measure the power. The mirror directed each beam, with very little loss, back to the specular detector for measurement of the incident power. During calibration, a set of four scatter readings were taken from the Spectralon™ surface, and three specular readings were taken from the mirror (the seven dots in Figure 2-18 indicate the measurement locations). Each set was then averaged and used to calculate the correction factor according to Equation (2). A special holder was designed in the sample carousel for the calibration sample which kept it covered at all times except for when it was under the TIS instrument.

Following calibration, each of the twenty 0.75-inch diameter test samples was rotated into place for measurement. Three measurements, each consisting of scatter and specular detector voltages at each wavelength, were made per sample. Switching between wavelengths was accomplished by cycling power to the choppers. Each chopper, when powered down, effectively shuttered the laser beam. The voltage readings, along with their automatically-adjusted electronic gain factors were saved in OPM permanent memory. Some diagnostic voltages from the lasers were also saved at the beginning of each sequence. Following the one hour measurement sequence, the TIS system was powered down.

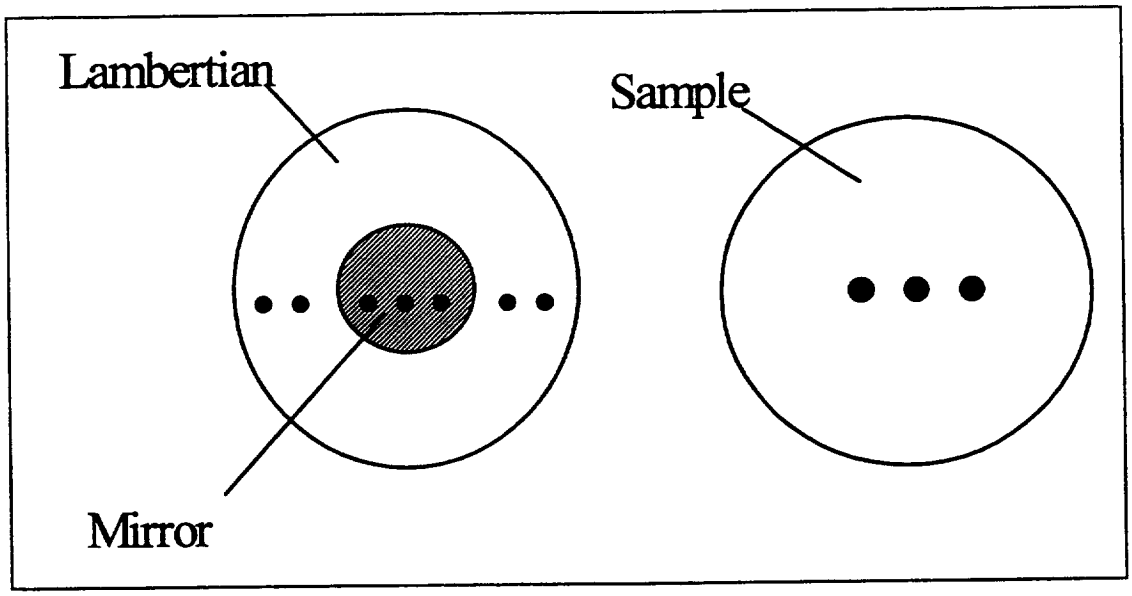

Figure 2-18. Calibration (Left) and Test Sample (Right) Layout.

2.5 Vacuum Ultraviolet Spectrometer Subsystem

The VUV spectrometer measured the specular reflectance and transmittance of test samples in the vacuum UV spectrum from 121.6nm (Lyman α) to 250nm. The VUV instrument was to characterize the change in specular reflectance and transmittances over time due to

exposure to the space environment. The performance specifications for this instrument are listed in Table 2-3.

Table 2-3. VUV Instrument Specifications

Accuracy:	± 5%
Repeatability:	± 2 %
Measurement wavelengths:	121.6nm 140.0nm 160.0nm 170.0nm 180.0nm 200.0nm 250.0nm

2.5.1 Optical Design

The OPM VUV instrument is a classical single beam (see Figure 2-19) spectrometer to measure specular reflectance and transmittance. A filter wheel monochrometer is used to select the desired measurement wavelength. As with all single beam spectrometers, a method must be provided to calibrate the detectors. For the OPM VUV instrument this was accomplished in two steps. At selected positions in the carousel, there were empty sample positions provided that served as calibration holes. When a calibration hole is in position, as shown in Figure 2-20 a and b, the transmittance detector views the full incident optical beam. This reading is the 100% reference reading for transmittance measurements. In order to calibrate the reflectance detector, the optical path is changed as shown in Figure 2-20c by rotating the 20 mm fold mirror and 20 mm spherical mirror. In this position, the reflectance detector directly views the full incident beam providing the 100% calibration signal.

A ruggedized deuterium lamp with a magnesium fluoride window provided the vacuum ultraviolet energy for the instrument. An off-axis ellipsoidal mirror focused the light energy through an eight-position filter wheel monochromator to a fold mirror, a collimating mirror, and to the test sample. The light was either reflected from or transmitted through the sample to identical detectors above and below the sample. At the filter wheel, seven narrow band pass UV filters selected the desired wavelength. One position in the filter wheel was a "hole" (i.e. no filter) used for end-to-end system calibration. A small stepper motor, controlled by the DACS, rotated the filter wheel for individual filter selection. The monochromatic beam was chopped using a 150Hz tuning fork light chopper to increase the signal-to-noise ratio. The fold mirror and collimating mirror were mounted to a rotator arm that rotated at pre-defined intervals for detector calibration.

The detectors were commercial Si photodiode detectors with the UV quartz window removed. A Lexan cylinder coated with Vacuum Deposited Aluminum (VDA) along its axial length ("light pipe") and sodium Salicylate coating of the exposed end converted the UV energy

could sense. The detector outputs were read by a phase-sensitive detection circuit and processed by the DACS.

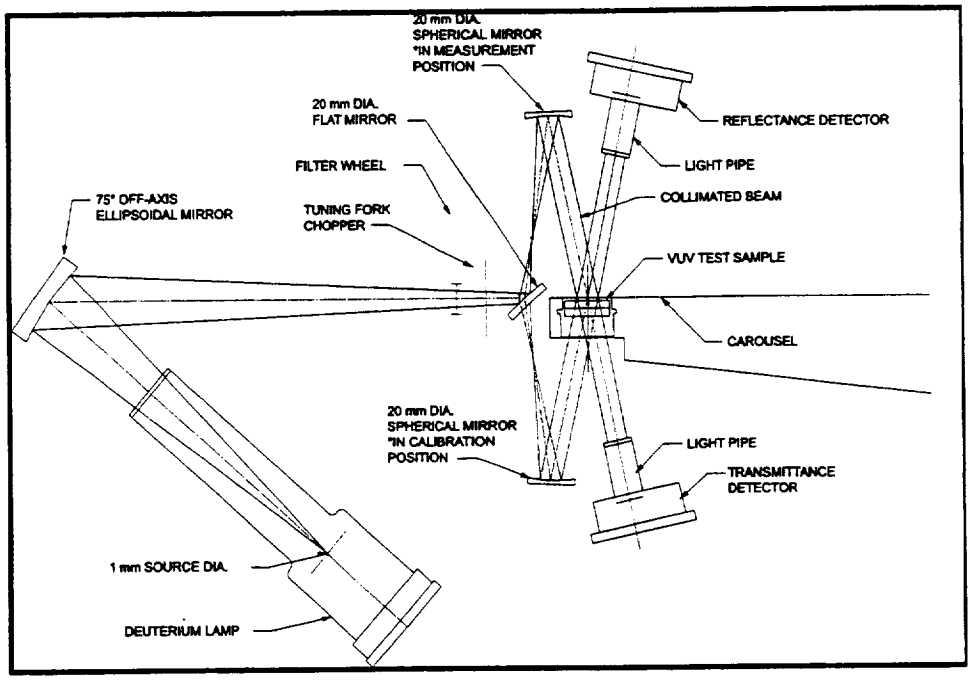

Figure 2-19. VUV Spectrometer Optical Schematic.

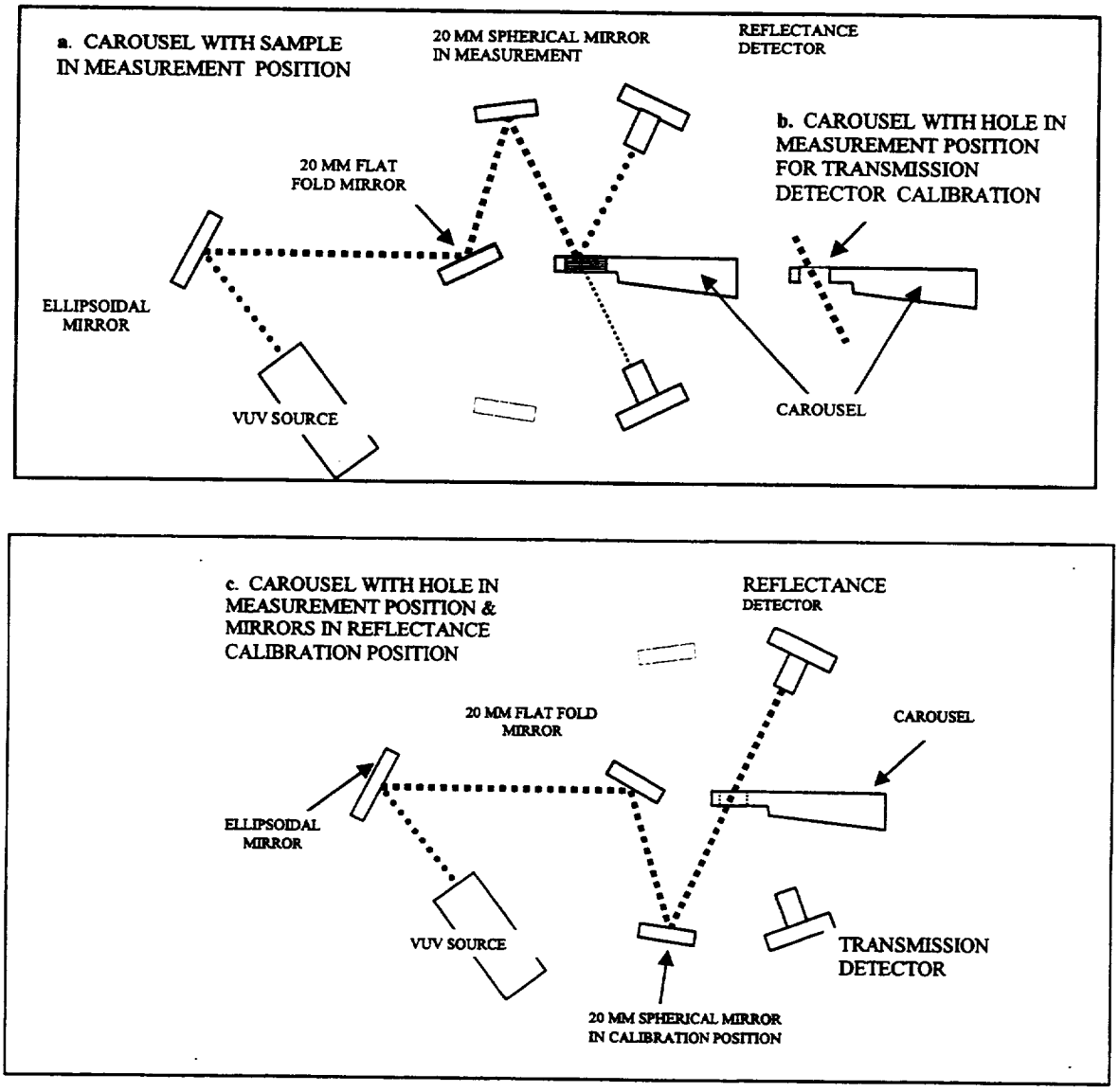

Figure 2-20. Operational Schematic of VUV Specular Reflectometer (not to scale)

The light source used for the VUV instrument was the V05 Deuterium Arc Lamp manufactured by Catheodeon, LTD. This lamp was an arc lamp complete with an anode, cathode, and heater. The heater heated up the cathode prior to the anode being struck. Once the cathode was heated, the anode required a high voltage strike to turn the lamp on. The lamp produced UV light in the wavelength range of 121.6 - 250.0nm.

A custom precision tuning fork chopper used in the instrument was manufactured by TFR Laboratories, Inc. The chopper ran at a frequency of 150Hz with Type S shutters for sine wave modulations. The shutters were coated with a non-reflecting optical flat black coating. The chopper chopped/shaped the light beam into a sinusoidal beam as it passed through a filter

assembly. The filter assembly consisted of a filter wheel with eight holes. Seven of the eight holes contained UV filters in the wavelengths of 121.6nm, 140nm, 160nm, 170nm, 180nm, 200nm, and 250nm. The eighth hole was a small aperture hole used for calibration.

The VUV instrument utilized two identical detector assemblies for the reflectance and transmission data collection. Each detector assembly consisted of a detector and a light pipe. Both detectors were HUV4000B silicon photodiodes manufactured by EG&G Optoelectronics, Canada. The detectors utilized an UV-enhanced PIN photodiode with an internal pre-amp. This detector is sensitive down to a wavelength 185nm but not to the required 121nm.

To extend the detector sensitivity to 121nm, each detector was fitted with a short light pipe that was coated with a fluorescing coating of sodium salicylate. This is a common technique in VUV spectroscopy to use a coating that will fluoresce when exposed to vacuum ultraviolet energy and re-emit energy in the visible wavelength band at approximately 500nm. This visible light can then be easily measured using a silicon detector. The short light pipe was also used to provide some light ray mixing for more uniform detector response. The light pipe was a custom cut cylinder of Lexan. All surfaces of the piece were polished to remove all scratches, burrs, and sharp edges. The exterior cylindrical face of the Lexan light pipe was coated with vacuum deposition aluminum. One end was coated with sodium salicylate. The other end of the Lexan piece was placed against the detector aperture.

2.5.2 Electrical Design

The VUV electronics system is shown in Figure 2-21 and is very similar to the reflectometer described in Section 2.3.2. The VUV instrument uses a chopped optical system and the same synchronous detection system used for the reflectometer.

Power for the deuterium lamp and stepper motors was provided from the PAC under DACS control.

The OPM DACS controlled all aspects of VUV operation. Small magnets and magnetic sensors provided positional feedback for operating the filter wheel and detector reversing rotor

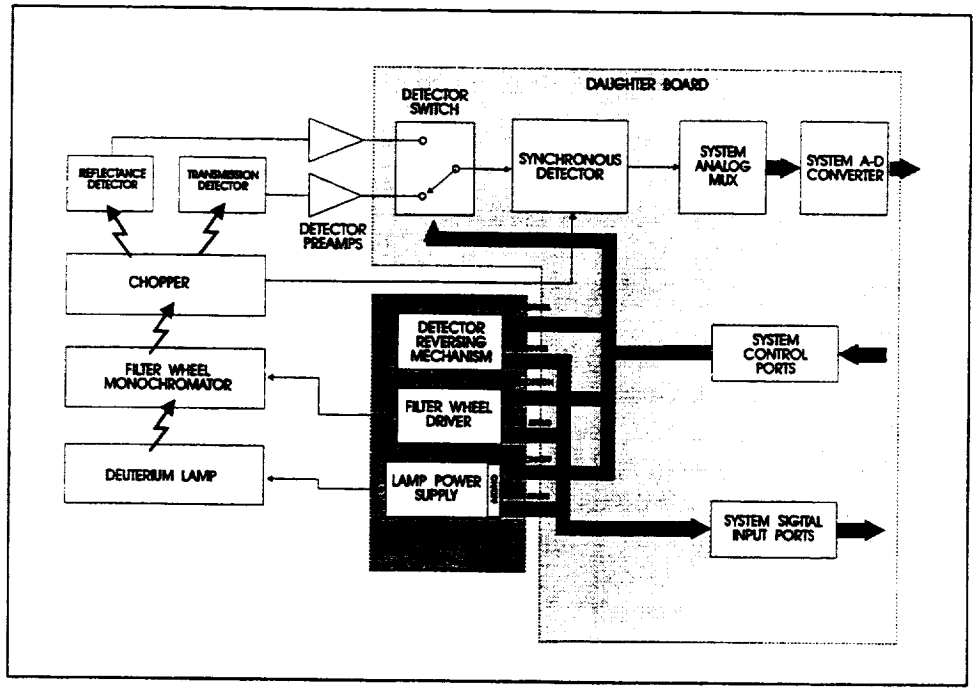

Figure 2-21. VUV Spectrometer Subsystem

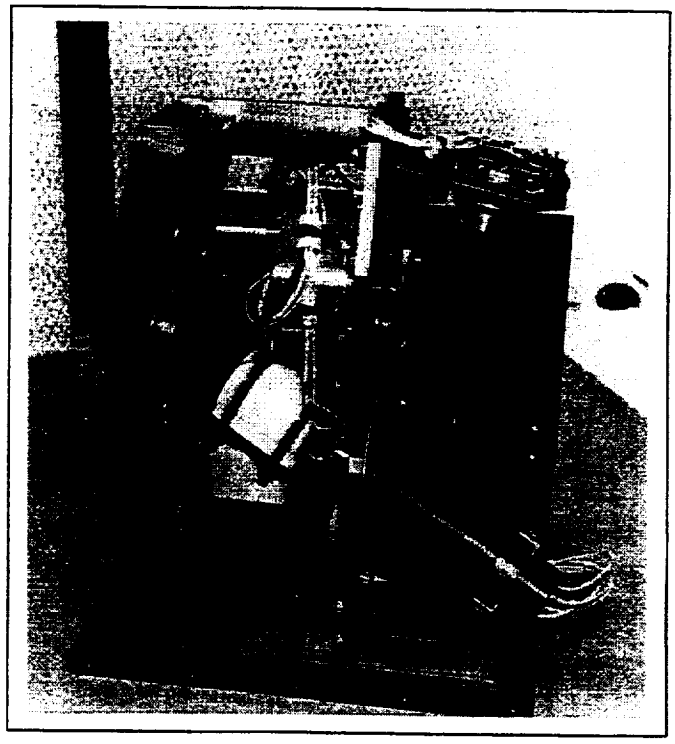

Figure 2-22. Assembled VUV Instrument

2.5.3 Mechanical Design

The mechanical design incorporated concepts to keep the optical path simple, minimize moving parts, and minimize volume. The VUV instrument was designed as an upright assembly that utilized a single light source with a simple optical path. This engineering design for the VUV instrument included support brackets, main support frame, mirror supports, rotator arm assembly, and a lamp holder assembly. Additionally, thermal analysis and structural stress analysis was performed on the design to ensure environment conditions could be met.

The VUV instrument was designed as an independent modular instrument. The VUV assembly design used its baseplate as the main support structure. The VUV assembly was mounted near the top of the OPM, and under the Top Cover. Its two detectors were placed on either side of the sample carousel (see Figures 2-19 and 2-22). The instrument was designed as a functional modular unit for easy removal and re-assembly in the OPM.

The use of the deuterium lamp required special attention in the mechanical design. A custom lamp holder had to be designed because the deuterium lamp was very fragile and it had to withstand the vibration and acoustics environment induced by the Shuttle launch. Likewise, the deuterium lamp holder was designed to protect and hold the lamp in the launch environment. The holder was made of Teflon material to protect the lamp. An electrical connector, made of Vespel, was custom designed to clamp to the electrodes protruding from the end of the lamp. When the lamp was struck, the lamp electrode differential voltage ranged from 600V to 900V. Vespel was selected because it could accommodate the lamp operating temperature and had a high dielectric voltage that accommodated the high voltage differential between the lamp electrodes.

The VUV instrument had two motors for the two movable assemblies: rotator arm assembly and the filter wheel assembly. The rotator arm assembly was designed to direct the light source to the top and bottom of the sample for calibration of the single beam system. For calibration of each detector, the rotator arm assembly would rotate up and down 180°. A custom Geneva drive system with a stepper motor drove the rotator arm assembly.

The filter wheel assembly was designed to hold seven different wavelength filters for the VUV instrument. The wheel had eight holes: seven holes for the filters, and one aperture hole for instrument calibration. A custom Geneva drive system with a stepper motor drove the filter wheel assembly.

The VUV dimensions were approximately 4.8-inches wide, 9.3-inches deep, and 10.1-inches high. The approximate weight of the VUV Assembly was 6.5 lbs.

2.5.4 Measurement Sequence

VUV was the second instrument operated during the weekly measurement run. During initialization processing, the instrument relays were enabled, a "zero offset" reading was made of the detectors, and the Deuterium lamp was struck and allowed to warm up/stabilize.

The carousel contained 41 positions for VUV measurements with calibration holes set at positions 0,5,10,15,20,25,30,35,40. Thirty-two samples were at all remaining positions. The VUV arm remained in the up/transmission position for sample readings. The VUV arm was moved up and down at each calibration hole to calibrate the detectors. Each sample was measured using seven filters plus a calibration hole on the rotating filter wheel. Two detectors, transmission and reflectance, recorded the reflected light. Detector readings and status data was stored for each of the test samples and calibration positions.

2.6 Temperature Controlled Quartz Crystal Microbalance Subsystem

The OPM Experiment used TQCM sensors to monitor the molecular contamination environment to which the flight test samples were exposed. There were two TQCM units used on the OPM. The purpose of a TQCM was to measure the mass deposition rate and total accumulation of contamination materials that deposited on its surface. The TQCM units used on OPM were designed and built by Faraday Laboratories in La Jolla, California. The measurement and control electronics were designed by AZ Technology.

The TQCM module consisted of a precision matched set of AT cut quartz crystals that operated at 15MHz. Their resonant frequency versus temperature is the parameter selected for matching. The crystals were 1.27cm in diameter and were optically polished. Inside the module were a temperature sensor (thermistor), a two stage Thermo-Electric Device (TED), crystal drive electronics and a Beat Frequency Oscillator (BFO). Output signal consists of the difference in frequency (beat frequency) between two identical oscillating circuits, each incorporating one of the crystals. Only one surface of one of the sensor crystals was exposed to the contamination flux. The mass loading, m, on the crystal will increase the output beat frequency. The beat frequency is directly proportional to the mass of contamination collected on the exposed crystal. This is a linear relationship, unless very thick deposits are accumulated.

$$m=1.56 \times 10^{-9}\ g/cm^2\ Hz$$

The thickness of the contamination deposit is calculated from the measured mass by assuming a density. The normal assumption for contamination is a density of "1." If the actual contamination can be identified, then a more accurate number can be used. When thickness is given is this report, a density of "1" was utilized.

The TQCM units were mounted in the OPM front corner adjacent to the flight samples. Indium foil was used to insure good thermal contact of the TQCM sensors to the OPM structure. The mounting bracket also insured the top of the TQCM sensor was in the same plane as the flight samples.

The TQCM sensors were controlled and monitored by the OPM DACS under software control. The TED was used in heating or cooling mode to control the temperature of the TQCM crystals. This allowed the TQCM to be driven to temperatures below ambient for contaminant collection. If the TQCM sensor became saturated, it could be driven hot (up to 100°C) to drive contaminants off the exposed crystal. The second order closed loop analog temperature control circuits for the TED was located in the OPM PAC. The controller was designed to maintain the TQCM temperature within 1°C for the full range of 100°C to -40°C. The control circuits for the

TQCM sensors were set to maintain sensor temperatures of -10°C and -30°C throughout the OPM mission to Mir.

The frequency measurement circuitry in the DACS had a resolution of 1/2Hz from 1Hz to about 20KHz. The TQCM software drivers were used to monitor TQCM beat frequencies and set TQCM operating temperatures. Each TQCM beat frequency was measured and recorded once every minute. Each TQCM operating temperature was checked and, if necessary, adjusted once every minute. If a TQCM beat frequency reached levels greater than 30KHz, the TQCM software drove the sensor into bakeout mode. In this mode, the sensor temperature would rise to 80°C for 1 hour in order to drive volatile contamination off of the exposed crystal's surface.

2.7 Irradiance Monitor Subsystem

The OPM irradiance monitor was designed to measure incident energy from the sun, earth Albedo, and earth IR emission. It was also to provide a measure of the exposure time of the flight samples to the direct solar environment.

Two radiometers were used for irradiance measurements: one for the combined direct solar incidence and earth Albedo, and the second for earth-emitted energy (infrared). The design was a simple one using standard detectors and optics. The spectral range of the three energy sources (direct solar, earth Albedo, and earth emitted IR) overlap, and, therefore, could not simply be separately measured by the radiometers. The radiometer with the quartz lens was designed to see mainly the direct solar and earth Albedo. The radiometer with the germanium optics was designed to see mainly the earth emitted IR. By knowing the OPM mission attitude, the direct solar, earth Albedo, and earth-emitted energy could be calculated from these two radiometers.

The radiometers for this experiment (reference Figures 2-23 and 2-24) consisted of thermopile detectors (a multiple-junction thermocouple) painted flat black covered with optics that selectively passed the external energy flux. Multiple junctions increased the sensitivity of the detector to the incident energy flux and gave a greater voltage output. Thermistors internal to the detector were used to monitor the detector thermal response. Baffles mounted over the lenses tailored the FOV of the radiometers to be close to the same as for the flight test samples. The lens material was selected to tailor the spectral response of the radiometer. For the solar spectral region of 0.2 to 3 microns, a quartz lens was used. A germanium lens was used for the infrared spectrum (between 2 and 20 microns). The irradiance monitor accuracy at near normal angles of incidence was not significantly degraded because of errors in attitude data. However, due to the near cosine response of the radiometer, the "system" accuracy approached five percent for low angles of incidence. The radiometer performance criteria are listed in Table 2-4.

Table 2-4. Radiometer Performance Criteria

	Solar Radiometer	Infrared Radiometer
Spectral Range	200nm - 3,000nm	2,000nm - 20,000nm
Optical Window	Quartz	Germanium
Accuracy	5%	5%
FOV	150°	150°
See Figure	2.7-1	2.7-2

The radiometers were mounted on the OPM sample carousel, as shown in Figures 2-1 and 2-2 OPM Assembly, and flush with the carousel top plane to enable the carousel to rotate inside the OPM. The radiometers were placed into a pilot hole in the carousel, pinned by a dowel, and bolted to the carousel. The lens was mechanically clamped to the radiometer housing to comply with the "frangible" material safety issues of the Safety Panels

Each of the two radiometers had a pre-amp on the carousel sub-multiplexer board for signal conditioning prior to routing through the OPM cable harness to the DACS. The radiometers were read once per minute during monitoring mode by the DACS under software control.

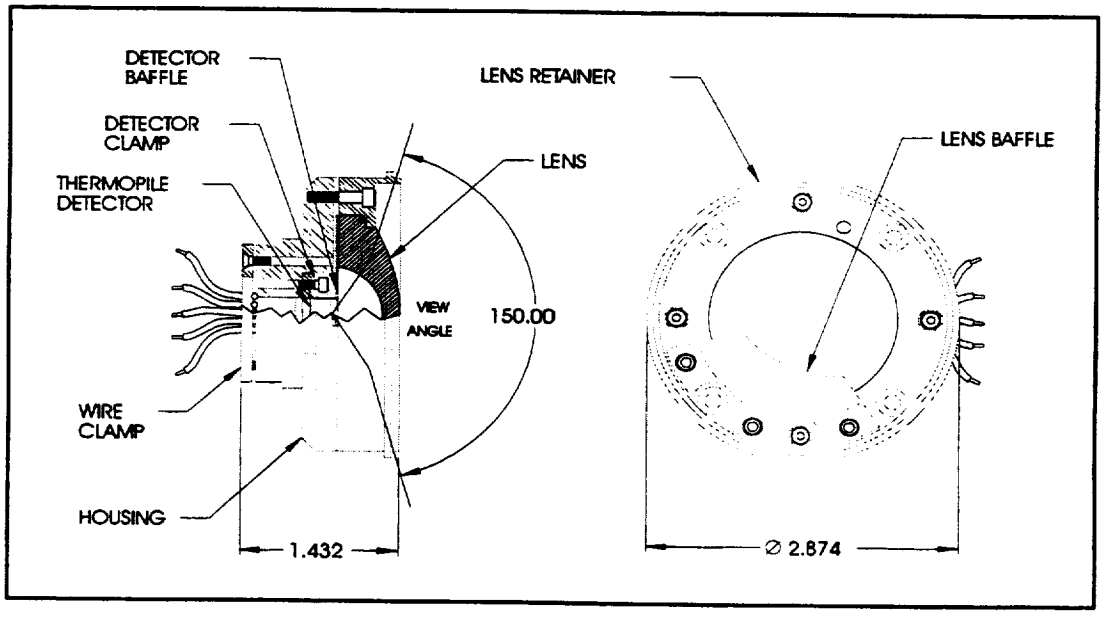

Figure 2-23. Solar Radiometer.

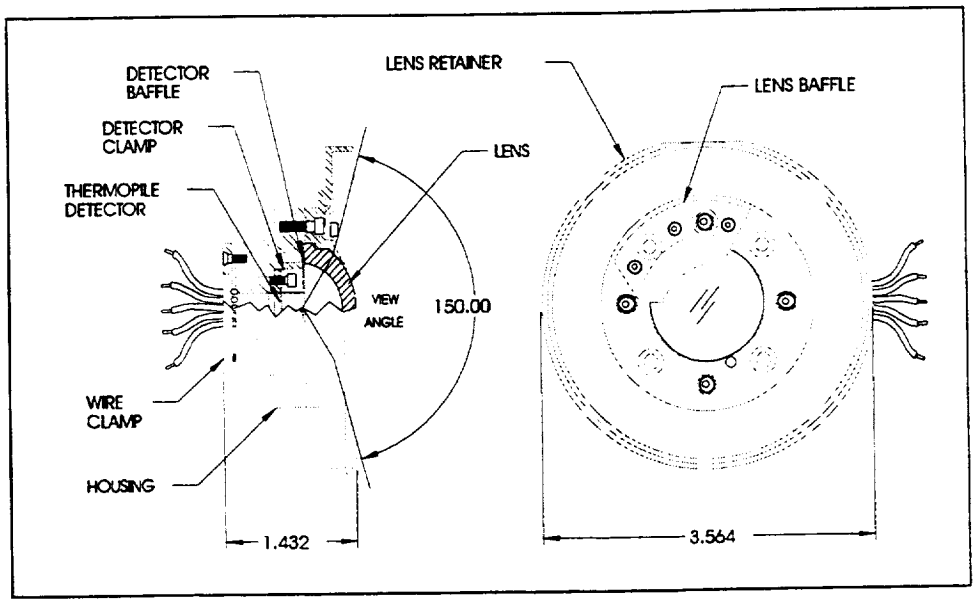

Figure 2-24. Earth IR Radiometer.

2.7.1. Radiometer Calibration

Both OPM radiometers were calibrated using equipment and laboratory facilities of the U.S. Army Radiation Standards and Dosimetry Laboratory at Redstone Arsenal. The radiometer electrical output produced by a known source of total irradiance was recorded for each unit under test. A standard 1,000 watt quartz-halogen Tungsten lamp was used as the calibrated source for the solar radiometer. A laboratory blackbody operating at 600° Kelvin was used as the source for the IR radiometer calibration. Because of the extremely wide FOV associated with the radiometers, calibration using an extended source large enough to completely fill the FOV was considered to be impractical, although this was the preferred method for achieving direct calibration. Alternatively, the radiometer response to a small source was determined for all incidence angles up to and including the maximum field angle to determine any departure of the radiometer response from that of an ideal cosine receiver.

The radiometers were mounted on a rotary stage that permitted adjustment of the incident angle by rotating the radiometer with respect to the source. Angular response was determined for field angles of -100 to +100° at 5° intervals in both x and y axes. In order to establish repeatability of the measurements, three runs were made for each setup. The results were averaged to determine the calibration factors. Additional information regarding the radiometer calibration may be found in the *Radiometer Calibration Test Report, AZ Technology Report No. 91-1-118-142.*

2.8 Atomic Oxygen Monitor Subsystem

The effects of AO are one of the primary concerns for materials operating in the LEO space environment. To characterize the effect of AO exposure on materials, the total exposure or fluence and the time history of the exposure must be determined. To provide this required flexibility, the OPM AO monitor was designed to be sensitive enough to measure low AO flux

levels where sensitive materials begin to exhibit changes. It must also provide a wide dynamic range for long duration OPM missions.

At the lower LEO altitudes (about 300km) where the Shuttle normally operates, the fluence rate is 10^{13} to 10^{16} atoms/cm^2/sec depending on the solar activity. The total fluence on typical Shuttle missions ranges from 6.5×10^{19} to 3.5×10^{20} atoms/cm^2.

At the higher altitudes (up to 500km) where the Space Station will operate, the fluence rate is significantly lower in the 10^{12} to 10^{14} atoms/cm^2/sec range, for a total fluence per year of 10^{19} to 10^{21} atoms/cm^2.

Given the wide range of potential AO fluence rates and the AO sensitivity of different materials, the OPM AO monitor sensitivity needed to be less than 10^{18} atoms/cm^2/sec and provide a wide dynamic range.

The OPM AO monitor consisted of four carbon film sensors which were exposed sequentially to provide the needed sensitivity and wide dynamic range. The AO sensor used a carbon film as the active element for detecting AO. The carbon sensor was exposed to the AO environment and was eroded away by the reaction of carbon with AO. The resistivity of the carbon element was measured by the OPM system to determine the erosion rate of the element. Combining this rate with AO Reaction Efficiency (RE) for carbon, the total fluence of the exposure was determined. Carbon was chosen as the sensor material because it has zero order reaction kinetics with AO with the resultant products leaving the surface. It was also electrically conductive for ease of measurement. The AO sensors for the OPM were built by Dr. John Gregory of the University of Alabama in Huntsville (UAH). The RE for carbon has been measured at 1.2×10^{-24} cm^3/atom, and to lie in the range of 0.9 to 1.7×10^{-24} cm^3/atom depending on the temperature and form of the carbon. The thickness and dimensions of the carbon film can be selected for each mission to accommodate the expected total fluence. Using multiple sensors in the AO monitor, the full fluence can be accommodated even with the failure of one sensor

The AO sensor is shown in Figure 2-25. It used two carbon film elements. One of the elements was overcoated with a protective coating of Sodium Silicate ($NaSiO_4$) to prevent it from eroding and to account for temperature effects in the resistivity measurements of the sensor. The other element was left exposed to the AO environment. The resistance of each element and the temperature of the substrate were recorded by the OPM data system.

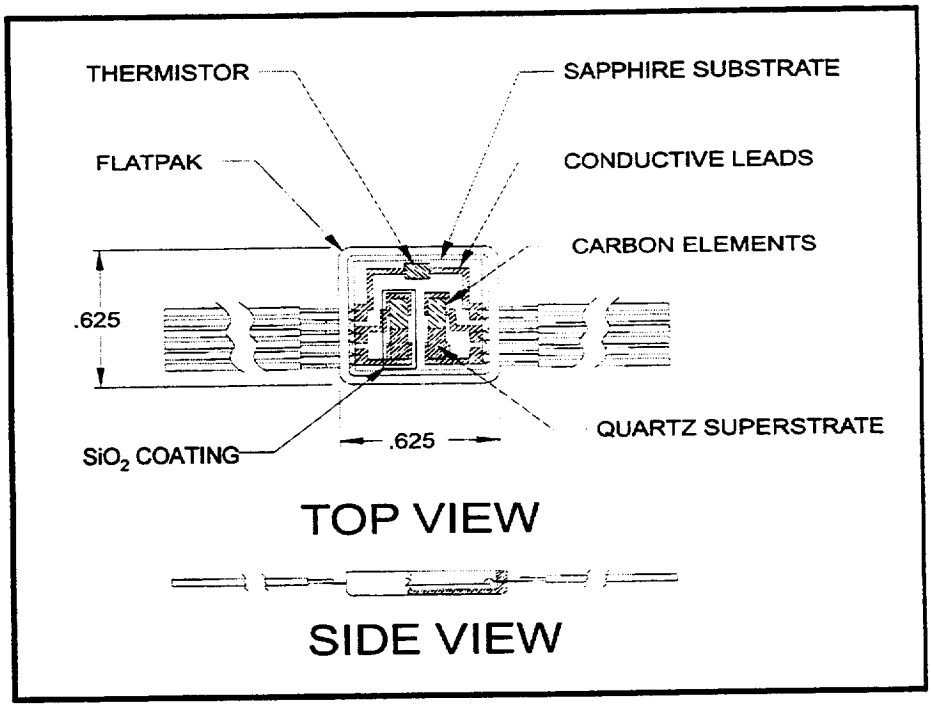

Figure 2-25. AO Sensor Assembly

The AO monitor assembly is shown in Figure 2-26 and consists of four AO sensors mounted on a common sensor plate assembly, and a stepper motor driven cover that exposed one sensor at a time. The sensor plate assembly, as shown in Figure 2-27, placed the four sensors and one "blank" position in a circular pattern. The cover plate fit tightly over the sensor plate and exposed one of the positions at a time. During ground processing and launch, all sensors were protected by the AO cover plate and the "blank" sensor position was exposed. During the OPM initialization, the AO cover plate was rotated to expose the first sensor. When the resistance of an element rose above a preset value, the next sensor was to be moved into position. A measurement multiplexer board was also fastened onto the AO Monitor. This multiplexer interfaced the AO sensors and other sensors inside OPM to the DACS for measurement and control. The AO monitor was mounted in the OPM front corner (opposite the TQCMs) adjacent to the flight samples to monitor the AO fluence incident on the test samples.

The OPM DACS controlled the operation of the AO Monitor and measured sensor resistance and temperature. Resistance measurement was performed using a dual multiplexer design, which allowed 4-wire Kelvin measurements. The four wire measurement minimized errors due to resistance losses in wiring to the AO sensors. The AO cover plate was rotated by a stepper motor under software control. Magnetic sensors and small magnets on the mechanism provided position feedback to the DACS to aid in the positioning sequence.

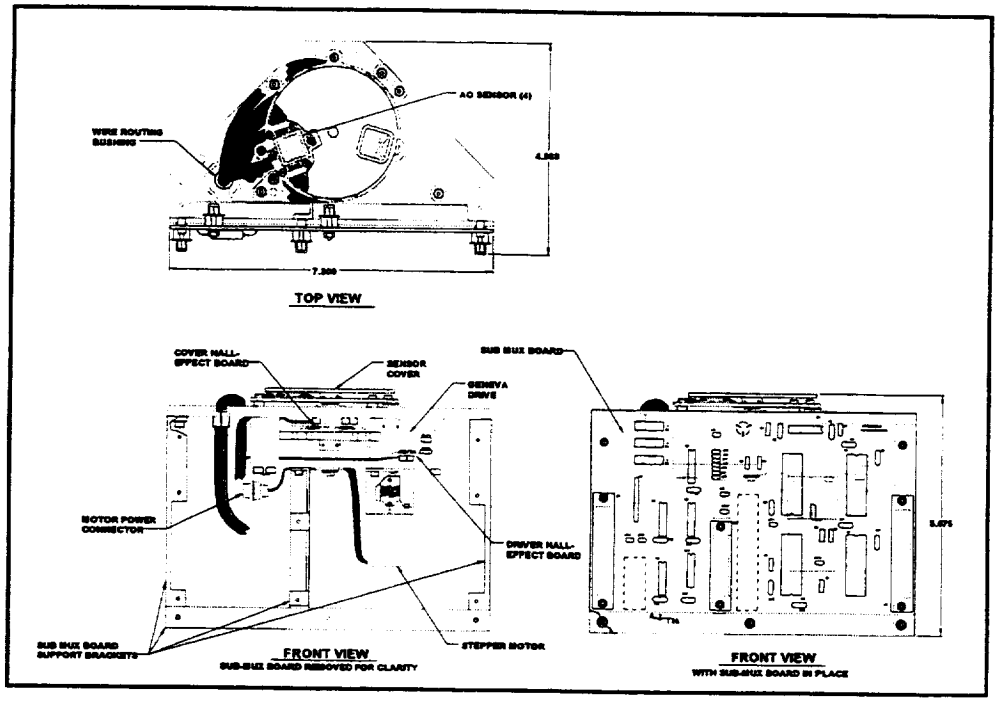

Figure 2-26. AO Monitor Assembly

The software for the AO monitor provided great flexibility in when and how the AO sensors were exposed and for how long. For the OPM mission on Mir, the expected attitude was to be stabilized with respect to the velocity vector (and AO flux) for the majority of the time. For the location of OPM on Mir, this would have resulted in an extremely large fluence of AO on the AO sensors. This fluence level would have eroded away all four of the AO sensors prior to the end of the mission. To avoid this problem, the AO sensors were only exposed for 2-hours per every 24-hour day. This process would extend the life of the AO sensors for the complete mission. While exposed, AO sensor and temperature data were taken at a rate of once per minute. As will be seen in the later mission discussions, the Mir attitudes were rarely velocity vector stabile. Mir was almost always in a solar inertial attitude to maximize solar array power. These attitudes resulted in a small fluence. Mission flight attitude and environment are discussed in Section 3.

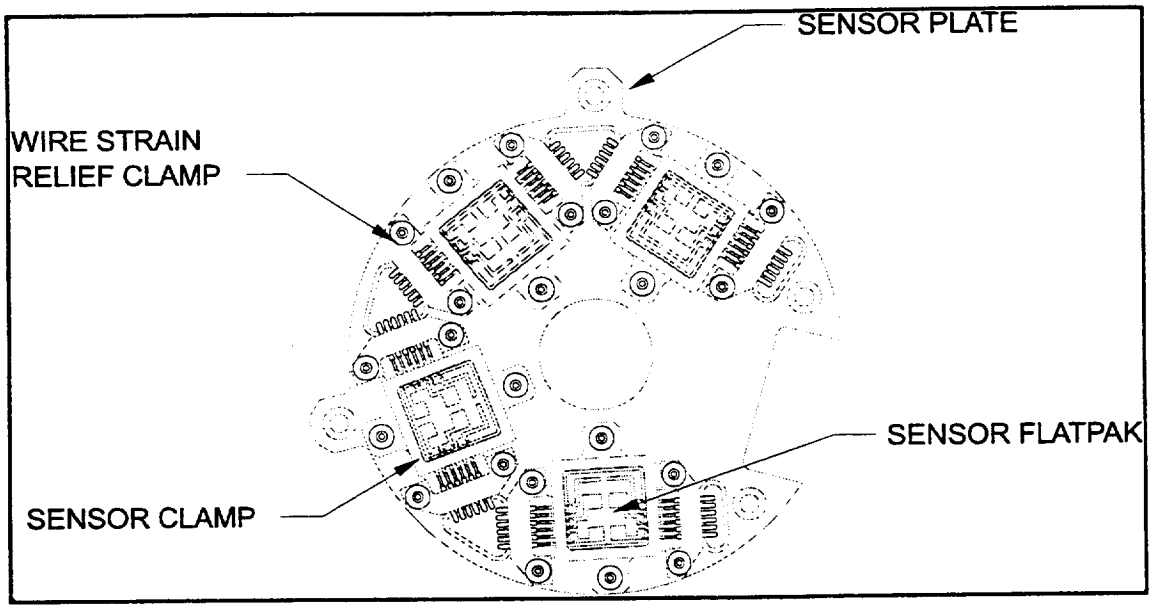

Figure 2-27. AO Sensor Plate Assembly

3.0 OPM/MIR MISSION

The OPM mission to Mir was a complex mission that combined both manned IVA and EVA operations. During this mission there were several events that affected the OPM deployment and operation. The OPM mission and these events will be described in the next section followed by a discussion of the OPM/Mir mission environment. In Section 3.3 the performance of the OPM systems and instruments will be discussed.

3.1 Mission Overview

The OPM was transported to the Mir space station, inside the SpaceHab module on the Space Shuttle mission STS-81 in January 1997. During this mission, OPM was transferred via internal vehicle activity (IVA) into the Mir and was tethered to the wall inside Mir. The OPM was to have been deployed on the outside of Mir soon after the end of the Shuttle mission. Due to other activities on Mir, the deployment of OPM was delayed until the end of April 1997. During the storage period in Mir, there was a fire (February 23, 1997) that caused considerable difficulty for the crew and the environmental system. There was significant water condensation reported inside the Mir. Post-flight inspections of the OPM showed signs of this condensation on the internal OPM surfaces.

The OPM was deployed on the exterior of the Mir Docking Module (DM) by a joint US/Russian EVA and activated on April 29, 1997. The OPM was mounted on the exterior of the DM as shown in Figure 3-1. Figures 3-2 and 3-3 are photos of the mounting location of OPM on the DM. This site and orientation was chosen because it was one of two available mounting locations, it provided a view of the Mir core and other modules, and also a good exposure to the natural space environment. The OPM was mounted on the Mir Space Station with customized interface hardware. The Russians supplied a latch that mechanically interfaced to standard interfaces used on the Mir exterior modules.

Within one hour of power up, the OPM initiated its first measurement sequence and then operated continuously except during several Mir power outages from activation at deployment until just before retrieval. When the OPM received power, the OPM ran autonomously performing environmental monitoring and weekly optical properties measurements. Data were stored internally inside the OPM and periodically dumped by the crew using the Mir Interface to Payload System (MIPS). The MIPS allowed the data to be down-linked to the ground through Russian ground stations. A high priority subset of the collected data was also archived in the OPM DACS in case the data was not recovered from the telemetry process.

OPM operated until January 8, 1998 except for a period of time from June 25, 1997 to approximately September 9, 1997 where the power was off due to the Progress accident. Even after power was restored, there were a number of other power outages in the days following power restoration. The OPM was retrieved from the Docking Module on January 9, 1998 Moscow Time (MT) by Russian EVA and returned to ground on STS-89 later that month. The OPM was returned to the AZ Technology laboratories for post-flight analyses.

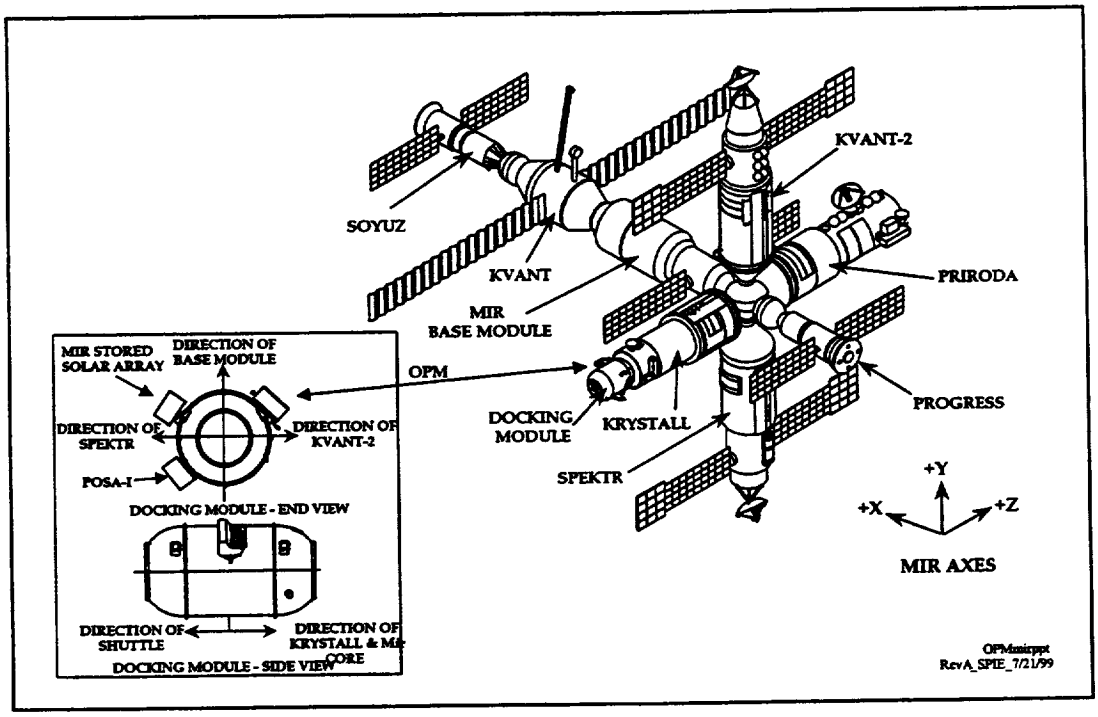

Figure 3-1. OPM Mounted on the Mir Docking Module.

Figure 3-2. OPM Mounted on the Docking Module.

Figure 3-3. Close-up of OPM on Mir.

3.2 OPM/Mir Environment

The natural space environmental constituents of concern for the OPM mission on Mir and for the ISS are the solar irradiance and the residual atmospheric atomic oxygen. The exposure condition of any surface on a spacecraft is dependent on the orbit and the attitude of the vehicle and the time integrated value of this exposure. Transient spacecraft maneuvers are not of significant importance unless the new attitude results in a significant change in the thermal environment that could cause increased molecular contamination accumulation or thermally induced artificial aging. This situation is true for the OPM mission on Mir.

To address the need to understand the OPM exposure environment, the actual Mir attitudes were analyzed and translated to the OPM coordinate system by the Russian Space Company Energia (RSC-E) and the Russian Space Agency (RSA)[15]. The elevation and azimuth data were provided at one-minute intervals for both the solar vector and the velocity vector relative to the OPM test samples (See Figure 3-4). The detailed attitude data were analyzed to determine the exposure levels of the OPM samples and surfaces for both solar and AO exposure. Table 3-1 shows the integrated solar and atomic oxygen exposure by month for the OPM samples and for the four other sides (as defined in Figure 3-4) of OPM.

Some general observations can be made from the OPM/Mir attitude data. Figure 3-5 shows the solar elevation and azimuth to the OPM sample array for May 1997 which is representative of the OPM mission except for the two months following the Progress accident on June 26, 1997. The preferred attitude for the Mir during the OPM mission was solar inertial with the sun off the left end of the OPM and slightly below the plane of the sample array most of the

time. This results in a very small direct solar exposure for May 1997 of only 37 equivalent sun hours (ESH) for the samples. Conversely, the left end of OPM saw over 400 ESH for this same time period. There were operational attitude changes performed periodically but were usually short followed by a return to the preferred attitude.

For the couple of months following the Progress accident, the attitude was still solar inertial most of the time but the attitude was somewhat different with the sample array seeing much more solar exposure. Figure 3-6 shows the solar attitude data for July 1997, the month following the accident. The integrated exposure data in Table 3-1 indicates that, in September 1997, the Mir returned to the preferred flight attitudes that were observed before the Progress accident.

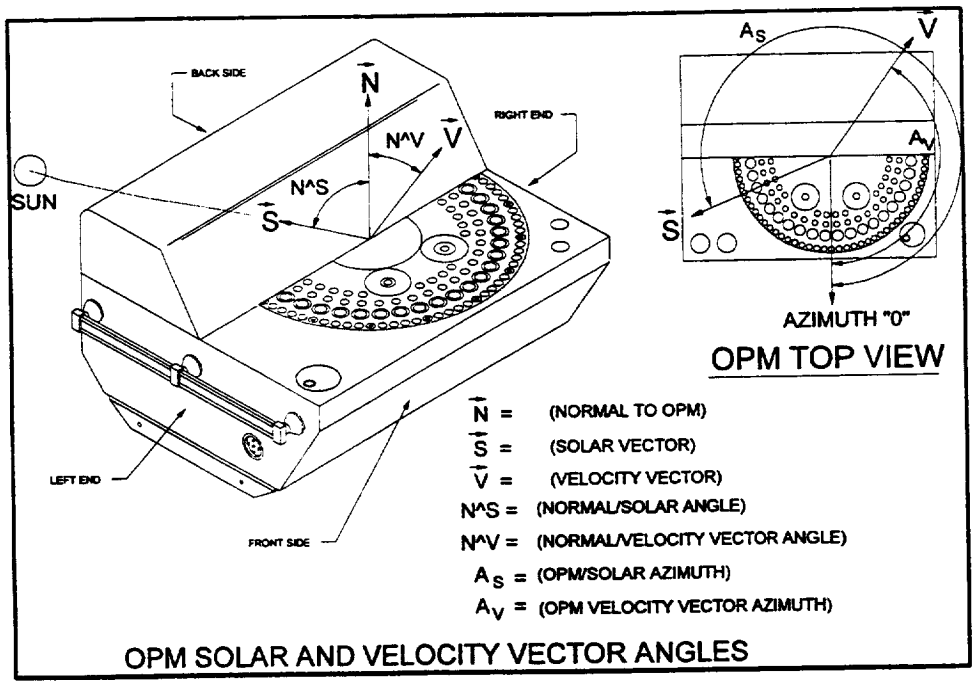

Figure 3-4. OPM Attitude Data Coordinate System.

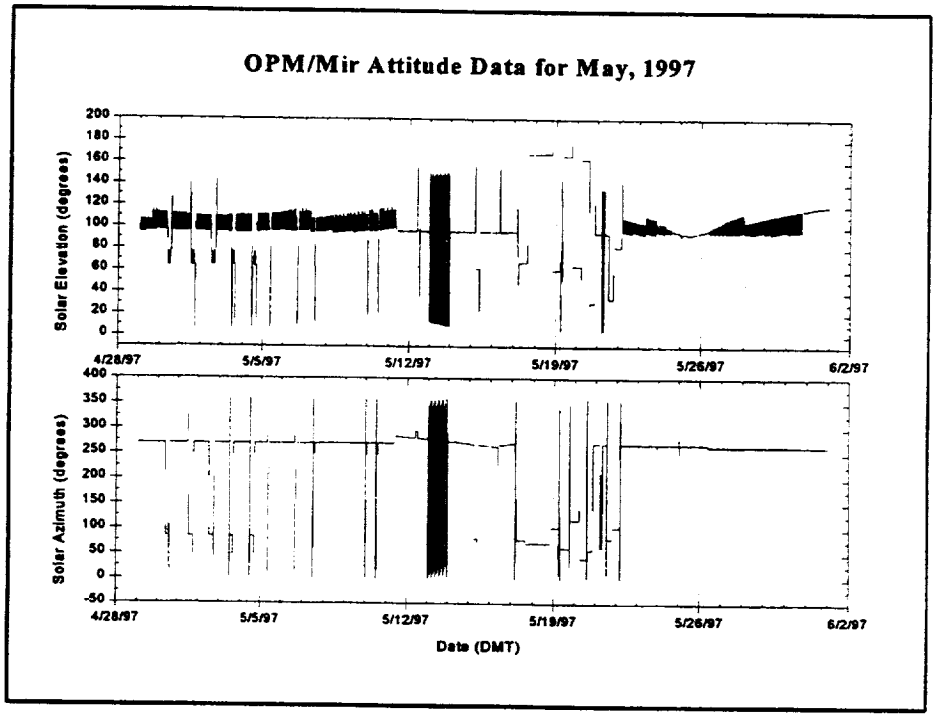

Figure 3-5. May 1997 Solar Elevation and Azimuth for the OPM Sample Array

Table 3-1. OPM Solar and AO Exposure by Month

Month	Direct solar exposure (ESH)					AO fluence(atoms/cm2)				
	OPM Samples	Left end	Front side	Right end	Back side	OPM Samples	Left end	Front side	Right end	Back side
May, 1997	37	403	20	59	20	9.3E+19	9.4E+19	1.0E+20	1.0E+20	1.0E+20
June, 1997	73	366	8	56	24	8.4E+19	8.8E+19	8.5E+19	9.0E+19	8.3E+19
July, 1997	353	164	12	68	12	8.9E+19	9.2E+19	9.9E+19	9.4E+19	9.9E+19
August, 1997	224	256	18	48	23	8.8E+19	8.4E+19	1.0E+20	8.5E+19	1.0E+20
September, 1997	13	394	13	22	17	9.0E+19	9.2E+19	6.8E+19	9.3E+19	6.9E+19
October, 1997	26	443	19	16	27	9.6E+19	9.7E+19	7.8E+19	9.6E+19	8.0E+19
November, 1997	62	345	24	38	12	8.9E+19	8.8E+19	6.9E+19	9.0E+19	7.1E+19
December, 1997	39	427	26	65	12	9.5E+19	9.5E+19	8.9E+19	9.6E+19	8.4E+19
January, 1998	5	105	1	6	5	1.9E+19	1.8E+19	2.7E+19	1.8E+19	2.7E+19
Mission total	832	2903	141	379	152	7.4E+20	7.5E+20	7.2E+20	7.6E+20	7.2E+20

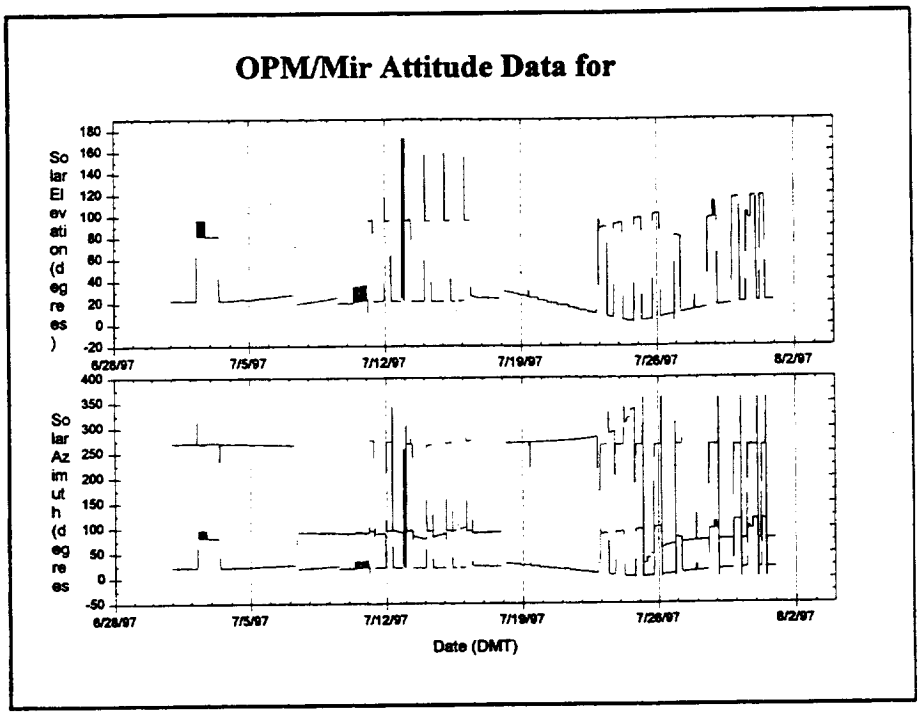

Figure 3-6. July 1997 Solar Elevation and Azimuth for the OPM Sample Array

3.3 OPM Performance

The OPM systems and instruments overall worked extremely well for the difficult mission to Mir. The OPM is a very complex space experiment that was exposed to the internal and external space environment and several off-nominal events. In this section, the performance of the OPM instruments, monitors, and support systems will be discussed. There were a few anomalies that occurred during the mission. These overall anomalies will be discussed here along with their effect on OPM mission science. More detail on the OPM systems and the anomalies can be found in the *OPM Systems Report, AZ Technology Report No. 91-1-118-164.* The performance of the OPM instruments and monitors will be discussed in Section 4.

Most OPM instruments and subsystems performed extremely well over the Mir mission providing unique data on the behavior of materials in the Mir environment. The reflectometer and the TIS optical instruments performed extremely well over the difficult mission. There was only one anomaly that had a significant effect on mission data. This anomaly was on the VUV instrument that prevented any in-space VUV optical measurements. The other anomalies were the failure of the reflectometer tungsten lamp at the end of the mission and solar radiometer detector.

The support systems performed very well and as designed. There were no anomalies in these systems. There are a few general observations that can be made about the OPM system:

- The OPM performed well in the space environment, and withstood unexpected conditions;
- The OPM returned intact. There were no frangible material (broken glass) issues. The external surfaces had some obvious "wear," but had not broken;
- There were no signs of "self-contamination." The OPM was a "clean" payload;
- The software control program maintained good control over the autonomous OPM operation;
- The data storage memory in the DACS survived with only a few "upsets" that were easily corrected in post-flight data reduction;
- The operational memory in the DACS did see a few single bit errors. This memory was protected with single bit error detection and correction (EDAC) and periodic memory scrubbing that resulted in no anomalous operations of the data system;
- Thermal margins were adequate. Station attitude went to full sun twice during the mission, creating over temperature conditions, but core systems remained operational;
- OPM was unpowered for two and one-half months while OPM was deployed in the space environment; but the OPM systems still powered up successfully and completed the mission.

The most significant unexpected event affecting OPM operation was the Progress collision with the Spectr module in late June 1997. This resulted in the loss of power to OPM for over two months. There was concern that OPM may have gotten too cold and would not operate properly if power was restored. Analysis showed that, while OPM was very cold, it would start up and work properly. The system did turn on and operate but did suffer two minor additional problems after power was restored. These were:

- The VUV filter wheel rotation was intermittent after power restoration. The filter wheel began "sticking" on the tenth timeline, the first measurement timeline after the two and one-half month powered down period. The filter wheel had intermittent problems rotating on approximately half of the subsequent timelines and during post-flight testing.
- The carousel motor did not find the proper start position on six of sixteen timelines after power restoration. Of those six timelines, four started with the motor temperature below 0°C. On two of those six timelines, the carousel position self-corrected during the timelines and successfully completed the measurement set. This condition has not reoccurred in post-flight testing.

The major anomalies encountered during the mission are discussed in the following Sections.

3.3.1 VUV Lamp Anomaly

The deuterium lamp in the VUV spectrometer did not function during the OPM mission on Mir. While the other parts of the VUV and OPM system did function, no valid VUV

lamp was functional during the last pre-flight tests at KSC before the OPM was integrated into the SpaceHab for launch. The lamp did not function when operated in the first on-orbit measurement cycle. Post flight investigations by the lamp manufacturer found a leak at the glass-to-metal seal on the electrical pin/s at the lamp base. This damage could have occurred either prior to launch or during launch from the induced launch vibration loading on the pins and socket. The lamp drive electronics were verified to be operating properly during post-flight testing. A replacement lamp was plugged into the lamp socket and powered up with no problem.

3.3.2 Reflectometer Tungsten Lamp Anomaly

During the last measurement sequence (Timeline 27) made on Mir, and prior to the retrieval of OPM, the tungsten lamp failed approximately half-way through the reflectometer measurement set. This was the only anomaly for the reflectometer. Post-flight microscopic inspection revealed the lamp filament had broken. The probable cause of failure was the bulb reached its end-of-life due to pre-flight testing. No problems were identified with the lamp drive electronics. When the lamp was replaced, the reflectometer was able to perform again within specifications.

3.3.4 Solar Radiometer Anomaly

The solar radiometer failed in June 1997 during a period that the Mir was in a full-sun orbit. Periodically, the high inclination Mir orbit will precess to where the Mir never goes into the earth's shadow. At these times the Mir surfaces become very hot. The radiometers had a large view factor of these hot Mir surfaces, a direct view of the sun and Mir reflected sunlight. The solar radiometer was designed to tolerate full sun exposure but not to the additional energy in this full sun orbit. Data were recorded from this radiometer, but it was not valid.

The solar radiometer anomaly was investigated once the OPM was returned to ground. The analysis revealed that the thermopile detector was "open." A spare detector was attached to the OPM cable harness and the OPM DACS was able to record valid data.

The infrared radiometer had a germanium window over the thermopile that did not transmit much of the solar energy. The infrared radiometer performed without any anomalies.

4.0 DATA AND ANALYSIS

4.1 Reflectometer Data

One of the major objectives for the OPM experiment flown on the Mir space station was to measure the optical effects of the space environmental exposure on a series of spacecraft external materials. This section will discuss the data and findings for samples measured by the reflectometer subsystem. All of the samples measured by the reflectometer were applied to calorimeters and are mostly thermal control type coatings. There were 20 samples flown on the OPM that were measured by the reflectometer. Table 4-1 summarizes the performance of these samples on the OPM mission. The solar absorptance readings are calculated from the OPM reflectometer spectral data. The emittance data in this table was measured pre- and post-flight with an AZ Technology TEMP 2000.

An Optical Solar Reflector (OSR) sample was included on the OPM carousel for measurement by the reflectometer instrument. The purpose of flying the OSR was to let it serve as an in-flight measurement control sample. The OSR sample is a thin second surface fused silica/silver mirror mounted on the aluminum substrate sample disk of the calorimeter, refer to Section 2.2. OSR's have been shown to be very stable in the natural space environment. Any reflectance change detected on the OSR would be attributed to either spacecraft contamination or instrument error/malfunction. Figure 4-1 shows the measured spectra for the OSR flown on the OPM. As can be seen in the graph, the sample was essentially unchanged in-flight and during post-flight measurements. There may be a slight (<1%) change in reflectance at the knee of the absorption band at about 400 nm, but this is within the accuracy of the instrument or could be the result of the very thin ~100 to 180 Angstroms of contamination (see Section 4.1.4 on the TQCM data and Section 4.3 on the post flight material analysis). The OSR data demonstrates that the reflectometer operated extremely well and within specifications for the OPM mission. In addition, it says that there were no significant optical effects caused by contamination that were measured by the reflectometer. The OSR establishes confidence in the data for the other samples that did show changes throughout the mission which were dependent upon the changing space environmental exposure conditions. In other words the changes detected and measured by the OPM reflectometer subsystem are real changes and not instrumentation errors.

A listing of all of the OPM samples is provided in Appendix A, giving the carousel position number of each sample, a brief description, the supplier, and the main technical contact. The minimum and maximum temperatures recorded for each of the 20 calorimeter samples is listed in Appendix B. In addition minimum and maximum values for the measured solar absorptance are also shown in Appendix B. Spectral data for all 20 calorimeter samples is presented in a series of plots in Appendix C. Pre-flight, selected in-flight, and post-flight measurements are shown. Not all of the flight data is shown since it would be hard to distinguish between the different scans when plotted on the same chart.

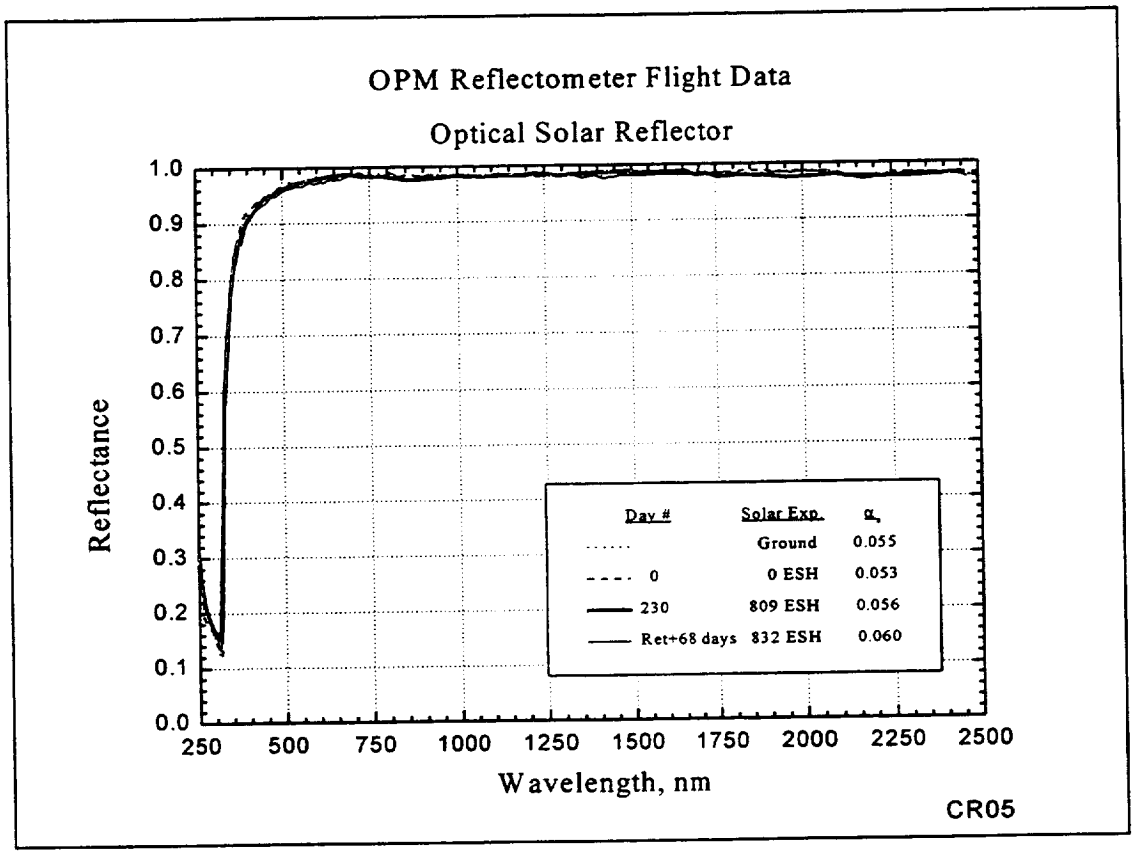

Figure 4-1 Optical Solar Reflector

The performance of the flight samples including post-flight measurements with time can be seen from the data in Appendix D, where the calculated solar absorptance is plotted versus exposure time on orbit and versus the solar exposure in ESH. The reason for including both plots is that damage sensitivity of material is dependent upon either solar ultraviolet radiation or on orbit atomic oxygen and in some cases a combination of the two. The atomic oxygen flux was on a daily basis fairly constant throughout the mission, so a plot of optical properties versus calendar days or atomic oxygen fluence is equivalent. This is not the case for the solar ultraviolet radiation. Orientation of OPM on Mir (see Section 3) resulted in very low levels of incident solar flux during most of the mission except for the approximately two months period after the Progress docking accident in late June 1997. This is shown in Appendix E in a plot of solar exposure (in ESH) versus actual dates (in Decreed Moscow time (DMT)). During the period from late June 1997 until early September 1997, OPM samples saw the largest increase in accumulated solar flux. This imposed a non-linear exposure between time and solar ultraviolet radiation. The data is presented both formats which helps in determining whether solar ultraviolet radiation or atomic oxygen is the dominate environment for a particular material.

As can be seen in Table 4-1 and Appendix C, many of the test materials such as Z93 white paint were very stable for the OPM missions while others changed significantly. Notice that for many samples there was significant bleaching of the in-space degradation from the final measurements to the final post-flight measurements in air. This bleaching effect is common to

many spacecraft materials.[1-3] The bleaching effects and the need for the true history of any materials degradation including environmental parameters are the major reasons to perform in-situ space experiments. In addition to these two variables of exposure, solar UV and AO, the TQCM has shown how the induced environment (mainly contamination) is event driven. All of these effects clearly demonstrate the absolute necessity of in-space measurements to accurately determine the level of damage, when it occurred, what caused the damage and to predict when and if replacement of hardware is required.

Table 4-1. OPM Reflectometer Samples Solar Absorptance/Emittance Change

OPM Reflectometer Samples Solar Absorptance/Emittance Change								
Sample Description	Supplier	ε Emittance Pre-Flight	ε Emittance Post-Flight	Δε	α_s, Solar Absorptance Pre-Flight	$\Delta \alpha_s$ 0 days (space v. grnd)	$\Delta \alpha_{s\ final}$ 237 days (space v. grnd)	$\Delta \alpha_s$ Post-Flight
Silver- COR - Triton	NASA MSFC	0.823	0.834	+0.011	0.118	0.023	0.150	0.145
TMS-800AZ, yellow	AZ Technology	0.872	0.868	-0.004	0.352	-0.008	-0.010	0.011
ESD white	AZ Technology	0.912	0.905	-0.007	0.244	0.011	n/a	n/a
Low alpha white	AZ Technology	0.903	0.898	-0.005	0.088	0.007	0.011	0.002
Optical Solar Reflector	AZ Tech/T&M Eng	0.758	0.767	+0.009	0.055	-0.002	0.001	0.005
AZ-93 over MLP-300 primer	AZ Technology	0.906	0.904	-0.002	0.160	0.001	0.005	0.006
AZ-93 w/ Teflon overcoat	NASA MSFC	0.902	0.892	-0.01	0.171	-0.002	0.096	0.063
TP-co-2, ZnO silicate & glass base	RSC Energia	0.918	0.907	-0.011	0.161	-0.004	-0.001	0.001
TP-co-12, ZnO silicate & glass base	RSC Energia	0.914	0.906	-0.008	0.148	0.000	0.005	0.002
Chromic Acid 6061 Al	Boeing (Huntsville)	0.463	0.463	0	0.361	-0.003	0.051	0.057
Boric-Sulfuric Anodized 6061 Al	Boeing (Huntsville)	0.569	0.564	-0.005	0.360	-0.002	0.071	0.052
Chem film 1A on 2219 Al	Boeing(Canoga Prk)	0.064	0.058	-0.006	0.461	0.004	0.074	0.062
Z-93CLM55 White coating	IIT Research Inst	0.909	0.901	-0.008	0.126	-0.002	0.011	0.004
Sulfuric Acid Anodized 7075-T7351	Boeing (Hunt. Bch)	0.869	0.877	+0.008	0.424	-0.004	0.053	0.053
Sulfuric Acid Anodized 2219-T851	Boeing (Hunt. Bch)	0.820	0.831	+0.011	0.393	-0.004	0.121	0.115
Z-93P White coating	Boeing (Hunt. Bch)	0.901	0.893	-0.008	0.163	-0.016	-0.002	-0.008
Z-93P w/500A silicone	Boeing (Hunt. Bch)	0.899	0.895	-0.004	0.154	-0.005	0.052	0.040
Z-93P w/500A Tefzel	Boeing (Hunt. Bch)	0.899	0.896	-0.003	0.188	-0.004	0.003	-0.008
Z93P w/2000A silicone	Boeing (Hunt. Bch)	0.895	0.893	-0.002	0.146	0.004	0.127	0.089
Z-93P w/2000A Tefzel	Boeing (Hunt. Bch)	0.899	0.893	-0.006	0.256	0.005	0.026	-0.007

In the following part of this section, the flight data for specific types of samples will be discussed. Most of the discussion will be concentrated on the materials of the most immediate significance to the ISS mission. As briefly mentioned before, a few of the samples are experimental coatings either new materials or modifications of older versions. Some of these will be discussed also, but only briefly, since more detailed analysis is required to fully understand their significance.

4.1.1 COR/Silver Triton Sample CR01

This sample from Triton Systems Inc., is a Clear Oxygen Resistant (COR) polymer that is basically stable when exposed to atomic oxygen. The original polymer was developed by Langley Research Center (LaRC), then further refined into a product by Triton Systems Inc., under contracts with LaRC and MSFC. Upon exposure to AO this polymer forms a glassy type surface which impedes any further erosion. The original version was the color of Kapton, a translucent amber. Triton modified the polymer to form a clear version, which was then coated with silver to form a second surface mirror with low solar absorptance and reasonably high thermal emittance, see Table 4-1. As can be seen from the data the sample solar alpha increased during the exposure, also refer to the in-flight data in Appendix D. The physical appearance of the COR sample after return to the ground, was a very bright specular gold color. It looked like a gold mirror, but with a slightly lighter gold color. Since this formulation was flown and the ultraviolet sensitivity was discovered, the formulation has been revised to reduce or eliminate the ultraviolet sensitivity.[16]

4.1.2 TMS-800AZ Yellow Marker Coating; CR02

The yellow marker coating TMS-800AZ was developed by AZ Technology under contract with NASA/MSFC. This is a ceramic based coating that can be applied to metal and non-metal surfaces to provide a bright yellow marker identification color on spacecraft. Previous ground space environmental testing performed at the MSFC indicated the coating was very stable when exposed to the space environment including high levels of electron and proton fluxes.

As can be seen from the flight data summary in Table 4-1, the coating had only a very slight change in solar absorptance from pre-flight to post-flight measurements. Interestingly the solar absorptance in-space was lower than pre-flight values and seemed to improve slightly with time. Upon return to the ground and exposure to atmospheric moisture the infrared reflectance returned to pre-flight values (bleaching affect) resulting in the slight overall increase in solar alpha. These affects can be seen in the spectral reflectance data in Figure C-2 of Appendix C, where the infrared had the typical increase in reflectance as the water vapor is leaves the coating in a high vacuum environment and then recovers after return to the ground. Also in the visible region a slight reduction in reflectance can be seen. This change is difficult to detect visually unless compared to the ground control and then the slight change can be detected. This change is similar to the affect change that occurred during ground testing. This sample was also exposed

on the MEEP/POSA I flight experiment[17] for a longer period (18 months) and still retained its bright yellow appearance even after heavy levels of surface contamination.

4.1.3 ESD White Coating; CR03, AZWEC-II(MST450-ICW)

This is a experimental coating developed by AZ Technology, that is a electrical static dissipative white ceramic type thermal control coating. The coating delaminated from its substrate after 161 days of exposure. Since we had on orbit insitu measurements, we still obtained valuable information. The coating degraded fairly quickly once exposed, reference Figure C-3 in Appendix C and Appendix D for the CR-03 sample. The coating did survive the impact accident, which is advantageous since this provided data including the larger dose of solar ultraviolet radiation. As seen from the data, the coating stabilized after approximately 50 ESH, in fact after 700 ESH it appears to recover slightly. In sufficient coating was recovered for post-flight optical analysis.

4.1.4 Low Alpha White Thermal Control Coating, CR04, AZW/LA-11 (MST600-IUCW)

This is a new experimental coating developed under research contract by AZ Technology sponsored by Wright-Patterson AFB (WPAFB) and managed by J. Sanders and P. Carlin.[18] Ground testing at AZ Technology had indicated good stability which was demonstrated during exposure on the Mir space station, reference Figure C-4 in Appendix C and data in Appendix D. The goal was to maintain a solar absorptance below 10% and still have a thermal emittance above or close to 90%, these goals were met. Other coatings developed under this research contract are part of a series of formulations that have promise to provide thermal control coatings with the high thermal emittance and solar absorptance values less than half of this coating.

4.1.5 AZ93P Over MLP-300 Primer, CR06, AZ93/MLP300

As can be seen from the data in Appendix C and D, this coating is very stable. In fact the spectral data shows clearly that this while on orbit was as stable as the control sample (OSR). This coating is the standard Z93P coating manufactured by AZ Technology, but applied over a primer which was developed by AZ Technology to enhance the bonding of Z93 type coatings to aluminum and non-metallic substrates. The goal was also to provide a means of applying Z93 type coatings with personnel having less skill, since Z93 type coatings applied directly to aluminum require considerable skill and experience to be successful. Flight data demonstrates that no detrimental affects occurred by using this primer.

4.1.6 AZ93 with a Teflon™ Overcoat, CR07

This sample is the standard AZ93 manufacture by AZ Technology but with a special Teflon type overcoat. The purpose of the overcoat was to provide a temporary cover for the AZ93 coating for ground handling. Since Z93 type ceramic coatings are very porous they are

susceptible to ground handling contamination. This coating fills in the voids on the surface of the porous ceramic thereby preventing contamination infiltrating the porous structure. Since contamination does not bond well to Teflon, the surface contamination can be removed with ordinary solvents prior to flight. In addition, the Teflon is sufficiently transparent as not to significantly change the starting solar absorptance. Ground tests at MSFC by R. Kamenetzky have shown that the Teflon is eroded off of the AZ93 fairly quickly. The data shown in Appendix D for CR07 show that towards the end of the exposure the solar absorptance was starting to return to its initial on orbit value. This particular Teflon formulation degrades under solar ultraviolet radiation as seen in Appendix C, Figure C-7, but eventually the AO will remove it the coating will return to its original value. The post-flight material analysis as discussed in Section 4.3.2 shows that the Teflon coating was slowly being removed, but the Teflon further into the porous structure was coming off even slower. The apparent difference in recovery rates between the MSFC tests and the flight data may be explained by the synergism between AO fluence and solar ultraviolet fluence on the erosion rate of Teflon. This particular formulation has not been investigated enough to understand this relationship, but it should be noted that the tests at MSFC utilized their 5eV AO source which has a high flux of AO but also includes a very large flux of vacuum ultraviolet radiation. In comparison to the exposure on Mir which while having a reasonable AO fluence was very low in solar ultraviolet fluence.

4.1.7 TP-co-2 & TP-co-12 ZnO Silicate & Glass Base; CR08 and CR09

Both of these samples were provided by Naumov/RSC Energia. They are similar to the Z-93 type coatings. The Russian coatings performed basically identical to the Z93 and AZ93 coatings as would be expected from their similar formulation and past performance on Russian spacecraft. As for the AZ93/CR06 and Z93P/CR16 these coatings were very stable with changes in solar absorptance within instrumentation error.

4.1.8 Anodized Aluminum Samples; CR10, 11, 14, and 15

Spectral reflectance data for the anodized aluminum samples flown on OPM are plotted in Figures 4-2 through 4-4. These samples were provided by Boeing Company and are aluminum conversion coatings being utilized on the International Space Station. The Chromic Acid Anodize (CAA) and Boric Sulfuric Acid Anodize (BSA) samples were provided by Dr. Gary Pippin of Boeing Seattle, while both of the Sulfuric Acid Anidize (SAA) coatings were provided by Mark Hasagawa, of McDonnell Douglas Company, now Boeing Huntington Beach.

The OPM performed reflectance measurements 27 times over the 8-month mission. Data is provided for the anodized samples in Tables 4-1 and –2, only for the initial ground scan, the initial in-space measurement, on orbit day 237, and post-flight (68 days after return to ground). Reference Table 4-2, which lists the solar absorptance values calculated from the reflectance data in Figures 4-2 through 4-4. All of the solar absorptance data is provided in Appendix C and D.

In general, the anodized samples degraded more than was expected. The SAA on Aluminum substrate 2219-T851 degraded almost twice as much as the other anodized aluminum surfaces. Since all samples received the same amount of contamination (150 to 180 Angstroms) and since the OSR sample showed very little change due to this level of contamination, the degradation observed results from the natural space environment. Since the samples only received 832 ESH's of solar ultraviolet radiation, compared to a typical 2000 ESH per year, this degradation was much greater than expected. Sadly the OPM data for the mid-point of the exposure period was not taken because of Mir power problems after the collision accident. Without this midpoint data, it is very difficult to accurately predict the long term degradation of the coatings based on this limited data. Certainly a straight line estimation can be made, but this would lead to excessive predictions of degradation. Either long term ground testing is required or a re-flight of the OPM is required to obtain the necessary data to predict long term degradation of these coatings.

Another finding that is of interest is shown in Table 4-2, listed in the right two columns. Results of reflectance measurements are summarized for day 68 after OPM was returned to the ground. Note that the BSA sample had significant bleaching, over 4%. Although the magnitude of the bleaching effect is not nearly as great as for ZnO pigmented coatings[4], it again demonstrates the importance of insitu or in-vacuum optical measurements.

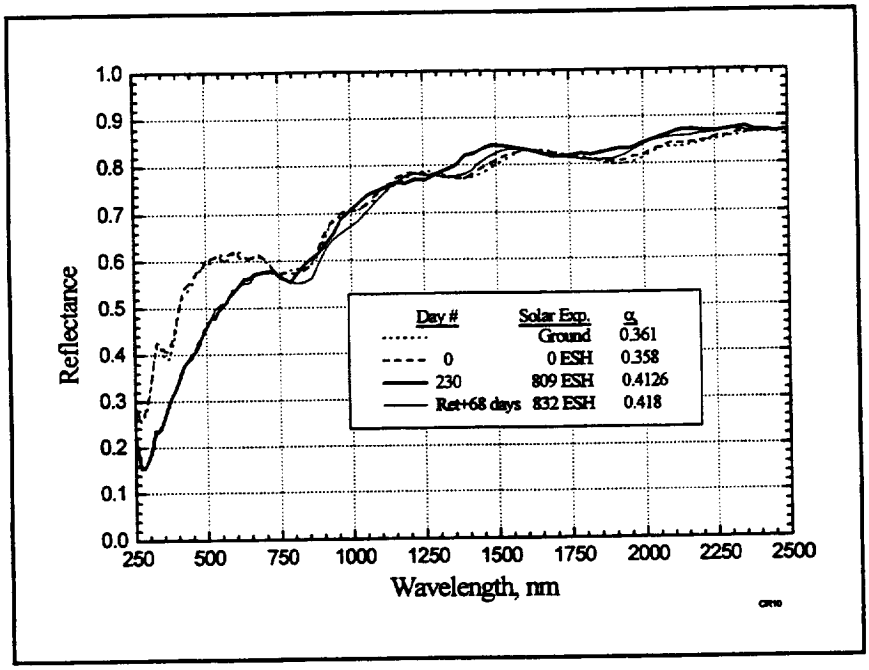

Figure 4-2. OPM Reflectometer Flight Data
Chromic Acid Anodized 6061 Aluminum Alloy

Table 4-2. Solar Absorptance Values for Anodized Samples

Sample	Initial α_s	Day 237 on orbit	$\Delta\alpha_s$	$\Delta\alpha_s/\alpha_s$ (%)	Post Flight α_s +68 days	Post Flight Recovery (%)
CAA on Al. 6061	0.361	0.412	0.051	14	0.418	1.5
BSA on Al. 6061	0.360	0.431	0.071	19	0.412	4.4
SAA on Al. 7075	0.424	0.477	0.053	13	0.477	0
SAA on Al. 2219-T851	0.393	0.514	0.121	31	0.508	1
* α_{237}-α_{+68} / α_{237} in %						

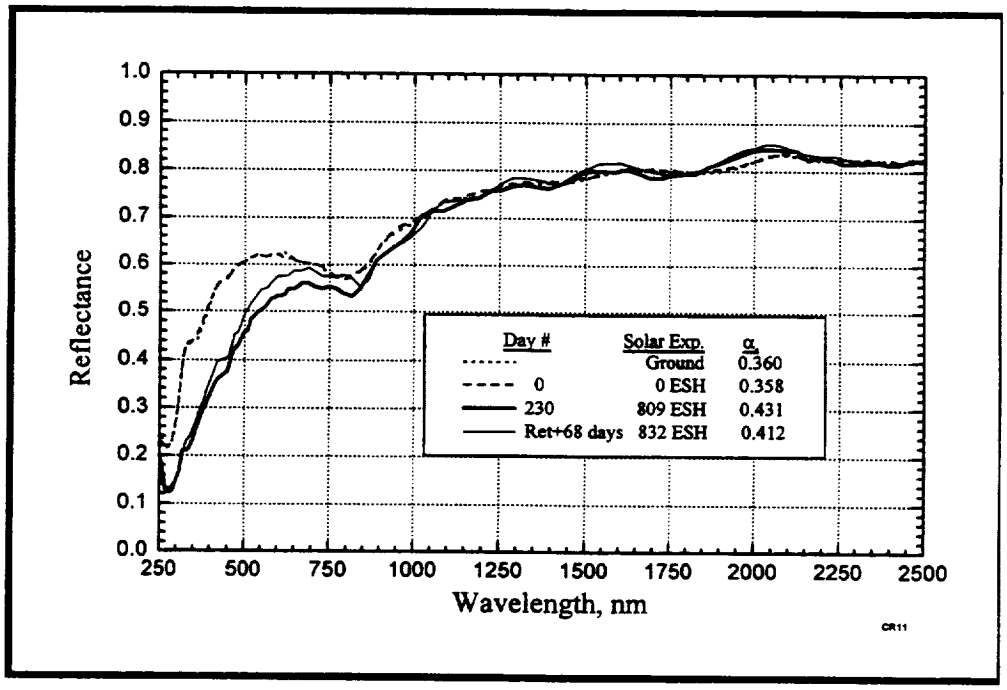

Figure 4-3. OPM Reflectometer Flight Data Boric-Sulfuric Anodized 6061 Aluminum Alloy

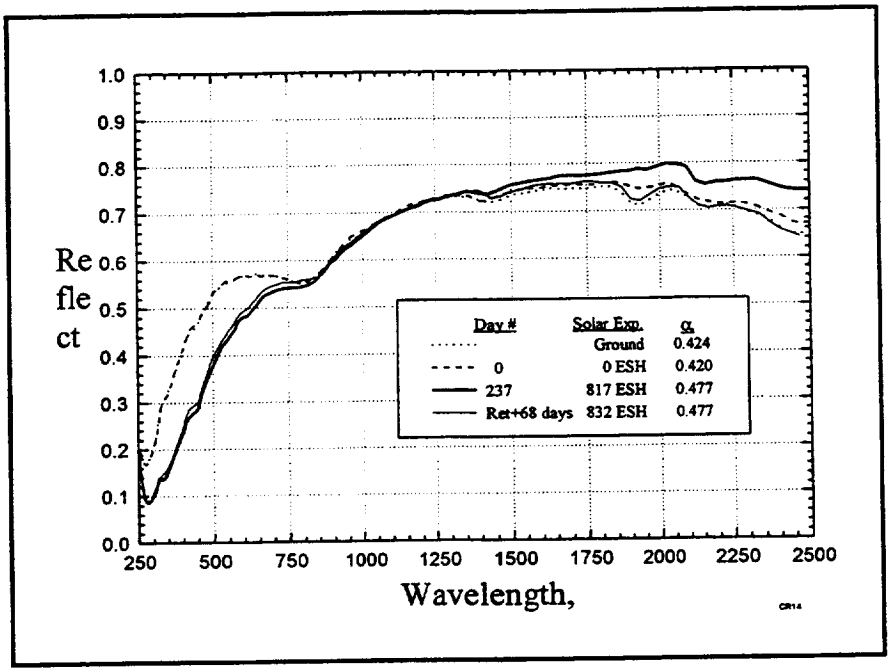

Figure 4-4. OPM Reflectometer Flight Data
Sulfuric Acid Anodized 7075-T7351

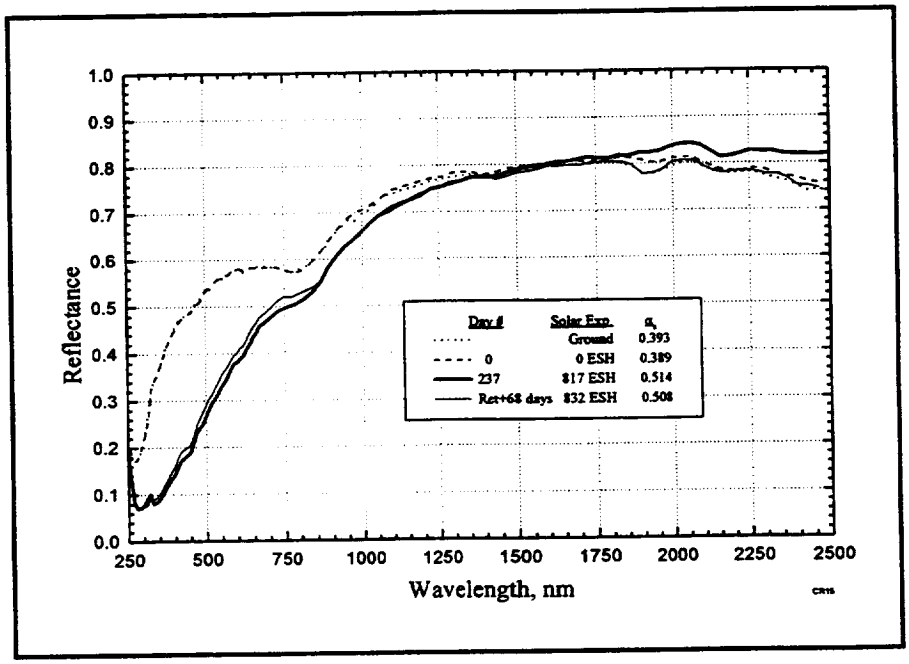

Figure 4-5. OPM Reflectometer Flight Data Sulfuric Acid Anodized 2219-T851

4.1.9 Chem Film Sample, CR12

This sample behaved very similar to the anodized samples. The sample coating was provided by P. Dano of Rocketdyne. Reference Figure C-12 in Appendix C and data in Appendix D for the flight data on CR12. Further post-flight analysis is anticipated by the sample supplier which should be published in the open literature.

4.1.10 Z-93ClM55 White Coating, CR13

This is a another experimental type coating provided by M. Deshpande of IITRI which is modified Z93 type coating. Referencing the data plots in Appendix C and D, the coating appears to be not quite as stable as the other standard Z93 type coatings (CR06 and CR16). The solar absorptance does appear to stabilized at less than 14%. Further analysis by the sample supplier investigator is anticipated and will be published in the open literature.

4.1.11 Uncontaminated Flight Control Z93P, CR16 and Pre-Contaminated Z93P Thermal Control Coating, CR17, 18, 19, And 20

One set of samples with significant importance for the ISS is the pre-contaminated Z93P white thermal control coating samples. Z93P is the coating for the large ISS Active Thermal Control System (ATCS) radiators and its optical properties must remain stable for the required ten-year lifetime. Z93 samples were pre-contaminated with either silicone or Tefzel offgassing products. These contaminants were photofixed with UV irradiation which prevented cross contamination of other flight samples. These samples were also pre-damaged with 5000 ESH of VUV irradiation. Refer to Section 4.4 on a discussion of the Contamination results for a detailed description of these samples, objectives, and findings. Briefly it is sufficient to mention here that the original objective of these samples was to determine if and the magnitude that atomic oxygen would be affective in removing heavily contaminated surfaces of Z93P with both silicone and Tefzel offgasing products. These surfaces also had a large fluence of simulated solar ultraviolet radiation to simulate potential long term accumulation of contamination during the ISS mission. Results of this experiment provide other interesting results as is discussed in detail in Section 4.4.

Figures C-17 through C-20 in Appendix C show the spectral reflectance data for the Tefzel and Silicone pre-contaminated Z93P samples. Figure 4-6 shows the comparison of the solar absorptance data for the uncontaminated Z93 and the "2000" Angstrom pre-contaminated samples. This data starts with the uncontaminated Z93P samples up through post-flight ground measurements. Note that the uncontaminated Z93 was very stable for the mission. The Tefzel contaminated sample degraded (increased solar absorptance) significantly early in the mission followed by a marked improvement later in the mission. In fact, the post-flight solar absorptance value was slightly lower (better) than the pre-flight value. The silicone contaminated sample did not degrade as quickly as did the Tefzel sample but continued to degrade for the complete mission. The reason for the recovery of the Tefzel contaminated sample is believed to be due to

the erosion of the Tefzel contaminant layer by the incident AO. Fluorocarbon polymers are susceptible to erosion by AO where silicone contaminants are converted to a non-volatile silicate by AO and solar UV. The incident AO fluence is believed to be sufficient to erode away the Tefzel contaminant.

The long term post flight bleaching affect even on these contaminated surfaces continues for an extended period as can be seen in Figure 4-6. Normally bleaching affects are rapid.[1-3] This long term or extended bleaching affect was unexpected. This data further demonstrates that the chemical mechanisms of material degradation are extremely complex and interesting. Also, the varying behavior in space with time clearly defines the requirement for in-space insitu measurement in order to obtain accurate data to understand the damaging mechanism behaviors that occur in a true combined space environment.

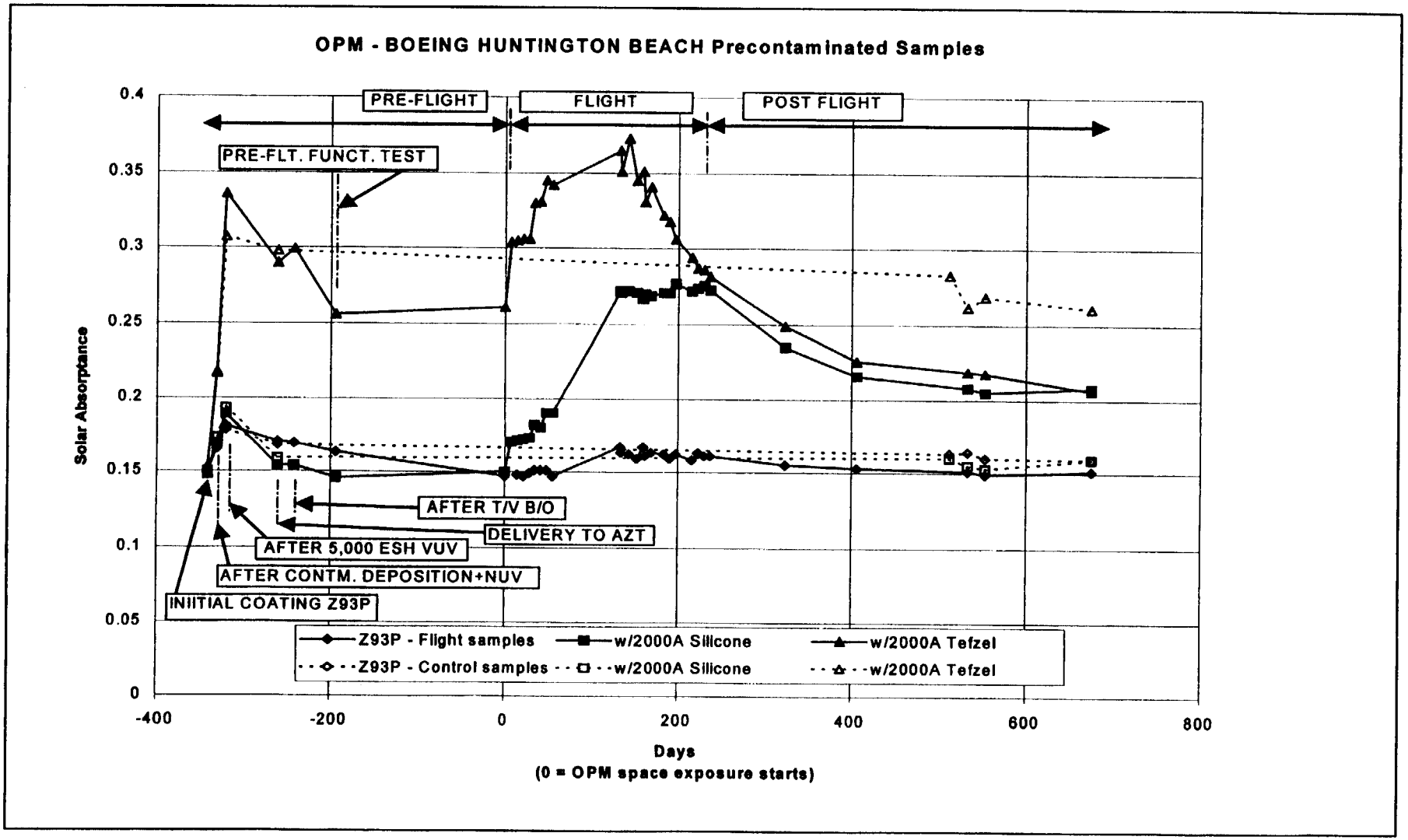

Figure 4-6 Solar Absorptance for Pre-Contaminated Z93P Samples from Original Coating Through Post-Flight

4.2 Total Integrated Scatter (TIS)

The OPM mission was the first time that TIS measurements had been performed in space.[14,19,20] The TIS instrument provided excellent measurements during the mission to Mir. Twenty TIS sample were flown and exposed on the carousel. Optical measurements, including TIS, were performed at weekly intervals while OPM was deployed and was powered. In addition to flight measurements, these samples were characterized prior to flight and then re-measured post flight. Appendix A and Appendix K, Table K-1, provide a listing of these samples along with a sample description and the sample supplier. Table K-1 provides detailed information including all identification numbers relating to each TIS sample. The samples were protected before and after the OPM deployed mission. This was accomplished by rotating the sample carousel to the closed position inside the OPM enclosure. This protected the samples from direct damage, but was not a hermitic sealed enclosure. The samples were still exposed to temperature, humidity, etc. inside the MIR. TIS was measured at 532nm and 1064nm before flight, during exposure in LEO, and post-flight.

In this Section, the results for the OPM TIS samples will be discussed. In Appendix K graphs are shown for the TIS flight data versus exposure time for 532 nm, for 1064 nm, and for the 532/1064 ratio of TIS values. Tables of TIS measurements, thermal emittance, and solar absorptance are also presented in Appendix K. Table 4-3 is a summary of the OPM TIS data for the twenty TIS samples. Detailed interpretation of the TIS sample results will be left to the sample supplier, to be published in the open literature.

Table 4-3. Summary of TIS Measurements for Flight Samples

Sample Number	Description	TIS Preflight 532 nm	TIS Week 35 532 nm	TIS Post-Flight 532 nm	[illegible]	TIS Preflight 1064 nm	TIS Week 35 1064 nm	TIS Post-Flight 1064 nm	[illegible]
ST01	Niobia/Silica multilayer	0.000661	0.002194	0.002455	[illegible]	0.000815	0.001391	0.002623	[illegible]
ST02	Zirconia/Silica multilayer	0.001444	0.002396	0.002626	[illegible]	0.000652	0.001083	0.001417	[illegible]
ST03	Diamond like carbon on Si	0.002130	0.002463	0.004321	[illegible]	0.001687	0.001537	0.002584	[illegible]
ST04	Titanium Diboride on Si	0.001165	0.002119	0.002469	[illegible]	0.001198	0.001637	0.002841	[illegible]
ST05	Zirconium Diboride on Si	0.000942	0.001935	0.001904	[illegible]	0.000699	0.001374	0.001648	[illegible]
ST06	$Ti_xB_yN_z$ film on silicon	0.000886	0.001617	0.002255	[illegible]	0.001059	0.001324	0.002326	[illegible]
ST07	CVD Diamond, as-grown	0.998164	0.997887	0.998503	[illegible]	0.877207	0.880383	0.870900	[illegible]
ST08	$Ti_xB_yO_z$ film on silicon	0.001882	0.001987	0.003048	[illegible]	0.001709	0.031255	0.090026	[illegible]
ST09	$Zr_xB_yN_z$ film on silicon	0.000829	0.001778	0.002030	[illegible]	0.000875	0.001485	0.002274	[illegible]
ST10	CVD Diamond, as-grown, doped - 5 atomic percent B	0.998371	0.997795	0.998703	[illegible]	0.951499	0.953960	0.951668	[illegible]
ST11	CVD Diamond, as-grown, doped - 5 atomic % P	0.994694	0.994164	0.994764	[illegible]	0.85718	0.862174	0.852681	[illegible]
ST12	Carbon nitride (C_xN_y) on Si	0.009086	0.003612	0.004320	[illegible]	0.00166	0.002136	0.002289	[illegible]
ST13	Titanium nitride (TiN) on Si	0.00182	0.002549	0.002378	[illegible]	0.000946	0.00106	0.001511	[illegible]
ST14	1st surface aluminum-coated levelized aluminum mirror	0.008679	0.007518	0.008942	[illegible]	0.005754	0.005097	0.00655	[illegible]
ST15	ISS Solar Array Face Sheet	0.966294	0.996364	0.998422	[illegible]	0.916701	0.993817	0.999596	[illegible]
ST16	Gold Mirror	0.001595	0.002158	0.002219	[illegible]	0.001168	0.001595	0.001838	[illegible]
ST17	Kapton H (four 5 mil layers)	0.917017	0.987365	0.993218	[illegible]	0.918294	0.942891	0.947124	[illegible]
ST18	MgF_2 / Aluminum Mirror	0.001314	0.001750	0.001909	[illegible]	0.000824	0.001135	0.001668	[illegible]
ST19	Platinum Mirror	0.000939	0.001484	0.001596	[illegible]	0.000745	0.001153	0.002070	[illegible]
ST20	Silver / Teflon	0.162412	0.168390	0.155528	[illegible]	0.051435	0.049860	0.044508	[illegible]

4.2.1 Sample Selection

Samples flown for TIS evaluation were chosen from three categories: optical samples, engineered scattering surfaces, and engineered materials. For the purpose of evaluating the measurements, the samples were categorized into four groups based on the preflight TIS values (Table 4-4). All of the *optical samples* are contained in the TIS "Lowest" category and have the least amount of scatter. The *engineered materials* are spread through the other three categories. The "controlled scattering" surfaces, supplied by the Naval Air Warfare Center (NAWC), are spread throughout all categories. The graphs in Appendix K are grouped by these categories.

Table 4-4. Sample Categories Based on Preflight TIS Values.

Lowest TIS< 0.002	Low .002<TIS< 0.01	Medium .01<TIS< 0.5	High TIS>.5
ST01	ST03	ST08 (1064 nm)	ST07
ST02	ST12		ST10
ST04	ST14	**ST20**	ST11
ST05			ST15
ST06			
ST08 (532 nm)			**ST17**
ST09			
ST13			
ST16			
ST18			
ST19			

4.2.2 Overall Results

In addition to TIS measurements, the samples were evaluated on Nomarski microscopes and some on an Atomic Force Microscope (AFM). Nomarski microscopes from the UAH and from NAWC were used. The AFM was located at Digital Instruments. The purposes of the Normarski investigations were to characterize the particulate contaminate and to chose areas to measure with the AFM. The TIS co-investigator, Dr Bennett, used the AFM to validate the TIS measurements and to provide more detailed interpretation of the TIS sample results for a later journal publication.

The 532 nm scatter for most samples increased slightly for the first on-orbit measurement relative to the initial preflight values. Then there was a slow decrease over the next 5 weeks before the general gradual rise that continued for the rest of the flight. During the same period, the 1064 nm scatter did not show the initial rise and gradual decrease, only a slight upward rise to week 9 and then a slower constant rise for the rest of the period. One possible explanation for the increased 532 nm scatter may have been molecular contamination during shipping, launch, and/or MIR onboard storage prior to deployment which was then partially cleaned off upon exposure to the space environment.

Post-flight inspection and measurements of the TIS samples show particle contamination on all surfaces. The films were nearly particle free when they were loaded into the carousel and tested before the flight. The Figures in Appendix K show this effect. Note that the 1064nm scatter, which is more sensitive to particles than the 532nm scatter[12], changed very little during the flight, indicating that very few particles settled on the samples during exposure to the space environment. The major increase in the 1064nm scatter occurred after the flight, so that is likely when the particles accumulated on the samples as seen in post-flight inspections. Figure 4-7 clearly shows the large increase in the 1064nm scatter from the last on orbit measurement to the post flight measurement. The samples in Figure 4-7 are ordered based on increasing preflight TIS values for 532nm.

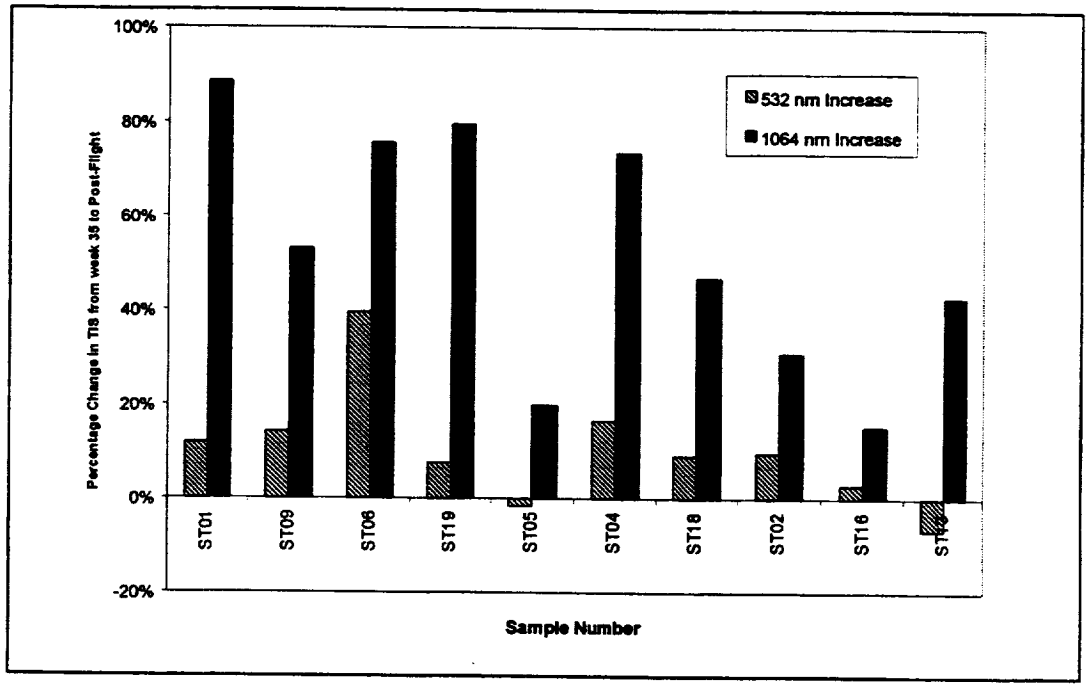

Figure 4-7. Last Space Measurement versus Post-Flight Ground Measurement

Many of the samples were either transparent or partially transparent at one or both wavelengths, so the TIS values could not be converted into effective rms roughness. Rms surface roughness was calculated for the magnesium fluoride coated aluminum mirror and the platinum mirror. The values are reported versus AFM measures in Table 4-5. The rms deviation for ST18-01 is due to possible recrystallization and is discussed in the sample section.

Table 4-5. Comparison of TIS Calculated RMS With AFM Determined RMS

Sample Serial No.	Description	1064 TIS RMS Angstroms	AFM RMS Angstroms
ST18-01	Al/MgF2 mirror Flight sample	34.6	48.6
ST18-02	Al/MgF2 mirror Backup sample	NA	37.0
ST19-01	Pt mirror Backup sample	NA	38.3
ST19-02	Pt mirror Flight sample	38.5	30.0

Some changes were seen due to the LEO environment. As expected, Kapton eroded due to AO exposure. Other samples based on carbon and nitrides showed severe susceptibility to AO erosion. Three of the TIS samples were severely degraded. Only clumps of initially uniform films remained on the exposed surfaces of the carbon nitride (CN) film as can be seen in the AFM image in Figure 4-8. Silver Teflon did not reach the threshold level necessary for significant erosion. In general, direct solar ultraviolet radiation exposure was minimized due to OPM/MIR attitude (see Section 3.2). However there was significant solar exposure on the OPM samples for the two-month period following the Progress accident. This may account for some of the step changes seen between weeks June 24 and September 13, 1997 (Weeks 9 to 20).

Solar absorptance and room temperature emittance was measured both preflight and post-flight for the TIS samples. The emittance measurements did not show significant changes for most TIS samples. Solar absorptance, on the other hand, indicated sample degradation when pre- and post-flight TIS measurements did not. See the discussion of sample ST03 later in this section. In general the solar absorptance was not useful for the low to lowest scattering samples except when there was sample decomposition. For the high scattering samples, the change in reflectance was sometimes more telling than the change in TIS.

The impact of storage inside the MIR was minimal despite the high humidity and smoke that was present during storage. The first space measurements on April 29, 1997 are not too far off from the preflight baseline measurements taken October 17, 1996. The OPM was stored just over 3 months inside the MIR. After deployment, evidence of the collision with the Progress module is seen by the unidirectional scratch marks under the protected areas of the samples. Similar scratch marks were present on samples across the carousel. These marks did not enter the measurement areas, and no TIS aberrations could be directly attributed to the collision.

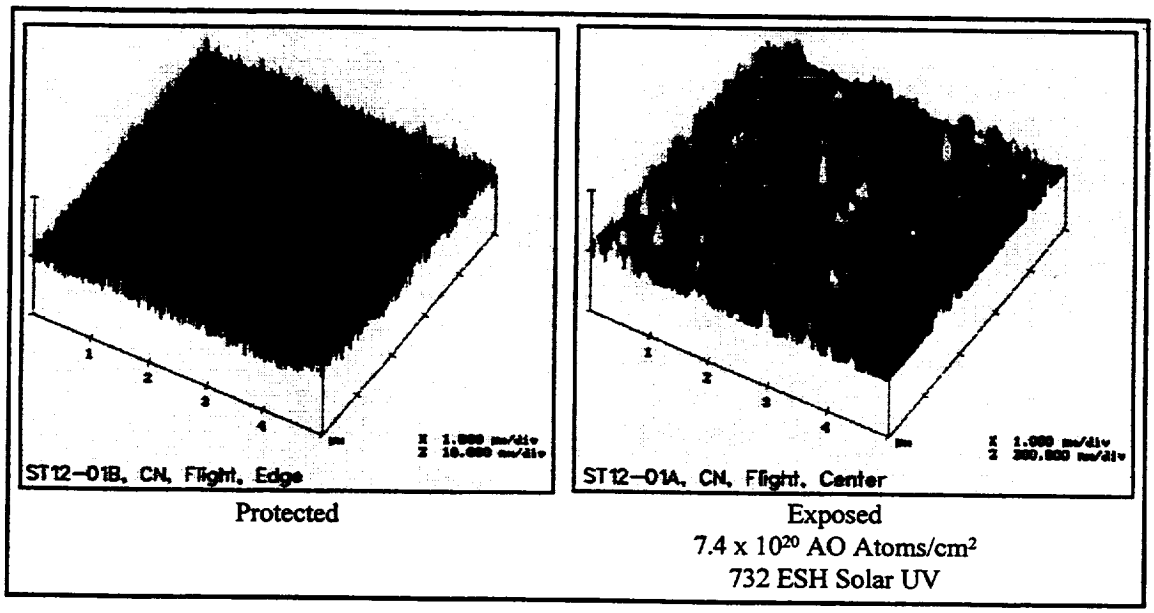

Figure 4-8. AFM Image of ST12 Showing CN Islands Left After AO Erosion

The 1064 nm calibration factors averaged 1.400 running within the expected 1.3 to 1.5 range. The 532 nm calibration factor ran higher and was stable around 1.550. There was less variance in the 532 values. This is thought to be due to a heater that is incorporated in the 532 nm laser for the frequency doubler. The only bad sample points that can really be tagged to temperature occur in week 24 when the 1064 laser temperature dropped to –5 °C. Erratic measurements are recorded at this time. This is most likely due to thermal drift from the time that the calibration is done until the samples are measured. Measuring the entire twenty samples takes about 2 hours.

The significance of the above discussion is that the overall instrument operation was validated and good TIS value measurements of the sample were obtained. Just as important, because of in-flight measurements, it was proven that most of the particulate contamination occurred after the OPM was packed up for return to Earth, not during on-orbit exposure to the space environment. No indications of misalignment or any other component failures were seen.

4.2.3 Specific Sample Results

4.2.3.1 USAF Research Laboratory Sample (ST01, ST02)

ST1-01 Niobia on Silica: This sample was composed of 18 pairs of Nb_2O_5 and SiO_2 films and a final Nb_2O_5 film on a fused silica substrate. This sample had the lowest 532nm scatter of the 20 samples. The scatter value rose more or less uniformly throughout the flight. The pre-flight value at 1064 nm was fourth from the lowest. The scatter increased more or less uniformly throughout the flight, but doubled from the last flight measurement to the post-flight

measurement. Investigation with the Nomarski microscopes revealed that the flight sample had a partial coverage of particles, one large scrape mark near the center, lint, and some small drops of dried liquid, mostly near the edge. The control sample (ST1-04) was nearly particle free. The AFM images of the flight and control samples were essentially identical with rms roughness values of 1.42nm and 1.22nm, respectively. The AFM image of the flight sample contained one large particle which would have slightly increased the rms value. Undoubtedly the 1064 nm scatter increased because of contamination on one or more of the measurement spots. In summary, the small TIS increases were caused by particle contamination rather than film degradation. Solar absorptance was unchanged. The multilayer coatings withstood the space environment well.

ST2-01 Zirconia on silica: This sample was composed of 22 pairs of ZrO_2 and SiO_2 films and a final ZrO_2 film on a fused silica substrate. Both flight and control samples were provided for the post-flight inspection. The zirconia sample had a larger 532nm scatter than the niobia coating (but there were more layers which would tend to increase the scattering). The zirconia sample had the lowest 1064 nm scatter of the 20 samples. This is surprising because one would expect the infrared scatter also to be higher because of the increased number of layers. The TIS at both wavelengths uniformly increased during the flight, but the slope of the increase at 532nm was smaller than for the niobia coating. At 1064nm TIS increased moderately. Nomarski microscope inspection revealed that the flight sample had fewer particles than the niobia sample, while the control sample (ST2-04) was nearly particle free. However, the China Lake Olympus Nomarski microscope showed that the surface texture was slightly more pronounced than for the niobia sample. The AFM images of the flight and control samples looked essentially identical with rms roughness values of 2.79nm and 2.73nm, respectively (a large particle on the image of the flight sample was deleted from the roughness measurements). Both of these samples were rougher than the pair of niobia samples, in agreement with the visual Nomarski microscope observations. Solar absorptance was unchanged. In summary, this coating withstood the space environment well.

4.2.3.2 NAWC Samples (ST03 – ST13)

All the silicon substrates used for the NAWC films were polished by General Optics. They were single crystal, (100) orientation, 0.125 inches thick, flat to one-quarter wave or better, and had an rms roughness of ~ 5 Å.

ST3-01 Diamond-like carbon on silicon, NAWC: The initial TIS measurements showed that the film had a somewhat higher scatter than the lowest scatter films. The first space measurements showed large scattering increases of more than 2 times in the visible channel and about 7 times in the infrared channel. The TIS values continued to increase with large fluctuations up to a maximum of 0.016 in the visible and 0.0093 in the infrared for week 9, then dropped to low values close to the initial readings at week 20. (No measurements were made during the intervening period.) Both visible and infrared scatter levels remained low for the rest of the measuring period, and the post-flight TIS values were only slightly larger. The Nomarski micrographs showed a large difference in the character of the film between the exposed region

and the protected region around the edge of the sample where the film had been under a Teflon retaining ring. In addition, the China Lake Olympus microscope showed what appeared to be a roughened region in the form of a partial ring on one side close to the edge. It looked as though the sample surface was shadowed from the full space exposure in this region (see Figure 4-9 A and B). The AFM images were quite different in the three regions. At the sample edge where the film was protected, it looked uniform and had an rms roughness of 4.44nm. In the exposed region there appeared to be clumps of the film remaining on a nearly bare silicon substrate, suggesting that most of the film had been eroded away by atomic oxygen. The roughness was 21.7nm rms. In the shadowed region, the film appeared to be deeply pitted, as though it was starting to be eroded away. The roughness was the highest in this region, 38.2nm rms. All the measurements suggest that the film started to be eroded immediately after it was exposed to atomic oxygen in space, and that the erosion process was essentially complete by week 20. After that, the scattering at both wavelengths was caused by unreacted clumps of diamond-like carbon remaining on the silicon surface.

The film of the diamond-like-carbon, sample ST03, has similar TIS values to the silicon substrate underneath. During flight the TIS value rose as described above, but when the sample eroded away TIS value dropped to a post-flight value that was similar to the preflight value. The change in solar absorptance picked up this change in preflight versus post-flight measurements. Solar absorptance dropped 25 percent. Emittance dropped 13 to 14 percent from preflight to post-flight, but the emittance generally shows less change relative to other TIS measurements.

ST4-01 Titanium diboride on silicon, NAWC: The TIS in the visible was initially low, but increased by 50% during the first space exposure, continued to increase in week 2, then gradually decreased until week 5, after which the scatter level gradually increased during the period of exposure in space. The post-flight TIS measurement increased by a modest amount. The infrared TIS scatter trend was quite different. The initial scatter was also low, and more or less uniformly increased during the entire space mission, but the post flight value was nearly twice the last value in week 35 in space. With the exception of numerous particles on the film and one dried liquid mark, the surface was featureless. The film was not photographed in the China Lake Nomarski microscope and no AFM images were taken. Further work will be done on this sample at China Lake.

ST5-01 Zirconium diboride on silicon, NAWC: The TIS values in both the visible and infrared were initially lower than those of the titanium diboride film. On the average, both the visible and infrared TIS uniformly increased throughout the space flight, and hardly increased after the flight. The surface was featureless except for particles. The film was not photographed in the China Lake Nomarski microscope and no AFM images were taken. Further work will be done on this sample at China Lake.

ST6-01 TiBN on silicon, NAWC: It had similar scatter characteristics to films of niobia on silica, ZrBN on silicon, and zirconium diboride on silicon. Both scatter channels increased slightly during the flight, probably caused by accumulation of particles. The post flight visible TIS increased somewhat, and the infrared TIS nearly doubled relative to the last space

measurement. The surface was featureless except for particles. No AFM images were taken. Further work will be done on this sample at China Lake.

ST7-01 CVD diamond on silicon, NAWC: The three CVD diamond films were all very rough and had high scatter because of the large crystallites in the polycrystalline films. The TIS levels did not change at the beginning of the flight and remained essentially constant throughout the flight, as well as for the post flight measurement. There were no obvious differences in the film structure in the exposed and protected regions. The film looked exceedingly rough everywhere. No AFM images were taken. Step height measurements will be taken between the protected region under the gold film and the exposed region to see if any of the film was removed by the atomic oxygen.

ST8-01 TiBO on silicon, NAWC: With the exception of the TiN film, the initial TIS value was the highest of the low scatter samples. The initial scatter in the visible dropped to 0.00128 for the first exposure in space and continued to drop to a minimum of 0.000935 (week 5), then increased and oscillated around 0.002 during the rest of the flight. The infrared scatter increased dramatically, first to 0.00679 (week 1) and then to 0.0150 (week 2), and 0.0207 (week 3). It continued to rise and then erratically rose and fell throughout the rest of the flight. The maximum value measured in flight was 0.0599 for week 27, but the post-flight value was much larger. The film was nonuniform in thickness across the sample, as evidenced by the color gradations, and in addition had a different color under the ring at the edge of the sample. There may have been a particle in the field of view of one measuring spot. There were many circular features (sizes 1μm to 40μm) on the surface that may have been dried spray. In addition, there was a discolored brown area in the outer ring on one side and two bubbles ~30μm diameter. The Nomarski micrographs emphasized the color differences on different parts of the sample and a displaced outline of the gold half-moon area suggested that some or all of the film had been eroded away (see Figure 4-9B). The AFM images showed that the center exposed region was dominated by many small contamination particles, giving an rms roughness of 0.79nm. Two AFM images were taken in the edge region, opposite each other. The film was very smooth on one edge, 0.33nm rms, but appeared to have a longer range mottling with a spacing ~0.5μm. On the opposite edge, the film appeared to be more blotchy with a slightly shorter spacing and a larger roughness, 0.75nm rms. Since the initial film was nonuniform, the variations between the two opposite edges may simply represent differences in the initial film roughness. There is a strong possibility that the entire film was eroded away in the central region and only the particle-covered silicon remained; this guess will be confirmed after part of the gold mask is removed and the film is profiled to see if there is a step.

ST9-01 ZrBN on silicon, NAWC: The first flight scatter value was 0.00108 at 532nm, but subsequent scatter values dropped to 0.000878 (week 3) and then rose again. The infrared values were quite similar. The film was uniform with a light particle coverage similar to the other samples. No AFM images were taken. Further measurements will be made on this sample at China Lake.

ST10-01 B-doped CVD diamond on silicon, NAWC: The TIS 532 nm values were very similar to those for the undoped CVD diamond film, but the 1064 nm values were very constant at a level of 0.951 – 0.954. There were no obvious differences in the film structure in the exposed and protected regions; the film looked exceedingly rough everywhere. No AFM images were taken. Step height measurements will be taken on this film that are similar to those to be taken on the other CVD diamond films.

ST11-01 P-doped CVD diamond on silicon, NAWC: The 532 nm scatter remained constant at 0.994 from the initial measurement, throughout the space flight, and for the post-flight measurement. The 1064nm scatter held nearly as constant at values between 0.854 and 0.863. There were no obvious differences in the film structure in the exposed and protected regions; the film looked exceedingly rough everywhere. No AFM images were taken. Step height measurements will be taken on this film that are similar to those to be taken on the other CVD diamond films.

ST12-01 CN on silicon, NAWC: The film had an initial moderate scattering level of 0.00909 at 532 nm, but it immediately increased to 0.0145 during the first week's exposure in space. After that it oscillated and finally decreased to a level close to 0.0038 (week 7) where it remained for the rest of the flight and post flight. The scattering level at 1064 nm behaved in a similar manner. The maximum increase (0.0389) occurred at week 3, but the scattering level then dropped gradually to 0.00279 at week 9 and remained at a slightly lower level, ~0.002 for the rest of the flight and post flight. In the Nomarski micrographs, there was a significant color difference between the central exposed region and the protected edge. In addition, there were several blotchy areas with small point-like centers, whose dimensions ranged from 8 to 400μm. The AFM image of the center showed clumps of material, similar to those at the center of the diamond-like carbon film, ST3-01, except that the clumps on the CN film were more dense. The roughness was 32.9nm rms, larger than for the diamond-like carbon film. At the two protected edges on opposite sides of a diameter, the CN film was uniform but contained particles. The roughness on the AFM images were 0.923nm rms and 1.119nm rms, respectively. The particles and also some residual polishing scratches on the silicon surface made these roughness values somewhat larger than the intrinsic roughness of the initial CN film. It is clear that much of the CN film had been eroded away by atomic oxygen and that only clumps of CN material remained in the exposed area. Solar absorptance revealed this erosion with a 17 percent decrease from preflight to post-flight.

ST13-01 Titanium nitride on silicon, NAWC: The film had a rather large initial scattering level at 532nm, and the scattering increased during the first few weeks in space. Following week 9, the scattering level behaved erratically during the rest of the flight, rising to a value of 0.00353 at week 25 but then decreased to the post flight value. The initial infrared scattering level was about average for the scattering levels of the NAWC dielectric films. The level remained nearly constant during the flight and increased slightly to the post-flight measurement. The film appeared to be uniform in both Nomarski microscopes, but the exposed area was slightly darker than the protected area; the particle density was lower than on some of the other films. The AFM images of the center and the protected area at the edge showed a dense

film which looked identical in both places; the rms roughness were essentially identical, 6.79nm at the center and 6.44nm at the edge. One possible explanation for the erratic behavior of the scattering level in the visible channel is that there was a large particle at the edge of the illuminated spot which added appreciable scatter when it was in the field, but the sample shifted slightly during the flight. Perhaps the illuminated spot for the infrared channel did not include the particle. Solar absorptance increased 4 percent over the exposure period. In summary, the TiN film did not seem to be affected by the space environment

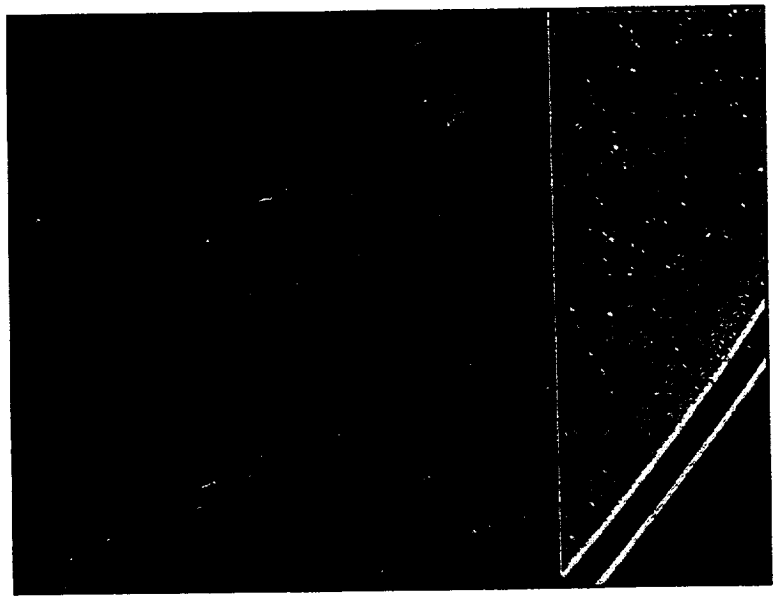

(A) – ST3-01

(B) – ST8-01

Figure 4-9. Nomarski Micrographs of (A) ST3-01 and (B) ST8-01

4.2.3.3 NASA Glenn Research Center Samples (ST14 – ST15)

ST14-01 Levelized Aluminum Mirror: The surface had a distinctive "orange peel" appearance, and would make a poor imaging optical surface. The initial 532 nm scatter level was close to that of the NAWC CN film and considerably higher than the scatter level for the MgF_2 overcoated aluminum mirror. The scatter levels in flight were erratic but there was no increase. The post-flight scatter was close to the initial value. The initial scatter level at 1064 nm was much higher than the initial scatter level of the MgF_2 overcoated aluminum mirror. During the flight the scatter level changed erratically but did not increase appreciably up to week 35, where the level was slightly lower than the pre-flight value; however, the post-flight value was considerably higher showing a similar increase to that of the MgF_2 overcoated aluminum mirror. Examination in the UAH Nomarski microscope revealed one large dried liquid drop away from the TIS measurement areas, various scrape marks (some of which could have been on the sample when it was submitted), and numerous particles. The dominant feature was the very obvious orange peel surface texture which would have caused the specularly reflected beam to shift and possibly to slightly impinge on the collecting hemisphere. In this case, the TIS values would increase. Probably all the changes with the exception of the post-flight increase in the 1064 scatter level can be explained by the non-optical sample surface. No AFM images were taken. In summary, the space environment apparently did not affect this sample.

ST15-01 ISS Solar Blanket Face Sheet: This was a thin sheet, like aluminum foil with parallel scratches, possibly from the rollers used to make the sheet. The exposed side was blackened to act as a solar absorber. The blackened surface had a very high scatter at both visible and infrared wavelengths. The 532nm scatter increased to 0.996 after the first week of exposure in space, and remained high, with oscillations, for the rest of the flight. The post flight scatter was very close to unity. The initial 1064nm scatter rose to 0.999 after one week exposure in space. The scatter remained high, with oscillations, throughout the flight, and the post flight value was 0.999. This sample had the highest scatter in the infrared and nearly the highest scatter in the visible of the 20 samples. With the exception of the initial preflight TIS values, the ratio of the visible to infrared scatter remained at unity all during the flight and for the post flight measurements. This was the only sample that had a ratio of 1 for the scatter from the two wavelengths. The sheet was so thin that it curled, making it difficult to look at under the Nomarski microscope. The material was quite rough, which is the reason it had such a high scatter. No AFM images were taken. Solar absorptance decreased 3 percent.

4.2.3.4 AZ Technology Samples (ST16 – ST20)

ST16-01 Gold mirror: The sputtered gold film on a fused silica substrate was intended to be a control. The initial scattering level at 532 nm was at the upper end of the low scatter coatings. The scattering gradually increased during the space mission, and the final post-flight value was not significantly higher than the values in space. The initial 1064 nm scattering value was at the high end of the low scatter samples. As with the visible channel, the infrared scattering gradually increased during the space mission and was only slightly larger than the last scattering level measured on week 35 in space. Inspection in the Nomarski microscope showed

particles on the surface, similar to those on the other samples. No AFM measurements were made on the mirror. It is probable that the gold mirror did not degrade in the space environment.

ST17-01 Kapton H: Four layers of 5 mil thick Kapton, were mounted in the sample holder; however, the exposure in space affected only the top sheet, which darkened appreciably. The lower sheets appeared to be unchanged from their initial condition. Since the material is transparent, the TIS before space exposure represents scattering from all of the sheets. After one week in space the 532nm scatter rose to 0.921 and continued to increase throughout the flight. At 1064nm, after one week exposure in space, the scatter was only slightly larger than preflight levels. During the flight the scatter oscillated between a high of 0.943 (week 35) and a low of 0.914 (week 9). The post-flight value was slightly higher. The NAWC Nomarski microscope showed that the film in its initial condition was lumpy, like a dried gummy plastic material, with numerous scratch marks crossing the surface; some parallel scratch marks may have been from the rollers forming the sheet. After exposure, the surface darkened appreciably, but the gummy texture appeared to be about the same. In some places around the edge there was a gradation in the darkening, possibly caused by shadowing of the sample from the full exposure to the space environment. When the Kapton sheet was examined in the AFM, the unexposed region around the edge showed parallel grooves at various orientations, probably caused by marks on the rollers, and a smaller texturing underneath the marks. The roughness was 3.90nm rms. It was very difficult to profile the exposed region. In the best attempt, the measured roughness was 122.95nm rms. As expected, the Kapton film had changed drastically due to AO exposure. Solar absorptance increased from 0.76 to 0.92 over the exposure period. This was a 16 percent increase.

ST18-01 MgF_2 Overcoated Al Mirror: This MgF_2 overcoated aluminum mirror on a fused silica substrate was also included as a control sample. The initial 532 nm scattering level was 0.00131, as expected for this type of sample. During the flight the scattering level gradually increased, with about the same slope as for the gold mirror. The post-flight level was 0.00191, only slightly larger than the week 35 value measured in space. The initial 1064nm scattering level was 0.000824, in the middle of the low scatter samples. During the flight, the level increased slightly, reaching 0.00113 on week 35. However the post-flight scattering greatly increased to 0.00167, which is similar to the increases shown by the NAWC boron-containing films. This large increase, which did not show in the visible channel, may have been caused by a light coating of particles that were of a size to affect the infrared scattering much more than the visible scattering channel. Inspection in the NAWC Nomarski microscope showed isolated particles on the control film, and a slight increase in particles on the flight sample, with about the same concentration of particles on the surface as were on the gold mirror. The AFM image of the control sample showed numerous small particles, possibly from defects in the MgF_2 film, giving the sample a roughness of 3.70nm rms. The flight sample had many more defects in the same size range, with an increased roughness of 4.86nm rms. Some of the particles were probably caused by the contamination that was on all the flight samples, but possibly the MgF_2 film also partially recrystallized.

ST19-02 Platinum Mirror: This platinum coated fused silica mirror was also included as a control sample, since similar platinum-coated mirrors have been flown on numerous previous space missions. The initial 532nm scattering level was 0.000939, as expected for this type of mirror. During the flight the 532nm scattering level gradually increased, with a slightly smaller slope than for similar samples. The post-flight scattering level of 0.00160 was only slightly larger than the week 35 scattering level. The initial 1064 nm scattering level was 0.000745, as expected for this type of sample. The 1064 nm scattering level gradually increased during the flight, with the same slope as that for the other low scatter samples, and reached a value of 0.00115 at week 35. There was a large increase in the post flight value, 0.00207, the same as was observed for all of the other low scatter samples with the exception of the gold mirror, and the NAWC zirconia and zirconium diboride films. The NAWC Nomarski microscope images of the flight sample and the control sample showed no differences in the structure of the film, except that there were more particles on the flight sample and scratch marks around the edge from mounting the sample in the Teflon holder. AFM images of both the flight sample and control sample looked similar except that the flight sample appeared to be slightly smoother, 3.00 nm rms roughness, than the control sample, 3.82nm rms. The sizes of the grains in the two films appeared to be about the same. In summary, the space environment apparently did not adversely affect the platinum film.

ST20-01 Silver Coated Teflon: This sample is a second surface mirror with the outer layer a 5 mil Teflon (FEP), coated on the underside with Silver and then a protective layer of Inconel. The surface quality was poor in TIS terms. It was not possible to obtain a specular reflection from the sample and there were wavy parallel cracks across the entire surface as well as numerous scratch marks. This is typical for this material. The center portion of the sample was raised relative to a circular ring at the edge that had been under the Teflon retaining ring in the sample holder. The scatter level rose to 0.179 after one week's exposure in space. After that, the values oscillated from a high of 0.183 (week 5) to a low of 0.139 (week 28). At 1064 nm TIS remained nearly constant throughout the flight, with maximum and minimum values of 0.0533 (week 3) and 0.0400 (week 28). A possible explanation for the erratic 532nm scattering level compared to the constant 1064nm scattering level is that there may have been a slight misalignment of the two beams such that the visible beam striking one of the sample areas was on the edge of a crack and slight shifts of the beam and/or sample caused large fluctuations in the reflected and scattered signals, while the infrared beam was on crack-free sample areas. The UAH Nomarski microscope showed the above mentioned cracks and sample waviness which dominated the scattering. Particles were also present, but their contribution to the scattering was smaller. The sample was not imaged in the AFM. Preflight and post-flight solar absorptance did not give any incite to this sample. In summary, it is probable that this sample was not affected by the space environment.

4.2.4 Summary of TIS Subsystem Experiment Findings

The TIS instrument performed successfully in the space environment. The strength of the instrument is in differentiating extremely small changes is surface roughness for specular

samples. Although the instrument works well for rougher materials, there are benefits to running other instruments such as reflectometers with these samples, particularly when film degradation occurs.

Because there were in-flight measurements, it was determined that the bulk of the particulate contamination occurred after space exposure. Monitoring in-flight calibration factors were used to validate the operation of the TIS instrument.

The 532 laser measurements of Kapton suggest that this method could possibly be used as a low fluence AO monitor. TIS values at 1064 were flat, so choice of wavelength is important. More work needs to be done in this area to judge the feasibility of this approach.

The TIS has successfully measured highly specular samples for surface changes in the space environment. The Air Force sample ST01 and ST02 are prime examples. A possible application for measuring highly reflective surfaces in space would be to qualify materials for critical optical programs such as the Space Based Laser program. The TIS instrument could be used to determine survivability requirements for space optics based on surface changes. A TIS instrument that measures in transmission as well as reflection could be developed for transparent materials.

4.3 Vacuum Ultraviolet (VUV) OPM Data

The original intention of the VUV samples was to obtain on orbit insitu measurement data using the OPM VUV reflectometer. This data was not obtained due to a malfunction of the VUV source as described in Section 2.5. Thirty-two (32) VUV samples were flown on the OPM and exposed to the Mir space. A listing of these samples along with a sample description and the sample supplier is provided in Appendix A and Appendix J. Many of the OPM VUV samples were measured pre- and post-flight in the VUV by Rachel Kamenetzky of the MSFC. This VUV spectral data is shown in Appendix J Table J.1 and Figures J-1 through J-10. All other samples were returned to the sample suppliers for post flight analysis. It is anticipated that the sample supplier investigators will publish their own results in the open literature.

It is important to note that, as discussed in other sections, these samples were exposed to a high humidity environment inside the Mir prior to deployment. Since many of the VUV samples are (at least to some extent) hygroscopic, this exposure can and did affect the data. Samples of exposed Lithium Fluoride and Magnesium Fluoride show the greatest effect, as can be seen in their reflectance data in Figures J-4, J-5, and J-6.

All VUV data plotted in the Figures in Appendix J include reflectance values for one or two control mirrors used with the reflectometer. This data is plotted on "transmission" plots without designating that it is reflectance data. The MSFC VUV reflectometer is a single beam, specular type instrument, built by Acton Research. This single beam type reflectometer utilizes a single detector light pipe design coated with sodium salicyate to convert vacuum ultraviolet radiation into visible range for the detector. This detector system is rotated such as to measure the 100% signal, transmission, and/or reflection. MSFC uses a special 6 sample holder, one sample position is left open for 100% calibration measurements (performed at each wavelength), a second sample position is for the laboratory "control" mirror, and the other four positions are for samples. In some cases two "control" mirrors may be used for cross referencing and checking laboratory control mirrors. Additional laboratory storage control mirrors are maintained to verify the measurement controls do not change. All data is corrected for any system changes as detected by the control mirrors. This system and procedure has been utilized by MSFC since the late 1960s and has proven very reliable. Repeatability on a long-term basis (over several years) is within ±3% delta R/R

Data is not shown for the UTEM samples from NASA/LaRC and the College of William and Mary. The ground controls and flight samples both changed dramatically. These samples basically lost their reflectance in the vacuum ultraviolet region between 120 to 250 nm. We did observe a major difference in appearance between the flight exposed and ground control samples. Flight samples had a diffuse appearance while the ground control were still semi transparent with not obvious scattering except for surface manufacturing irregularities. It is left for the sample supplier to perform his material analysis to understand the mechanisms involved.

All VUV data plotted in Appendix J show significant changes in reflectance. As stated before the samples coated or composed of hygroscopic type material degraded the most, but all samples showed a loss in reflectance. The gold and platinum mirrors should be stable but show a

fairly uniform loss in reflectance from 120 to 250 nm (see Figures J-1 & J-8). Compare this data to Figure J-6 for the magnesium fluoride over aluminum mirror. The post-flight analysis of one of the TIS gold mirror (discussed in Section 4.3.2) measured ~100 Angstroms of silicate contamination. This thin but significant contaminate layer does not affect solar absorptance to any significant level, but does result in very significant changes in the vacuum ultraviolet region. Since the MgF_2/Al mirror is an interference coating with a thickness on the order of 250 Angstroms (~1/4 wave at 120nm), a thin layer of contamination acts as an additional interference layer. Previous data published by Linton[21], demonstrated the effect shown between the gold and MgF_2/Al. mirror. Gold can experience an overall drop in reflectance whereas the MgF_2 mirror can undergo increases/decreases in reflectance at various wavelengths dependent upon the overlying contaminates optical properties (n & k) and thickness.

As a comparison to the mirrors, refer to the window data in Figures J-4 and J-5, for Lithium Fluoride and Magnesium Fluoride windows. Since these are too thick to form interference effects, you don't see the same strange changes as for the MgF_2/Al. mirror. Instead, the overall transmission is reduced. When compared to the data in Figure J-2, J-3 and J-10; for quartz crystal, fused silicate, and sapphire windows respectively, you see less loss in transmission. At this time we contribute this reduction in transmission to materials that are not hygroscopic and should not have been affected by the high moisture and humidity level in the Mir internal environment. The difference in levels of transmission loss between these "stable" samples could be results of variations in deposition thickness. Temperatures can also greatly affect deposition, but since these are all window materials whose thermal optical properties are close, one would not expect major temperature differences. The other cause can be the difference in optical properties (n & k) between window materials in the 120 to 250 nm wavelength range and those for the silicate contaminant in the same wavelength range. Further studies will be required to evaluate the specific cause for the observed variations in degradation between the quartz, fused silica, and sapphire samples.

Changes in optical baffle coatings are plotted in Figure J-7 and J-9, for MLS85 and RM550B. Both of these are black diffuse type coatings. The reflectance values in the VUV were low to start with and did not change significantly after on orbit exposure, even with the 100 to 200 Angstroms of contamination.

4.4 Temperature Controlled Quartz Crystal Microbalance Data

The OPM Experiment used two TQCM sensors to monitor real time the molecular contamination environment to which the flight samples were exposed. TQCM sensors have become the standard for insitu measuring molecular deposition (contamination) in the space environment. These sensors have sufficient sensitivity and stability to measure partial monolayers of contamination, under a wide range of operating temperatures typical of the space environment, and capability of "self-cleaning" by driving off (at high temperature) volatile contaminants deposited on the sensor. One TQCM was held at –30 °C while the other was held at –10 °C. The sensitivity of the OPM TQCM is 1.6×10^{-9} g/cm^2/Hz. The beat frequency (difference) between the two crystals is monitored and recorded at one minute intervals by the OPM Data Acquisition and Control System (DACS). Over 190,000 data points were recorded

for the OPM TQCM sensors. Refer to the Experiment Description section for details of the TQCM design and integration into the OPM.

Figures 4-10 and 4-11 are summary graphs of the TQCM data from the OPM mission to Mir. Since the OPM power was off from June 26 until approximately September 9, 1997, the temperature of the TQCM crystals floated with the ambient thermal environment. The OPM TQCM data is presented for the two time periods. Figure 4-10 is for the time period from OPM deployment until power loss due to the Progress accident and is characterized by a number of mass gain events.

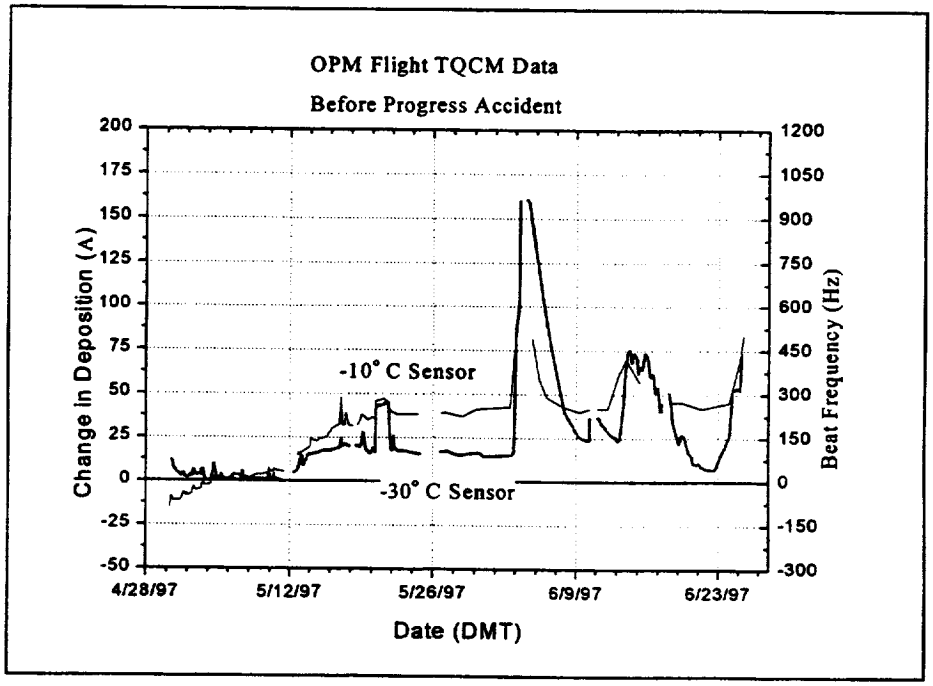

Figure 4-10. OPM Flight TQCM Data – Before Progress Accident

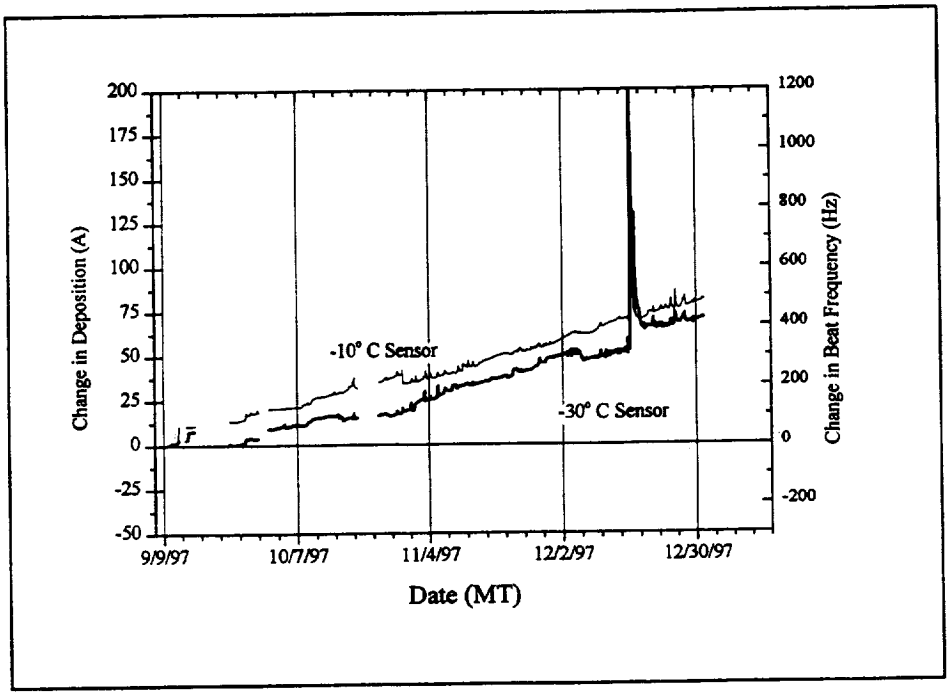

Figure 4-11. OPM Flight TQCM Data – After Power Restored

Most of the mass gain events are followed by the slower re-evaporation of this mass. This re-evaporation may have occurred because the mass gained was a volatile species that was not "fixed" on the surface by solar UV. The TQCM sensors had the same viewing angle as the sample array resulting in a minimum solar exposure for this time period. Without sufficient solar UV, a contaminant that condenses on a surface will re-evaporate but at a slower rate due to the sensor temperature. Solar UV can "fix" the contaminant on the surface by crosslinking the contaminant, which reduces the vapor pressure and prevents re-evaporation.

The mass event in early June 1997 is noteworthy because this occurred during a period of time when the Mir was in sunlight for the complete orbit. Figure 4.12 shows, for this time period, the measured beat frequency from both TQCM's on OPM compared to the time in shadow for the Mir space station. For this orbital condition, the Mir surfaces became significantly hotter, increasing outgassing rates. This resulted in a film thickness gain on the –30°C sensor of about 145Å (based on an assumed film density of 1 g/cm^3). As with the other events, most of the contaminant re-evaporated within a few days.

The TQCM data shown in Figure 4-11 is for the time period from September 9 until the end of the mission. Except for the major event in mid-December, the molecular deposition is very different from the earlier period with a fairly uniform accumulation rate for both sensors of about 20Å per month. This would seem to be a fairly small contamination rate except that it is significantly above the maximum rate allowed for ISS[17]. This rate is also of concern since the TQCM sensors viewed Mir modules that had been in space for six to eleven years and should be thoroughly baked out.

The mass event that occurred in mid-December is by far the largest TQCM event recorded on the OPM mission. Figure 4-13 is a more detailed view of this event for the –30° C sensor. This event represented a mass gain of 380Å for the –30°C sensor and 250Å for the –10°C sensor (based on an assumed density of 1 g/cm^3) This event did not occur instantaneously but rose in three steps over 28 minutes to its peak. As with most of the other events the accumulated film re-evaporated almost completely. The OPM attitude for this time period also resulted in a minimum of solar exposure for the TQCM sensor.

Attempts were made to correlate the mass gain events with Mir mission events but have been largely ineffective. Even the large event in December has not been correlated with a particular mission event. There were mission events in this time period that could have possibly caused a mass gain event. It has been very difficult to correlate the OPM system time with the Mir mission time. One of the problems is the difference between the OPM clock and the Mir mission clock that was caused by the numerous power interruptions in early September, 1997.

The molecular contamination levels measured by the OPM were lower than might have been expected from other measurements on Mir. This lower level is due to two factors. The view factor of the TQCM sensors (and test samples) is of 6-11 year old Mir modules that should be well baked out. In addition, the Mir attitudes resulted in minimum solar UV for much of the mission exposure on the OPM samples and TQCM sensors to "fix" the molecular contaminant onto the surfaces and prevent re-evaporation.

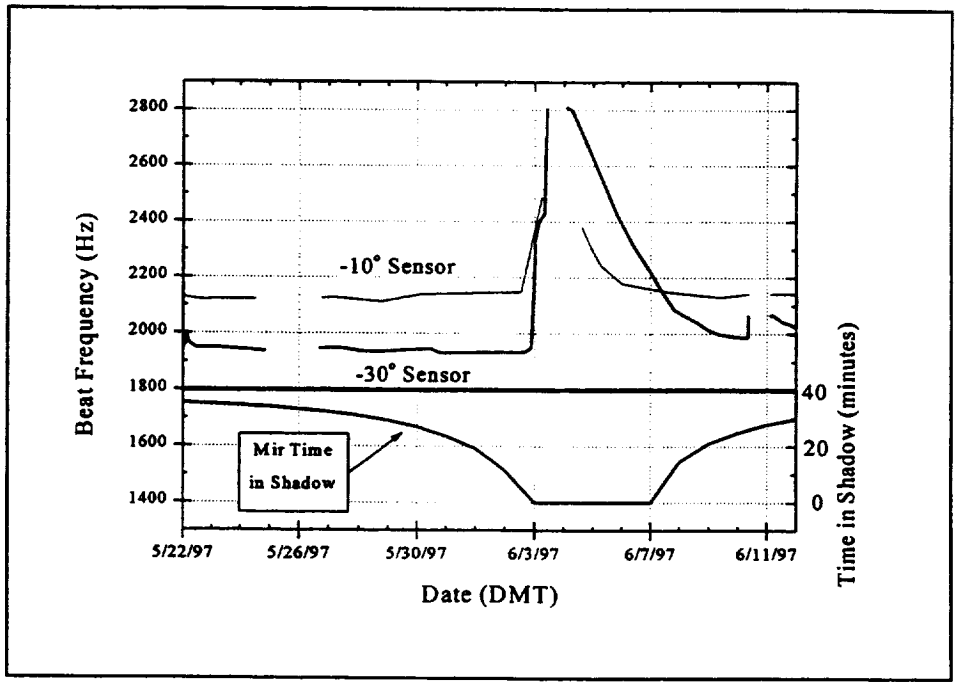

Figure 4-12. TQCM Flight Data vs. MIR Time In Shadow
For Full Sun Orbit Period – 6/3/97 to 6/7/97

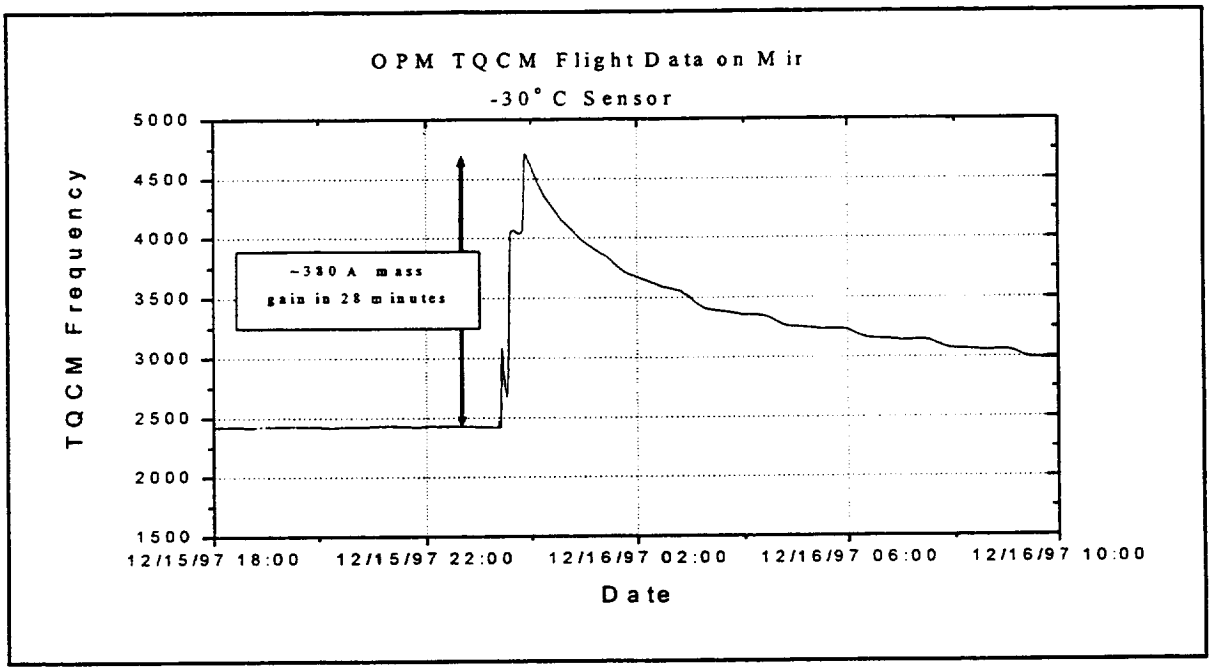

Figure 4-13. OPM TQCM Flight Data on Mir

The TQCM environmental monitor subsystem performed well. The control system performed exceptionally well and maintained thermal control at the defined set points of -10°C and -30°C, within ±2°C. The temperature data appeared to have noise on the reading of approximately 5° peak-to-peak. This noise was not observed in either pre- or post-flight testing. If these variations were really a variation in sensor temperature, this would have also significantly affected the frequency of the sensor, which was not observed.

One of the errors that must be considered in the analysis of TQCM flight data is the effect of orbital cycle solar heating on the TQCM crystals. Figure 4-14 shows the performance of the -30° TQCM sensor over several orbits on May 5, 1997. The OPM attitude data with respect to the sun is also shown. From this data the normal Mir attitude was solar inertial with the sun positioned just below the horizon for the OPM samples and TQCM sensors. The orbit to orbit variations of the sensor beat frequency during this period was due to the heating of the Mir surfaces in the field of view. Also, from this data, it can be seen that for one orbit, the Mir attitude changed to where the OPM TQCM sensors (and test samples) were at a near normal exposure to the sun. This resulted in a solar induced change of 90-100 Hz. This was typical of the maximum orbital variation observed for the Faraday laboratories TQCM sensors. The orbital variations, as shown in Figure 4-14 are very small due to the excellent thermal mounting of the two matched quartz crystals in the TQCM sensor.

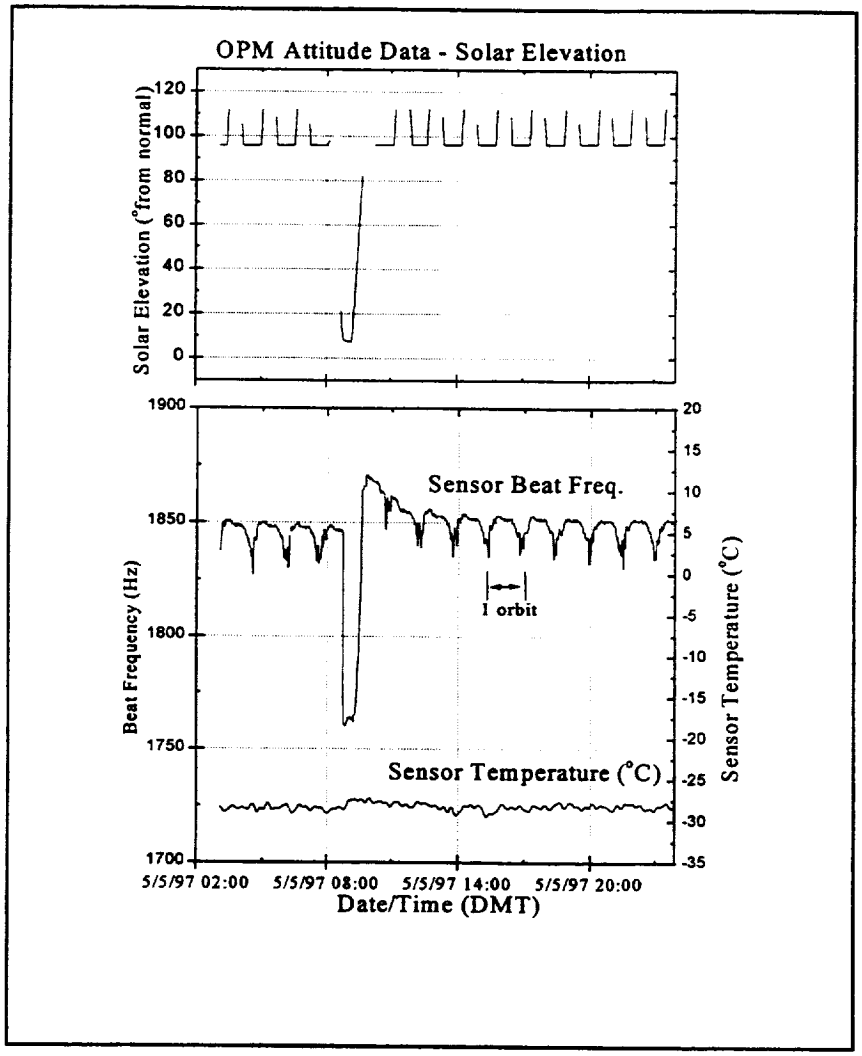

Figure 4-14. Comparison of TQCM and Attitude Data

4.5 Passive Samples

The OPM passive samples were exposed on the carousel along with the active samples but were not measured in-flight. There were twenty seven passive samples flown on the OPM. These samples were characterized prior to flight and then re-measured post-flight. Appendix A and Appendix I, Table I-1 provides a listing of these samples along with a sample description and the sample supplier. As the case for the active samples, the passive samples were protected until deployment and during retrieval by rotating the samples inside the OPM enclosure.

Detailed interpretation of passive sample results will be left to the sample supplier, to be published in the open literature. All of the thermal optical property measurements performed on the flight and control samples is listed in Appendix I. Table I-2 provides this detailed listing of thermal optical property measurements, including "pre-vacuum bakeout" data if taken. Samples that were not inherently "non-outgassing" went through a pre-flight thermal vacuum bakeout to

make sure they would not cross-contaminate the other samples. Table I-2 lists also the substrate used for the sample.

It is worthwhile to remember that any damage or changes measured on the ground may be different than what was the situation on-orbit. The atmosphere can bleach out some types of damage or might even enhance changes after return. Some of the samples returned from LDEF, on the TCSE experiment have continued to change since it returned in December 1989.[4-8] So one must be cautious in making conclusions only based on data from the passive samples.

The solar absorptance and thermal emittance of the passive samples were measured pre-and post-flight using AZ Technology LPSR-200IR and Temp-2000 instruments. The data are summarized in Table 4-6. Data are arranged so that the first line provides data for the flight exposed sample and directly below it is the data for the ground control sample. Two columns are highlighted which list the delta change measured for thermal emittance and solar absorptance. A quick scan of this data reveals that the majority of sample materials did not show any significant change in the 8 month exposure on the Mir. A few of the exceptions will be specifically discussed. Most of ISS baseline materials appear to be stable in that the change in the thermal optical properties is insignificant.

Sample SP15, which was a special thin film coating on a glass substrate (corning 7059), appears to have completely disappeared during on-orbit exposure. Since this coating was known to be very hygroscopic and since the OPM was exposed to excessive moisture and temperatures inside the Mir prior to deployment, this coating could have been compromised even before it was exposed. The excessive level of moisture was not anticipated. This occurred as the result of the on-board fire incident and resulting temporary lost in control of the internal environment. For this reason no post flight data was taken and any further analysis will be left to the sample supplier.

Sample SP28 appears to have changed significantly for both the flight and ground control. Figure 4-15 is a post-flight photograph of sample.

Since the measurement beam from the reflectometer overlaps the these measured changes are not accurate. The photograph of the flight sample does show the white background which is a form of "white anodize" did turn darker after the 8 month exposure on Mir. Note the difference in reflectance in the white background between the outer ring or edge and the inner area. The outer ring was protected by a Teflon retainer ring. A similar effect was found with the SP06 flight exposed sample shown in Figure 4-16. The white area is an anodized aluminum (alloy 1100 H14) supplied by Rocketdyne. The "X" is integrated into the anodized layer by a photographic process using silver compounds per Mil-P-15024D.

Table 4-6. Summary of Passive Sample Thermal Optical Properties

Description	Sample Number	Serial Number	Flight / Backup	Pre-Flight Hemispherical Total Emittance,	Post-Flight Hemispherical Total Emittance,	Delta Emittance	Pre-Flight LPSR Solar Absorptance	Post-Flight LPSR Solar Absorptance	Delta Absorptance
AO Resist. Diam.-like Nanocomp. Coatings (DYLYNTM) DLN-undoped	SP01	SP1-01	F	0.842	0.841	0.000	0.874	0.887	0.013
AO Resist. Diam.-like Nanocomp. Coatings (DYLYNTM) DLN-undoped	SP01	SP1-02	B	0.845	0.841	-0.004	0.874	0.879	0.005
AO Resist. Diam.-like Nanocomp. Coatings (DYLYNTM) DLN-30% Ti doped	SP02	SP2-01	F	0.711	0.744	0.033	0.762	0.795	0.033
AO Resist. Diam.-like Nanocomp. Coatings (DYLYNTM) DLN-30% Ti doped	SP02	SP2-02	B	0.713	0.721	0.007	0.758	0.769	0.011
TCOH-COTM - "6u" glass fabric	SP04	SP4-01	F	0.861	0.851	-0.010	0.317	0.307	-0.010
TCOH-COTM - "6u" glass fabric	SP04	SP4-02	B	0.859	0.861		0.293	0.296	0.003
Beta Cloth	SP05	SP5-01	F	0.877	0.877	0.000	0.299	0.344	0.045
Beta Cloth	SP05	SP5-02	B	0.878	0.876	-0.001	0.287	0.292	0.005
Black marking-Metalphoto	SP06	SP6-01	F	0.825	0.825	0.000	0.832	0.834	0.002
Black marking-Metalphoto	SP06	SP6-02	B	0.833	0.836	0.003	0.841	0.840	-0.001
Al 1st Surface Mirror Contam Monitor	SP10	SP10-01	F	0.015	0.017	0.002	0.079	0.083	0.004
Al 1st Surface Mirror Contam Monitor	SP10	SP10-02	B	0.016	0.012	-0.004	0.078	0.078	0.000
Defected Al on Kapton	SP11	SP11-01	F	0.026	0.023	-0.003	0.096	0.100	0.004
Defected Al on Kapton	SP11	SP11-02	B	0.023	0.023	0.000	0.115	0.114	-0.001
ISS Solar Array Blanket Face Sheet	SP12	SP12-01	F	0.871	0.871	0.000	0.934	0.938	0.004
ISS Solar Array Blanket Face Sheet	SP12	SP12-02	B	0.874	0.868	-0.005	0.933	0.939	0.006
Ir/Si Multilayer	SP14	SP14-01	F	0.172	0.182	0.010	0.410	0.438	0.028
Ir/Si Multilayer	SP14	SP14-02	B	0.170	0.183	0.012	0.410	0.415	0.005
OCLI coating over white Tedlar	SP16	SP16-01	F	0.796	0.799	0.003	0.328	0.335	0.007
OCLI coating over white Tedlar	SP16	SP16-02	B	0.797	0.801	0.004	0.329	0.329	0.000
Six layer stack on Si-wafer	SP17	SP17-01	F	0.727	0.723	-0.004	0.463	0.486	0.023
Six layer stack on Si-wafer	SP17	SP17-02	B	0.723	0.724	0.001	0.464	0.475	0.011
YB-71P, Zn2TiO4-Potassium silicate thermal coating	SP19	SP19-01	F	0.887	0.875	-0.012	0.128	0.128	0.000
YB-71P, Zn2TiO4-Potassium silicate thermal coating	SP19	SP19-02	B	0.895	0.893	-0.002	0.116	0.120	0.004
Z-93SC55	SP20	SP20-01	F	0.895	0.889	-0.006	0.136	0.135	-0.001
Z-93SC55	SP20	SP20-02	B	0.893	0.894	0.001	0.133	0.132	-0.001
S13GP/LO-1, Encapsulated ZnO in methyl silicone	SP21	SP21-01	F	0.902	0.895	-0.007	0.182	0.188	0.006

Description	Sample Number	Serial Number	Flight / Backup	Pre-Flight Hemispherical Total Emittance,	Post-Flight Hemispherical Total Emittance,	Delta Emittance	Pre-Flight LPSR Solar Absorptance	Post-Flight LPSR Solar Absorptance	Delta Absorptance
S13GP/LO-1, Encapsulated ZnO in methyl silicone	SP21	SP21-02	B	0.904	0.903	-0.001	0.180	0.180	0.000
Z24P binder w/ZnO pigment + 2% Sodium Salicylate by wt	SP23	SP23-01	F	0.910	0.905	-0.005	0.216	0.250	0.034
Z24P binder w/ZnO pigment + 2% Sodium Salicylate by wt	SP23	SP23-02	B	0.914	0.911	-0.003	0.215	0.209	-0.006
Silver Teflon 5 mil 2-1/2" x 3/4"	SP24	SP24-01	F	0.709	0.727	0.018	0.074	0.092	0.018
Silver Teflon 5 mil 2-1/2" x 3/4"	SP24	SP24-02	F	0.709	0.731	0.022	0.072	0.086	0.014
Silver Teflon 5 mil 2-1/2" x 3/4"	SP24	SP24-03	B	0.704	0.711	0.008	0.073	0.067	-0.006
White Paint Z24P Binder w/ZnO Pigment	SP25	SP25-01	F	0.905	0.898	-0.007	0.240	0.251	0.011
White Paint Z24P Binder w/ZnO Pigment	SP25	SP25-02	B	0.899	0.897	-0.002	0.236	0.235	-0.001
EVA Label - Blue	SP26	SP26-01	F	0.787	0.804	0.017	0.519	0.544	0.025
EVA Label - Blue	SP26	SP26-02	B	0.786	0.791	0.005	0.518	0.520	0.002
EVA Label - Red	SP27	SP27-01	F	0.754	0.770	0.017	0.507	0.510	0.003
EVA Label - Red	SP27	SP27-02	B	0.756	0.764	0.008	0.509	0.506	-0.003
EVA Label Decal	SP28	SP28-01	F	0.829	0.834	0.005	0.380	0.467	0.087
EVA Label Decal	SP28	SP28-02	B	0.815	0.816	0.001	0.663	0.504	-0.159
ATR Crystal-Zinc Selenide	SP29	SP29-01	F	0.741	0.744	0.003	0.701	0.710	0.009
ATR Crystal-Germanium	SP30	SP30-01	F	0.535	0.542	0.007	0.542	0.561	0.019
ATR Crystal-Germanium	SP30	SP30-02	B	na	0.538		na	0.543	
Kapton (1 layer)	SP31	SP31-01s	F	0.883	0.881	-0.001	0.879	0.909	0.030
Kapton (1 layer)	SP31	SP31-02s	B	0.885	0.881	-0.004	0.879	0.883	0.004
AZBEC-1	SP32	SP32-01	F	0.879	0.876	-0.003	0.955	0.956	0.001
AZBEC-1	SP32	SP32-02	B	0.880	0.876	-0.004	0.954	0.961	0.007
AZWEC-2I	SP33	SP33-01	F	0.911	0.901	-0.010	0.171	0.168	-0.003
AZWEC-2I	SP33	SP33-02	B	0.913	0.910	-0.003	0.174	0.172	-0.002

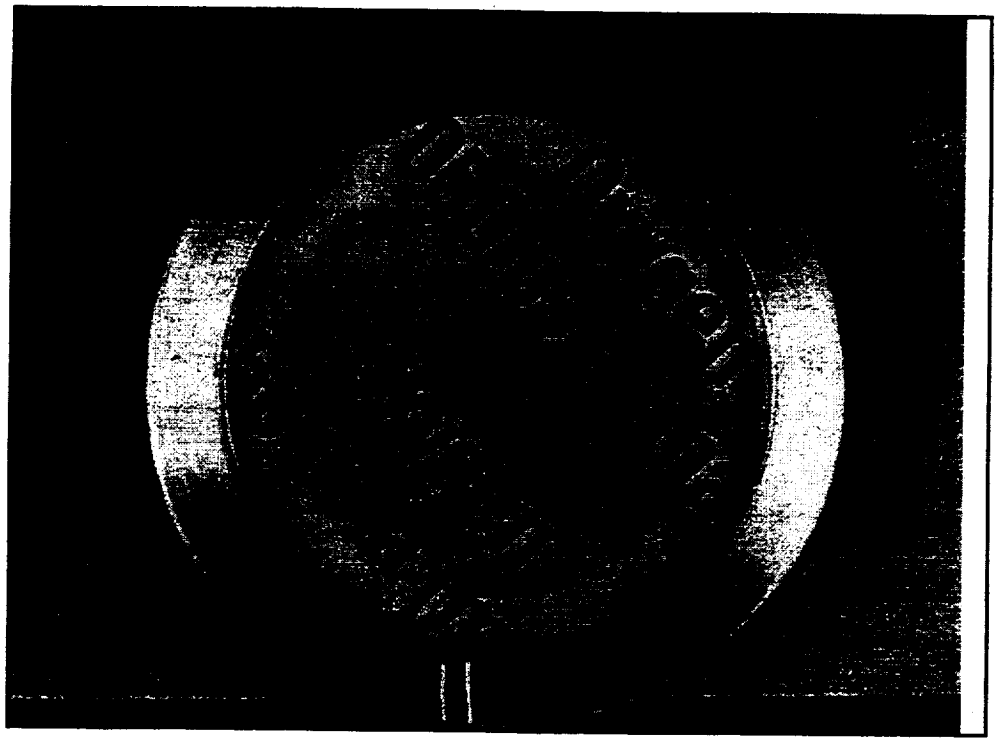

Figure 4-15. Post Flight Image of Sample SP28; Space Exposed

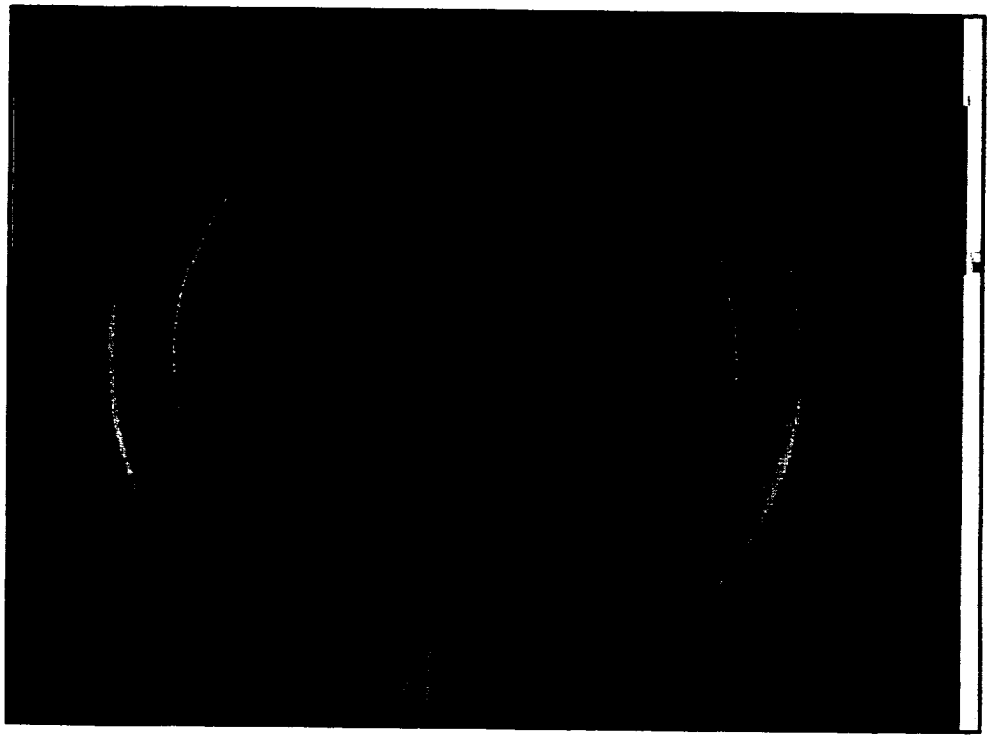

Figure 4-16. Post Flight Image of Sample SP06; Space Exposed

4.6 Multi-layer Insulation (MLI)

As part of the thermal control system, the sides of OPM were covered with multi-layer insulation (MLI) blankets. The outer layer of the MLI is a Beta Cloth (type 500F) manufactured by Chemfab. This particular Beta Cloth material was procured with one side treated with DF-1100 by Chemfab in order to achieve good bonding of the required identification labeling. The treated side of the Beta Cloth was the side exposed to the space environment.

Figures 4-17 is a pre-flight photograph of OPM showing the initial condition of the MLI blankets and other OPM surfaces. Figure 4-18 shows the post-flight condition of the OPM. Notice that the left end of OPM is significantly discolored. A distinct shadow is evident behind the EVA handrail on the MLI. The degradation of the MLI is due to a combination of UV degradation of the beta cloth outer covering of the MLI and molecular contamination (which was also degraded by solar UV). Measurements of the MLI show that the solar absorptance increased to a value of 0.49 from the initial value of 0.25. As discussed in Section 3, the sides of the OPM were exposed to very different levels of solar exposure. This solar exposure difference is evident by the degradation observed on the sides of OPM.

As shown in Section 4.7, contamination analysis shows that only a small level of contamination (~40 Angstroms) was deposited on the left end of the OPM. This data indicates that the darkening of the Beta Cloth was the result of mainly solar ultraviolet radiation with only a very insignificant amount due to contamination. In order to confirm the ultraviolet darkening effect, samples from the same lot of Beta Cloth as used on the OPM were supplied to the NASA/MSFC, R. Kamenetzky/M. Finckenor for an exposure test in a space environmental effects solar ultraviolet simulation system. Results from these tests[22] confirmed the magnitude of the degradation of the OPM MLI on the Mir mission. Table 4-7 compares the results of the MSFC ground tests using Beta Cloth samples from the same lot as the flight MLI. These tests also show that the DF-1100 treatment does cause increased degradation in a solar UV environment.

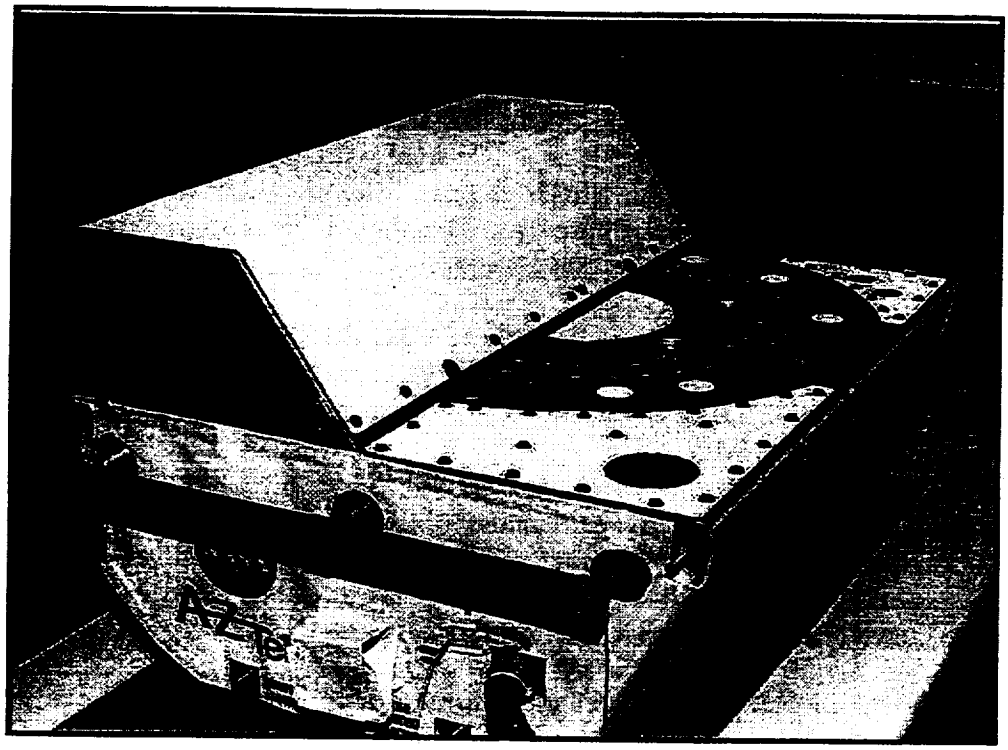

Figure 4-17. Pre-flight Photograph of the OPM.

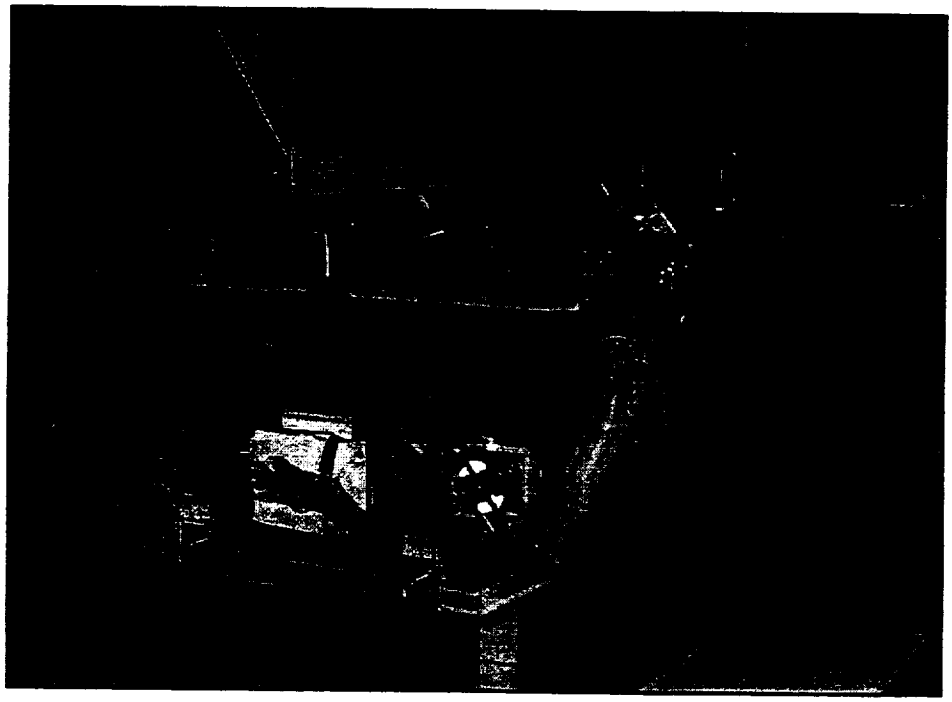

Figure 4-18. Post-flight Photograph of the OPM.

Table 4-7. Degradation of Beta Cloth in Flight and Ground Testing

Sample	Flight/Ground	UV Exposure	Initial α_S [*]	Final α_S	Change in α_S
OPM Flight MLI Blanket Left End - Treated	Flight Exposed	2903 ESH	0.25	0.49	0.24
OPM Flight MLI Blanket Right End - Treated	Flight Exposed	379 ESH	0.25	0.36	0.11
OPM Flight Material Same Lot Treated	Ground Test	500 ESH	0.37	0.53	0.16
OPM Flight Material Same Lot Untreated	Ground Test	500 ESH	0.38	0.43	0.05
* Differences in the initial measurement of α_S result from the high transparency of Beta Cloth. The backing material affects the absolute α_S value. Flight exposed Beta Cloth values were measured on the assembled MLI blanket while the ground test Beta Cloth sample was measured separately.					

4.7 Material Analysis XPS/ESCA

Chemical analysis of several of the OPM surfaces and samples was performed to better understand the amount and composition of the contaminant films deposited during the Mir mission. Additional analysis was performed on selected samples and ground controls to analyze their surface composition and how this changed due to exposure to the Mir space environment.

4.7.1 XPS/ESCA Chemical Analysis of OPM Surface Hardware

ESCA chemical analysis of two sections of the OPM structure were performed by N. Carl Miller, of Raytheon System Company, in Lexington, Massachusetts. Depth profiling was also performed on the exposed side of each of the two samples, in order to determine the thickness of contamination layers. The sample from the Carousel Cover Panel was exposed to the same environment as the TQCM sensors and the OPM samples. The interface plate sample was exposed in the same direction as the MLI blanket on the left side of the OPM as viewed in Figure 2-1 and 3-4. Table 4-8 presents a summary of the data showing the composition of the contamination measured on the exposed surfaces. ESCA analysis found that the major contaminate was silicate in the form of silicon dioxide on the exposed surface, which agrees with other analysis on samples exposed to the space environment[4-8,17] Depth profiling of the hardware samples indicated that the sample from the Carousel Cover Panel had a 150 Angstrom layer of silicon dioxide on the surface of the aluminum, while the sample from the interface plate had a 40 Angstrom layer of silicon dioxide on the aluminum.

Table 4-8. ESCA Surface Composition (Atomic Percent)

Sample	Al.	Si.	O	C	N	F	S	Cl	Na	Zn	Ca
Interface Plate	6.12	9.72	54.89	24.56	1.59	1.95	.46	.46	0.24	-	-
Carousel Cover Panel	2.5	17.28	59.9	19.19	0.4	0.22	-	.23	-	.09	.19
"control" not exposed	-	1.72	27.8	66.02	2.01	1.03	.21	.25	0.55	.18	.22

4.7.2 XPS/ESCA & SEM/EDAX Chemical Analysis of Selected OPM Calorimeter Samples

Referencing the depth profile scans are included in Appendix F and the survey spectrum runs are in Appendix G, and the SEM/EDAX data is in Appendix H.

Another set of OPM samples was taken to WSTF for X-ray photoelectron spectroscopy (XPS) analysis. Twelve of the calorimeter samples used for the reflectometer were selected. In addition one gold mirror and one sample of the inorganic binder (potassium silicate) as used with Z93P and AZ93P were analyzed. The binder data was used to provide accurate binding energy values for both potassium and silicate in the potassium silicate compound in order to help discriminate the types of bonding species from the flight and control sample XPS data.

These measurements were performed by Steve Hornung of the WSTF as directed by the JSC Materials and Failure Analysis Branch in support of the ISS Boeing contamination analysis and control team under the direction of Ron Mikatarian. This analysis was coordinated by Jim Visentine of Boeing. The following section incorporates the summary report from Steve Hornung/WSTF expanded to include additional data and interpretation of results.

The purpose of this analysis was to provide for additional in-depth material analysis in an effort to determine the effect of the space environment including contamination on thermal control coatings used on the ISS. XPS and SEM/EDAX were used for this analysis to determine the elemental composition and chemical state of the contaminant layer and to characterize the chemical composition of the surface as a function of depth.

4.7.2.1 Samples Tested

The calorimeters consisted of an aluminum body which supported a thermally and electrically isolated substrate to which the thermal control coating was applied. The thermal control coating, designated Z93P or AZ93, consists of zinc oxide with a potassium silicate binder. Some of the samples were pre-contaminated with offgased products from heated Tefzel or silicone. One pair of samples was coated with a special DuPont fluorocarbon formulation (designated as Teflon in this report). All pre-contaminated samples were exposed preflight to 2-days exposure to near UV radiation and 5000 equivalent solar hours of vacuum UV before flight. This was done in an effort to determine the magnitude of atomic oxygen cleaning of contaminated surfaces after extensive solar ultraviolet irradiation, that served to fix or cross-link the material on the surface, prevent cross-contamination, and provide accelerated data (since the Mir exposure time was limited). A special mounting fixture had to be designed and fabricated to mount the calorimeter on the sample holder used for analysis. Twelve calorimeters and one gold mirror on a silica substrate were analyzed, reference Table 4-9 for a listing of the calorimeter samples, their ID's, description, ground environmental exposure, and fight environmental exposure.

4.7.2.2 Method

XPS was performed on selected areas of each calorimeter using a Physical Electronics 5600 surface analysis system. For each area analyzed, a survey spectrum was acquired using magnesium (Mg) kα x-rays with a nominal pass energy of 190 electron volts (eV) in the binding energy range of 0 to 1150 eV. The elements on the surface were identified, and high-resolution spectra of the primary photoelectron peaks of these elements were obtained using Mg kα x-rays at a nominal pass energy of 11 eV. From the high-resolution spectra, the atomic concentrations, given in atomic percent, were calculated using the peak area and sensitivity factors in the instrument software. The binding energies of the elements were also determined from the high-resolution spectra. Depth profiles were obtained on each of the calorimeters to determine the elemental distribution in the surface layers of the plates. Argon ions accelerated to 4 kV were used to remove material for the depth profile at a rate of 100 angstroms (Å) per minute as determined on a 1000 Å silicon dioxide on silicon (SiO_2 on Si) standard.

In addition to the XPS scans, small sections of each of the calorimeter samples were overcoated with a conductive layer and then SEM images were made of each of these areas. Along with the SEM images, three EDAX scans were made of interesting features on Z93P, sample AZC032 and the 2000A Silicone on Z93P AZC037.

4.7.2.3 Discussion of Results for Each Sample

Gold Mirror: High Purity Gold on a Polished Fused Silica Substrate

Figure G-1 shows the survey spectrum from the surface of gold mirror; carbon, oxygen, and silicon are detected on the surface in addition to a small amount of gold. The peaks are labeled with the associated energy levels (-Au 4f, -C 1s) or the Auger peak designation (-O KVV, -C KLL). Subsequent high-resolution spectra were processed to give the following atomic concentrations: Carbon 10.2 %, oxygen 58.6 %, gold 0.6 %, and silicon 30.6 %. The binding energy from the silicon 2p high resolution spectrum shown in Figure G-3 was determined to be 103.8 eV, which is consistent with a silica, most likely formed from the action of atomic oxygen on the silicone contamination deposited on orbit. Figure F-13 in Appendix F is the depth profile of this deposit and indicates a silica thickness of 90 to 100 Angstroms. Figure G-2 is a survey spectrum taken following the depth profile run and shows only the presence of gold.

Z93P White Ceramic Paint, AZC032 and AZC033.

The survey spectra from the ground control and the flight samples are given in Figures G-4 and G-5. The ground control sample shows the presence of carbon, silicon, potassium, oxygen, and zinc. The atomic concentrations calculated from the high-resolution spectra are given in Table 4-10 and show carbon, at a concentration of 61% to be the predominant constituent on the surface. The flight-exposed sample shows the same elements present on the surface with a greatly reduced carbon concentration and higher concentrations of the constituents of the Z93P paint. The depth profiles shown in Figures F-3 and F-4 in Appendix F confirm that the carbon layer is primarily confined to the top 200 Angstroms of the surface in both samples. This is consistent with the behavior of "adventitious" carbon, which is present on most samples due to the presence of organic contaminants in our environment. With respect to concentrations of the other elements the depth profiles are otherwise similar, the potassium and silicon drop slightly while the zinc steadily increases until a depth of approximately 800 Angstroms, where it reaches a steady value. Both profiles show transitions from the surface layer containing the adventitious carbon to a potassium, silicon, oxygen, containing layer and finally to a layer which also contains zinc. This behavior is expected since the zinc oxide particles are coated with a potassium silicate binder. This transition from surface layer to potassium silicate binder to binder and zinc oxide is seen in all subsequent Z93P samples. The binding energies from the zinc are consistent with the oxide and the silicon is consistent with a silicate. Figures G-6 and G-7 are survey spectra taken following the depth profile for the ground control and the flight sample. The elemental constituents of the paint, silicon, potassium, oxygen, and zinc are present.

An interesting phenomena occurred during the depth profile runs for all of the Z93 type coatings. Typically what was found, once the "adventitious" carbon layer was removed, was that

a thin layer of binder material composed of potassium silicate covers the zinc oxide pigment. The potassium and silicon signals drop off fairly quickly as sputtering progressed. The zinc and oxygen signals dominate, then reach fairly steady values within "800 to 1000" Angstroms sputter depth, dependent upon the sample. As can be seen in all of the SEM photos taken for Z93 type coatings (refer to Figure H-1 and H-2 for Z93P) this is a very rough surface and porous with a lot of structure. What occurs during the sputtering of the surface is the removal of the potassium silicate binder covering the pigment particles. In addition remember that the pigment (zinc oxide) to binder (potassium oxide) ratio is approximately 4 to 1 (by weight), so there is considerably more zinc than silicon. As this surface coating material is removed the "round" pigment particles of zinc oxide are exposed. As more material is removed their exposed surface area (Zn and O) increases rapidly with depth or erosion of the roughly spherical particles. Eventually the Zn and O nominates. Note that the O signal also derives from the oxygen in the binder. It is difficult to separate the oxygen spectra from that originating in the ZnO to that originating in the KSiO4. For other samples the oxygen signal also gets contributions from the converted contaminant layers of both the silicone and silicates.

On a rough surface, there is shadowing of the ion beam due to the topography of the sample on a microscopic scale, plus the differing angles of view of the ion gun, x-ray source, and electron energy analyzer. This means that even if a uniform layer of contaminant were on the surface, a sharp interface would not be evident in the depth profile. In other words it is difficult to distinguish the relative thin ~100 A of silicate contamination layer on Z93P type coatings given the existing silicate and oxygen elements and the very rough and porous nature of these ceramic coatings. Refer to Appendix H where the SEM photographs are included. They show clearly the level of porosity, approximately 40%, that is present on all of the Z93P and AZ93P surfaces.

AZ93 White Ceramic Paint with Teflon Overcoat, AZC017 and AZC018

The survey spectra from the ground control and flight samples are given in Figures G-8 and G-9. Carbon, fluorine and a trace of oxygen are the only elements detected on the surface of the ground sample. The flight-exposed sample shows predominantly carbon and fluorine with small amounts of oxygen and silicon. The atomic concentrations calculated from the high-resolution spectra are given in Table 4-10 and show carbon and fluorine to be the only elements with apparent high concentrations at the surface. Depth profiles on this pair of samples are shown in Figures F-1 and F-2. The fluorocarbon layer on the ground control sample shows near complete coverage to a depth of approximately 200 Angstroms. From 200 Angstroms to 400 Angstroms is a transitional layer between the complete coverage and the bulk concentrations, beginning at a depth of approximately 400 Angstroms. This transitional region may be due to shadowing of the ion gun by the rough surface. Also, due to this shadowing, fluorine is detectable throughout the depth profile. The flight-exposed sample shows similar behavior with slightly elevated carbon concentrations near the surface. Figure G-11 shows a Survey Spectrum of the flight-exposed sample following the depth profile. Carbon and fluorine are detected in addition to the silicon, oxygen, and zinc from the bulk coating. This post-depth profile spectrum is representative of both the ground control and the flight exposed sample. SEM images presented in H-7 and H-8 ground and flight exposed samples, show that the Teflon overcoat is indeed partly eroded away by atomic oxygen exposure. On the other hand the

surface survey spectrums in Figures G-4 and G-5 indicate that the Teflon coating is still present. The depth profiles in Figures F-1 and F-2 again show that some Teflon is still present. The magnitude of this difference does not appear to be as great as indicated from the SEM photos, which appear to show that most, if not all the Teflon has been removed from the flight exposed sample. What is interesting is the depth that the fluorine signal persists (> 800A), indicating that the Teflon overcoat is fairly deep into the porous coating or that the fluorine has reacted with the silicate form a fluoro-silicate.

500 Angstroms Tefzel on Z93 White Ceramic Paint, AZC027 and AZC028

The survey spectra for the ground and flight exposed samples show the constituents of the paint, silicon, potassium, oxygen, and zinc. The ground control sample shows significant carbon and a small amount of fluorine. The flight-exposed sample shows less carbon and only a trace of fluorine. The flight-exposed sample also shows high surface concentrations of zinc. The atomic concentrations calculated from the high-resolution spectra are given in Table 4-10. The depth profiles for theses samples are given in Figures F-5 and F-6. The flight sample shows a significant drop in both the amount and thickness of the surface carbon. Only a trace of fluorine was detected on the flight sample and was not detected throughout the depth profile.

2000 Angstroms Tefzel on Z93P White Ceramic Paint, AZC029 and AZC030

The survey spectra for the ground control and flight exposed samples treated with 2000 Angstroms of Tefzel offgas products are given in Figures G-12 and G-13. The 2000 Angstrom thickness was calculated from deposition rates calculated from a quartz crystal microbalance. The ground control sample, AZC030, shows the presence of carbon, oxygen, potassium, and fluorine with a trace of silicon. The flight exposed sample shows an elemental composition more consistent with the bulk potassium silicate/zinc oxide coating with a small amount of fluorine. The elemental compositions of the two samples determined from high-resolution spectra are given in Table 4-10. Figures F-7 and F-8 are the depth profiles for the ground and flight exposed samples. The ground control samples shows an enriched carbon layer approximately 500 Angstroms thick. Oxygen, potassium, and fluorine are also apparent in the top 500 Angstroms. The fluorine concentration drops to the noise level at approximately 700 Angstroms at which depth the elemental composition is characteristic of the bulk coating. The flight exposed sample shows much lower surface carbon and a nearly immediate appearance of the binder layer.

500 Angstroms Silicone on Z93P White Ceramic Paint, AZC034 and AZC035

The survey spectra for the ground control and flight samples show carbon, oxygen, silicon, and potassium. The flight-exposed sample shows much lower surface carbon and increased amounts of silicon, oxygen, and zinc. The atomic concentrations determined from the high-resolution spectra for both the ground control and flight sample are given in Table 4-10. From the silicon 2p high-resolution spectrum, the charge-corrected binding energy of the ground control sample was determined to be 102.3 eV, which is consistent with a silicone compound. The charge corrected binding energy of the silicon 2p peak on the flight exposed sample is 103.3 eV which is characteristic of a silica compound. For comparison, the silicon 2p binding energy obtained from a potassium silicate reference material is 102.4 eV, which again supports the interpretation that the flight sample has a silica coating. The depth profiles for these samples are shown in Figures F-9 and F-10. From the depth profile data, the ground control sample data indicates a carbon-rich surface layer approximately 400 Angstroms thick, which also contains

silicon, oxygen and potassium. From the elemental make-up of this surface layer, the silicone appears to have in some way permeated the potassium silicate layer. By a depth of approximately 500 Angstroms the bulk containing the zinc oxide along with the potassium silicate is evident. This agrees fairly well with the original data from MDAC/Boeing that showed a deposition of ~500 Angstroms of silicone, based on the TQCM data taken during sample preparation. The flight sample depth profile indicates only a very thin carbon layer on the surface of the sample, which disappears within the first 50 Angstroms. All of this data supports the analysis that the original (~500Å) silicone layer deposited on the flight sample was converted to a silicate during exposure to the Mir space environment. The residual thickness of the silicate layer on the flight exposed sample is difficult to determine with any exact value as is further discussed in the contamination section.

2000 Angstroms Silicone on Z93P White Ceramic Paint, AZC036 and AZC037

Survey Spectra for the ground control and flight exposed samples are shown in Figures G-16 and G-17. The ground control sample shows predominantly carbon and oxygen with silicon, potassium and a small amount of zinc. A trace of sulfur was detected as well. In addition, the silicone charge corrected binding energy from the high resolution silicon 2p spectrum is 102.2 eV originating from the surface contaminant on the ground sample correlates with silicon bonded in a silicone structure. Figure G-18 shows the details of this scan. The flight exposed sample shows much lower surface carbon with an increase in the silicon and oxygen concentration. Potassium and zinc were also detected. The atomic concentrations are given in Table 4-10. Binding energy analysis of the silicon 2p peak of the flight-exposed sample is 103.4 eV, which is consistent with a silica compound, see Figure G-21. One can see clearly that the original surface silicone has converted to a silicate after exposure to the space environment. Depth profile scans are given in Figures F-11 and F-12, indicating the depth in the coating that this conversion has occurred. It appears from Figure F-11 that the all of the silicone has been converted. If carbon is used as a guide, then depth profile data shows that the carbon reaches the Z93P residual level within ~800 Angstroms. From the high resolution data, we also know that the silicon on the surface of the flight sample is associated with a silicate not a silicone, similar to the Z93P sample with 500 Angstroms of silicone.

If we compare the depth profile data for the ground samples only in Figures F-10 and F-12, then it is easy to see that the indicated quantity of original silicone contamination is greater on the 2000A sample than on the 500A sample. The question is whether or not the mass per unit area is four times as great between the two samples as originally prepared?

Surface Features on Flight Samples

From the SEM imaging of the flight exposed Z93P control sample (AZC032), what appears as two different types of growth features were found on the surface of the Z93P coating. One is referred to as "crystal" since it has more of a bulk crystalline form, whereas the other is referred to as "mica" since it has more of a layered or platelet growth form. Figure H-2 clearly shows these two features. Figures H-3 and H-4 are close-ups of each of these two types of features. EDAX scans were performed on each of these two features as shown in Figures H-5 and H-6. Both show strong peaks of potassium (K) and zinc (Zn). Interestingly, the crystal type structure has a higher ratio of K than Zn, whereas the mica has more Zn than K. In order to verify the previous EDAX scans, another scan was performed on the 2000A Silicone on Z93P

verify the previous EDAX scans, another scan was performed on the 2000A Silicone on Z93P (AZC037) sample. SEM images of this sample also showed the "mica" type structure, but not the "crystal" type structure (see Figure H-14). An EDAX scan was made on this feature resulting is spectra shown in Figure H-15. These data are consistent in that the Zn signal is considerably greater than the K, which is the same result found for the mica structure on the Z93P (AZC032). It should also be noted that the samples coated with Teflon or the offgasing products of Tefzel did not show any of this growth.

This growth has not been seen before on space exposed Z93 coatings, including the 6-year exposed surfaces on LDEF, and the other passive samples on Mir (POSA I)[17]. The difference with these samples is that they were stored inside the Mir and exposed to its environment. The OPM was in a protective bag, but that bag "breathed". OPM was exposed during the on board fire on Mir and other events. Records indicate very high moisture levels. Post-flight inspection of OPM found what appears to be indications that considerable condensation occurred on some of the OPM surfaces. In the laboratory it has been found that if these coatings are exposed for extended times to high humidity and temperature, then carbonaceous type growth initiates at the aluminum/coating interface and grows through the surface. In time these appear as fine crystals. Normally, the coatings never see this kind of environment. Most environments in the laboratory and where spacecraft are handled never reach these excessive levels of moisture and temperature, so this normally is not a problem.

Table 4-9. OPM Carousel Samples for SEM/ESCA/XPS Analysis

SAMPLE ID # [1] SR#	SAMPLE ID # [1] CR#	SAMPLE ID # [1] AZC#	FLT OR GROUND EXPOSED	SAMPLE DESCRIPTION	GRD. PROCESSING		FLT. ENVIRONMENT		
					GRD EXP NUV (~2DAYS)	GRD VUV ESH'S	FLT. SOLAR ESH'S	AO FLUENCE [2]	FLT. CONTM. A
SR12-02	CR19	AZC037	FLIGHT EXPOSED	2000A silicone precontaminated on Z93P white ceramic paint	YES	5,000	832	7.4E20	150 to 180
SR12-01	NA	AZC036	GROUND CONTROL	2000A silicone precontaminated on Z93P white ceramic paint	YES	5,000	-0-	-0-	-0-
SR9-01	CR20	AZC029	FLIGHT EXPOSED	2000A Tefzel precontaminated on Z93P white ceramic paint	YES	5,000	832	7.4E20	150 to 180
SR9-02	NA	AZC030	GROUND CONTROL	2000A Tefzel precontaminated on Z93P white ceramic paint	YES	5,000	-0-	-0-	-0-
SR11-02	CR17	AZC035	FLIGHT EXPOSED	500A silicone precontaminated on Z93P white ceramic paint	YES	5,000	832	7.4E20	150 to 180
SR11-01	NA	AZC034	GROUND CONTROL	500A silicone precontaminated on Z93P white ceramic paint	YES	5,000	-0-	-0-	-0-
SR8-02	CR18	AZC028	FLIGHT EXPOSED	500A Tefzel precontaminated on Z93P white ceramic paint	YES	5,000	832	7.4E20	150 to 180
SR8-01	NA	AZC027	GROUND CONTROL	500A Tefzel precontaminated on Z93P white ceramic paint	YES	5,000	-0-	-0-	-0-
SR10-01	CR16	AZC032	FLIGHT EXPOSED	Z93P FLIGHT CONTROL	NO	-0-	832	7.4E20	150 to 180
SR4-01	CR07	AZC018	FLIGHT EXPOSED	AZ93 with Teflon overcoat	NO	-0-	832	7.4E20	150 to 180
SR4-02	NA	AZC017	GROUND CONTROL	AZ93 with Teflon overcoat	NO	-0-	-0-	-0-	-0-
SR10-02	NA	AZC033	GROUND CONTROL	Z93P white ceramic paint sample	NO	-0-	-0-	-0-	-0-

[1] CR: Carousel ID#; SR: Sample ID#; AZC: Number on Calorimeter

[2] Atomic oxygen fluence in atoms/cm^2 .

Table 4-10. Surface Elemental Concentrations from Optical Properties Monitor

AZC Number	Sample Description	Elemental Concentration (atomic percent)					
		Carbon	Oxygen	Potassium	Silicon	Zinc	Fluorine
AZC033	Z93 White Ceramic Paint Ground Control	61.1	23.7	8.2	6.6	0.4	--
AZC032	Z93 White Ceramic Paint Flight Exposed	30.7	41.4	7.2	18.5	2.2	--
AZC017	AZ93 with Teflon Overcoat Ground Control	38.6	0.4	--	--	--	61
AZC018	AZ93 with Teflon Overcoat Flight Exposed	35.1	4.2	--	1.6	--	59.1
AZC027	500 Angstroms Tefzel on Z93P Ground Control	66.9	19.6	8.6	3.5	0.2	1.2
AZC028	500 Angstroms Tefzel on Z93P Flight Exposed	26.5	44.2	7.4	19.3	2.6	0.1
AZC030	2000 Angstroms Tefzel on Z93P Ground Control	60.8	23.6	11.6	0.6	--	3.5
AZC029	2000 Angstroms Tefzel on Z93P Flight Exposed	28.0	42.9	8.3	16.8	2.8	1.4
AZC034	500 Angstroms Silicone on Z93P; Ground Control	68.5	20.2	6.3	4.6	0.4	--
AZC035	500 Angstroms Silicone on Z93P; Flight Exposed	24.7	44.7	5.6	23.3	1.8	--
AZC036	2000 Angstroms Silicone on Z93P, Ground Control	63.7	20.5	6.9	7.3	0.3	--
AZC037	2000 Angstroms Silicone on Z93P, Flight Exposed	19.3	52.1	4.8	23.2	0.7	--

4.8 Results/General Observations

4.8.1 Molecular Contamination

The molecular contamination levels measured by the OPM TQCM (180 Angstroms) and measured on the OPM hardware surfaces (40 to 150 Angstroms) were lower than might have been expected from other measurements on Mir[17] (260 to 10,000 Angstroms). This lower level is due to several factors. The view factor of the TQCM sensors (and test samples) was of 6-11 year old Mir modules that should have been thoroughly vacuum outgassed. In addition, the Mir flight attitude resulted in minimum solar UV exposure of the OPM samples to "fix" the molecular contaminant onto the surfaces and prevent re-evaporation. Exposure time to the Mir space environment was twice as long for the MEEP passive experiments than for the OPM samples. The large 10,000 Angstrom deposition measured on the MEEP/POSA-I experiment appeared to originate from a stored Mir solar array located on the docking module which had been in space approximately 4 months at the time of MEEP/POSA-I deployment. In addition, the side of POSA-I exposed to the solar array was only a couple of meters distance. The OPM samples did not have direct line-of-sight to this stored solar array.

Samples on the other side of the POSA-I experiment faced the older Mir modules similar to the OPM samples. The level of contamination (260 Angstroms) on POSA-I agrees with OPM data when the longer POSA-I exposure time (~x2) is considered. Table 4-11 compares the OPM contamination with the POSA-I levels for Mir. Only the samples facing the older Mir modules are compared. It can be seen that the correlation of deposition with time is very good, while the correlation with ESH is very poor. One would expect the ESH correlation to agree. Possible reason for the difference is the uncertainty in the ESH exposure level. OPM calculated ESH based on attitude data provided by the Russians, while the POSA-I data was based on a unique radiometer that recorded total UV fluence. Attitude data for the whole MEEP exposure period was not available to verify the measured fluence. Also, the solar radiometer on the OPM failed during the mission, therefore the OPM calculated fluence levels also cannot be verified by independent measurements.

Significant transient contamination events were detected by both of the OPM TQCM units as described in Section 4.4. Therefore not only is location and pointing direction important, but the actual time of exposure is also very important. Most major contamination deposition appeared to be from transient events instead of a long term steady build up as would have been expected. Although the POSA-I experiment was a passive type, some time resolved information was obtained. During the next Space Shuttle mission STS-79 (September 1996) after deployment on STS-76 (March 1996) photos were taken of the POSA-I which showed the heavy contamination on the side facing the stored solar array.[17] Later photos and post flight analysis indicated that most of the measured contamination occurred during this time period between STS-76 and STS-79. Note, that OPM was not even delivered on orbit to Mir until later (STS-81, December 1996) and samples not exposed until April 1997 (13 months between initial MEEP/POSA-I exposure and the OPM exposure). Subsequently POSA-I was retrieved approximately 3 months before OPM was retrieved from the Docking Module.

In addition to transient events, the time in sunlight was shown to be very significant in that all TQCM's flown measured high deposition rates when time in sunlight reached 100% for several days.[8] This is usually plotted as time in shadow, which translates to 0% time in shadow for full sun orbits. Refer to section on TQCM data, Figure 4-12 in Section 4.4 which shows this correlation of TQCM frequency to Mir time in shadow.

Table 4-11. Comparison of Contamination versus Environmental Exposure

Experiment	Exposure Period (months)	Solar UV Exposure (ESH)	Contamination Thickness (Δ)	Comparison Thickness/ESH	Comparison Thickness/Time
OPM Sample side	8	832	~165	0.20	20.6
MEEP/POSA-I Mir facing side	18	413	~260	0.63	14.4
Standard Deviation	--	--	--	103%	35%

4.8.2 Discussion of the Results of the Pre-contaminated Z93P Samples Flown on OPM

Some additional observations can be made from the results of OPM concerning in-space contamination. The data generated by OPM including results of the pre-contaminated Z93P thermal control coatings demonstrates the magnitude of our lack of understanding all of the events that can degrade a surface in space and the need for continued on-orbit insitu experimental systems to help untangle this web of data.

Most spacecraft thermal control surfaces for long term missions are based on ceramic based paints that provide the required optical properties, are stable in space for long periods, and can be applied to complicated spacecraft surfaces at reasonable costs. A better understanding of the processes involved in order to predict contamination effects on these porous surfaces. Also, we need to be able to correlate contamination effects between surface coatings such as Z93P relative to a smooth surfaces such as the mirrors and TQCM crystals as flown on OPM, which are much more easily modeled.

Analysis of the OPM samples exposed on the Mir space station clearly demonstrate that deposition of a molecular contaminant onto a rough porous surface is not a simple thin film layer on a smooth surface. Even on a smooth surface, a contaminant does not initially go down as a thin film. Contaminants normally form isolated islands that grow in size as the contaminant continues to deposit until the islands finally grow together to form a continuous film. For rough surfaces, a relatively thin contaminant may never form a simple surface layer. There will probably always be some of the rough surface material exposed.

The pre-contaminated Z93P sample experiment on OPM was proposed by Hank Babel, et.al. with MDAC now Boeing Huntington Beach, Calif. The original objective of this experiment was to evaluate the degree that Atomic Oxygen would clean heavily contaminated Z93P thermal control coatings after extensive solar exposure. This issue was and is till a high priority issue for the ISS materials contamination community. The large area thermal radiators and a multitude of other smaller radiators are coated with Z93P and AZ93 thermal control

coatings, and it is essential to predict their lifetime performance while on orbit. Past data from LDEF and on Mir have demonstrated the long term stability of these coatings in the LEO space environment, but contamination has the potential to negate this stability. If the coatings degrade faster than expected, then the operational performance of the ISS must be reduced to match the reduced ability to dump excessive heat. All excessive heat must be dumped (radiated) from the thermal control radiators. If they degrade optically (solar absorptance increases and/or thermal emittance decreases) the quantity of heat dumped is correspondingly reduced.

In order to accomplish this experiment, it was decided to prepare four samples of Z93, each in two sets having two thickness' of two different types of contaminants deposited in a vacuum from ISS baseline materials. Source of contamination was materials which were primarily selected for wire insulation. MDAC had already experienced contamination events from these two materials and was concerned about their usage and which material would be better for long term use on ISS.

First it is worthwhile to understand how the samples were prepared. The pre-contaminated Z93P was prepared by directly exposing pristine surfaces to the offgasing products of heated silicone or Tefzel in a vacuum system. During contamination deposition, in order to build up a layer and minimize re-evaporation, the surfaces were simultaneously exposed to a ultraviolet source.[23] The magnitude or thickness was determined by monitoring a quartz crystal microbalance (QCM), until the desired thickness was achieved (500 or 2000 Angstroms). Then additional vacuum ultraviolet exposure (estimated at ~5,000 ESH) was performed, to pre-damage the surface. A certain amount of UV coating damage was achieved, but much of this degradation was bleached out before flight for the silicone contaminated surfaces. Interestingly, the Tefzel contaminated surfaces up to launch still exhibited significant degradation, but also were on a recovery curve, refer to Figure 4-6 in Section 4.1.

From the SEM photos showing the extreme rough and porous nature of the Z93 coating, one certainly would not expect a well defined layer of contamination. Interestingly the optical data correlates fairly well with the initial deposition "thickness." In addition, the XPS survey scans indicate that contamination layers were indeed achieved and to some extent residing on the surface of the coating. In the case of the Tefzel source, the contamination is dominated by a hydrocarbon with very little fluorine present. Likewise the XPS depth profile data shows a reasonable thickness was achieved (ground control samples) but not exactly the 500 and 2000 Angstroms indicated by the QCM. In fact the layer thickness as derived from the XPS sputter depth profile data taken on the ground control samples is not a factor of four difference as planned, but appears closer to 500 Angstroms for both Tefzel contaminated surfaces. For the silicone contaminated surfaces the thickness appears to be more like 600 and 1000 Angstroms. In addition, the depth profile data indicates that the contamination reaches a steady value within 1000 to 1500 Angstroms. We were not able (due to time constraints) to determine the actual depth of this residual level, and determine if the residuals (located in the porous structure) and the partial surface deposition adds up to what the QCM monitored.

Given the extreme porous nature of the Z93 coating, the results are not a surprise. What it does demonstrate is the difficulty in trying to model the contamination effects on Z93 type coating using conventional techniques.

Given the extreme porous nature of the Z93 coating, the results are not a surprise. What it does demonstrate is the difficulty in trying to model the contamination effects on Z93 type coating using conventional techniques.

The manner in which the contamination deposits and accumulates on a very porous surface can be compared to trying to apply paint to a very porous concrete block, it absorbs the first few layers until a sufficient "primer" layer is formed. Likewise the first few layers of contamination during deposition must be "soaked" up into the porous region of the coating. If the contaminate layer is thick enough then one can talk about a continuous layer. Until that level is reached the surface must be treated as a very porous open structure. Of course if the contaminate level ever even begins to reach this continuous level, the coating would of long since lost its usefulness. It is much easier (not easy) to put known contamination layers (must measure in terms of areal density not thickness) down on known smooth surfaces and measure the resulting effects (thermal optical properties) under various simulated environmental conditions (solar ultraviolet radiation, atomic oxygen, and high energetic particulates).

Other complications arise for the actual surfaces exposed on a spacecraft. Contaminant sources are comprised of a multitude of materials including typical silicones, hydrocarbons, various polymers, greases, coolants, fuels, oxidizers, and waste dumps. Temperatures of the contamination sources and critical surfaces also play a very important factor. Rates of offgasing are a function of time in vacuum, temperature history, and area. Likewise the deposition levels depend upon geometry factors between source and critical surface and surface texture/type. In addition, the space environment (solar ultraviolet radiation, atomic oxygen, and high energetic particulates) will affect deposition rates and optical properties changes. It is still not possible to set up and experimentally perform this level of simulation testing in ground facilities.

Until very detailed and evolved models are developed, once must rely on these empirical techniques correlating the thermal optical properties with areal density (mass per unit area), contaminant type, and exposure (solar ultraviolet radiation and/or atomic oxygen). Whether the contaminant is a silicone or hydrocarbon makes a radical difference in terms of the long term degradation of optical properties. For hydrocarbon contaminants the AO is removing material whereas for silicone contaminants AO is converting the deposit to a silicate. The interaction of all of these forces present a major challenge to develop long term lifetime prediction models. For accurate modeling and to obtain a high level of confidence in the models, all of the interactions must be included.

Besides the need for more extensive ground testing to build up usable data bases, flight experiments must continue to collect flight data since this is the only location where all of the spacecraft and space environmental effects are present simultaneously. Ground testing is cheaper and quicker, but cannot simulate all of the flight environments. The specific reason that OPM was developed was to acquire this vitally needed data.

5.0 SUMMARY

The OPM is a unique, reusable flight instrument to study the behavior of materials in the space environment. The OPM performed well on the mission to Mir and demonstrated its capability to measure the in-space behavior of materials and monitor selected components of the space environment. The processed in-flight and post-flight OPM data from the Mir mission has already provided the ISS and aerospace community with unique and valuable data on the performance of materials in the Mir space environment. The OPM has provided the only in-space time-dependent data for critical ISS materials including contaminated surfaces.

The continuing post flight analysis of the OPM samples, hardware, and flight data is yielding valuable information, More analysis and ground testing is scheduled that will help to understand and verify the OPM findings. Comparing the OPM data with other experiments that were flown on Mir is also helping to understand both the magnitude and uniqueness of the Mir contamination environment. As can be seen in the data described is this report; location, time, temperature, and direction are all very important in predicting the quantity and effect of contamination on critical surfaces. Transient events which may not be possible to predict can also significantly contribute to the contamination environment.

New and modified materials/coatings need to be thoroughly tested on the ground and then exposed to the actual space environment in order to verify that anticipated improvements work the way they were planned. LDEF and Mir provided the platform necessary to carry out these important material tests. In order for the ISS to realize its full potential in the area of space environmental effects experimentation, the existing and flight proven OPM must be incorporated in the flight instrumentation available to material researchers and re-flown on ISS at an early date.

For more information on OPM, please see the Internet web sites at http://www.aztechnology.com and http://see.msfc.nasa.gov/see/see.html.

6.0 REFERENCES AND OPM BIBLIOGRAPHY

6.1 References

1. Zerlaut, G. A., Gilligan, J. E.; "Study of In-situ Degradation of Thermal Control Surfaces NASA Contract NAS8-21074 Final Report", IITRI Report U6061-17 & -29, March 7, 1969 and February 20, 1970.

2. Edwards, D. L., Zwiener, J. M., Meshishnek, M. J., et. al.; "Radiation Induced Degradation of the White Thermal Control Paints Z-93 and Z-93P", NASA TM-108518, October 1996.

3. Edwards, D. L., Zwiener, J. M., Meshishnek, M. J., et. al.; "Radiation Induced Degradation of the White Thermal Control Paint", 20th Space Simulation Conference, IEF-NASA/ASTM/AIAA/CSA, Oct. 26-29, 1998.

4. Wilkes, D. R.; "Thermal Control Surfaces Experiment" Final Contract Report NAS8-38939, AZ Technology Report No. 90-1-108-054, August 15, 1997.

5. Wilkes, D.R.; "Thermal Control Surfaces Experiment", NASA Report CR-1999-209008, January 1999.

6. Levine, A. S.; "69 Months in Space: First LDEF Post Retrieval Symposium" NASA CP-3134, Part 1-3, 1991.

7. Levine, A. S.; "69 Months in Space: Second LDEF Post Retrieval Symposium" NASA CP-3194, Part 1-3, 1993.

8. Levine, A. S.; "69 Months in Space: Third LDEF Post Retrieval Symposium" NASA CP-3275, Part 1-3, 1993.

9. Whitaker, A., and Gregory, J.; "LDEF Materials Results for Spacecraft Applications", NASA Conference Publication 3257, 1994

10. Wilkes, D.R., Bennett, J.M., Hummer, L.L. Clukman, R.A., Hadaway, J.B., Pezzaniti, L.; "Optical Properties Monitor, Experiment Definition Phase"; NASA Report CR4293; May, 1990.

11. Reichard, Penelope, J. and Triolo, J.J.; "Pre-flight Testing of the ATS-1 Thermal Coating Experiment" Proc. of the AIAA Thermophysics Specialist Conference, AIAA Paper 67-333, April 17-20, 1967.

12. Pezzaniti,J. L.,Hadaway, J. B.,Chipman, R. A.,Wilkes D.,Hummer L., and Bennett, J.M.; "Total Integrated Scatter Instrument for In-Space Monitoring of Surfaces Degradation." Proc. Soc. Photo-Opt. Instrum. Eng. 1329, 200-210 (1990).

13. Hadaway, James, Anees Ahmad, and Jean Bennett; "Final design, assembly, & testing of a space-based Total Integrated Scatter Instrument", SPIE Vol. 3141, pp. 209-219.

14. Hadaway, J. B., Bennett, J. M., Johnson, L., Kjoller, K., Crandall, D. G.; "Final Report of the Total Integrated Scattering Measurement Made on the Russian MIR Spacecraft as Part of the Optical Properties Monitor Experiment", unpublished, 1999.

15. Wilkes, D. R., Naumov, S., and Maslenikov, L.; "The Mir Environment and Material Effects As Observed On the Optical Properties Monitor (OPM) Experiment" AIAA #99-0102 presented at the 37th Aerospace Sciences Meeting and Exhibit, January 11-14, 1999, Reno, NV.

16. Lennhoff, J., Vaughn, J., Zwiener, J. et. al.; "Electrically Conductive Low Absorption Atomic Oxygen Resistant Films for Spacecraft Thermal and Charge Control", SAMPE March 25-28, 1996

17. Zwiener, J. M., Kamenetzky, R. R., Vaughn, J. A., and Finckenor, M. M.; "Contamination Observed on the Passive Optical Sample Assembly (POSA)-I Experiment", SPIE paper #3427A-20, July 1998.

18. Mell, R. J., Zwiener, J. M.; "Development of Highly Reflective Spacecraft Radiator Sprayable Coatings", Final Contract Report, AZT96-4-317-007, Air Force Report Number AFRL-ML-WP-TR-1999-4097, May 1999.

19. Wilkes, D. R.; Carruth, M. R.; "In-Situ Materials Experiments on the Mir Station"; SPIE Vol.3427, pp. 211-224, 1998

20. Wilkes, D. R., Zwiener, J. M. "Optical Properties Monitor (OPM) In-Situ Experiment Flown on the Mir Station", SPIE Vol.3784, pp. 72-83, July, 1999.

21. Linton, R. C.; "Measurement and Application of Contaminant Optical Constants", paper 71-460, AIAA 6th Thermophysics Conference, Tullahoma, Tenn., April 26-28, 1971

22. Kamenetzky, R. R., and Finckenor, M. M.; "MSFC Investigations of Beta Cloth Darkening Due to Ultraviolet Radiation Interactions", (to be published in 1999).

6.2 OPM Bibliography

1. Hadaway, James; Anees Ahmad, and Jean Bennett. "Final design, assembly, & testing of a space-based Total Integrated Scatter Instrument," SPIE Vol. 3141, pp. 209-219.

2. Hadaway, J. B.; Bennett, J. M.; Johnson, L.; Kjoller K.; Crandall, D. G. "Final Report of the Total Integrated Scattering Measurement Made on the Russian MIR Spacecraft as Part of the Optical Properties Monitor Experiment", unpublished, 1999

3. Kamenetzky, R. R., and Finckenor, M. M. "Comparison of Observed Beta Cloth Interactions with Simulated and Actual Space Environment," NASA/TM-1999-209575, September 1999

4. Pezzaniti,J. L.; Hadaway, J. B.; Chipman, R. A.; Wilkes D.; Hummer L., and Bennett, J.M. "Total Integrated Scatter Instrument for In-Space Monitoring of Surfaces Degradation." Proc. Soc. Photo-Opt. Instrum. Eng. 1329, 200-210 (1990)

5. Wilkes, D.R.; Bennett, J.M.; Hummer, L.L.; Clukman, R.A.; Hadaway, J.B. and Pezzaniti, L. "Optical Properties Monitor, Experiment Definition Phase"; NASA Report CR4293; May, 1990.

6. Wilkes, D. R.; Carruth, M. R. "In-Situ Materials Experiments on the Mir Station"; SPIE Vol.3427, pp. 211-224, 1998

7. Wilkes, D. R.; Naumov, S., and Maslenikov, L. "The Mir Environment and Material Effects As Observed On the Optical Properties Monitor (OPM) Experiment" AIAA #99-0102 presented at the 37th Aerospace Sciences Meeting and Exhibit, January 11-14, 1999, Reno, NV.

8. Wilkes, D. R.; Zwiener, J. M. "Optical Properties Monitor (OPM) In-Situ Experiment Flown on the Mir Station", SPIE Vol.3784, pp. 72-83, July, 1999

9. Hummer, L. "Optical Properties Monitor (OPM) System Report,", AZ Technology Report Number 91-1-118-164, Contract Number NAS8-39237, dated December 31, 1999

10. Wilkes, D.R.; Zwiener, J.M. "Optical Properties Monitor (OPM) Science Data Report", AZ Technology Report Number 91-1-118-169, Contract Number NAS8-39237, dated December 31, 1999

11. Schmitz, C.P., "Optical Properties Monitor (OPM) Mission Thermal Data Report", AZ Technology Report Number 91-1-118-166, Contract Number NAS8-39237, dated December 31, 1999

APPENDIX A

LIST OF ALL FLIGHT SAMPLES

APPENDIX A

OPM Flight Samples				
Carousel Position	**Description**	**Supplier**	**Contact**	**Phone**
Reflectometer Samples				
CR01	Thermal Control - COR - Triton	NASA MSFC	Jim Zwiener	205-544-2528
CR02	TMS-800AZ, yellow	AZ Technology, Inc.	Richard Mell / David Crandall	205-837-9877
CR03	AZWEC-1I (MST450-ICW), ESD white	AZ Technology, Inc.	Richard Mell / David Crandall	205-837-9877
CR04	AZW/LA-1I (MST600-IUCW), low alpha white	AZ Technology, Inc.	Richard Mell / David Crandall	205-837-9877
CR05	Optical Solar Reflector	AZ Technology, Inc.	Don Wilkes / David Crandall	205-837-9877
CR06	AZ-93 over MLP-300 primer	AZ Technology, Inc.	Richard Mell / David Crandall	205-837-9877
CR07	Thermal Control Paints - Z93 w/primer and Teflon overcoat	NASA MSFC	Jim Zwiener	205-544-2528
CR08	TP-co-2, silicate on ZnO & liquid glass base	RSC Energia, Moscow	S. Naumov	na
CR09	TP-co-12, silicate on ZnO & liquid glass base	RSC Energia, Moscow	S. Naumov	na
CR10	Chromic Anodized 6061 Aluminum Alloy	Boeing (AL)	Gary Pippin	206-773-2846
CR11	Boric-Sulfuric Anodized 6061 Aluminum Alloy	Boeing (AL)	Gary Pippin	206-773-2846
CR12	Chem film 1A on 2219 Alum.	Rocketdyne	Pol Dano	818-586-4176
CR13	Z-93CLM55 Thermal control coating	IIT Research Institute	M.S.Deshpande	312-567-4290
CR14	Sulfuric Acid Anodized 7075-T7351	McDonnell Douglas	Mark Hasegawa	714-896-3311 ext60988
CR15	Sulfuric Acid Anodized 2219-T851	McDonnell Douglas	Mark Hasegawa	714-896-3311 ext60988
CR16	Z-93P control	McDonnell Douglas	Mark Hasegawa	714-896-3311 ext60988
CR17	Z93P contaminated with silicone 500A	McDonnell Douglas	Mark Hasegawa	714-896-3311 ext60988
CR18	Z-93P contaminated with Tefzel 500A	McDonnell Douglas	Mark Hasegawa	714-896-3311 ext60988
CR19	Z93P contaminated with silicone 2000A	McDonnell Douglas	Mark Hasegawa	714-896-3311 ext60988
CR20	Z-93P contaminated with Tefzel 2000A	McDonnell Douglas	Mark Hasegawa	714-896-3311 ext60988

APPENDIX A

OPM Flight Samples				
Carousel Position	**Description**	**Supplier**	**Contact**	**Phone**
TIS Samples				
CT01	dc Magnetron Sputtered Optical Coatings-Niobia/Silica	USAF Phillips Laboratory	Angie Annaballi	505-846-5112
CT02	dc Magnetron Sputtered Optical Coatings-Zirconia/Silica	USAF Phillips Laboratory	Angie Annaballi	505-846-5112
CT03	NAWC-TIS-Diamond like carbon (DLC) on silicon	NAWC	Linda Johnson	619-939-1422
CT04	NAWC-TIS-7/Titanium Diboride	NAWC	Linda Johnson	619-939-1422
CT05	NAWC-Zirconium Diboride on silicon	NAWC	Linda Johnson	619-939-1422
CT06	NAWC-TixByNz film on silicon	NAWC	Linda Johnson	619-939-1422
CT07	NAWC-TIS-1/as-grown, undoped CVD Diamond	NAWC	Linda Johnson	619-939-1422
CT08	NAWC-TixByOz film on silicon	NAWC	Linda Johnson	619-939-1422
CT09	NAWC-ZrxByNz film on silicon	NAWC	Linda Johnson	619-939-1422
CT10	NAWC-TIS-2/as-grown, boron-doped CVD Diamond	NAWC	Linda Johnson	619-939-1422
CT11	NAWC-TIS-3/as-grown, phosphorus-doped CVD Diamond	NAWC	Linda Johnson	619-939-1422
CT12	NAWC-Carbon nitride (CxNy) film on silicon	NAWC	Linda Johnson	619-939-1422
CT13	NAWC-Titanium nitride (TiN) film on silicon	NAWC	Linda Johnson	619-939-1422
CT14	Gold Mirror	AZ Technology, Inc.	Don Wilkes / David Crandall	205-837-9877
CT15	MgF2 Overcoated Aluminum Mirror	AZ Technology, Inc.	Don Wilkes / David Crandall	205-837-9877
CT16	Platinum Mirror	AZ Technology, Inc.	Don Wilkes / David Crandall	205-837-9877
CT17	First surface aluminum-coated levelized aluminum mirror	NASA LeRC	Bruce Banks	216-433-2308
CT18	ISS Solar Array Blanket Face Sheet	NASA LeRC	Bruce Banks	216-433-2308
CT19	Kapton H (4 layers of 5 mil)	AZ Technology, Inc.	Don Wilkes / David Crandall	205-837-9877
CT20	Silver/Teflon (5 mil)	AZ Technology, Inc.	Don Wilkes / David Crandall	205-837-9877
VUV Samples				
CV01	Window Material with MgF2 AR Coating	Boeing (AL)	Gary Pippin	206-773-2846
CV02	Fused Silica Window	AZ Technology, Inc.	Don Wilkes / David Crandall	205-837-9877
CV03	Crystalline Quartz Window	AZ Technology, Inc.	Don Wilkes / David Crandall	205-837-9877
CV04	Lithium Fluoride (LiF) Window	AZ Technology, Inc.	Don Wilkes / David Crandall	205-837-9877
CV06	Magnesium Fluoride Window (MgF2)	AZ Technology, Inc.	Don Wilkes / David Crandall	205-837-9877
CV07	Sapphire Window	AZ Technology, Inc.	Don Wilkes / David Crandall	205-837-9877
CV08	VUV Neutral Density Filter, up	AZ Technology, Inc.	Don Wilkes / David Crandall	205-837-9877

APPENDIX A

OPM Flight Samples				
Carousel Position	**Description**	**Supplier**	**Contact**	**Phone**
CV09	VUV Neutral Density Filter, down	AZ Technology, Inc.	Don Wilkes / David Crandall	205-837-9877
CV11	Gold Mirror	AZ Technology, Inc.	Don Wilkes / David Crandall	205-837-9877
CV12	Platinum Mirror	AZ Technology, Inc.	Don Wilkes / David Crandall	205-837-9877
CV13	MgF2 Overcoated Aluminum Mirror	AZ Technology, Inc.	Don Wilkes / David Crandall	205-837-9877
CV14	OWS Mirrors - Gold/Fused Silica	NASA MSFC	Jim Zwiener	205-544-2528
CV16	OWS Mirrors - Iridium/Fused Silica	NASA MSFC	Jim Zwiener	205-544-2528
CV17	OWS Mirrors - MgF2/Al/Fused Silica	NASA MSFC	Jim Zwiener	205-544-2528
CV18	OWS Mirrors - Platinum/Fused Silica	NASA MSFC	Jim Zwiener	205-544-2528
CV19	Iridium	NASA GSFC	Ritva Keski-Kuha	301-286-6706
CV21	SiC	NASA GSFC	Ritva Keski-Kuha	301-286-6706
CV22	Boron Carbide	NASA GSFC	Ritva Keski-Kuha	301-286-6706
CV23	Al + MgF2	NASA GSFC	Ritva Keski-Kuha	301-286-6706
CV24	Boron Carbide	NASA GSFC	Ritva Keski-Kuha	301-286-6706
CV26	CVD Diamond	NASA GSFC	Ritva Keski-Kuha	301-286-6706
CV27	CVD-SiC	NASA GSFC	Ritva Keski-Kuha	301-286-6706
CV28	Iridium	Boeing (AL)	Gary Pippin	206-773-2846
CV29	Window Material with MgF2 AR Coating	NASA GSFC	Ritva Keski-Kuha	301-286-6706
CV31	Ir/Si Multilayer	College of William & Mary	Dick Kiefer	804-221-2553
CV32	ULTEM, pure	College of William & Mary	Dick Kiefer	804-221-2553
CV33	ULTEM / 10% BTO	College of William & Mary	Dick Kiefer	804-221-2553
CV34	ULTEM / 20% BTO	AZ Technology, Inc.	Richard Mell / David Crandall	205-837-9877
CV36	RM550IB Baffle Coating	AZ Technology, Inc.	Richard Mell / David Crandall	205-837-9877
CV37	MLS85 Baffle Coating	AZ Technology, Inc.	Richard Mell / David Crandall	205-837-9877
CV38	Alodine Baffle	AZ Technology, Inc.	Don Wilkes / David Crandall	205-837-9877
CV39	Black Anodize Baffle			
Passive Samples		USAF Phillips Laboratory	Chuck Miglionico	505-846-9363
CP01	AO Resist. Diam.-like Nanocomp. Coatings (DYLYNTM) DLN-undoped	USAF Phillips Laboratory	Chuck Miglionico	505-846-9363
CP02	AO Resist. Diam.-like Nanocomp. Coatings (DYLYNTM)			

APPENDIX A

OPM Flight Samples				
Carousel Position	**Description**	**Supplier**	**Contact**	**Phone**
	DLN-30% Ti doped			
CP03	YB-71P, Zn2TiO4-Potassium silicate thermal coating	IIT Research Institute	M.S.Deshpande	312-567-4290
CP04	Z-93SC55	IIT Research Institute	M.S.Deshpande	312-567-4290
CP05	S13GP/LO-1, Encapsulated ZnO in methyl silicone	IIT Research Institute	M.S.Deshpande	312-567-4290
CP09	Al 1st Surface Mirror Contam Monitor	NASA LeRC	Bruce Banks	216-433-2308
CP10	AZWEC-2I	AZ Technology, Inc.	Richard Mell / David Crandall	205-837-9877
CP11	AZBEC-1	AZ Technology, Inc.	Richard Mell / David Crandall	205-837-9877
CP12	Z24P binder w/ZnO pigment + 2% Sodium Salicylate by wt	Boeing (WA)	Gary Pippin	206-773-2846
CP16	Six layer stack on Si-wafer	Lockheed Martin	William Saylor	610-354-3979
CP17	Kapton (4 layers)	AZ Technology, Inc.	Don Wilkes / David Crandall	205-837-9877
CP18	TCOH-COTM - "6u" glass fabric	RSC Energia, Moscow	S. Naumov	na
CP19	Beta Cloth	Rocketdyne	Pol Dano	818-586-4176
CP20	Black marking-Metalphoto	Rocketdyne	Pol Dano	818-586-4176
CP Plate 1	Defected Al on Kapton	NASA LeRC	Bruce Banks	216-433-2308
CP Plate 1	EIC Electrochromic Coating	NASA GSFC	Lonny Kauder	301-286-5309
CP Plate 1	EVA Label - Blue	Boeing (TX)	John L. Golden	713-244-7929
CP Plate 1	EVA Label - Red	Boeing (TX)	John L. Golden	713-244-7929
CP Plate 1	EVA Label Decal	Boeing (TX)	John L. Golden	713-244-7929
CP Plate 1	ISS Solar Array Blanket Face Sheet	NASA LeRC	Bruce Banks	216-433-2308
CP Plate 1	OCLI coating over white Tedlar	NASA GSFC	Lonny Kauder	301-286-5309
CP Plate 1	White Paint Z24P Binder w/ZnO Pigment	Boeing (WA)	Gary Pippin	206-773-2846
CP Plate 2	ATR Crystal-Germanium	AZ Technology, Inc.	Don Wilkes / David Crandall	205-837-9877
CP Plate 2	ATR Crystal-Zinc Selenide	AZ Technology, Inc.	Don Wilkes / David Crandall	205-837-9877
CP Plate 3	Silver Teflon 5 mil 2-1/2" x 3/4"	Boeing (WA)	Gary Pippin	206-773-2846
CP Plate 4	Silver Teflon 5 mil 2-1/2" x 3/4"	Boeing (WA)	Gary Pippin	206-773-2846

APPENDIX B

Minimum and Maximum Calorimeter Temperatures

APPENDIX B

Minimum and Maximum Calorimeter Temperatures During Weekly Measurement Timelines					
Calorimeter Sample	**Temperature Sensor**	**Min Temp, °C 4/29/97**	**Solar Absorptance 4/29/97**	**Max Temp, °C 6/24/97**	**Solar Absorptance 6/24/97**
CR01	T00	-55.68	0.141	48.34	0.204
CR02	T01	-59.74	0.344	66.93	0.348
CR03	T02	-58.23	0.255	48.83	0.278
CR04	T03	-65.77	0.095	35.26	0.089
CR05	T04	-60.74	0.053	32.75	0.057
CR06	T05	-66.27	0.161	37.27	0.156
CR07	T06	-67.37	0.169	38.21	0.191
CR08	T07	-66.27	0.157	38.78	0.156
CR09	T08	-65.75	0.148	37.84	0.142
CR10	T09	-46.67	0.358	111.16	0.358
CR11	T10	-58.23	0.358	85.02	0.387
CR12	T11	-6.46	0.465	229.27	0.503
CR13	T12	-64.76	0.124	39.28	0.129
CR14	T13	-69.29	0.420	68.43	0.414
CR15	T14	-63.26	0.389	75.47	0.405
CR16	T15	-67.28	0.147	37.27	0.147
CR17	T16	-65.77	0.149	38.27	0.164
CR18	T17	-66.27	0.184	34.25	0.194
CR19	T18	-60.74	0.150	39.78	0.190
CR20	T19	-58.73	0.261	59.38	0.342
	T00 Emissivity Plate	-3.1		61.69	
	T01 Emissivity Plate	-3.8		62.81	
	T02 Emissivity Plate	-4.07		63.48	
	T03 Emissivity Plate	-3.34		61.99	
	IR Radiometer	-2.569		55.494	
	Solar Radiometer	-2.64		54.776	

APPENDIX C

REFLECTOMETER DATA

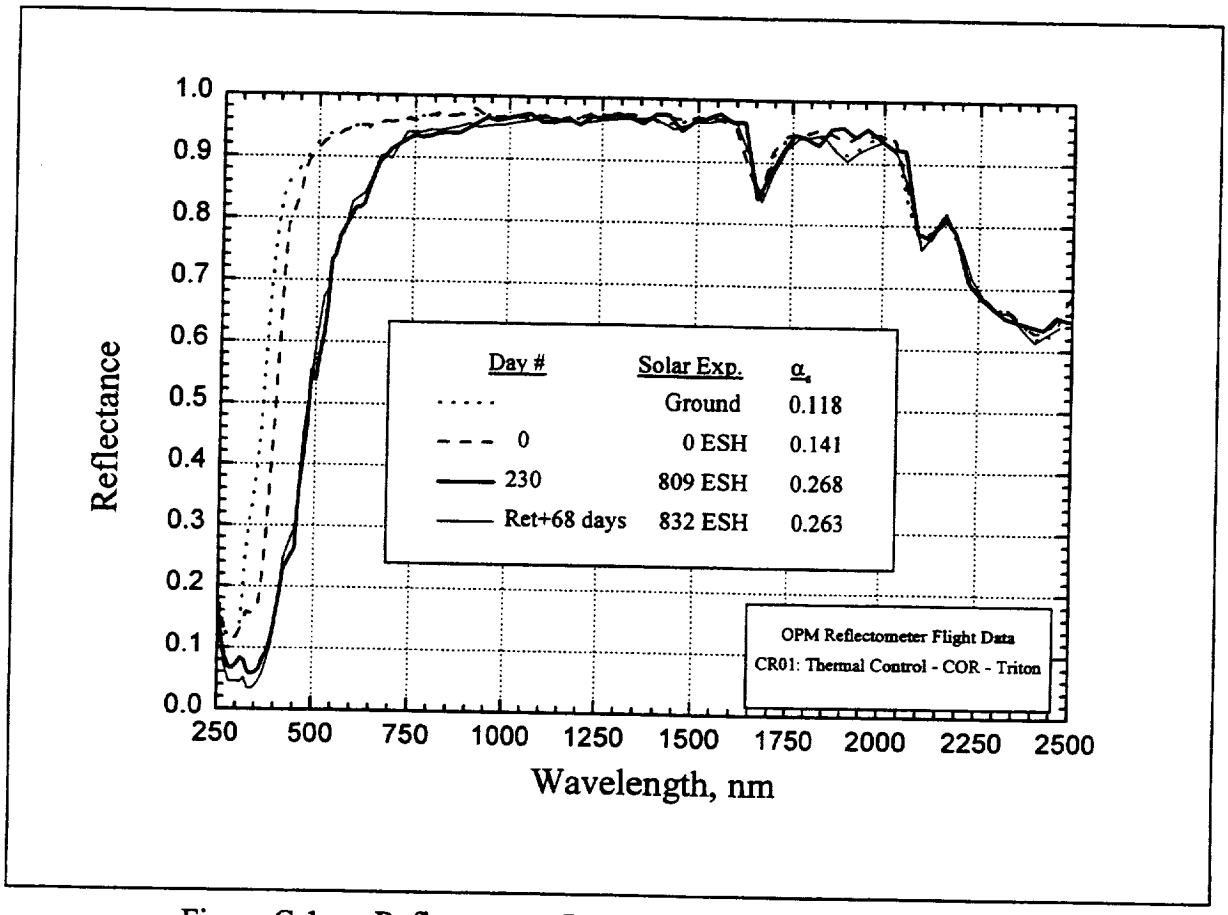

Figure C-1. Reflectometer Data for CR01, Triton COR Coating

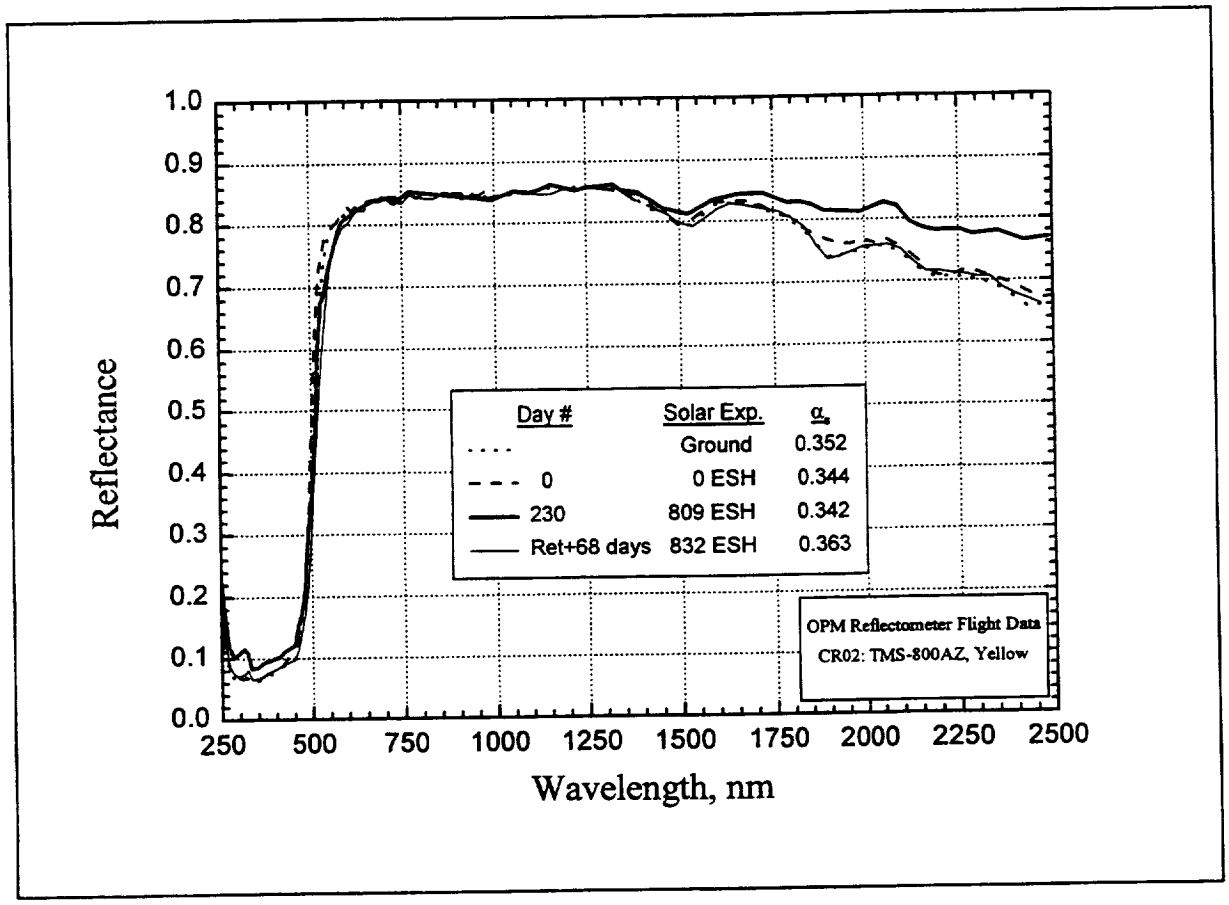

Figure C-2. Reflectometer Data for CR02, TMS-800AZ, Yellow Coating

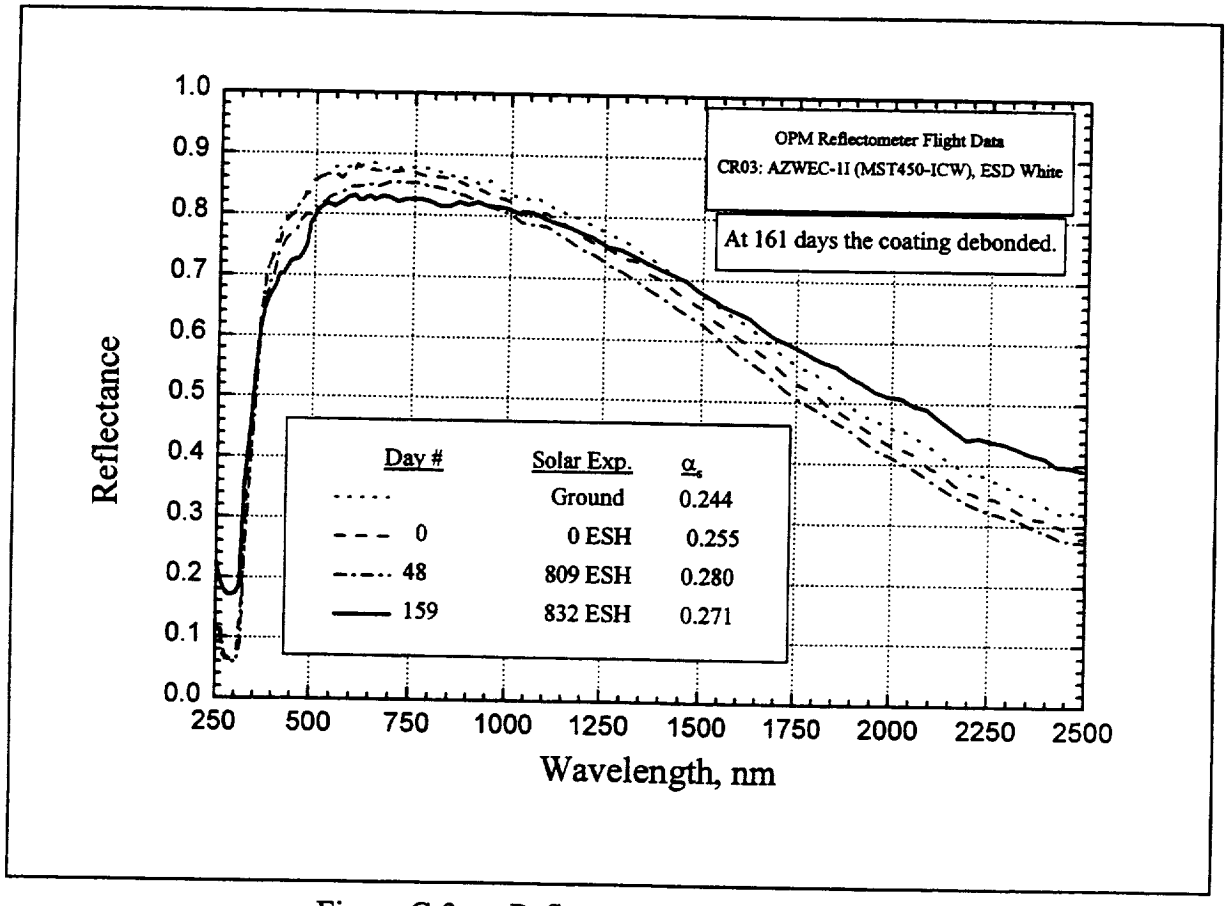

Figure C-3. Reflectometer Data for CR03, AZWEC-11 ESD White Coating

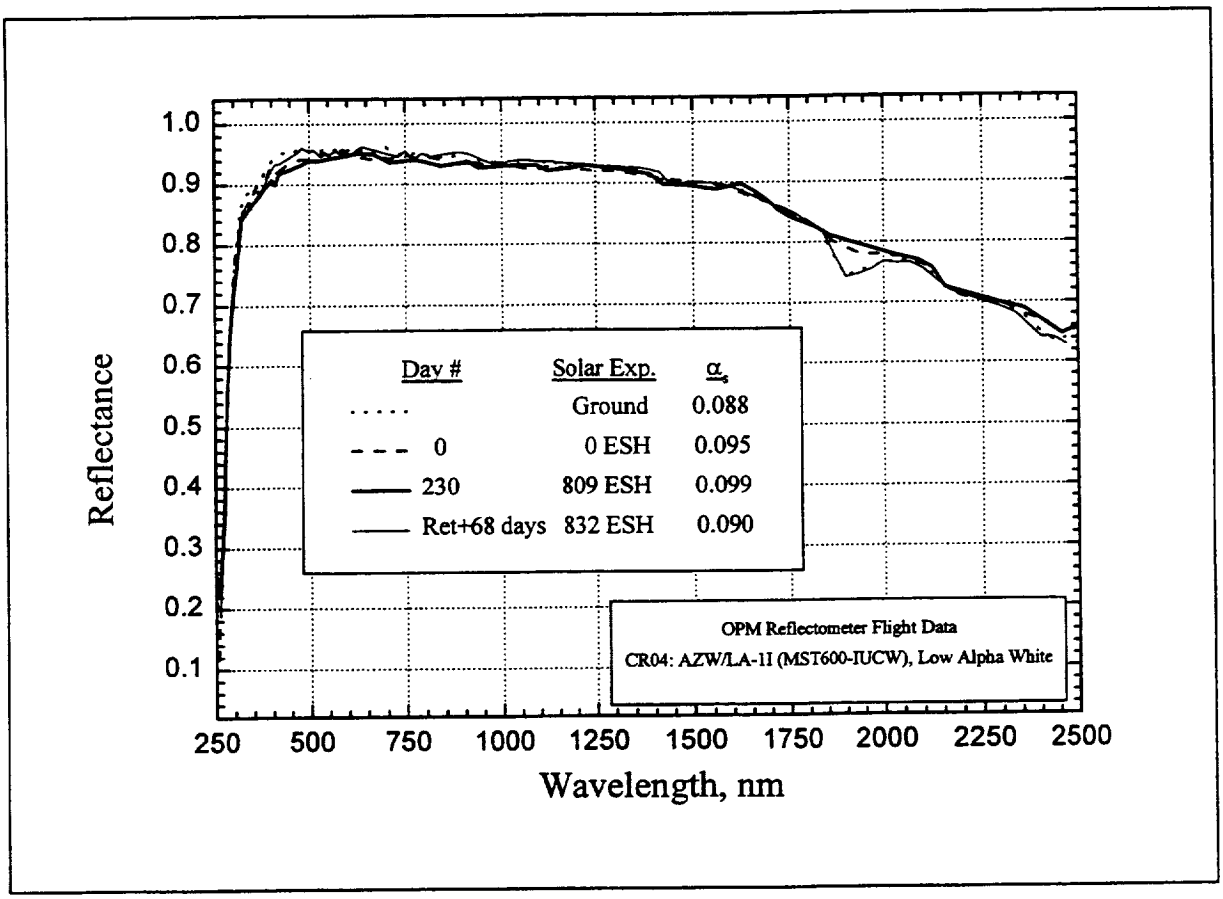

Figure C-4. Reflectometer Data for CR04, AZW/LA-11 Low Alpha White Coating

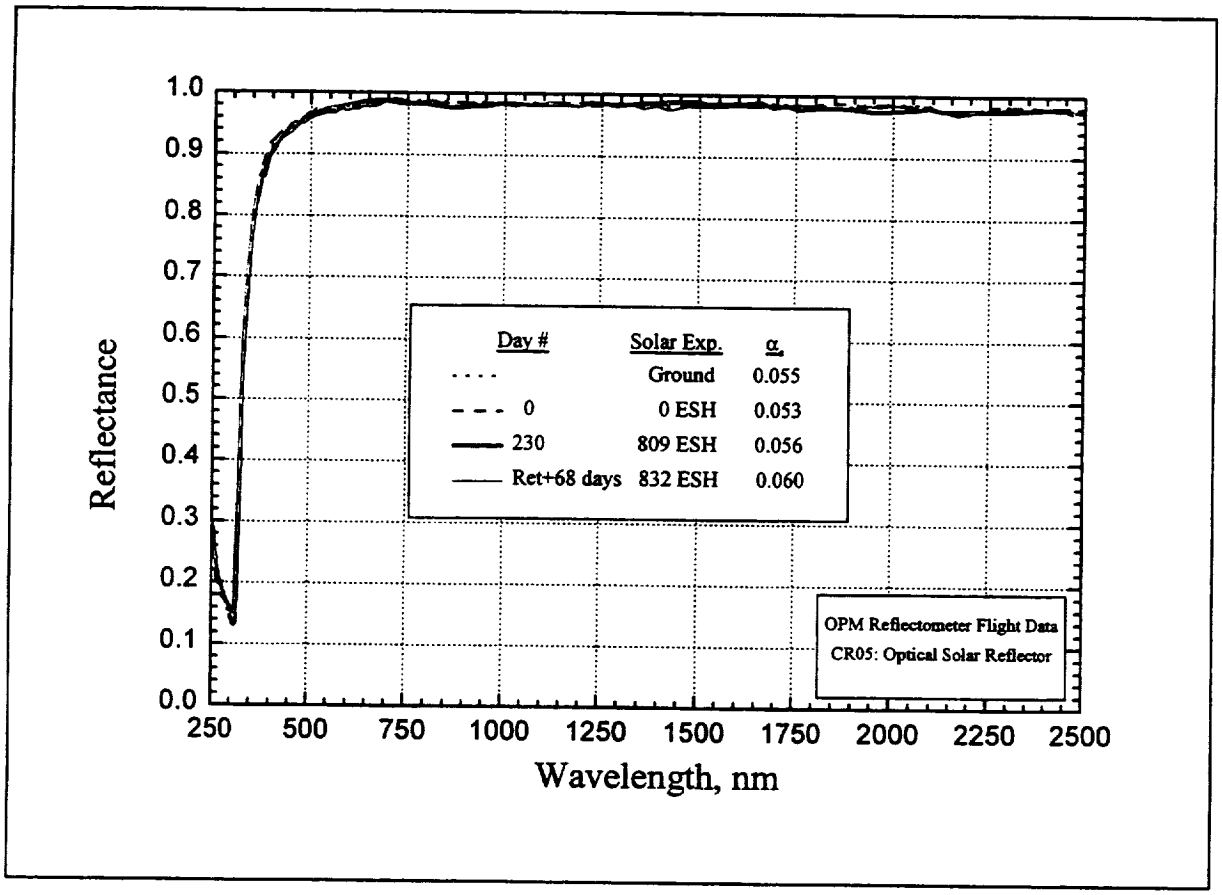

Figure C-5. Reflectometer Data for CR05, Optical Solar Reflector (OSR)

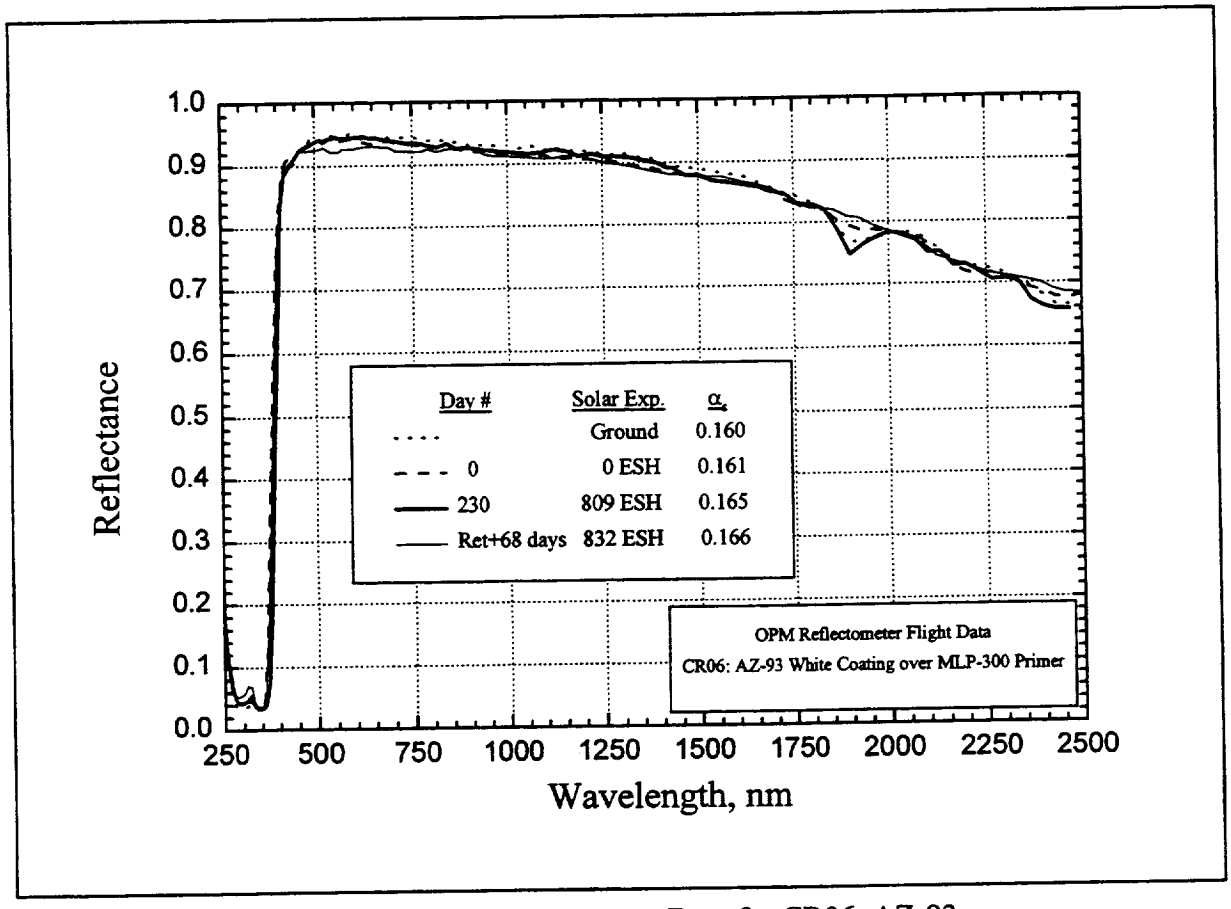

Figure C-6. Reflectometer Data for CR06, AZ-93 White Coating over MLP-300 Primer

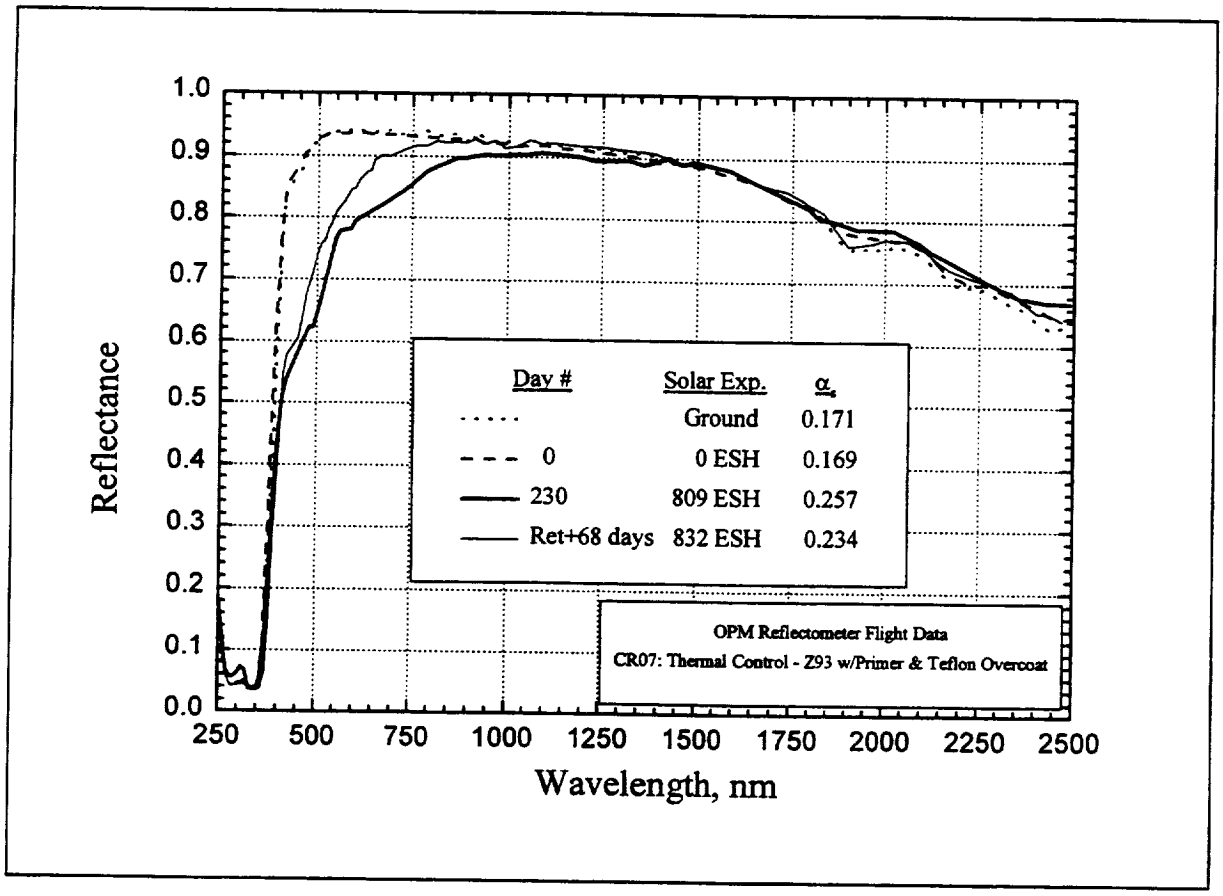

Figure C-7. Reflectometer Data for CR07, AZ-93 with Primer & Teflon Overcoat

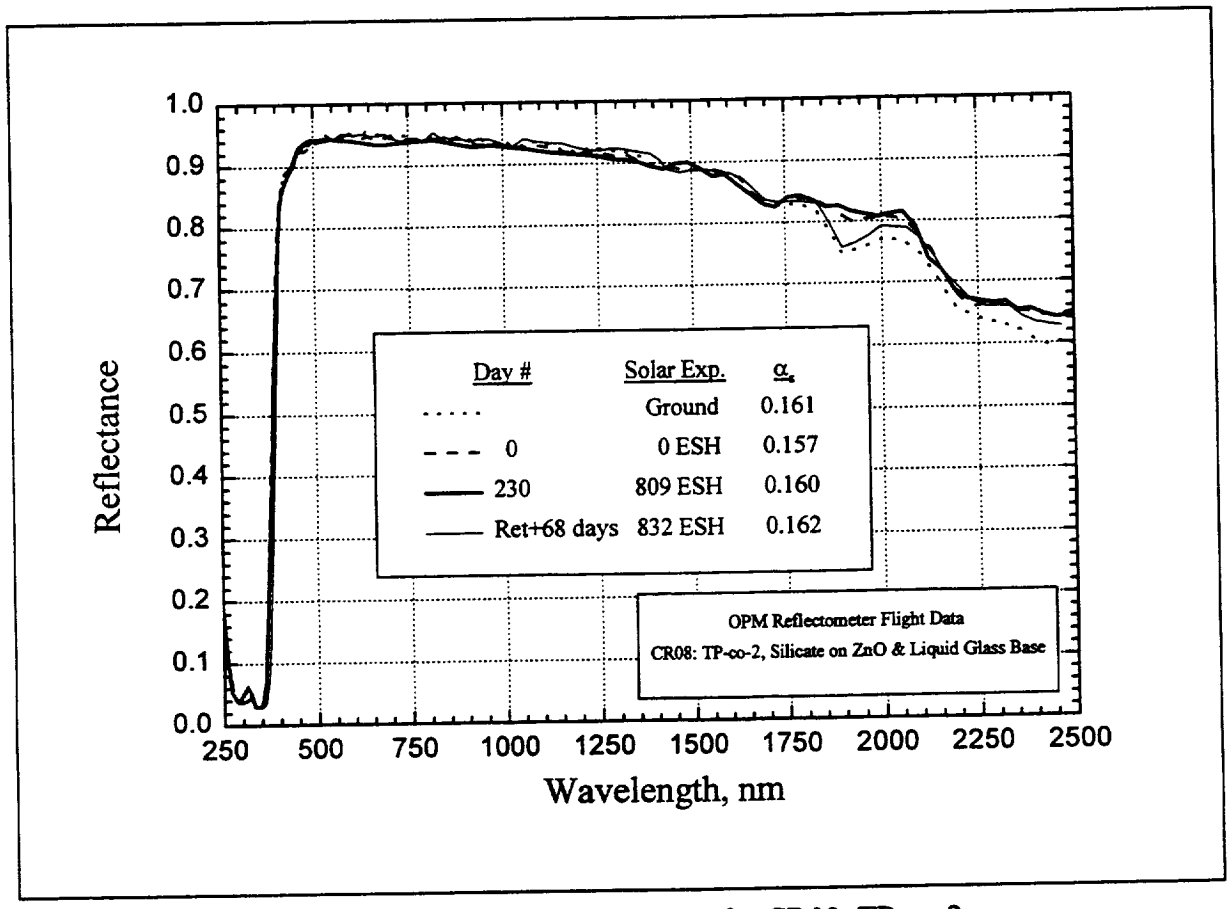

Figure C-8. Reflectometer Data for CR08, TP-co-2, Silicate on ZnO & Liquid Glass Base

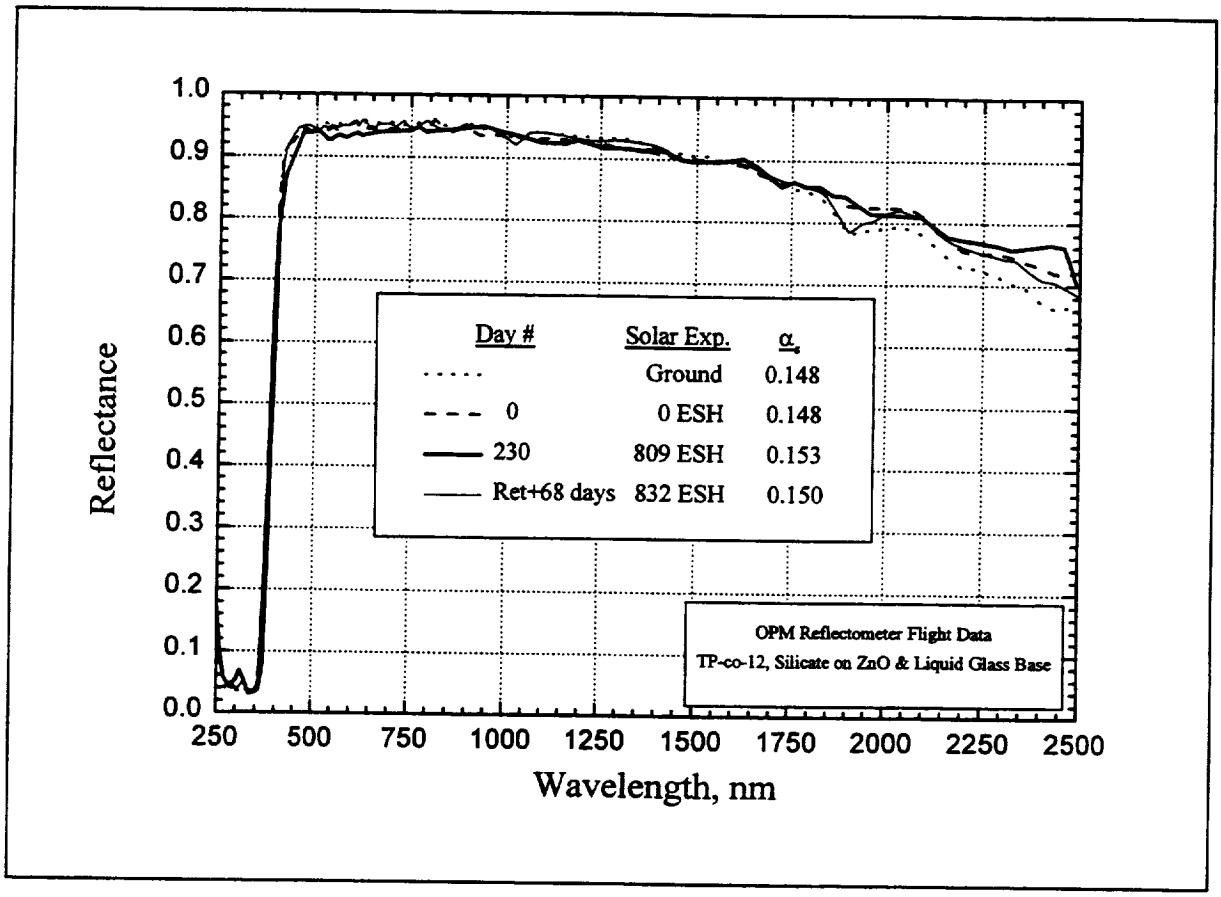

Figure C-9. Reflectometer Data for CR09, TP-co-12, Silicate on ZnO & Liquid Glass Base

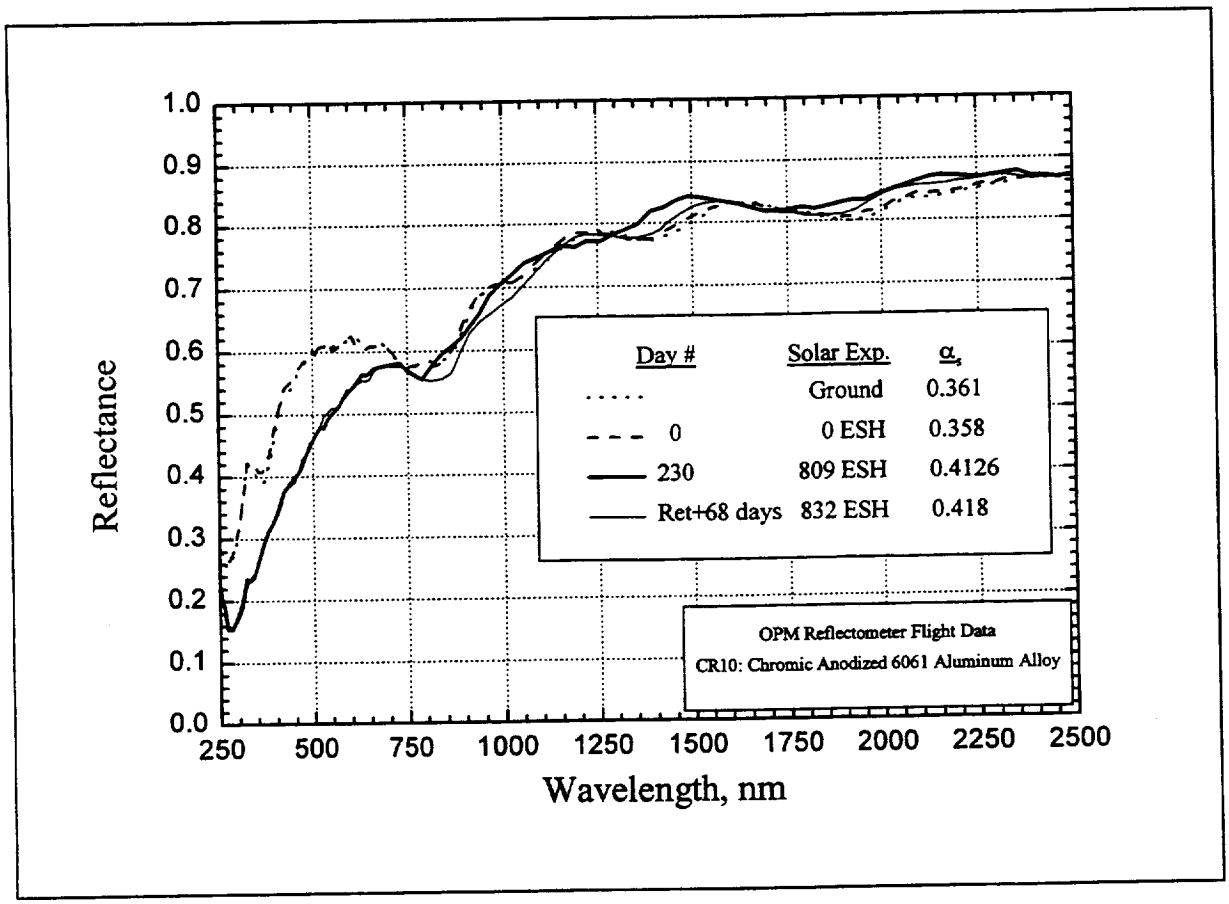

Figure C-10. Reflectometer Data for CR10,
Chromic Anodized 6061 Aluminum Alloy

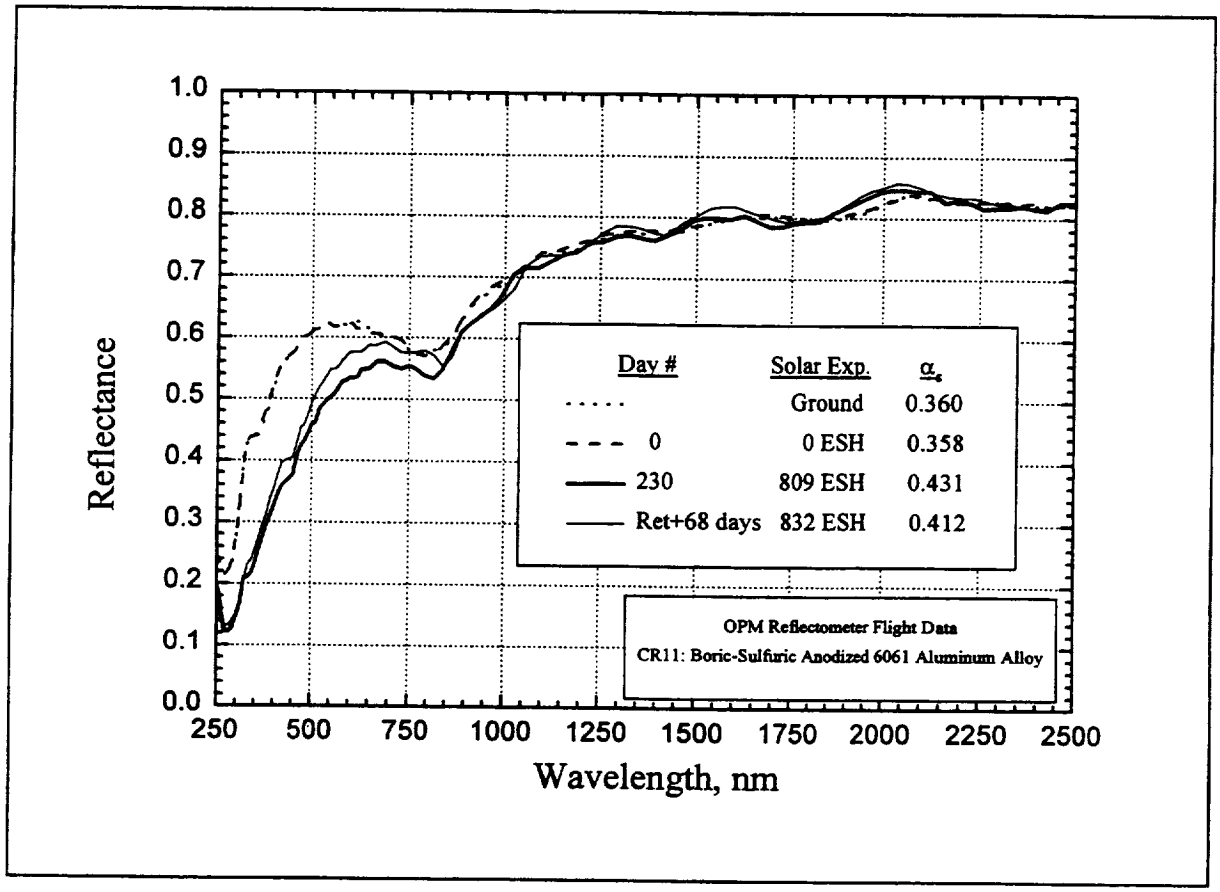

Figure C-11. Reflectometer Data for CR11,
Boric-Sulfuric Anodized 6061 Aluminum Alloy

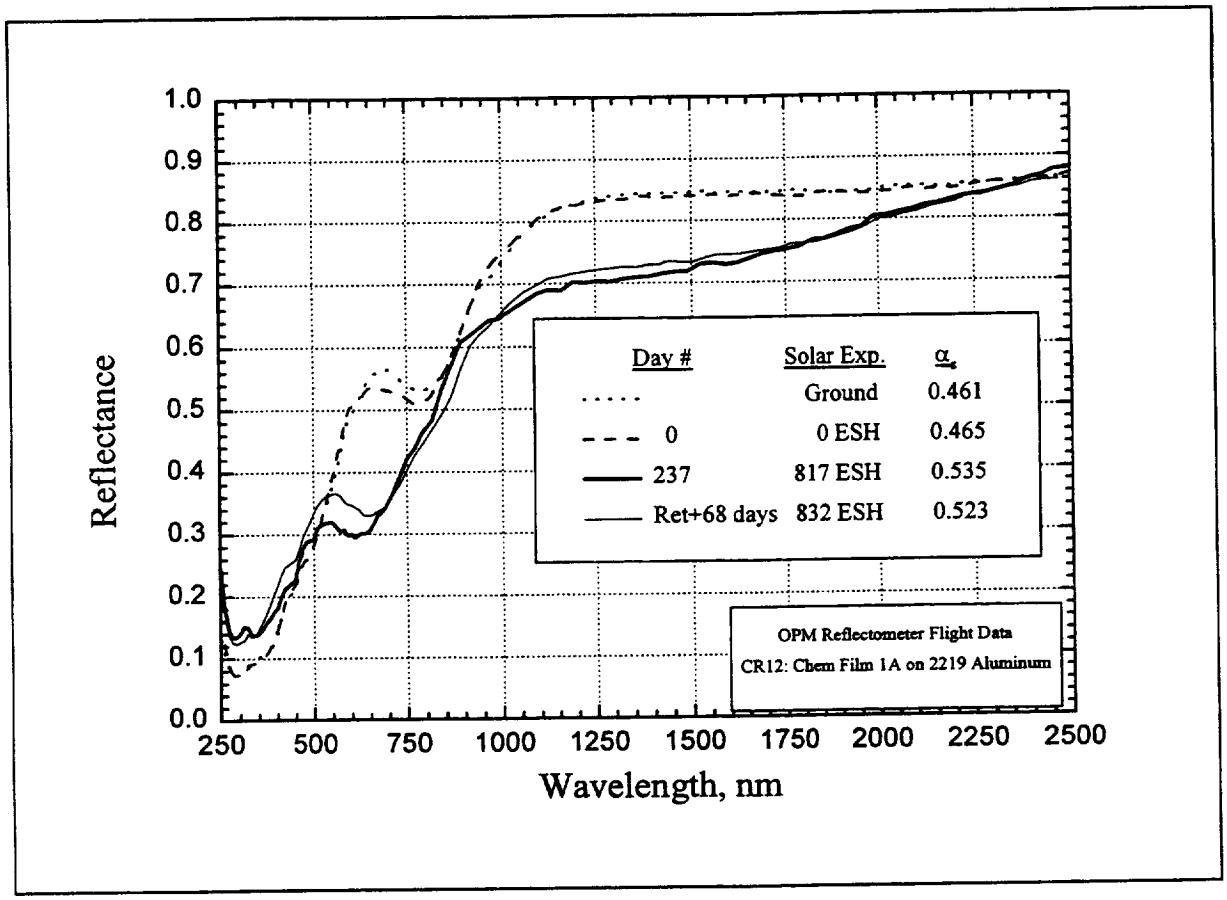

Figure C-12. Reflectometer Data for CR12,
Chem Film on 2219 Aluminum

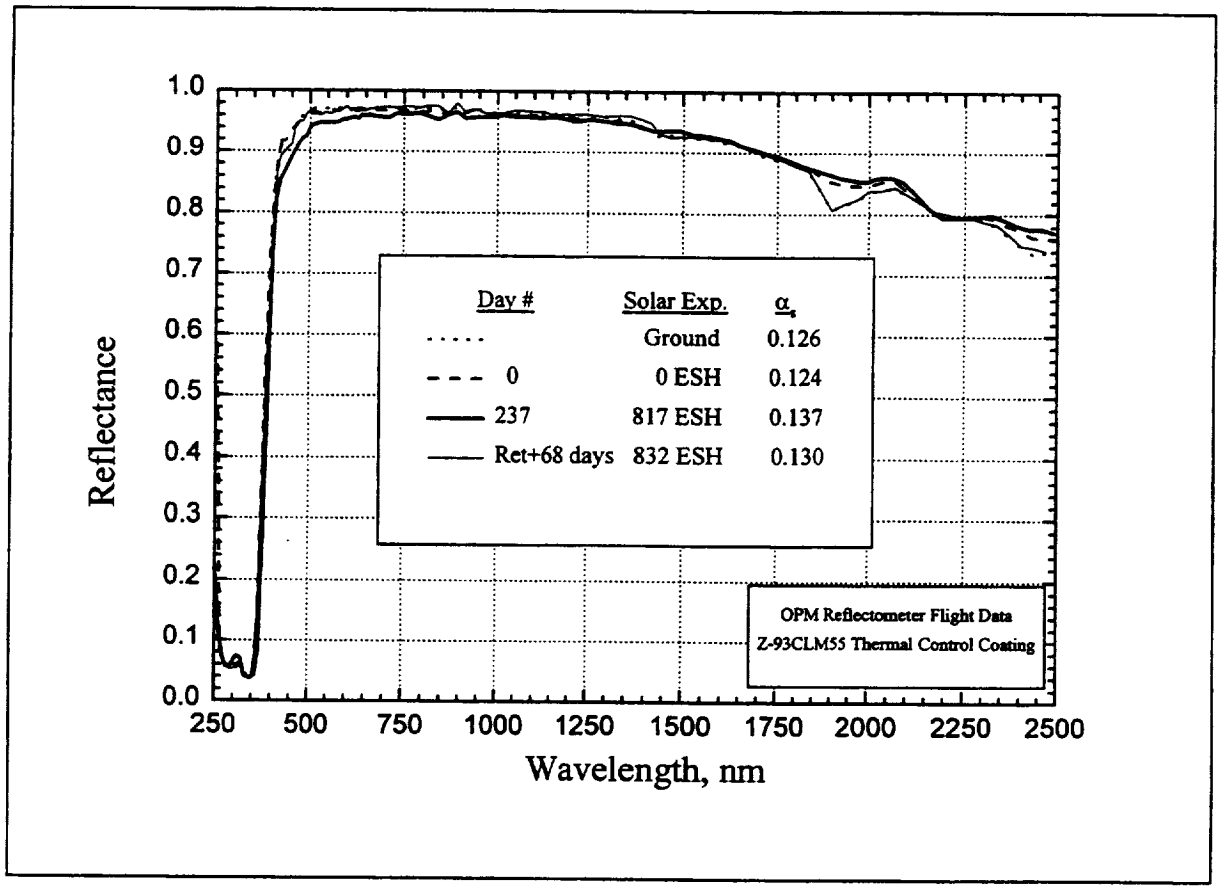

Figure C-13. Reflectometer Data for CR13,
Z-93CLM55 Thermal Control Coating

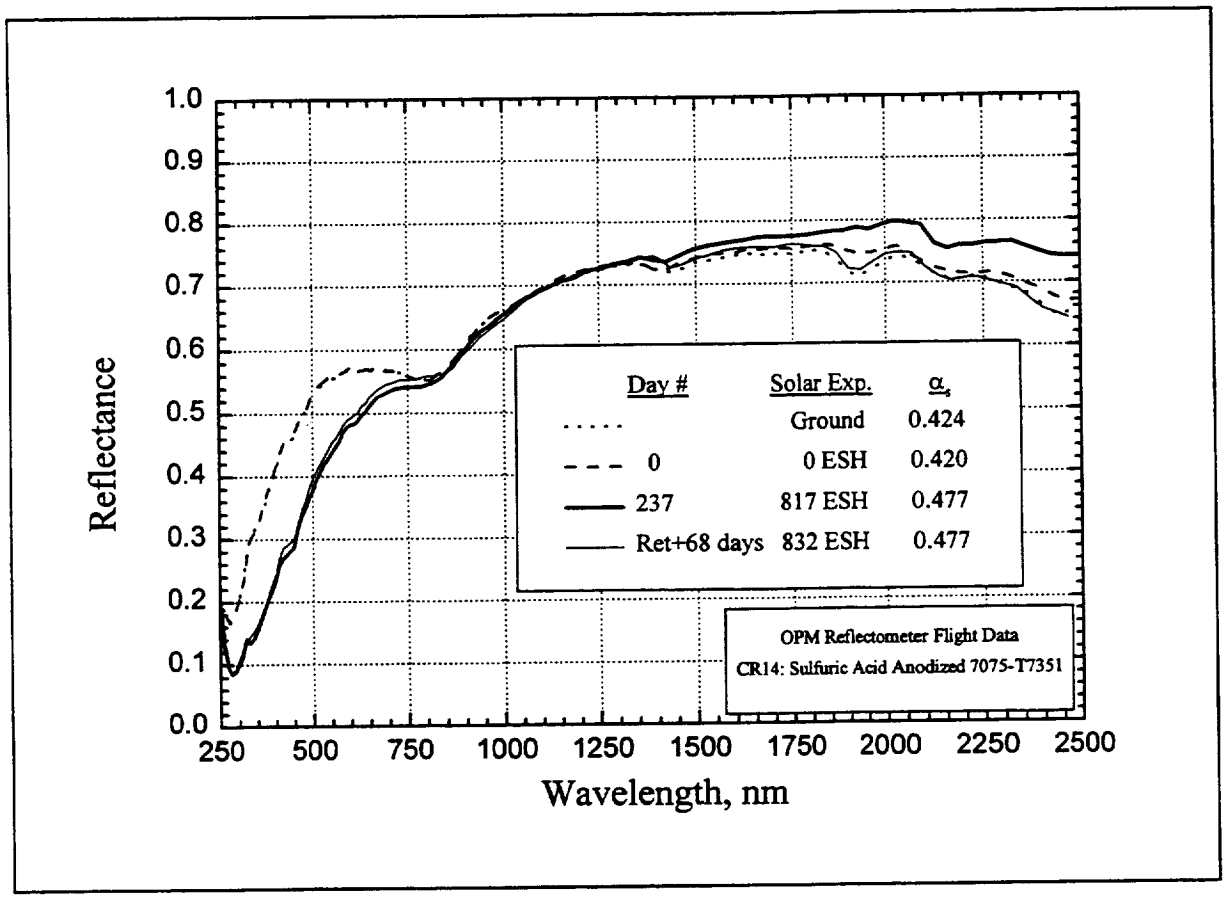

Figure C-14. Reflectometer Data for CR14,
Sulfuric Acid Anodized 7075-T7351

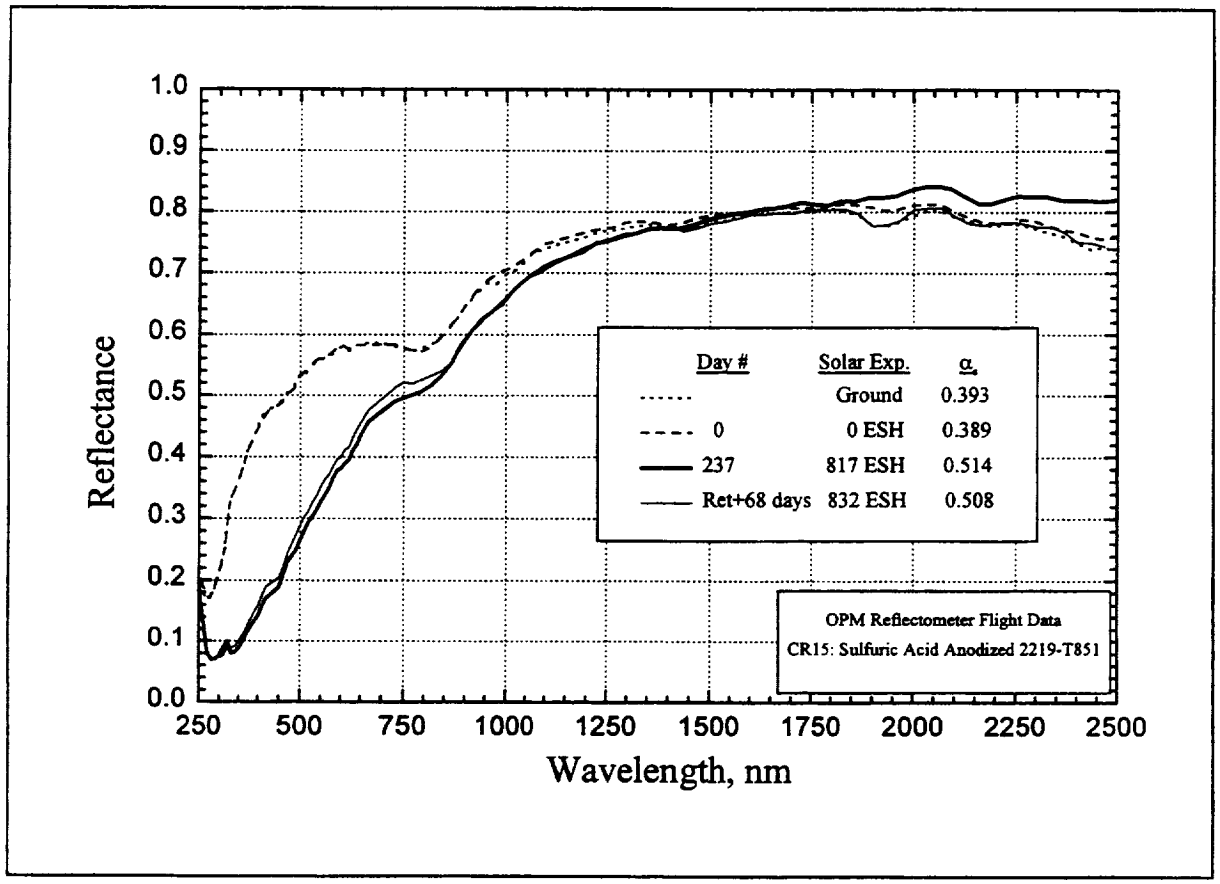

Figure C-15. Reflectometer Data for CR15,
Sulfuric Acid Anodized 2219-T851

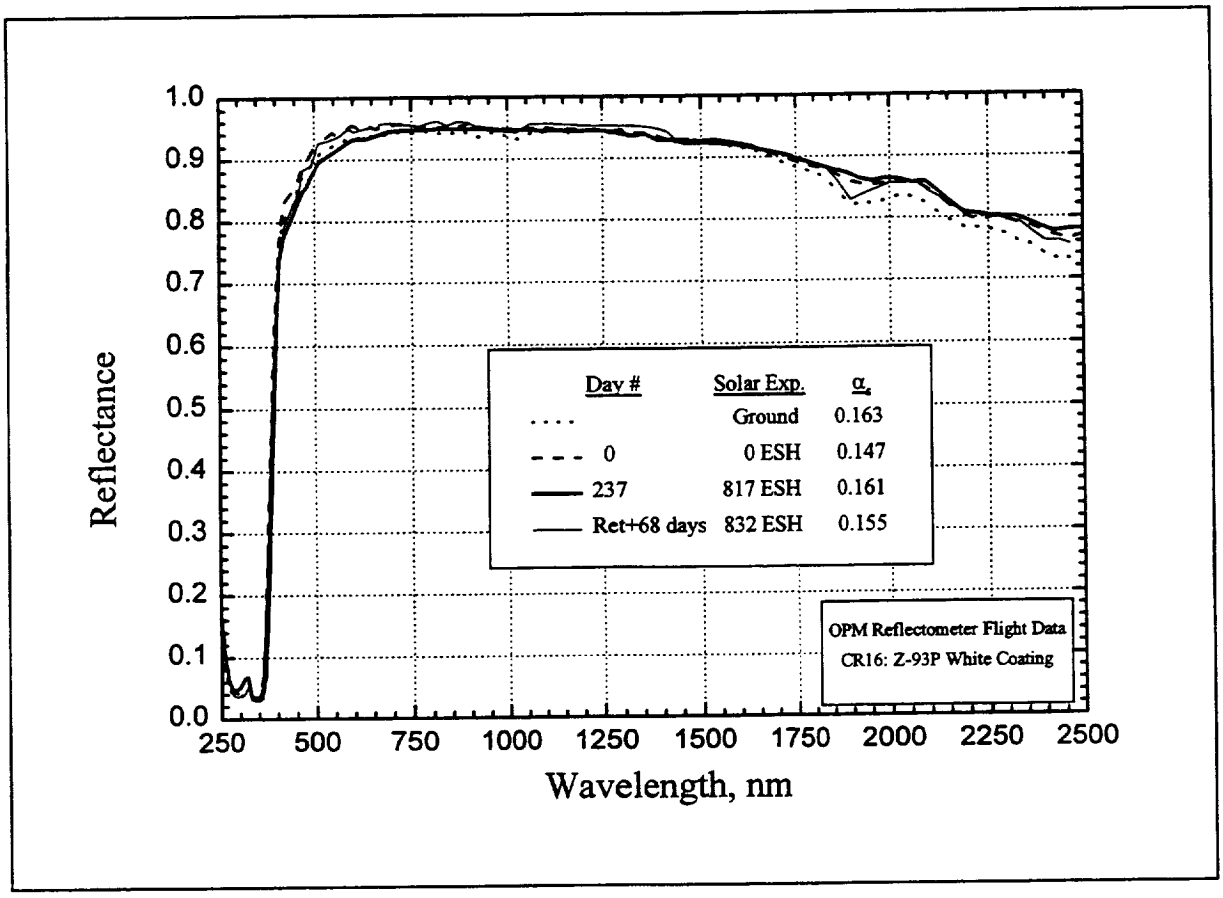

Figure C-16. Reflectometer Data for CR16, Z-93P White Coating

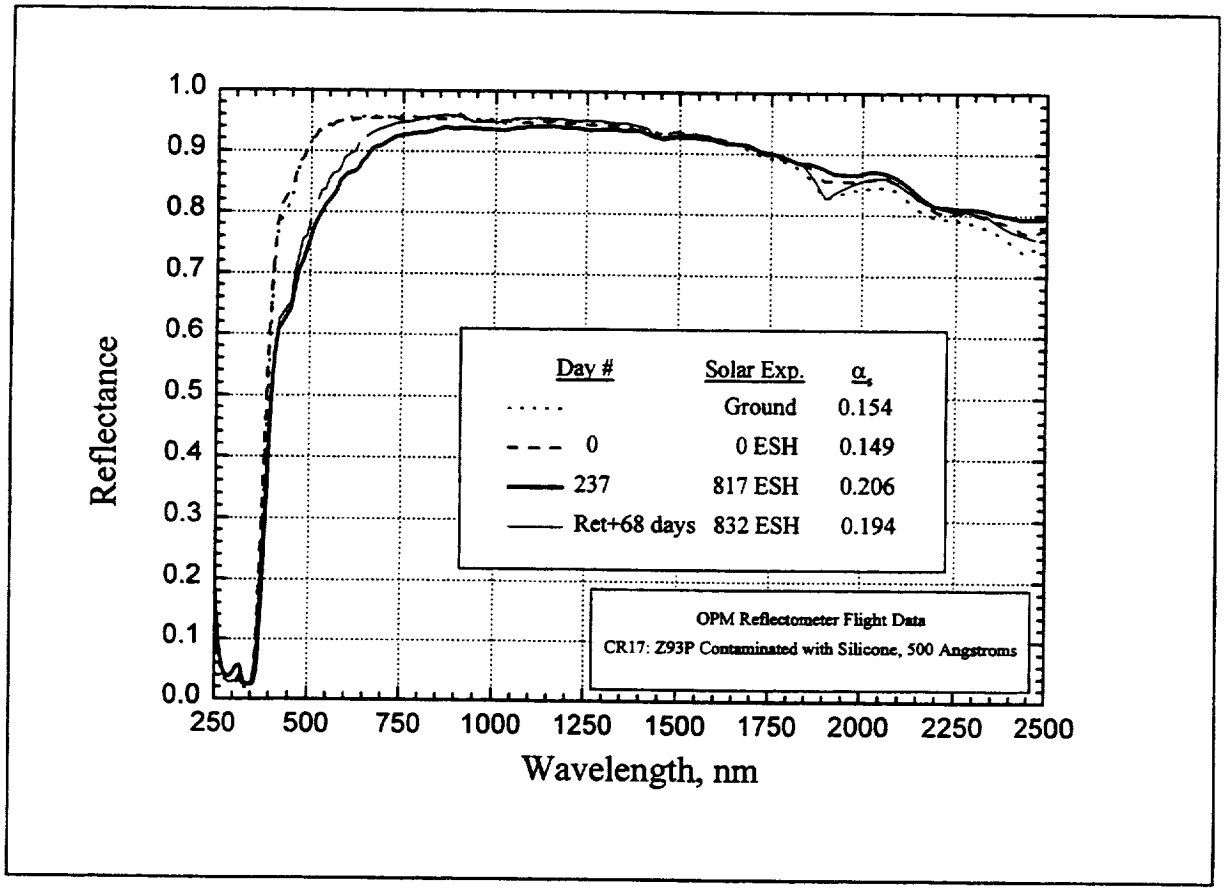

Figure C-17. Reflectometer Data for CR17,
Z93P Contaminated with Silicone, 500 Angstroms

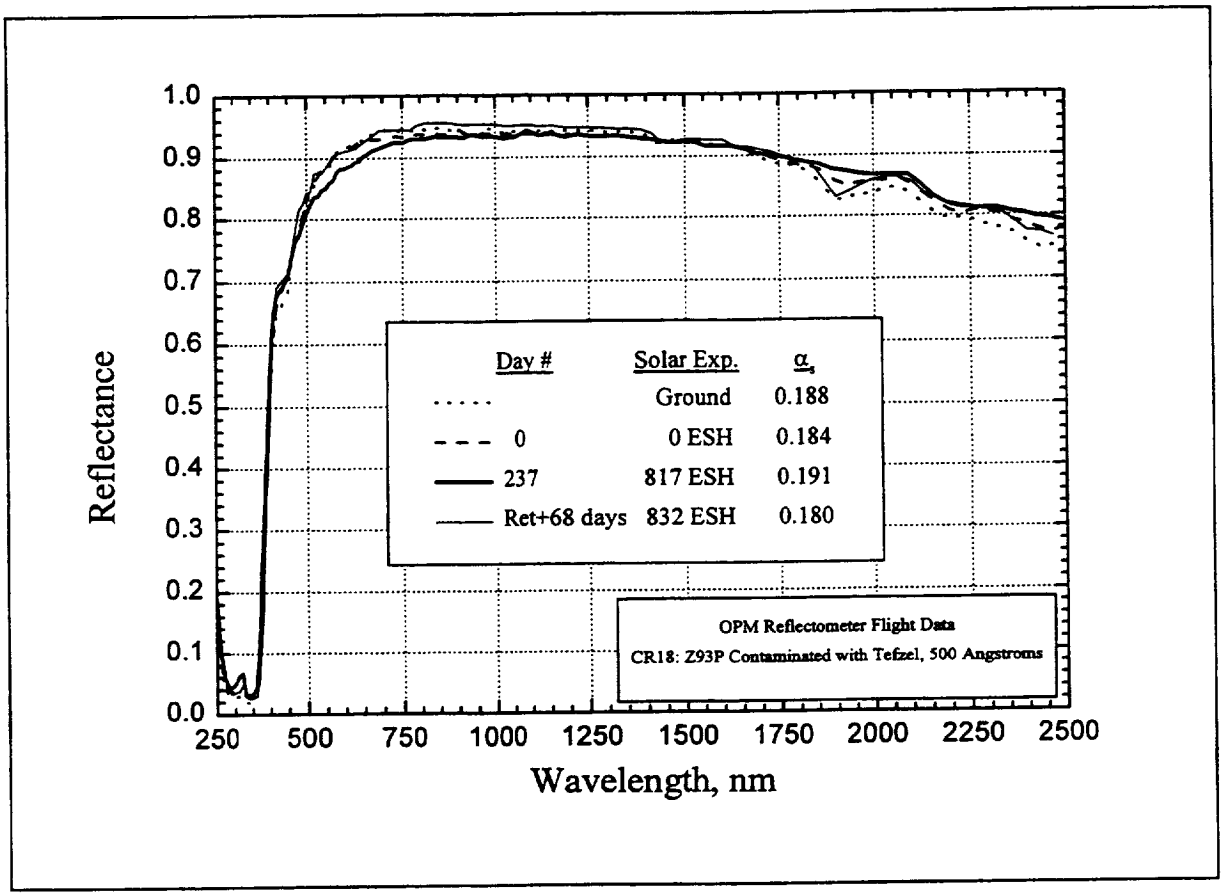

Figure C-18. Reflectometer Data for CR18,
Z93P Contaminated with Tefzel, 500 Angstroms

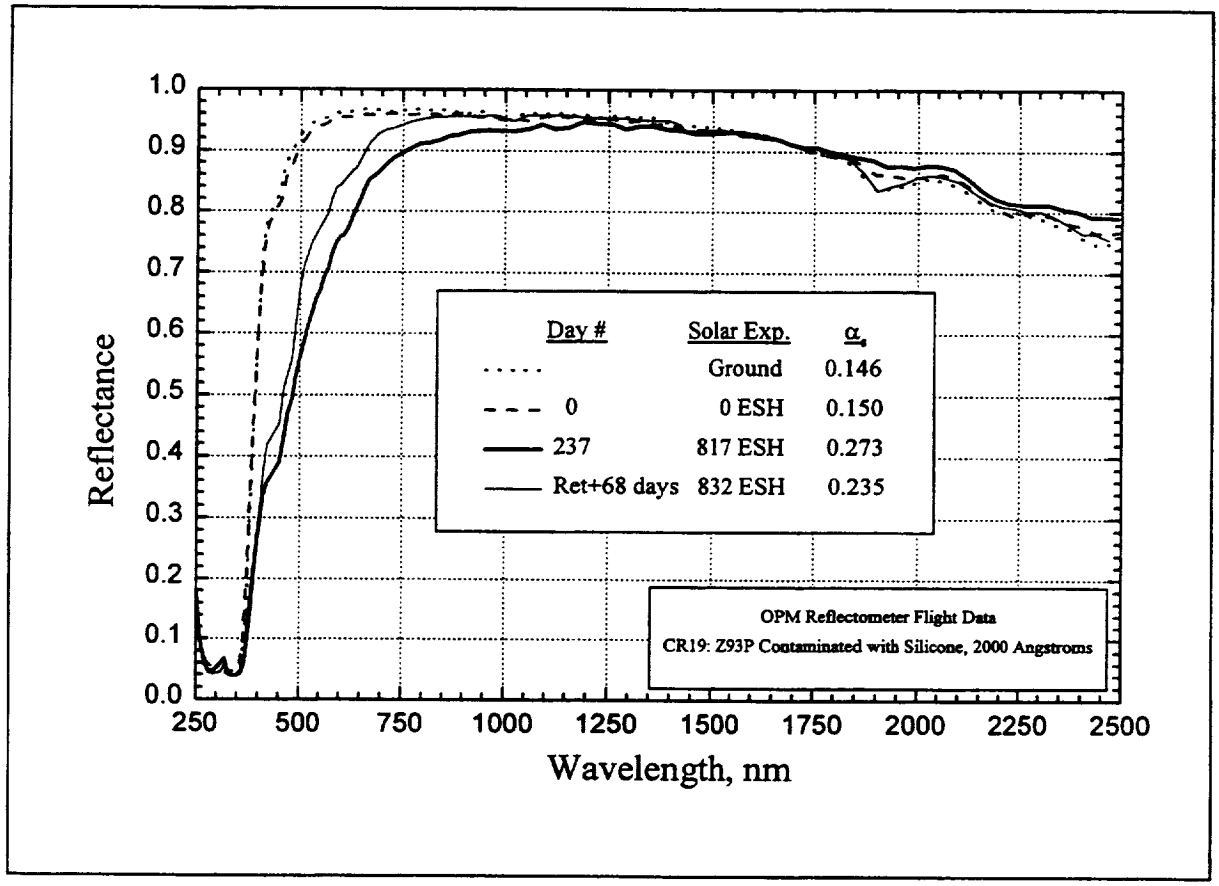

Figure C-19. Reflectometer Data for CR19, Z93P Contaminated with Silicone, 2000 Angstroms

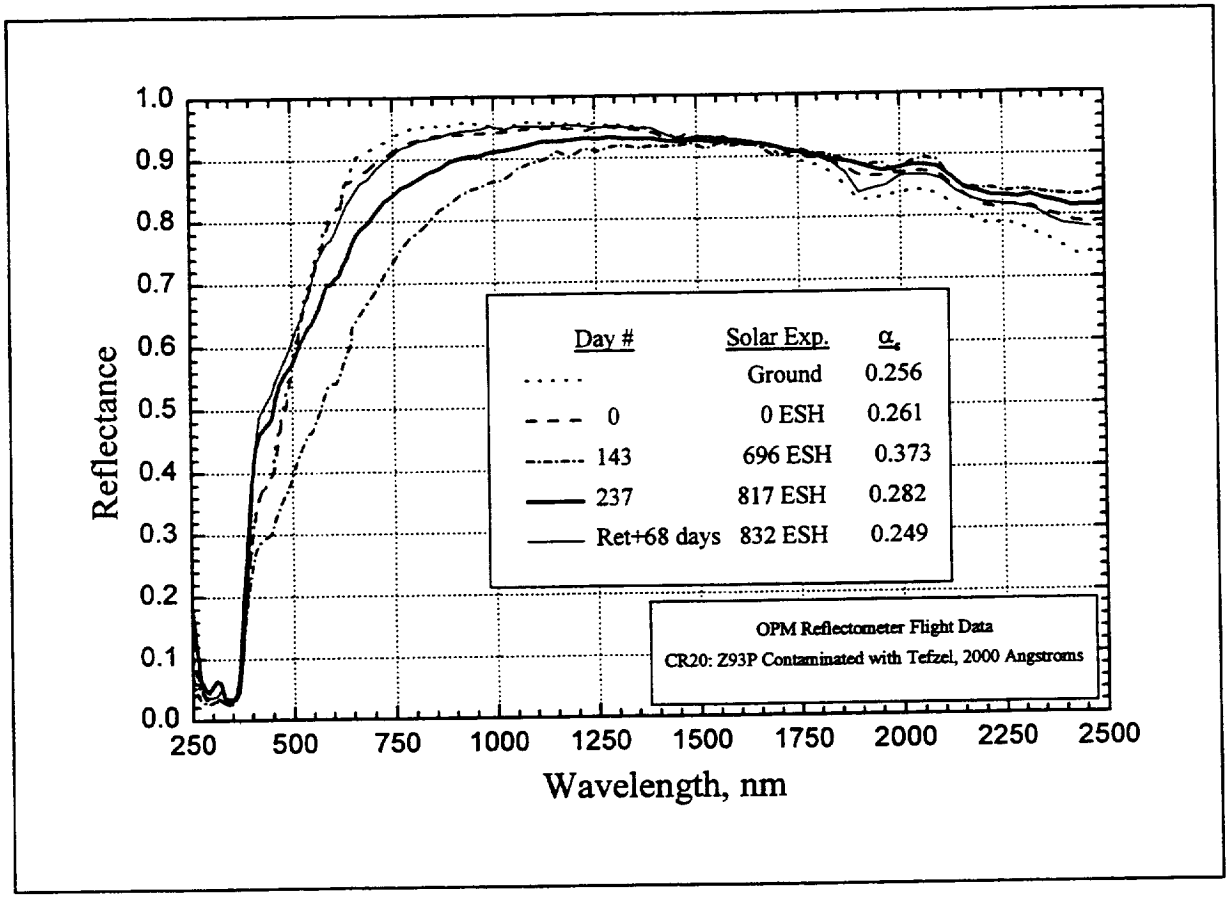

Figure C-20. Reflectometer Data for CR20, Z93P Contaminated with Tefzel, 2000 Angstroms

APPENDIX D

Delta Solar Absorptance for Calorimeters versus Exposure and ESH

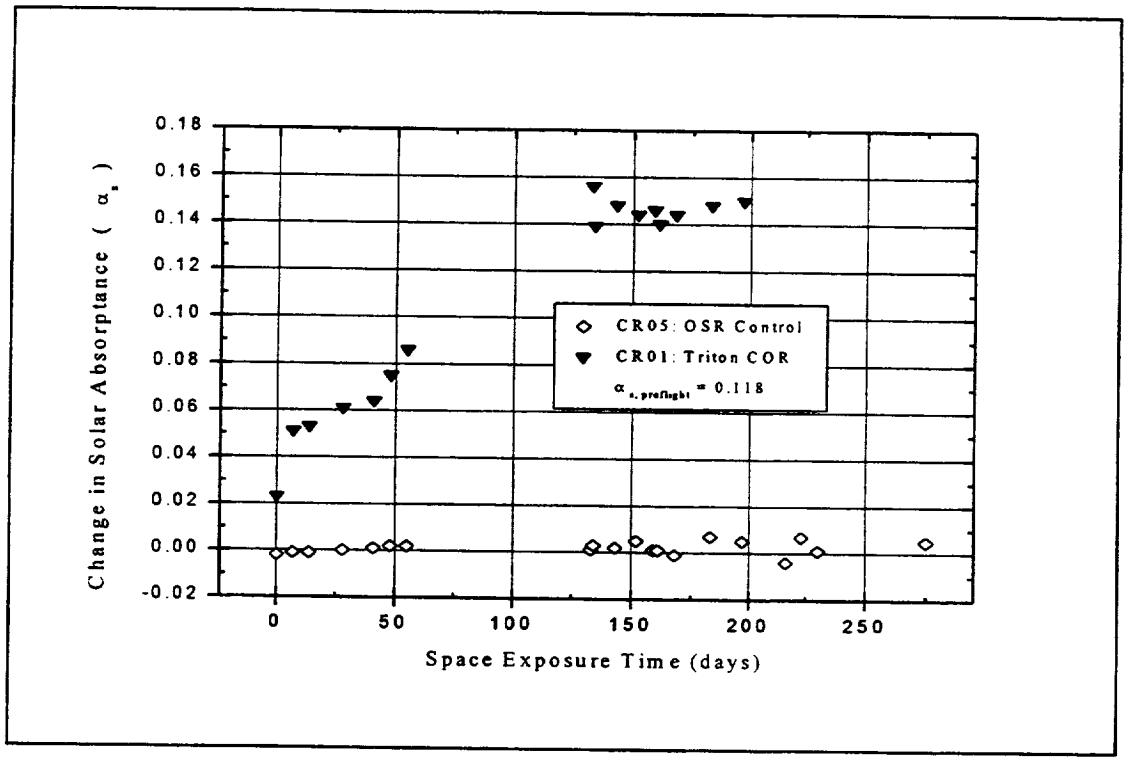

Figure D-1. CR01 Silver Coated COR, Triton – Space Exposure Time (Days)

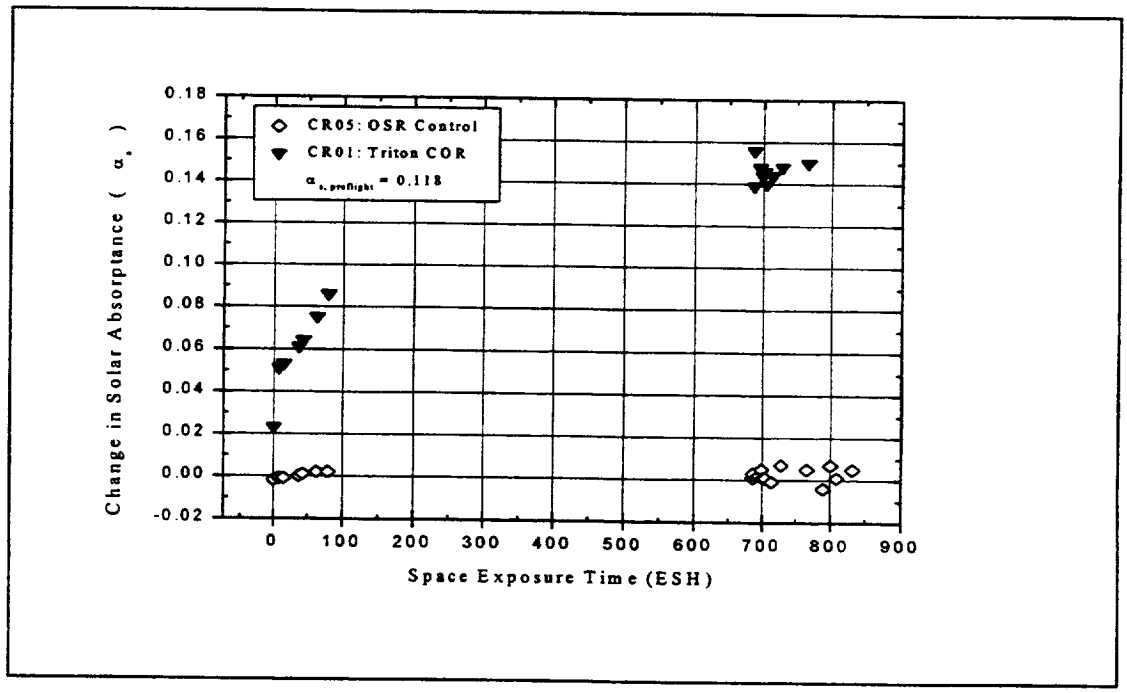

Figure D-2. CR01 Silver Coated COR, Triton – Space Exposure Time (ESH)

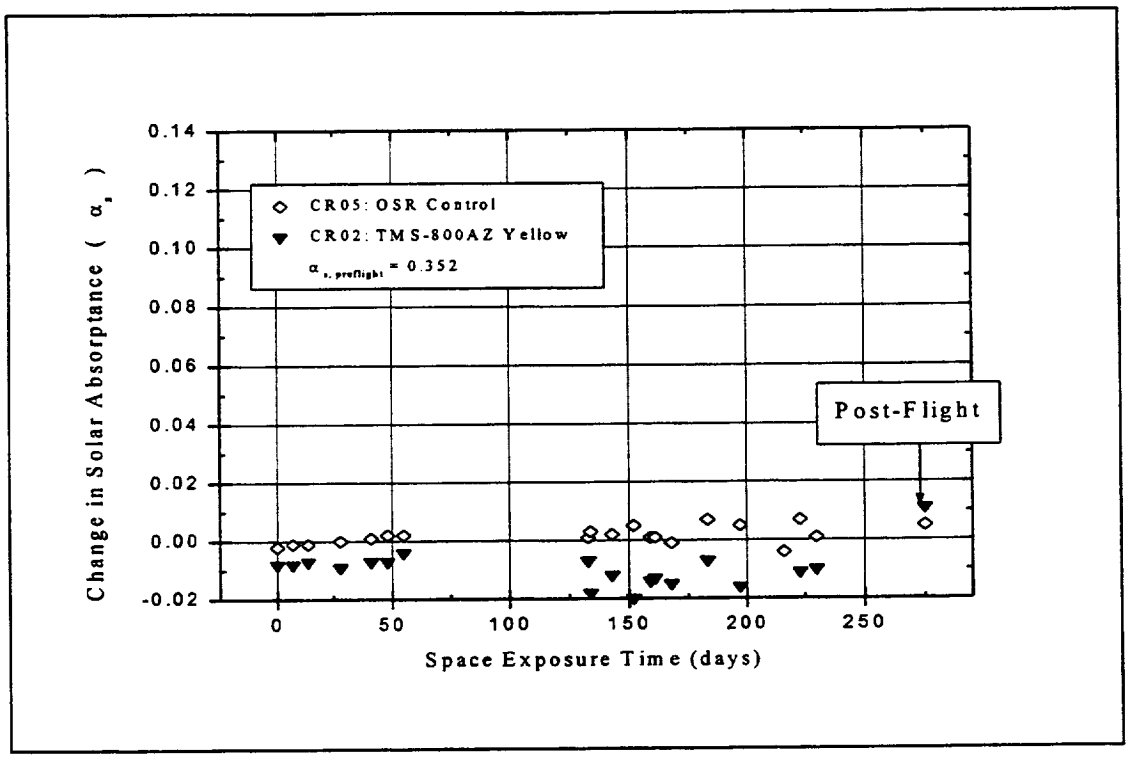

Figure D-3. CR02 TMS-800AZ Yellow – Space Exposure Time (days)

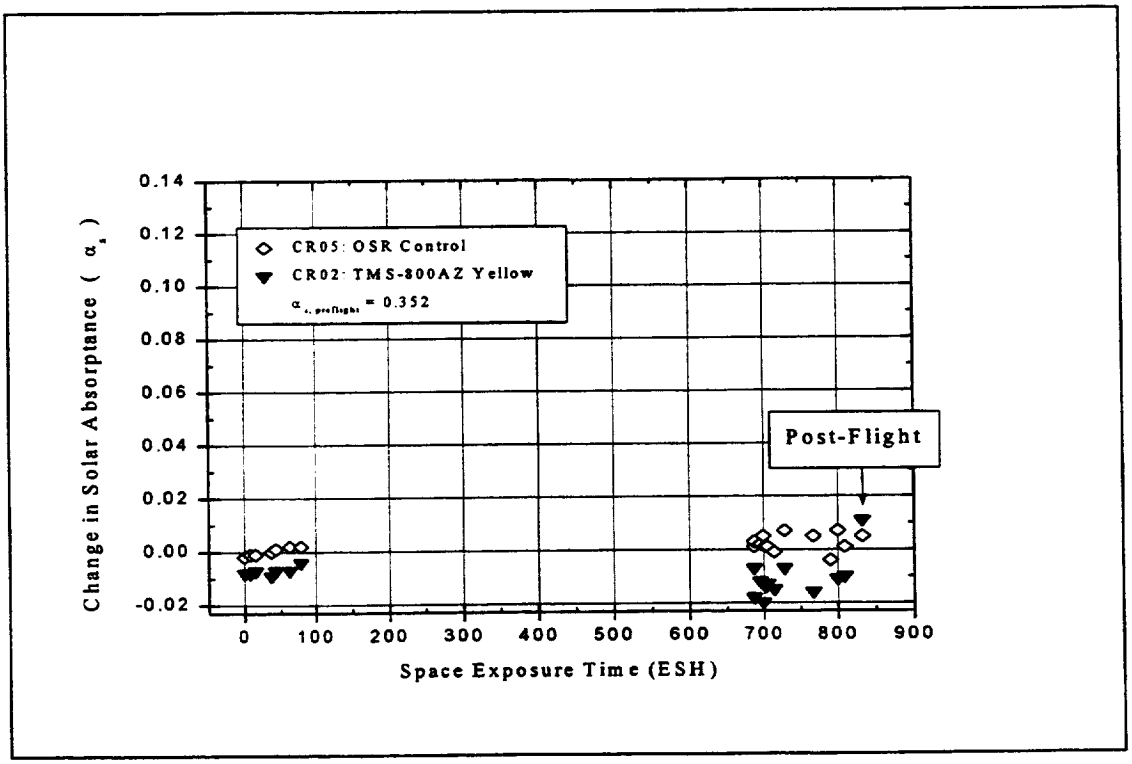

Figure D-4. CR02 TMS-800AZ Yellow – Space Exposure Time (ESH)

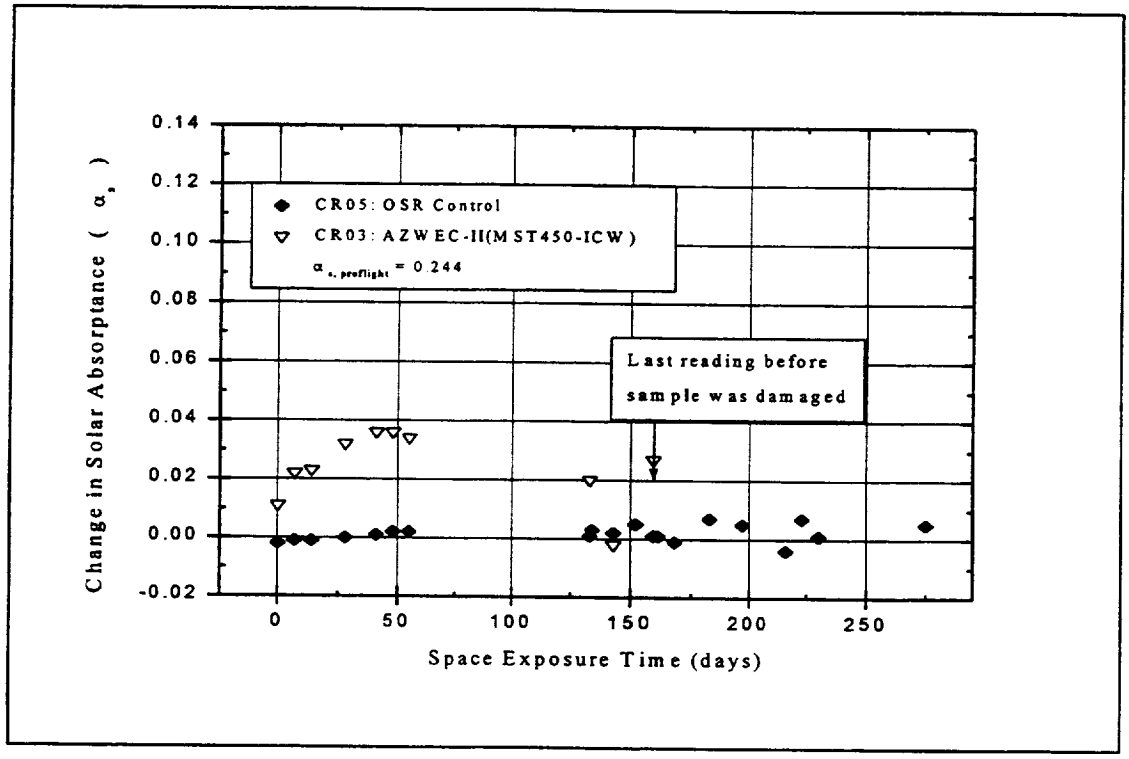

Figure D-5. CR03, AZWEC-II(MST450-ICW) – Space Exposure Time (Days)

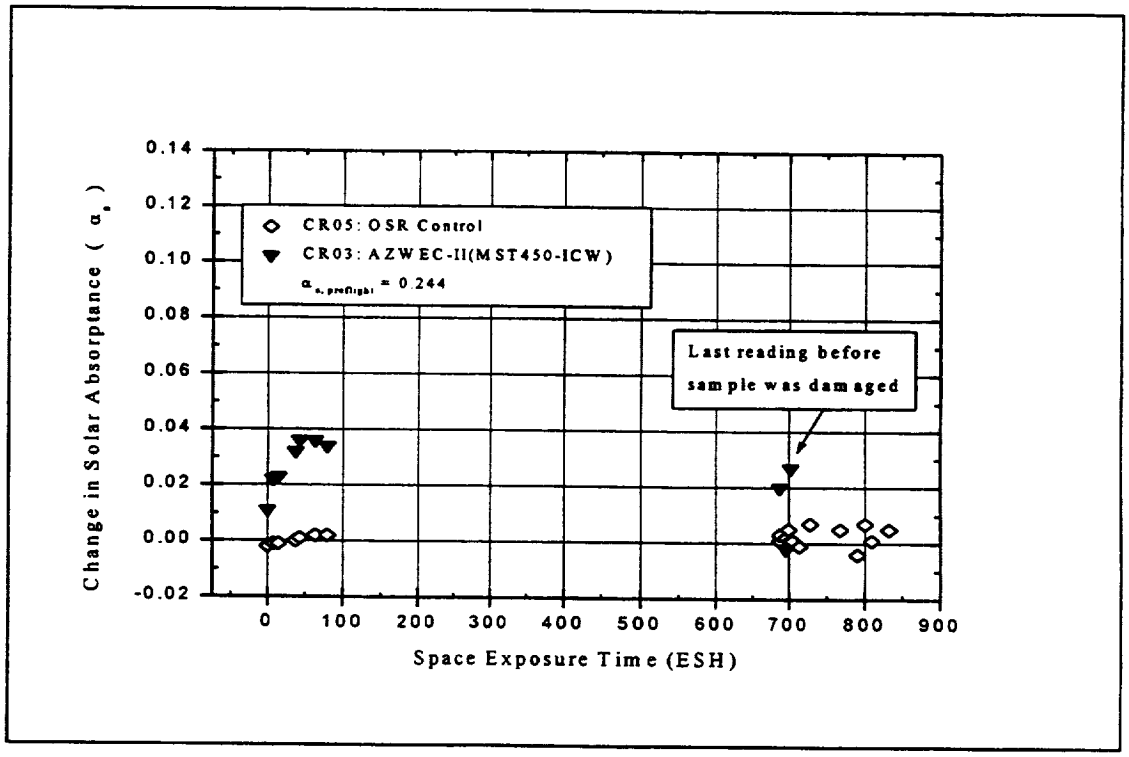

Figure D-6. CR03, AZWEC-II(MST450-ICW) – Space Exposure Time (ESH)

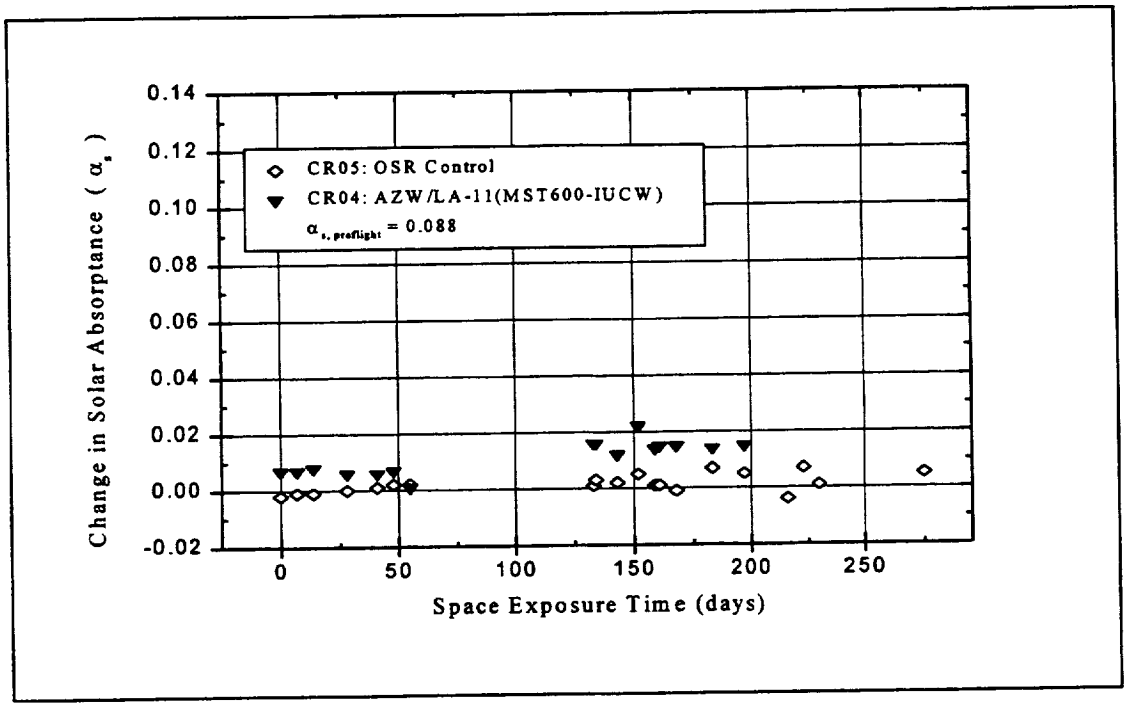

Figure D-7. CR04, AZW/LA-11 (MST600-IUCW) – Space Exposure Time (Days)

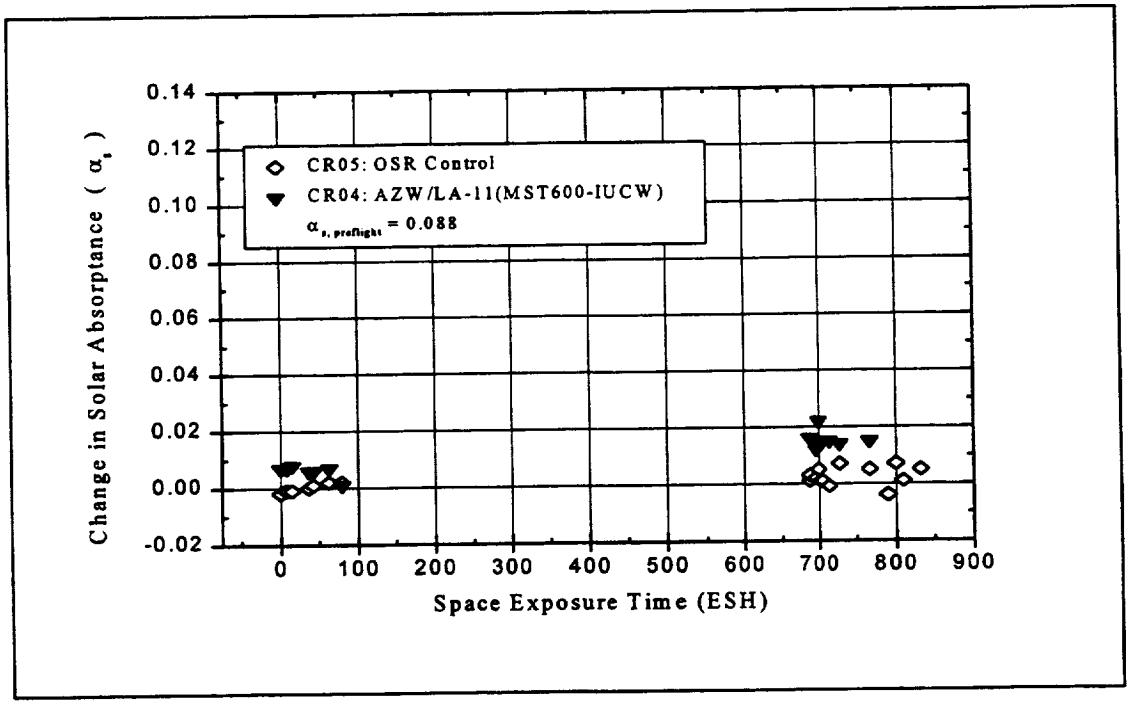

Figure D-8. CR04, AZW/LA-11 (MST600-IUCW) – Space Exposure Time (ESH)

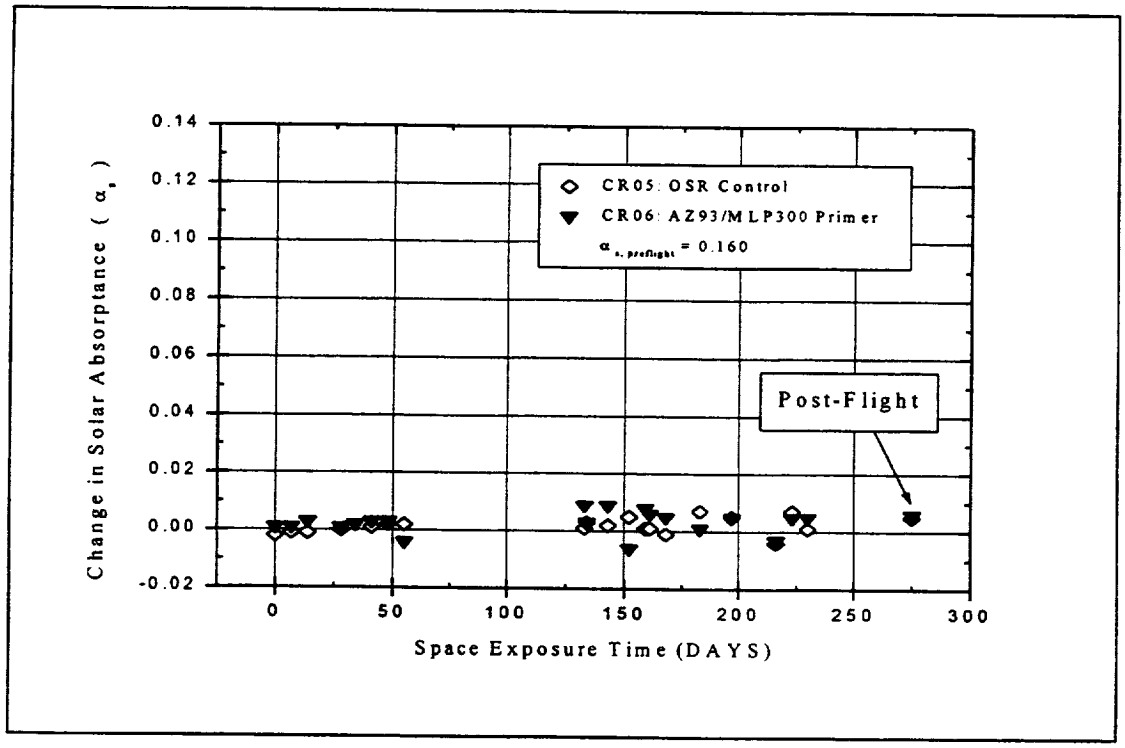

Figure D-9. CR06, AZ93/MLP300 – Space Exposure Time (Days)

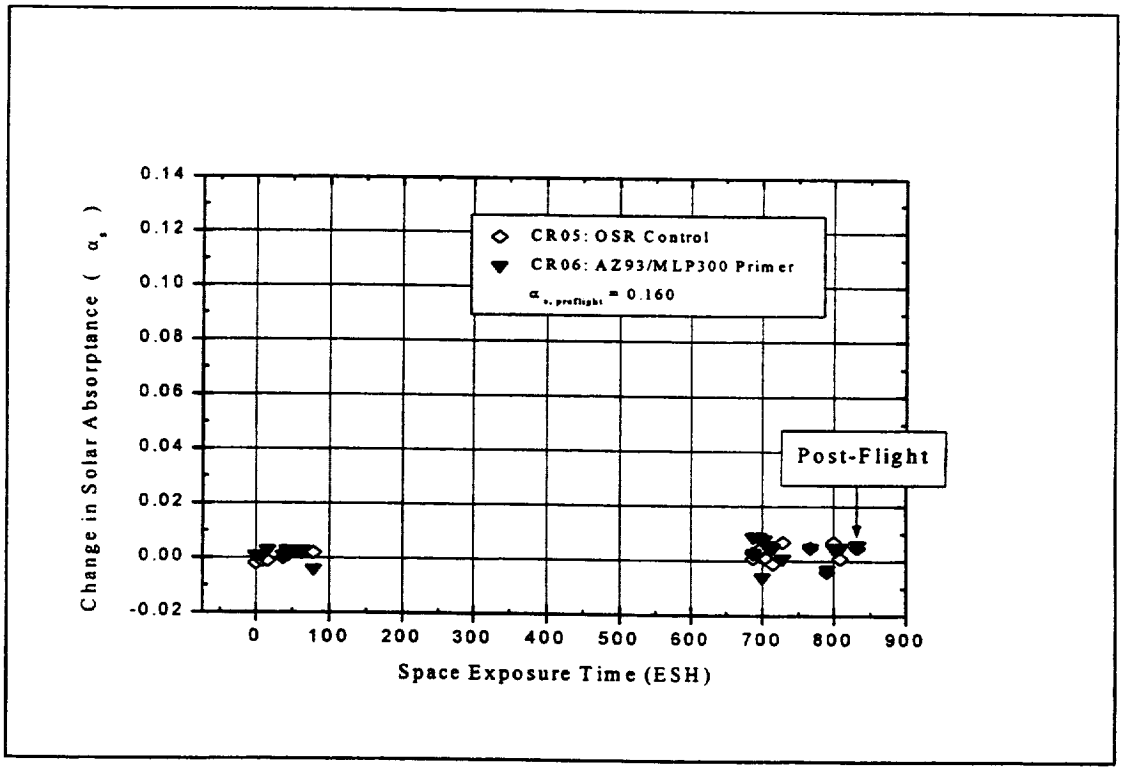

Figure D-10. CR06, AZ93/MLP300 – Space Exposure Time (ESH)

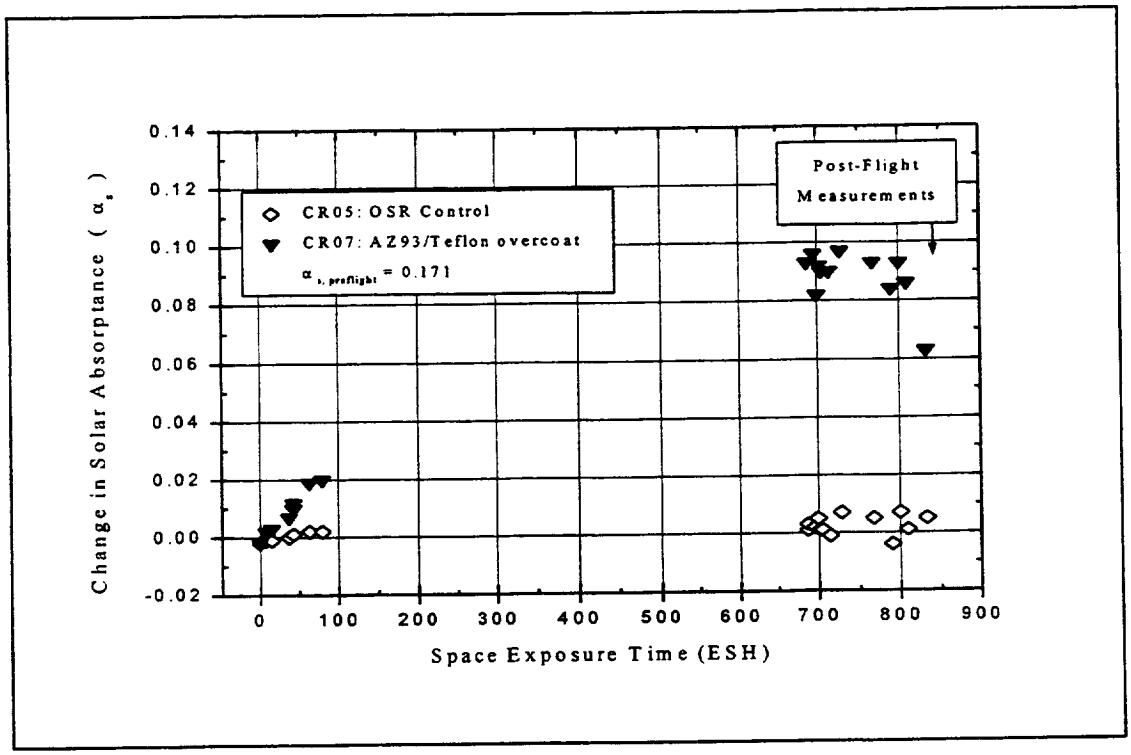

Figure D-11. CR07 Z93/TEFLON™ OVERCOAT – Space Exposure Time (ESH)

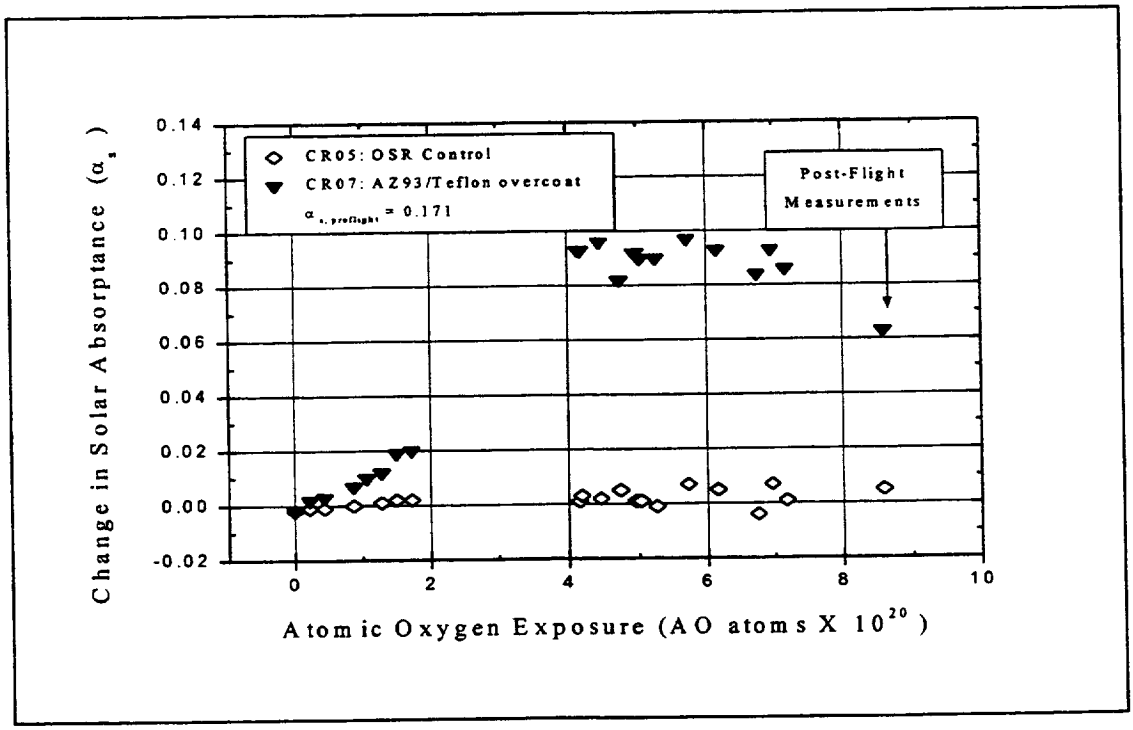

Figure D-12. CR07 Z93/TEFLON™ OVERCOAT – Space Exposure Time (AO)

™ trademark of DuPont Corp.

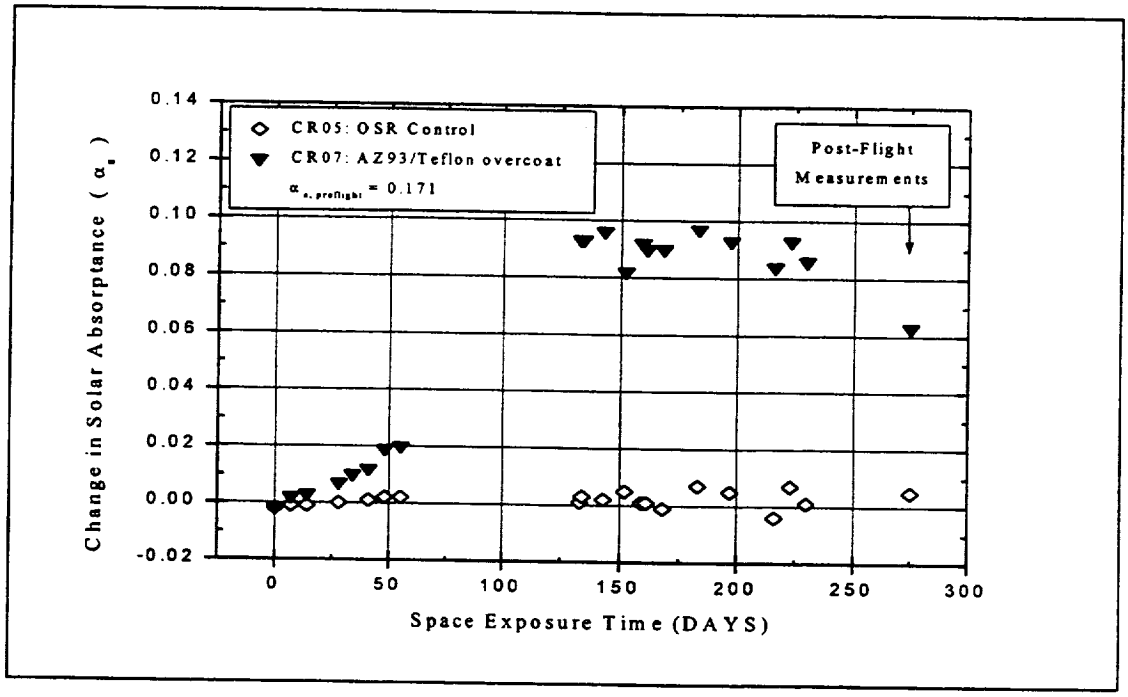

Figure D-13. CR07 Z93/TEFLON™ OVERCOAT – Space Exposure Time (Days)

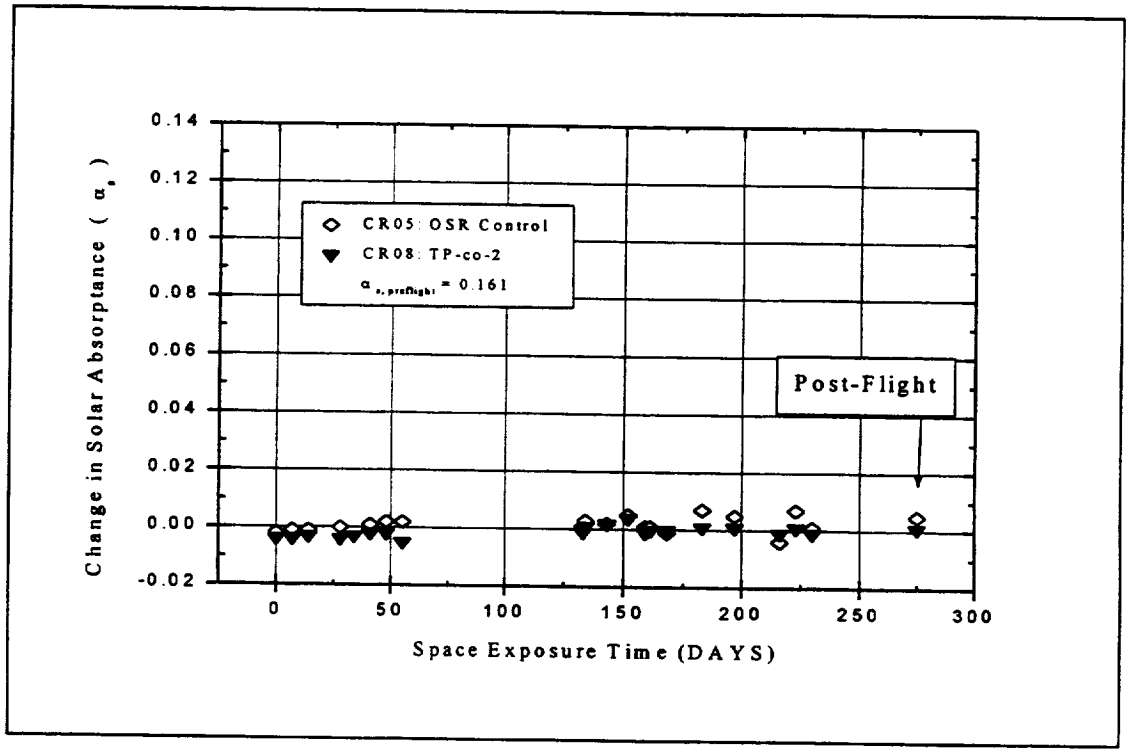

Figure D-14. CR08, TP-co-2 – Space Exposure Time (Days)

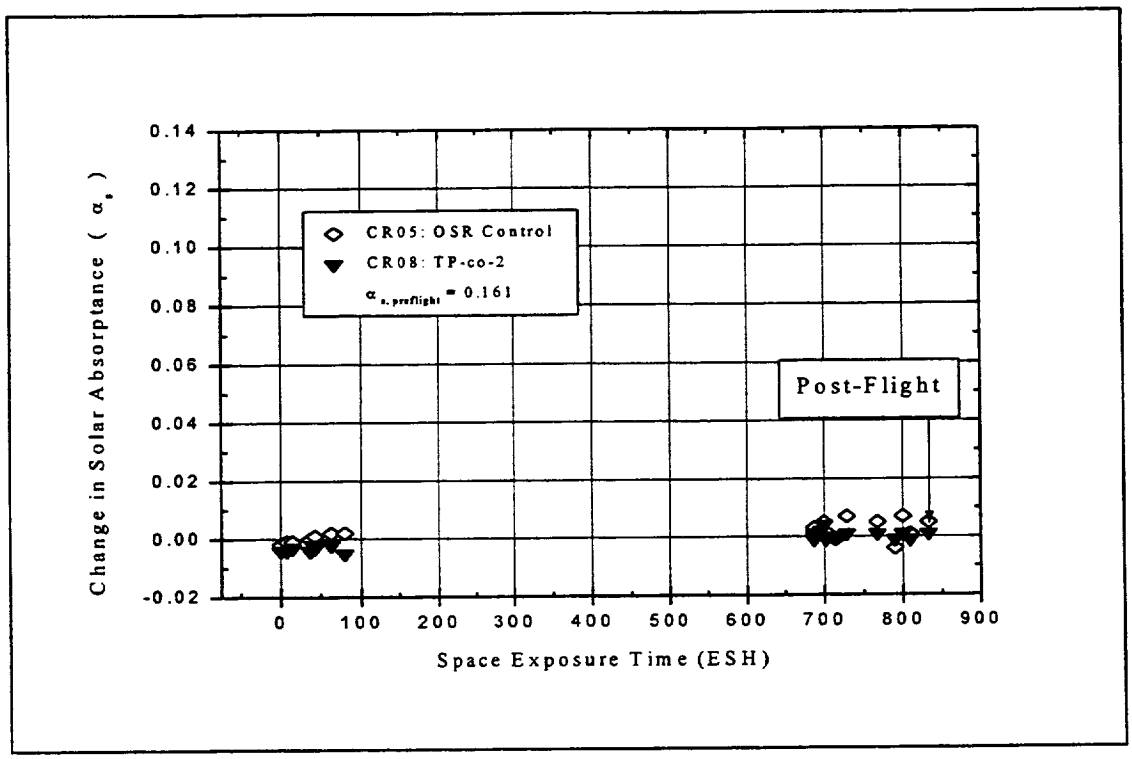

Figure D-15. CR08, TP-co-2 – Space Exposure Time (ESH)

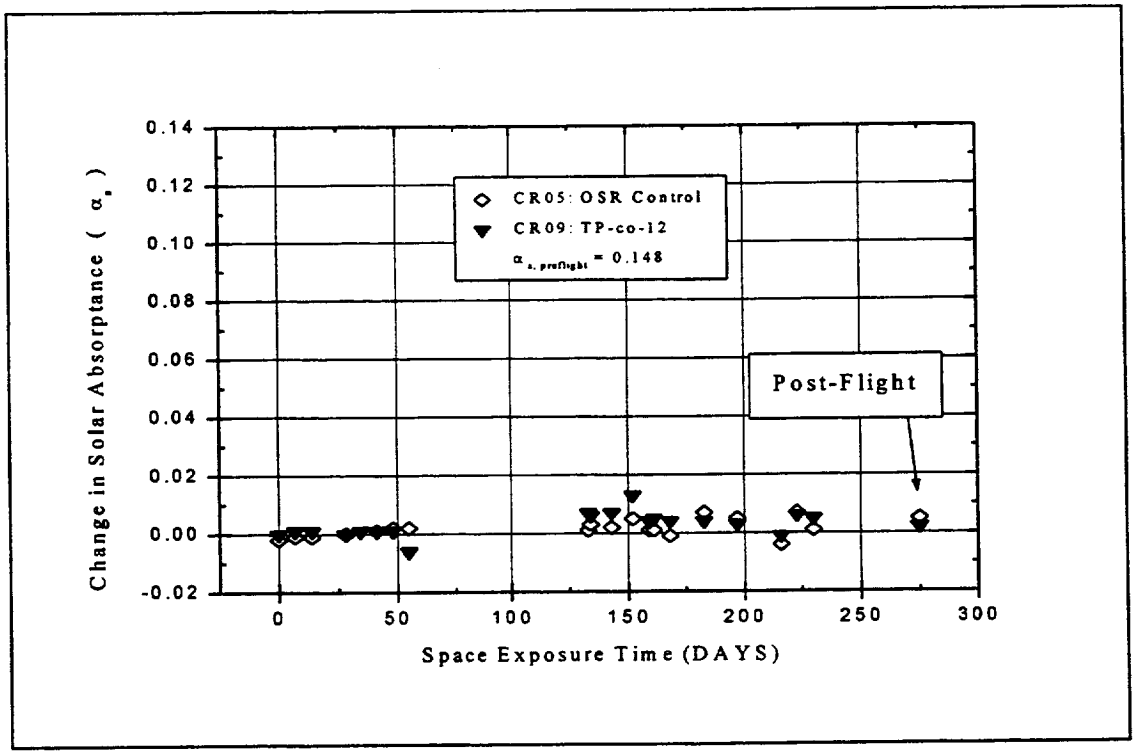

Figure D-16. CR09, TP-co-12 – Space Exposure Time (Days)

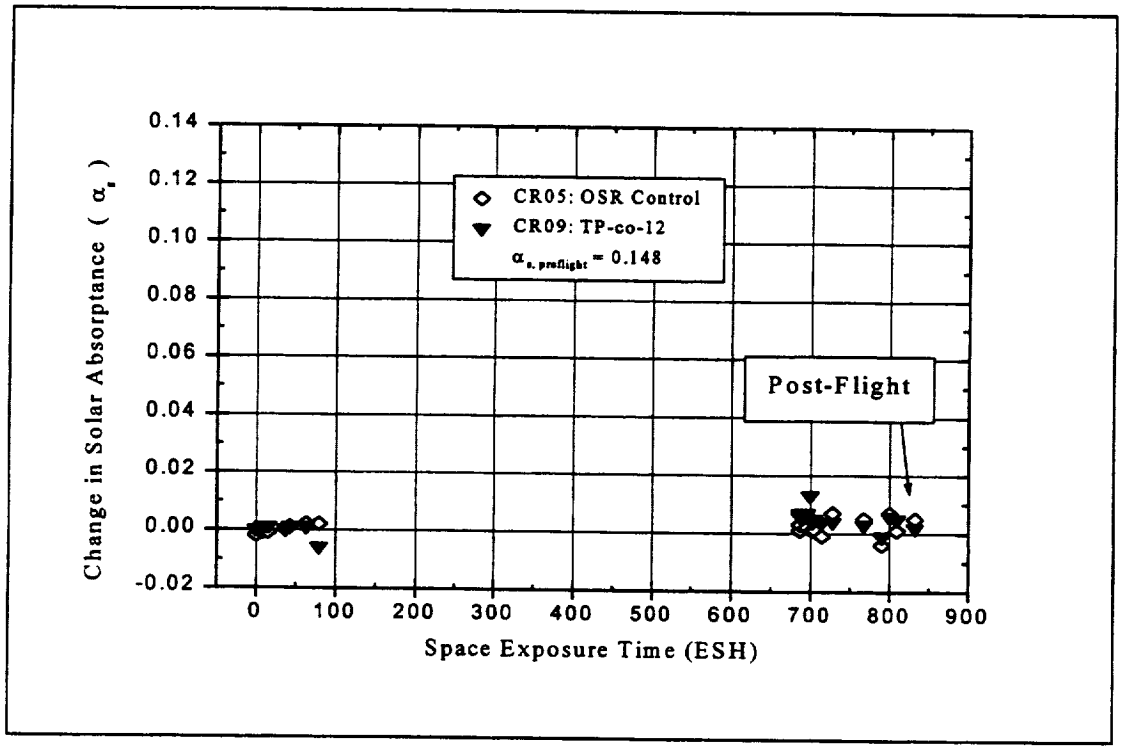

Figure D-17. CR09, TP-co-12 – Space Exposure Time (ESH)

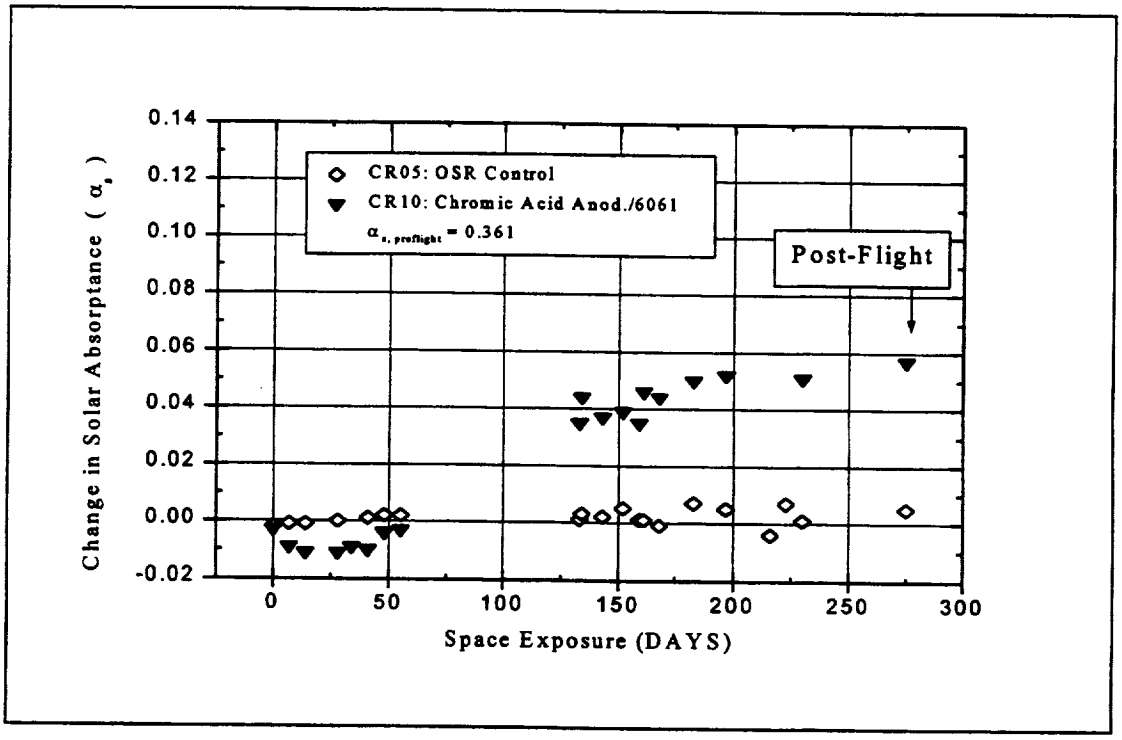

Figure D-18. CR10, Chromic Acid Anodize/6061 – Space Exposure Time (Days)

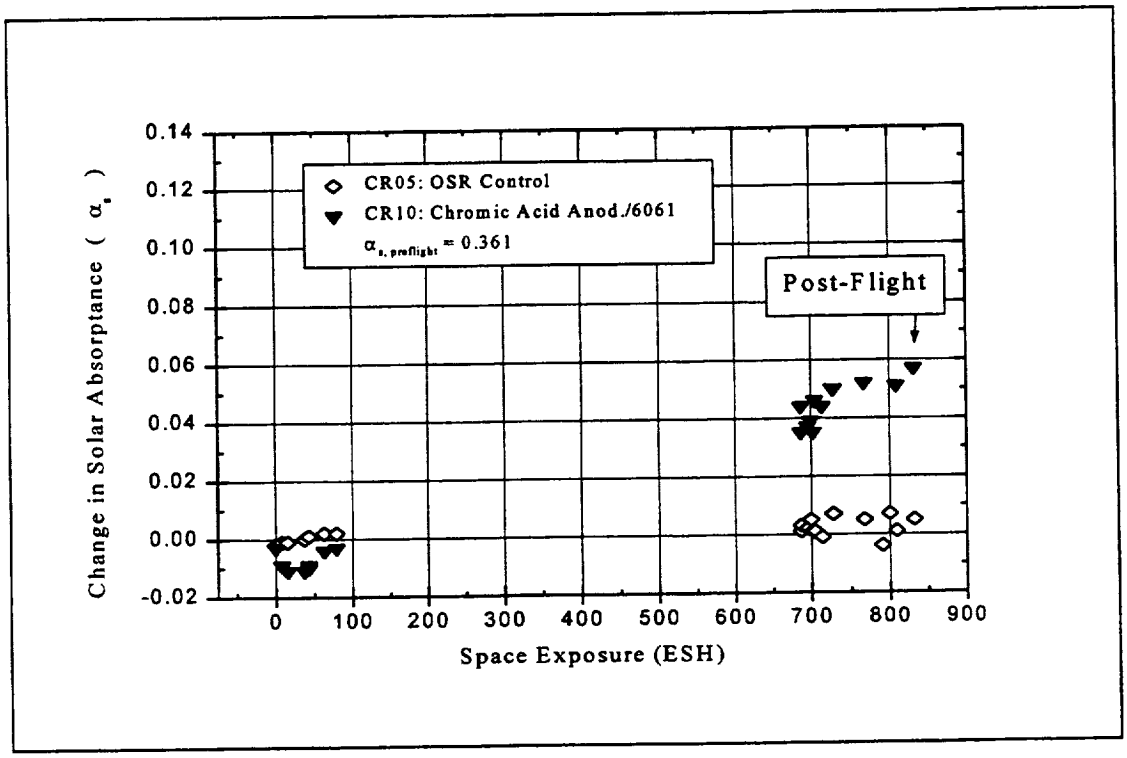

Figure D-19. CR10, Chromic Acid Anodize/6061 – Space Exposure Time (ESH)

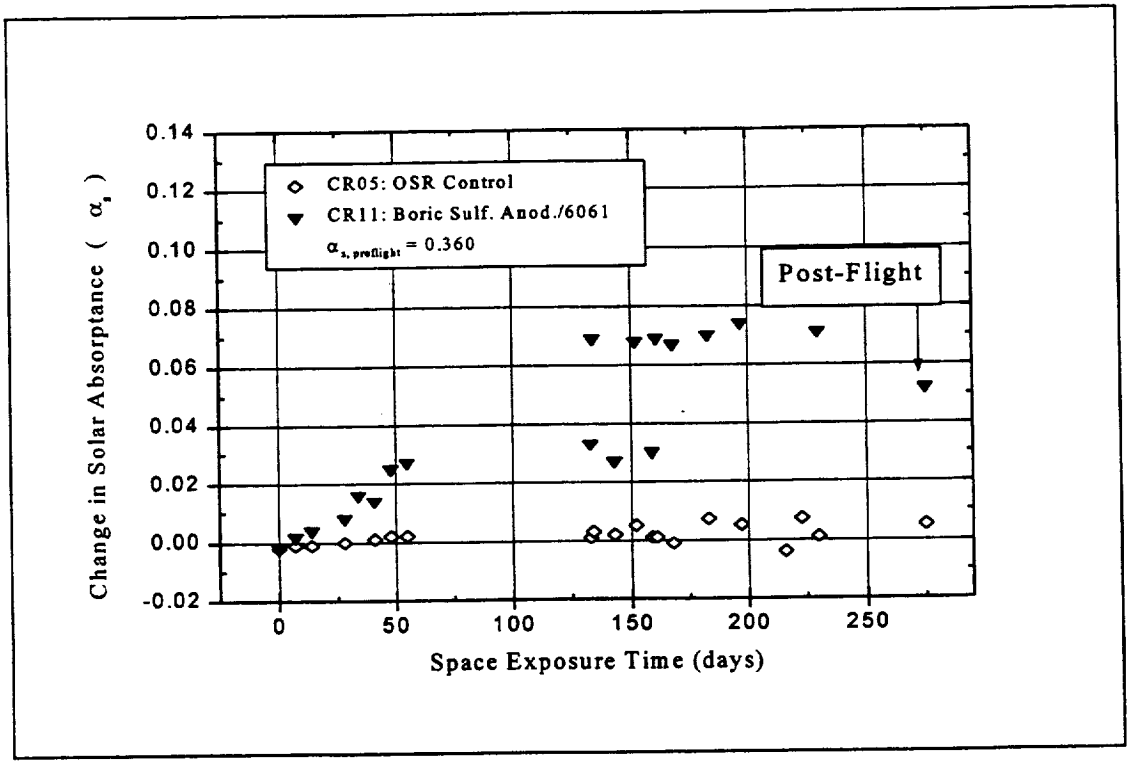

Figure D-20. CR11, Boric Sulfuric Anodize/6061 – Space Exposure time (Days)

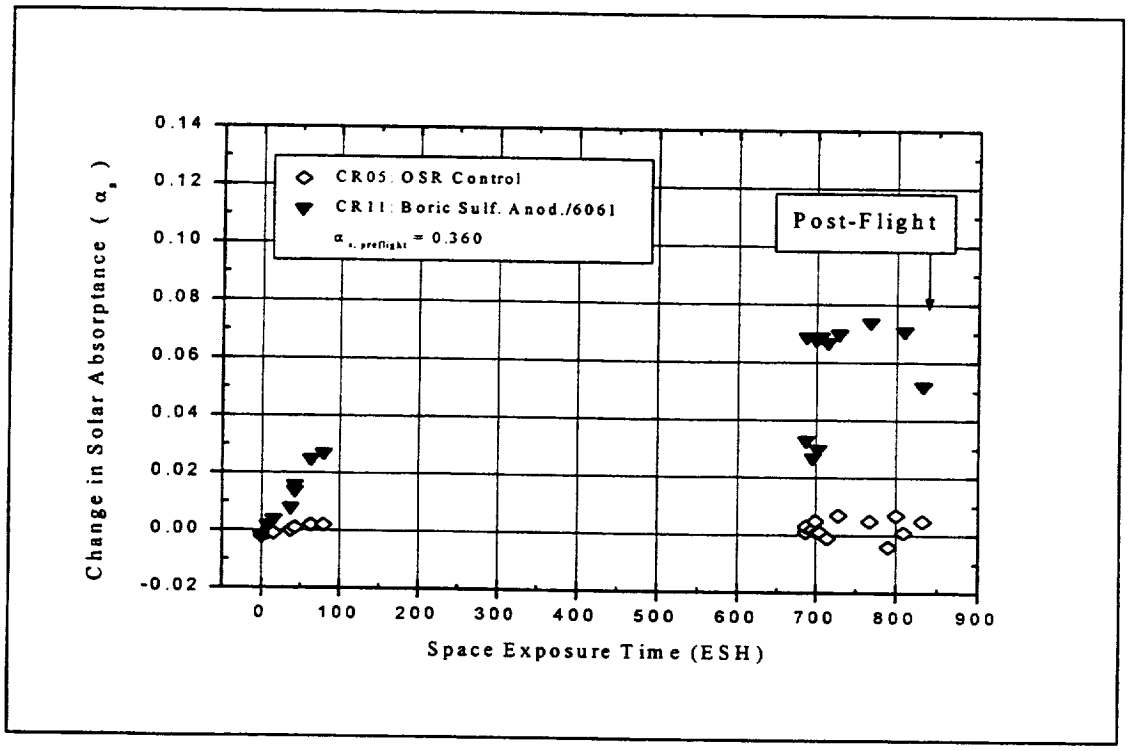

Figure D-21. CR11, Boric Sulfuric Anodize/6061 – Space Exposure time (ESH)

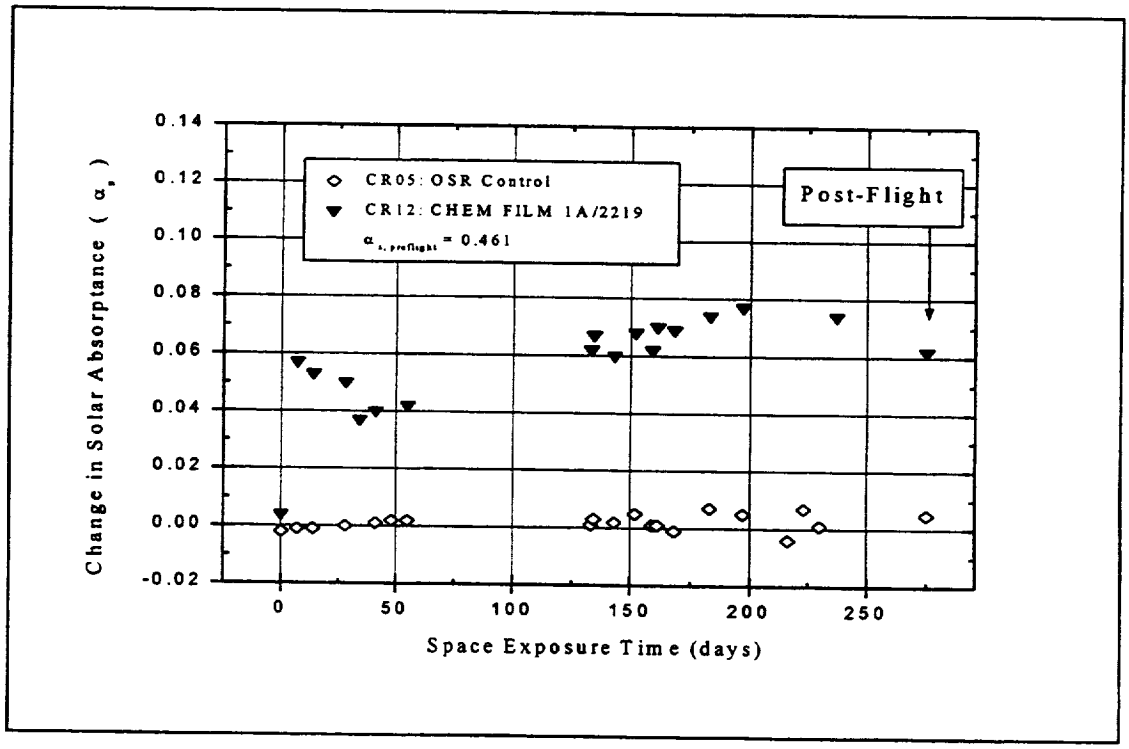

Figure D-22. CR12, Chem Film 1A/2219 – Space Exposure Time (Days)

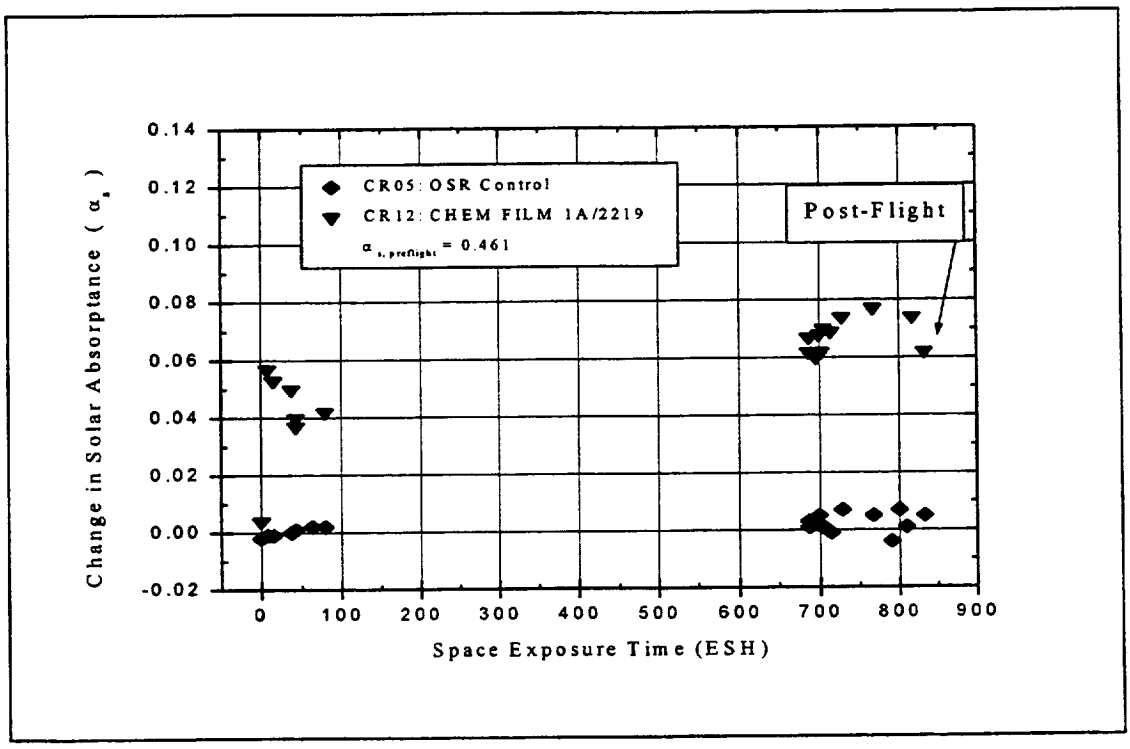

Figure D-23. CR12, Chem Film 1A/2219 – Space Exposure Time (ESH)

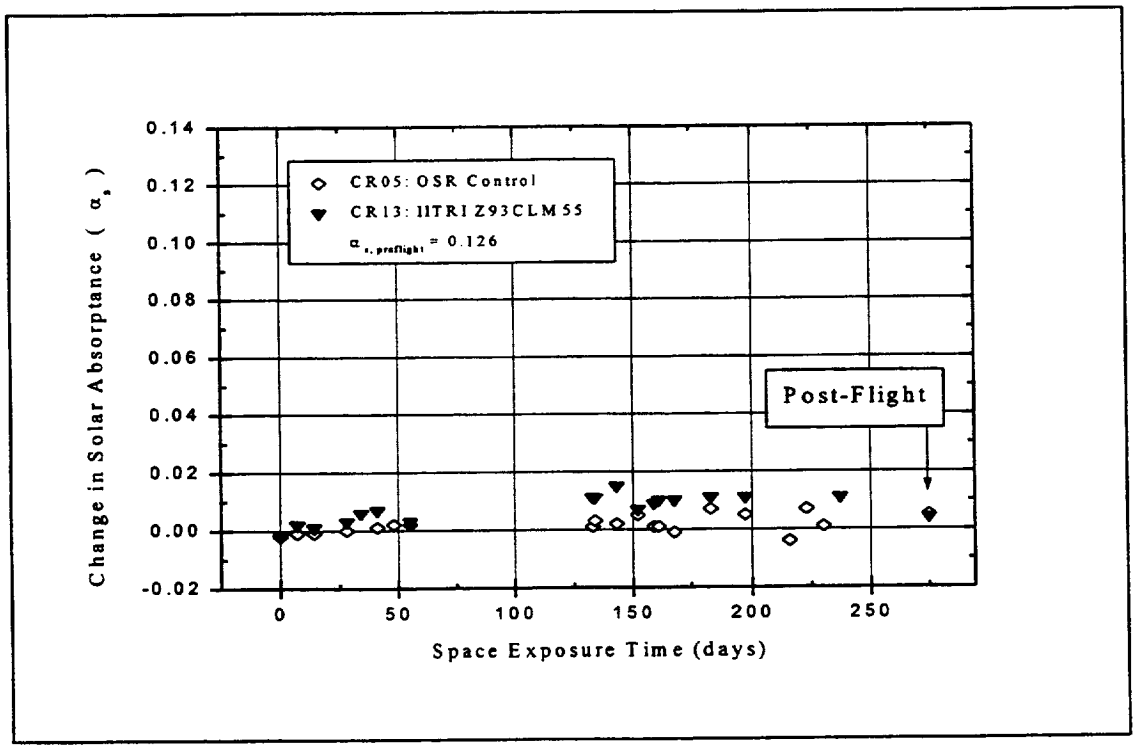

Figure D-24. CR13, IITRI Z93CLM55– Space Exposure Time (Days)

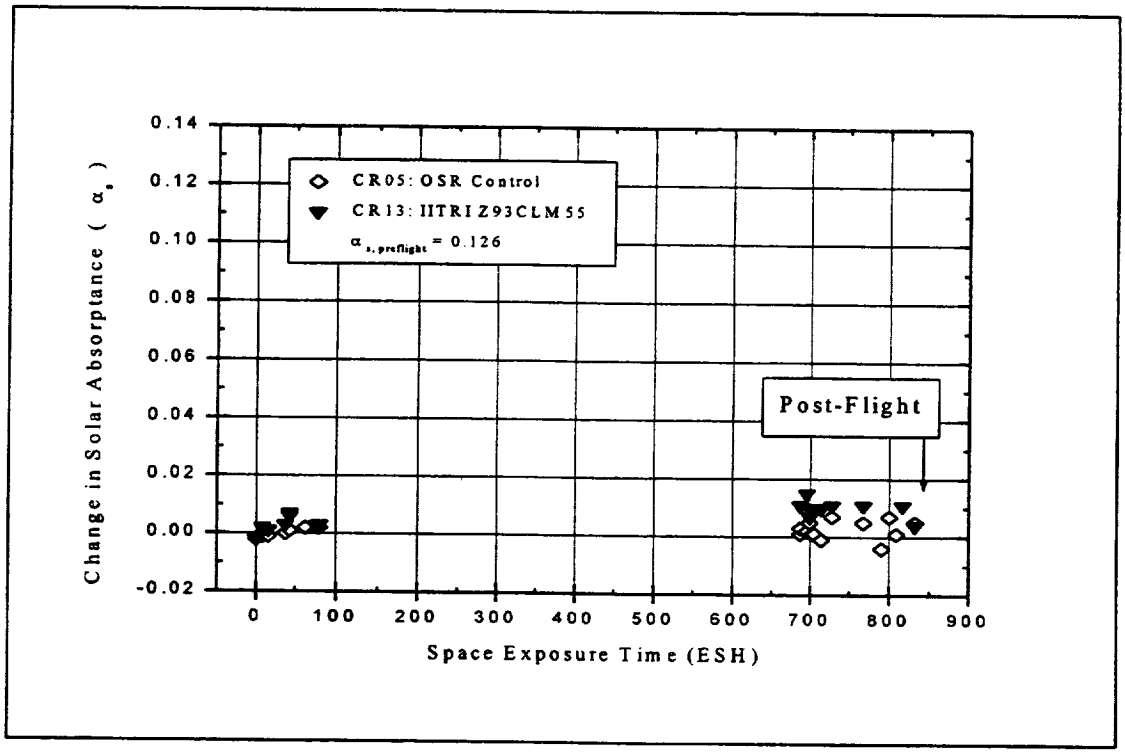

Figure D-25. CR13, IITRI Z93CLM55– Space Exposure Time (ESH)

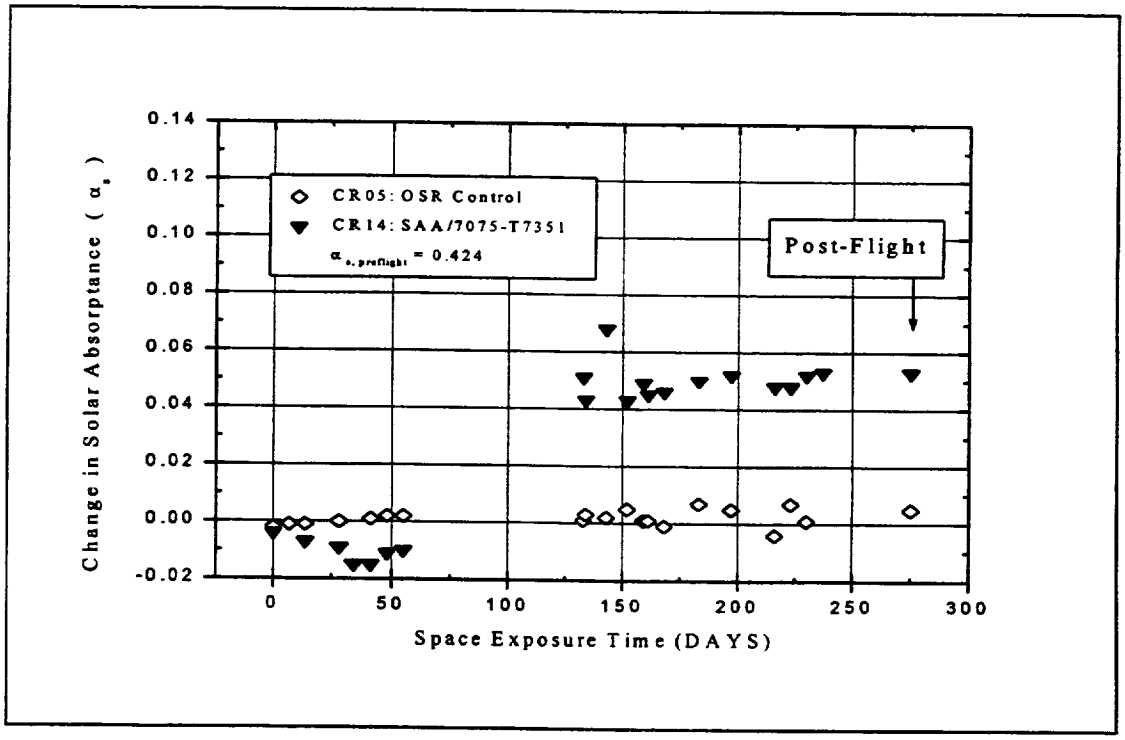

Figure D-26. CR14, SAA/7075-T7351– Space Exposure Time (Days)

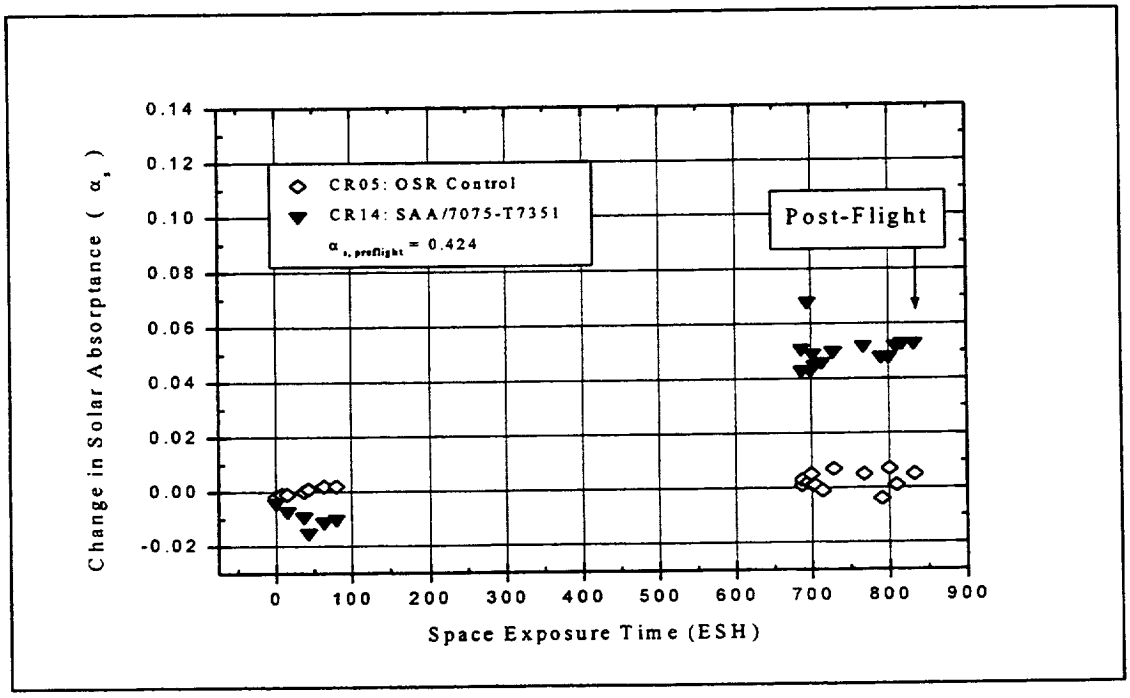

Figure D-27. CR14, SAA/7075-T7351– Space Exposure Time (ESH)

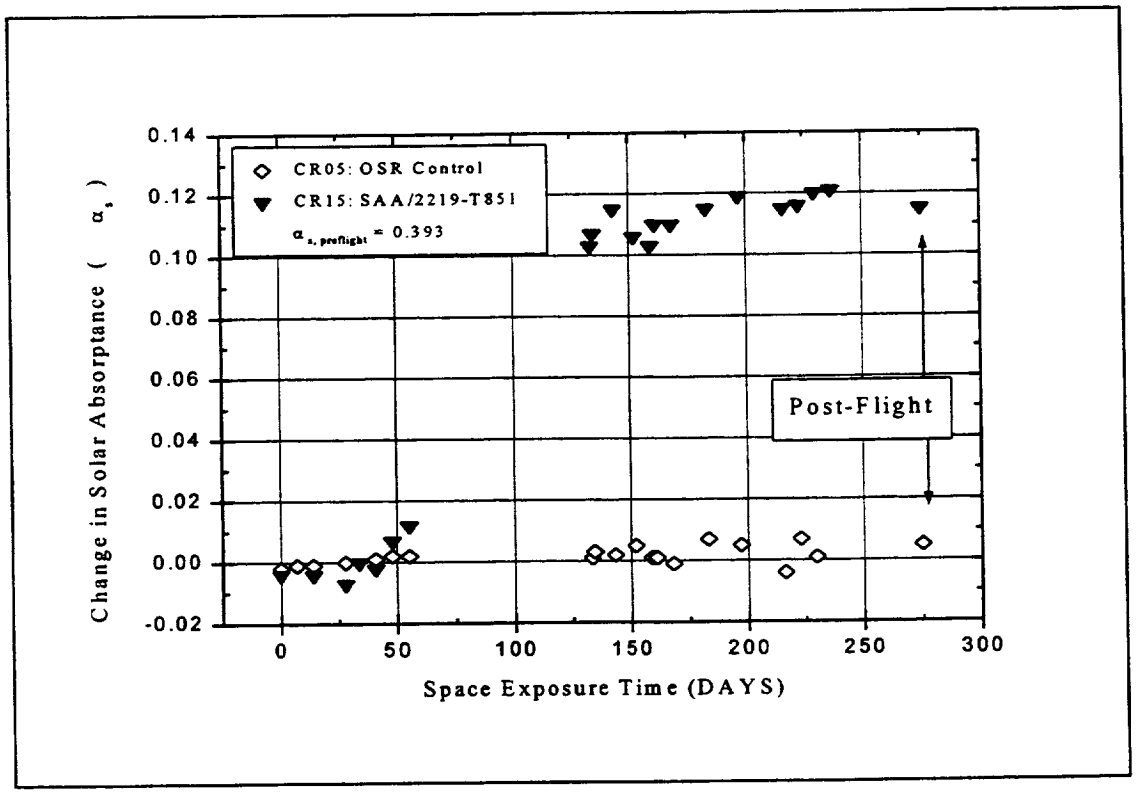

Figure D-28. CR15, SAA/2219-T851– Space Exposure Time (Days)

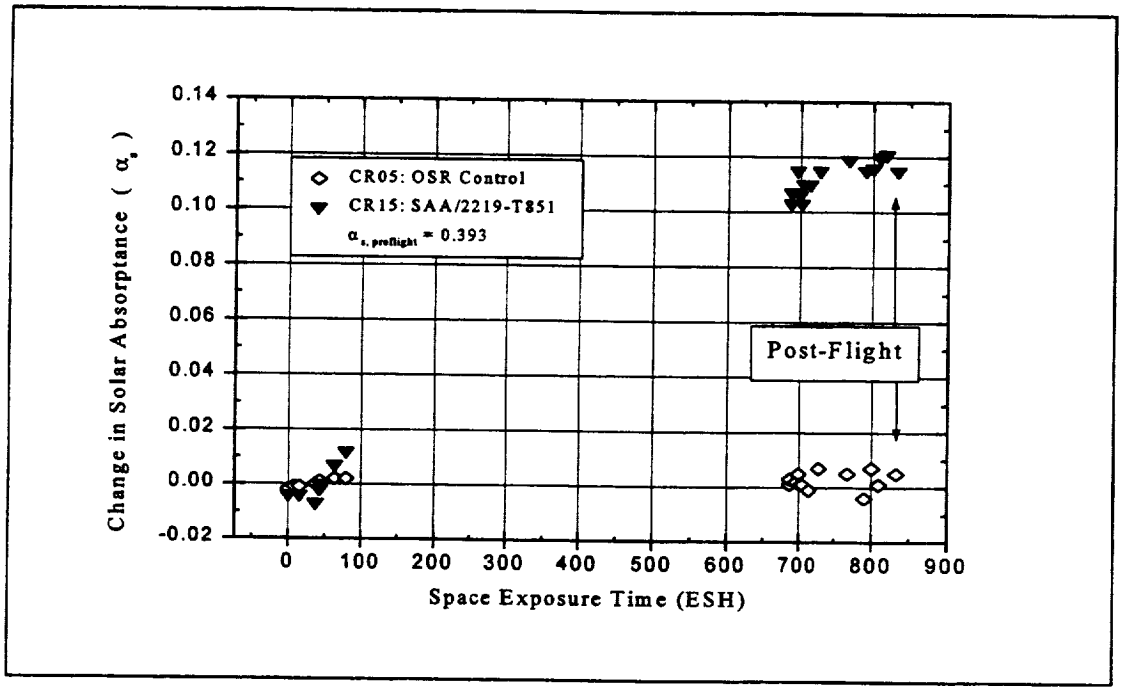

Figure D-29. CR15, SAA/2219-T851– Space Exposure Time (ESH)

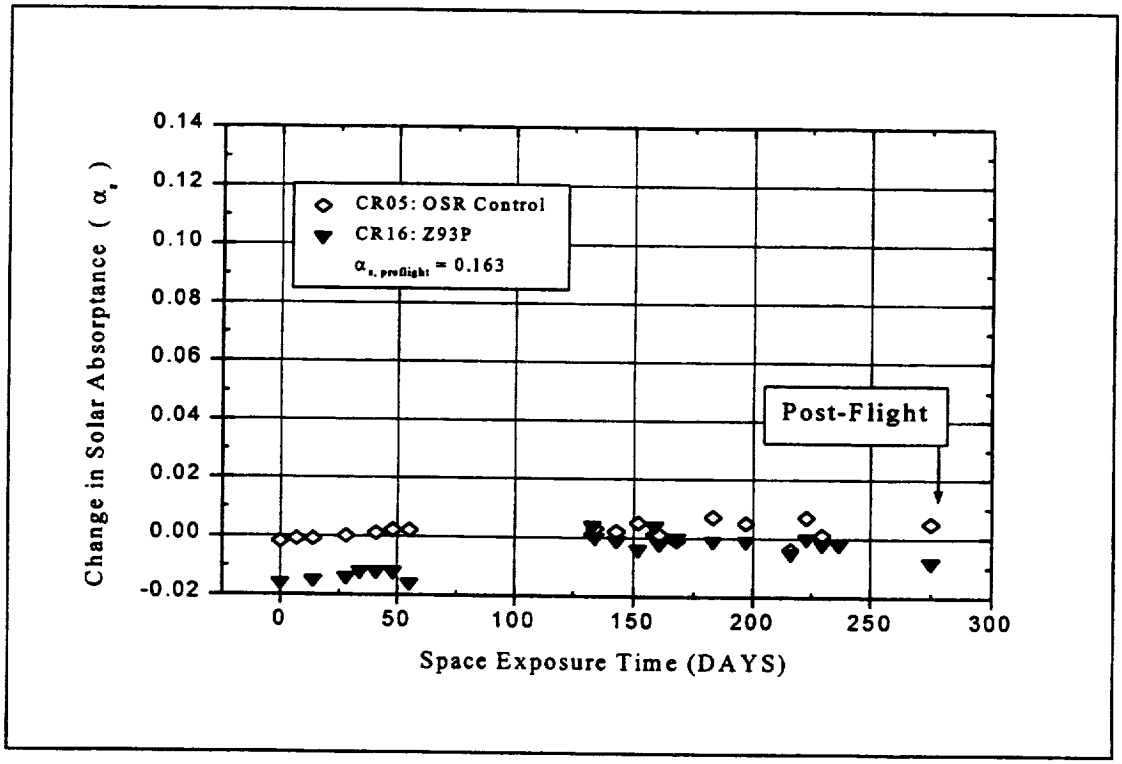

Figure D-30. CR16, Z93P – Space Exposure Time (Days)

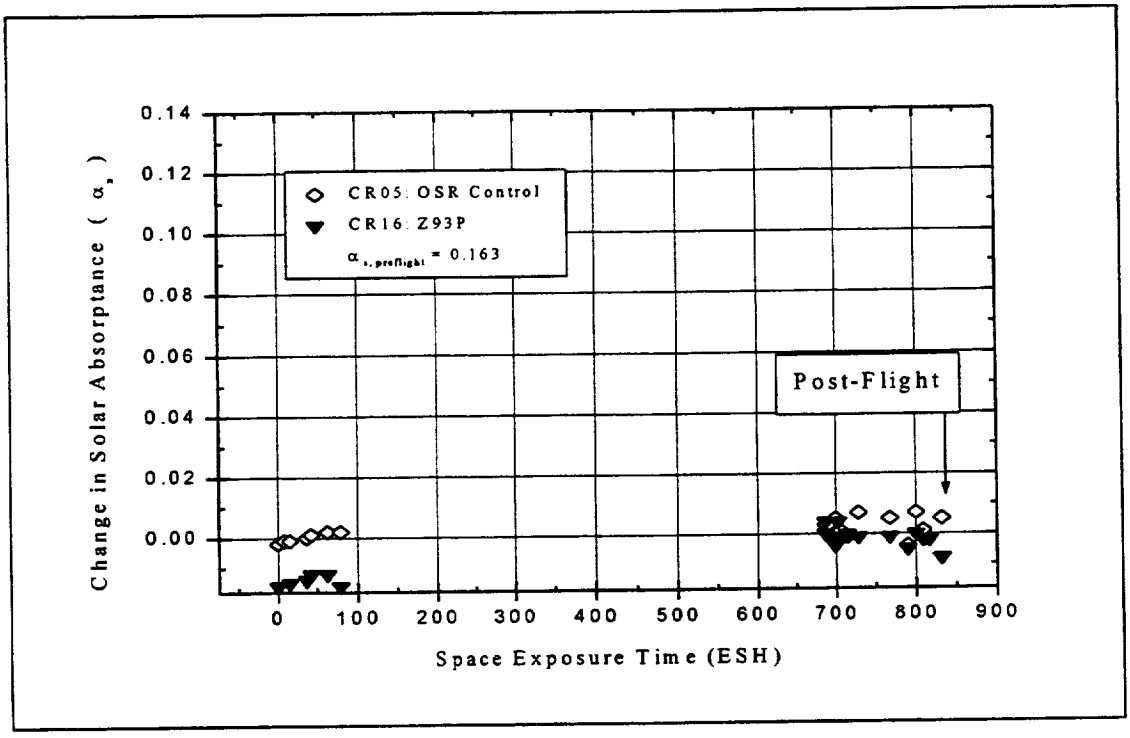

Figure D-31. CR16, Z93P – Space Exposure Time (ESH)

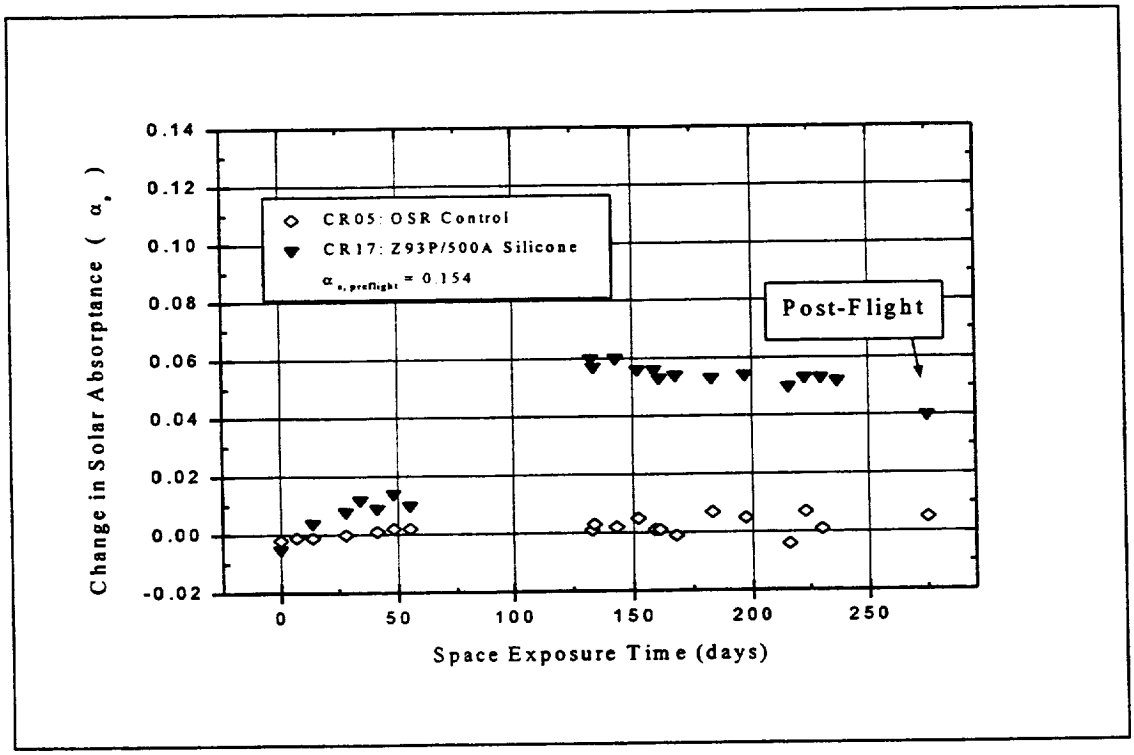

Figure D-32. CR17, Z93P/500A Silicone – Space Exposure Time (Days)

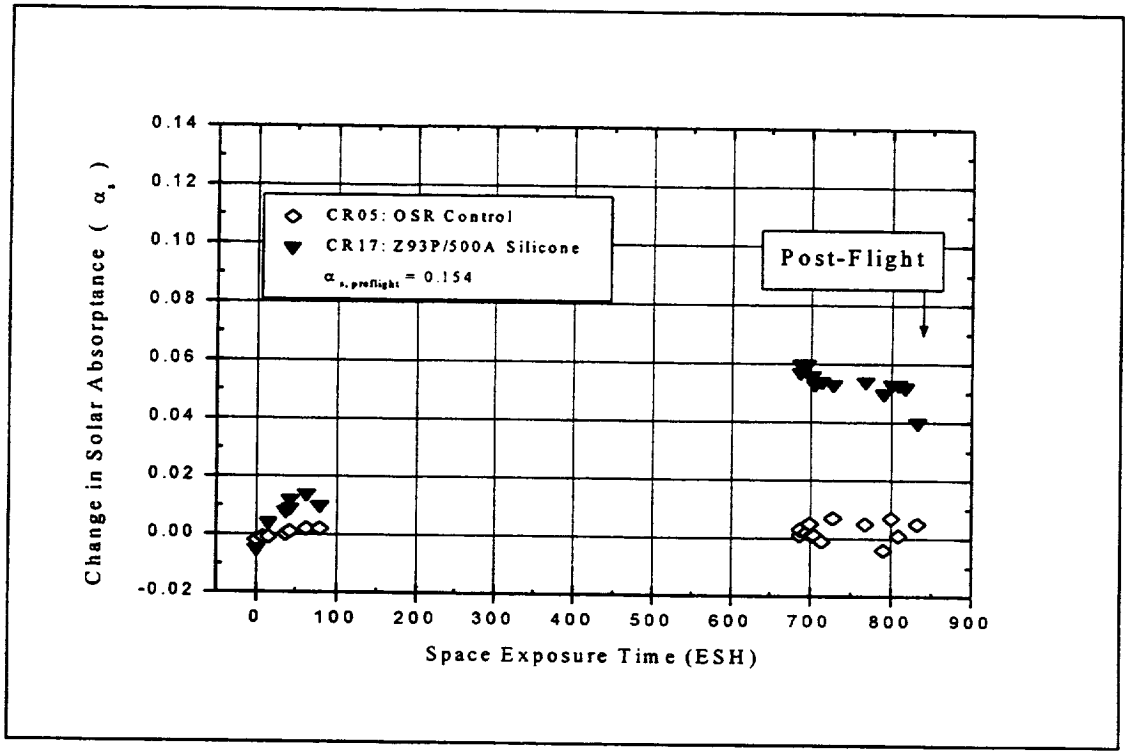

Figure D-33. CR17, Z93P/500A Silicone – Space Exposure Time (ESH)

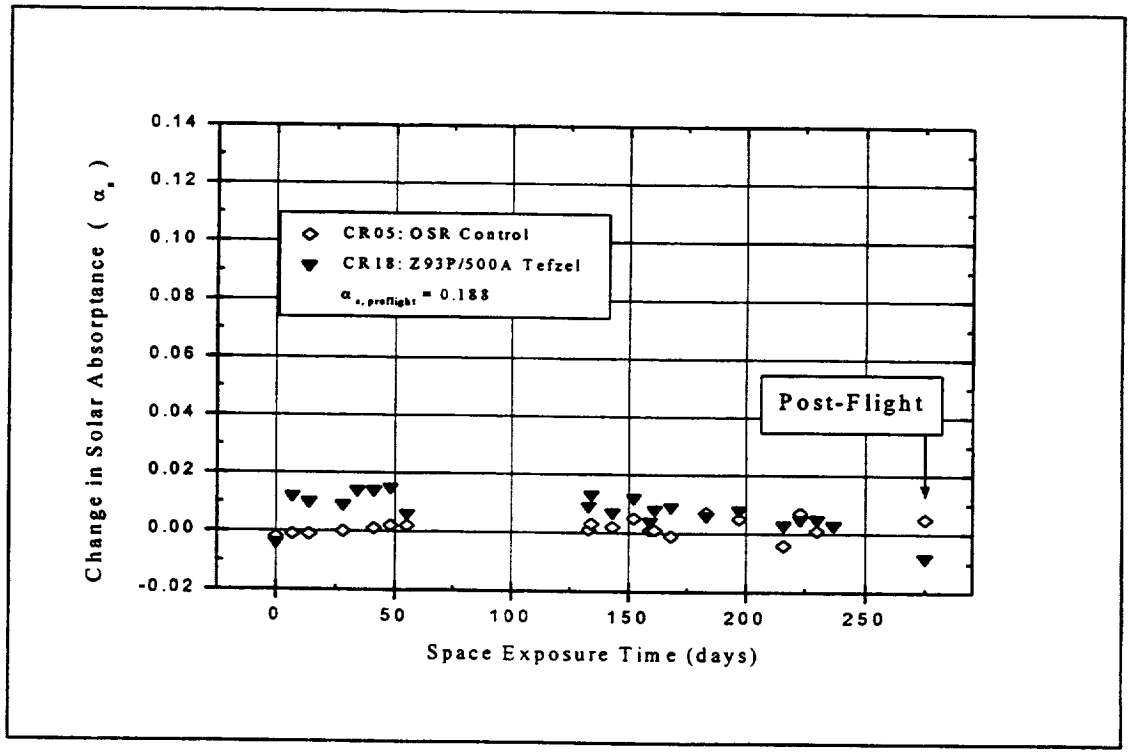

Figure D-34. CR18, Z93P/500 Tefzel – Space Exposure Time (Days)

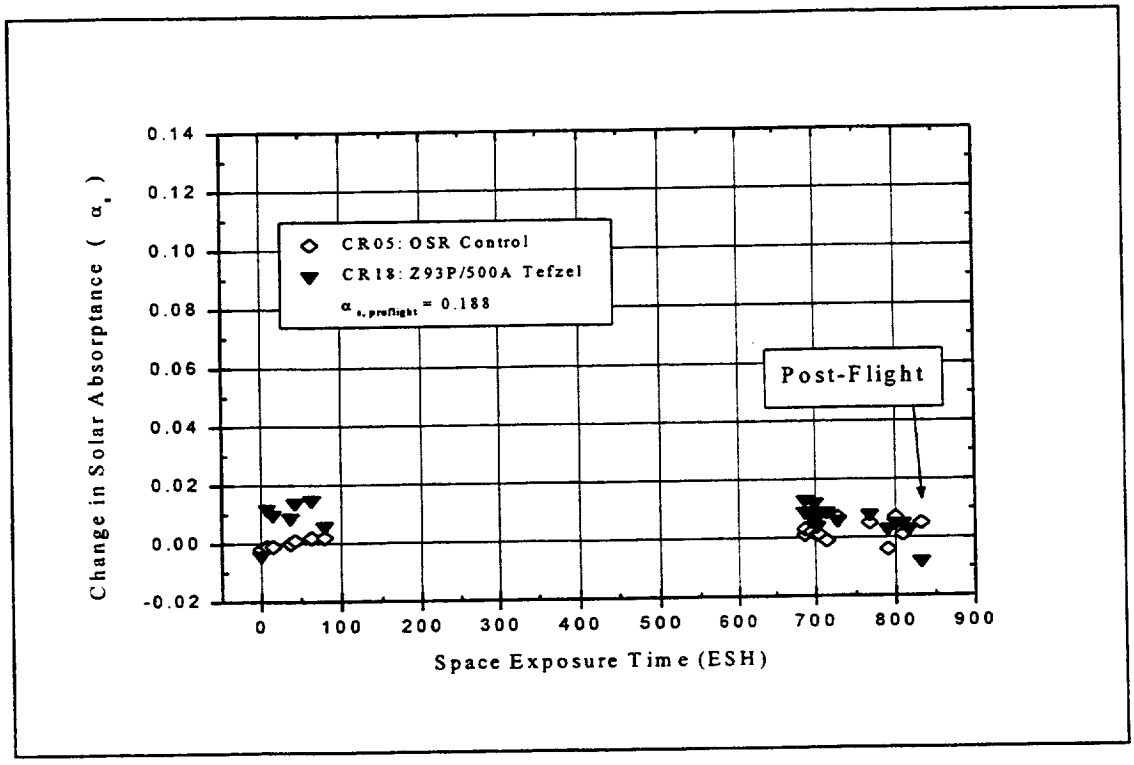

Figure D-35. CR18, Z93P/500 Tefzel – Space Exposure Time (ESH)

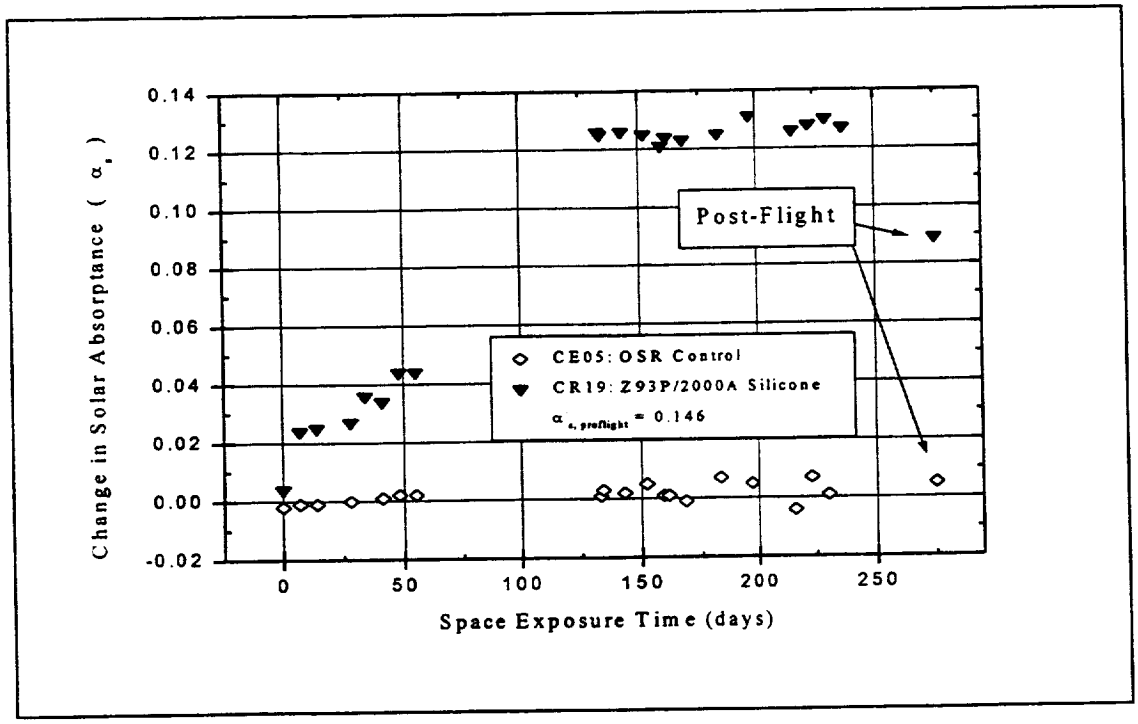

Figure D-36. CR19, Z93P/2000A Silicone – Space Exposure Time (Days)

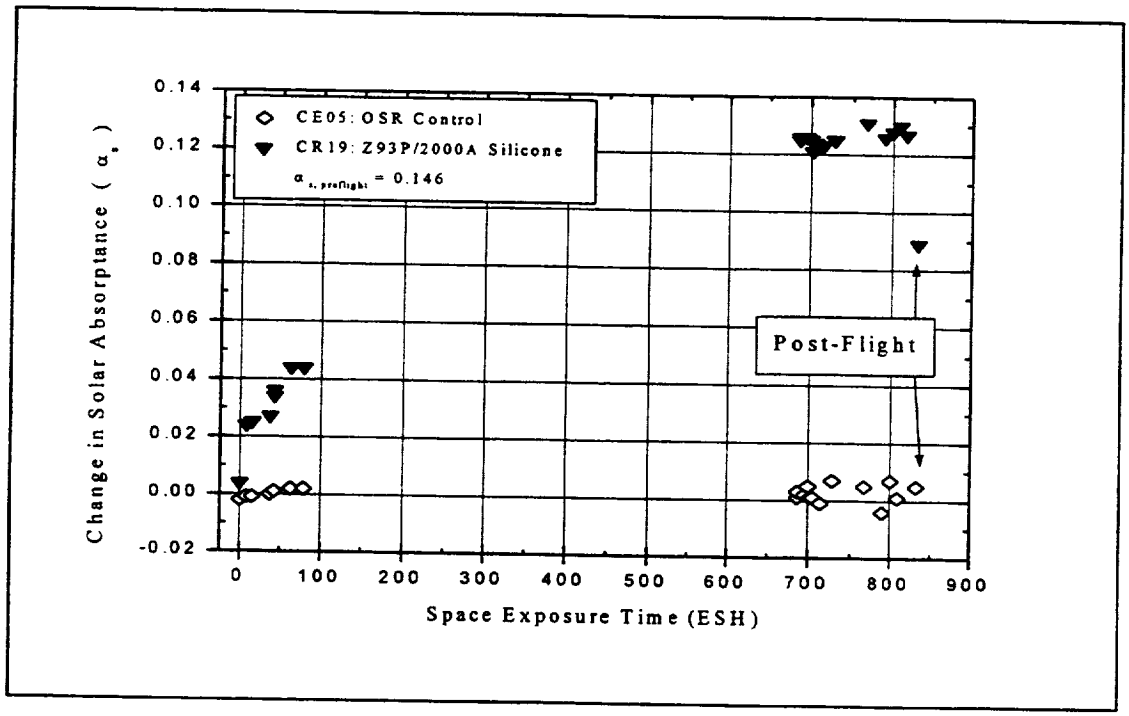

Figure D-37. CR19, Z93P/2000A Silicone – Space Exposure Time (ESH)

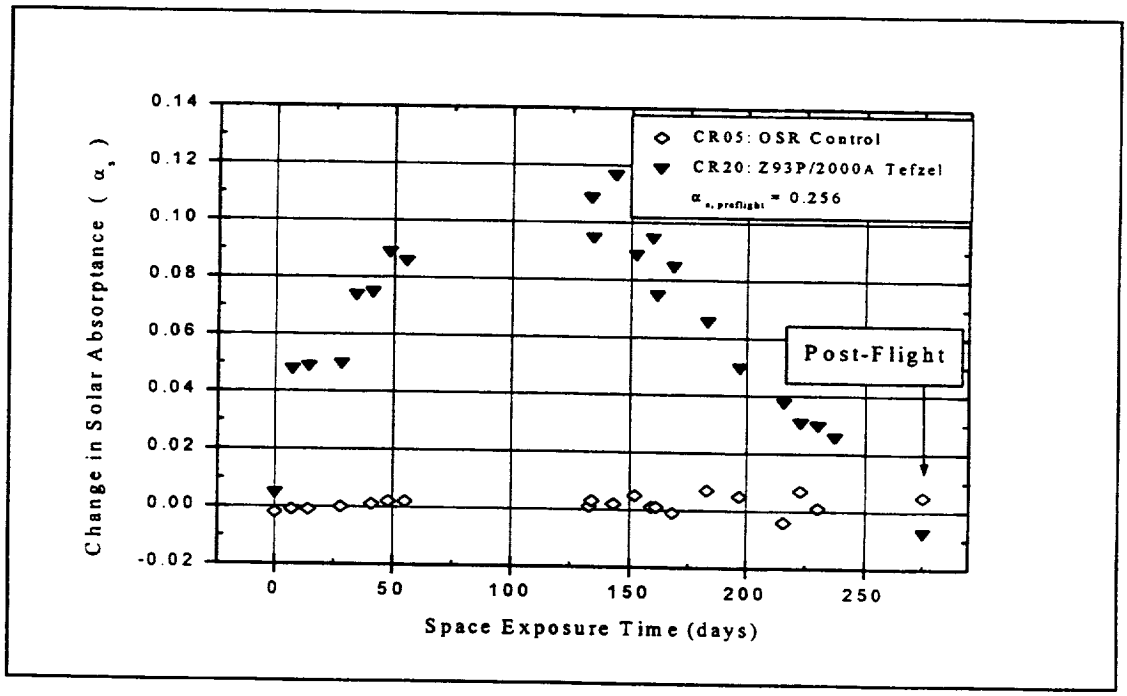

Figure D-38. CR20 Z93P/2000A TEFZEL – Space Exposure Time (Days)

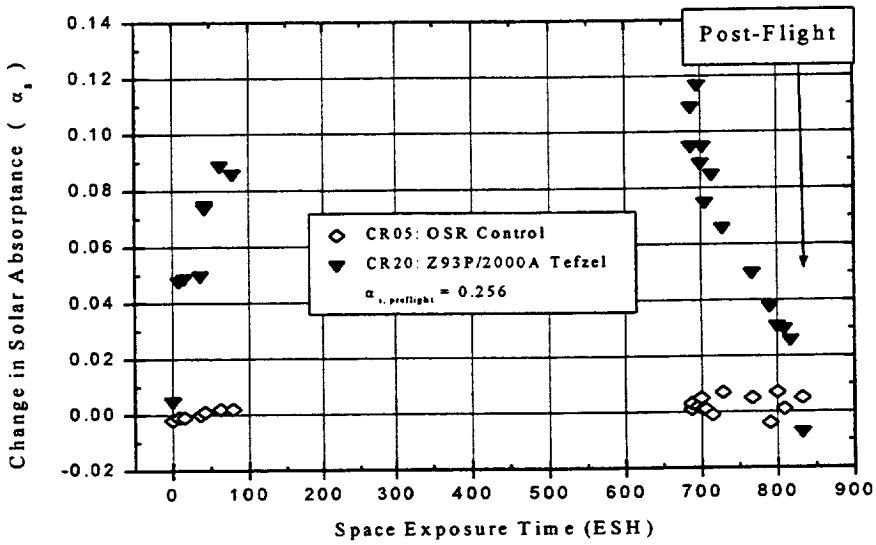

Figure D-39. CR19, Z93P/2000A Silicone – Space Exposure Time (ESH)

APPENDIX E

Solar Exposure in ESH and Atomic Oxygen Flux vs Exposure Time

APPENDIX E

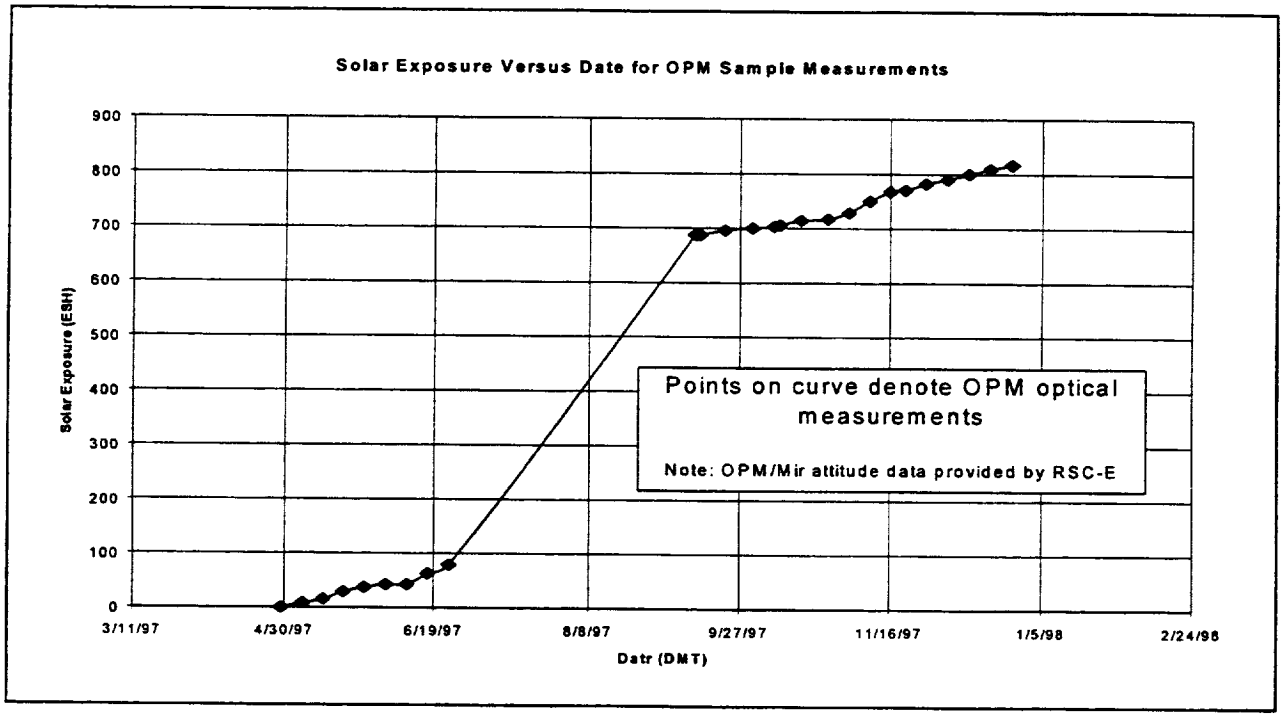

Figure E-1. Solar Exposure Versus Date for OPM Sample Measurements

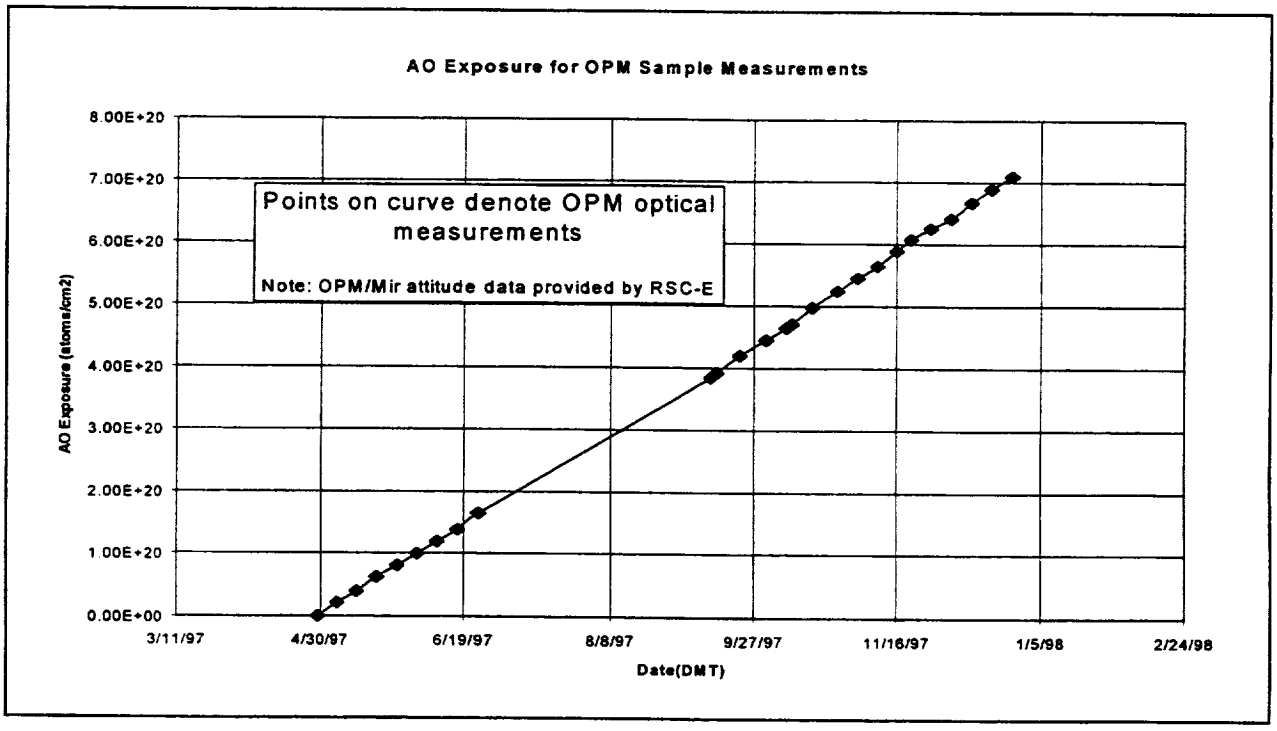

Figure E-2. AO Exposure for OPM Sample Measurements

APPENDIX F

MATERIAL ANALYSIS DATA

XPS/ESCA DEPTH PROFILE DATA

WHITE SANDS TEST FACILITY (WSTF)/JOHNSON SPACE CENTER (JSC)

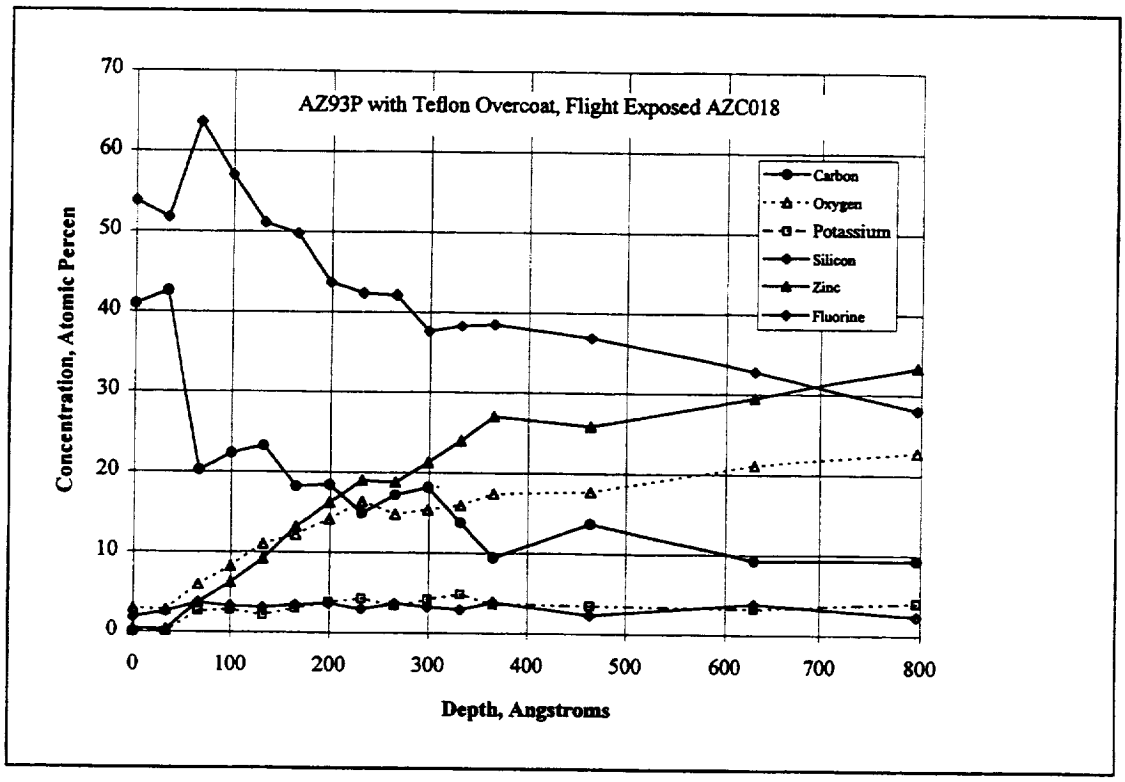

Figure F-1. AZ93P with Teflon Overcoat, Flight Exposed AZC018

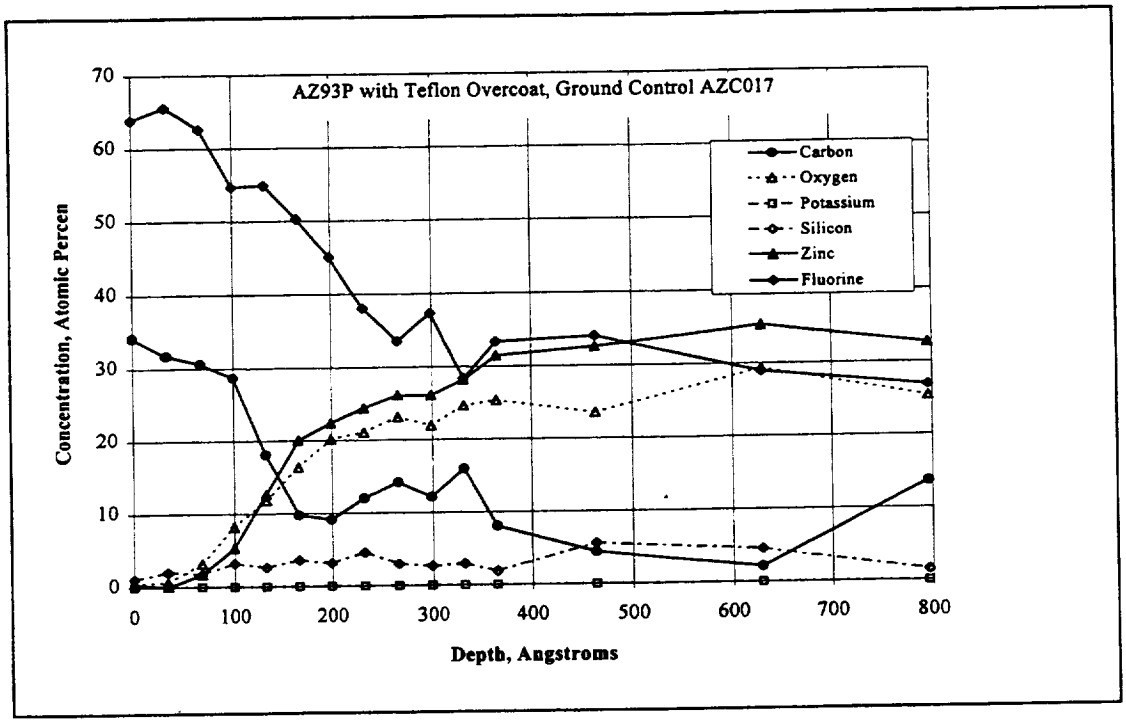

Figure F-2. AZ93P with Teflon Overcoat, Ground Control AZC017

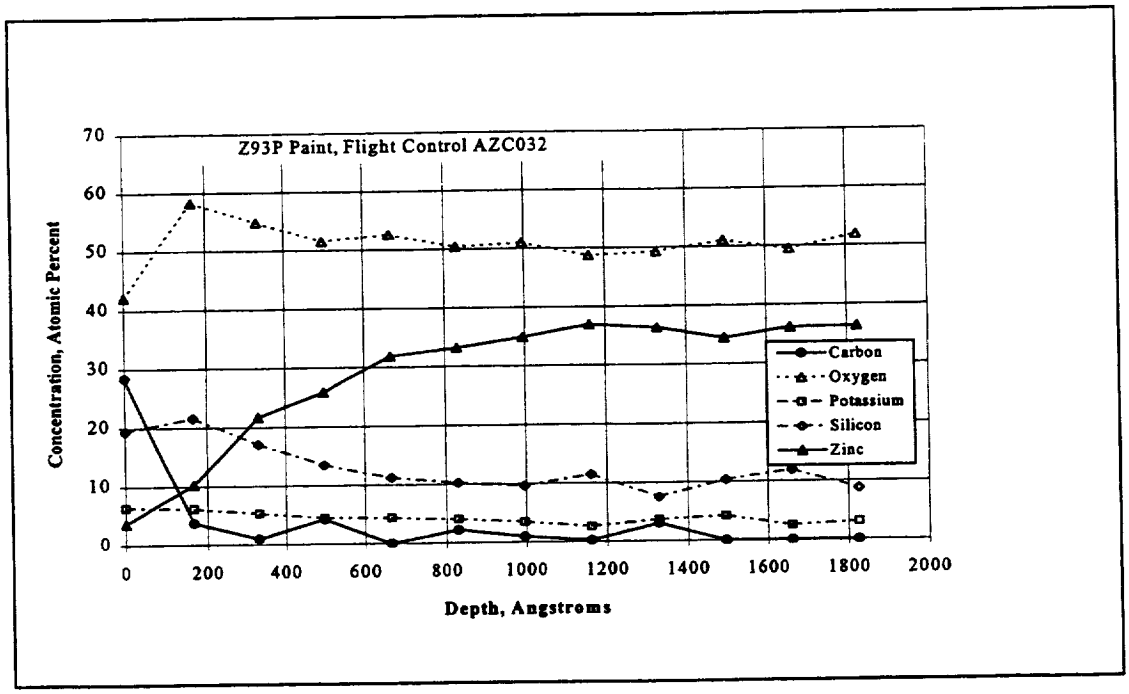

Figure F-3. Z93P Paint, Flight Control AZC032

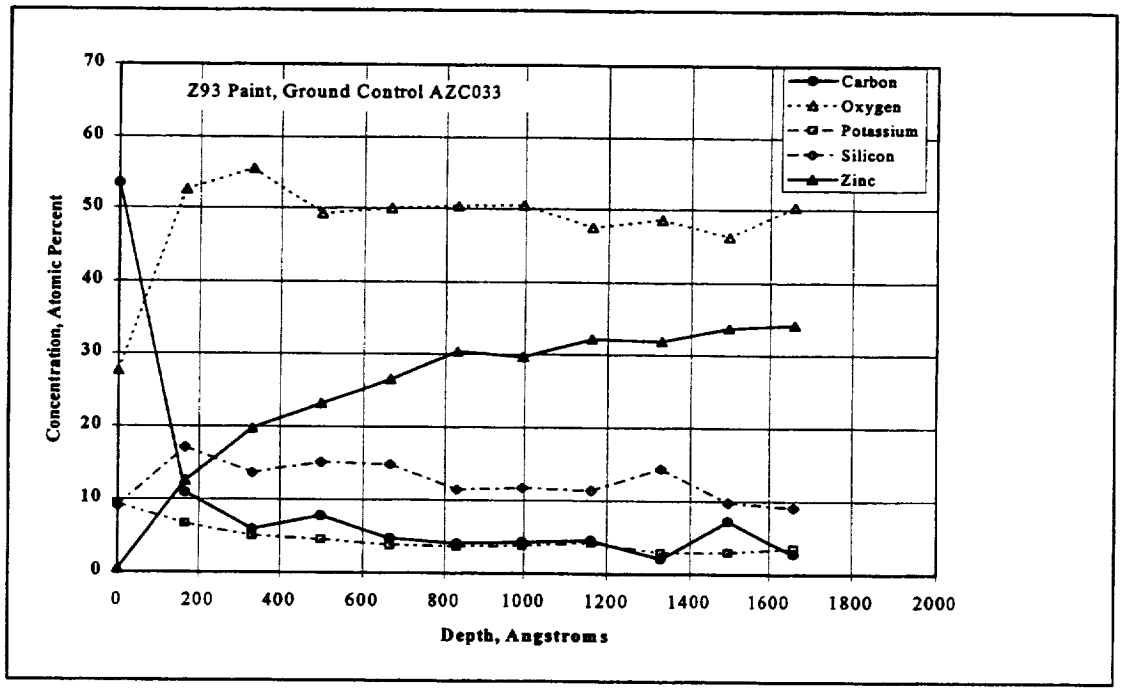

Figure F-4. Z93P Paint, Ground Control AZC033

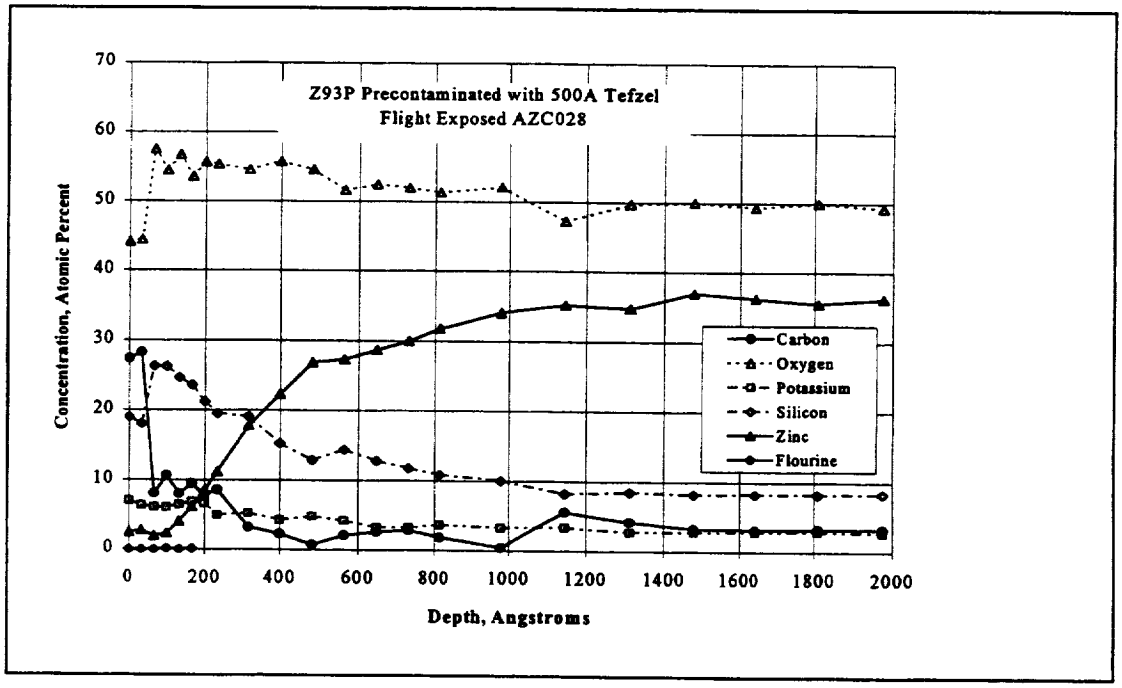

Figure F-5. Z93P Precontaminated with 500A of Tefzel, Flight Exposed AZC028

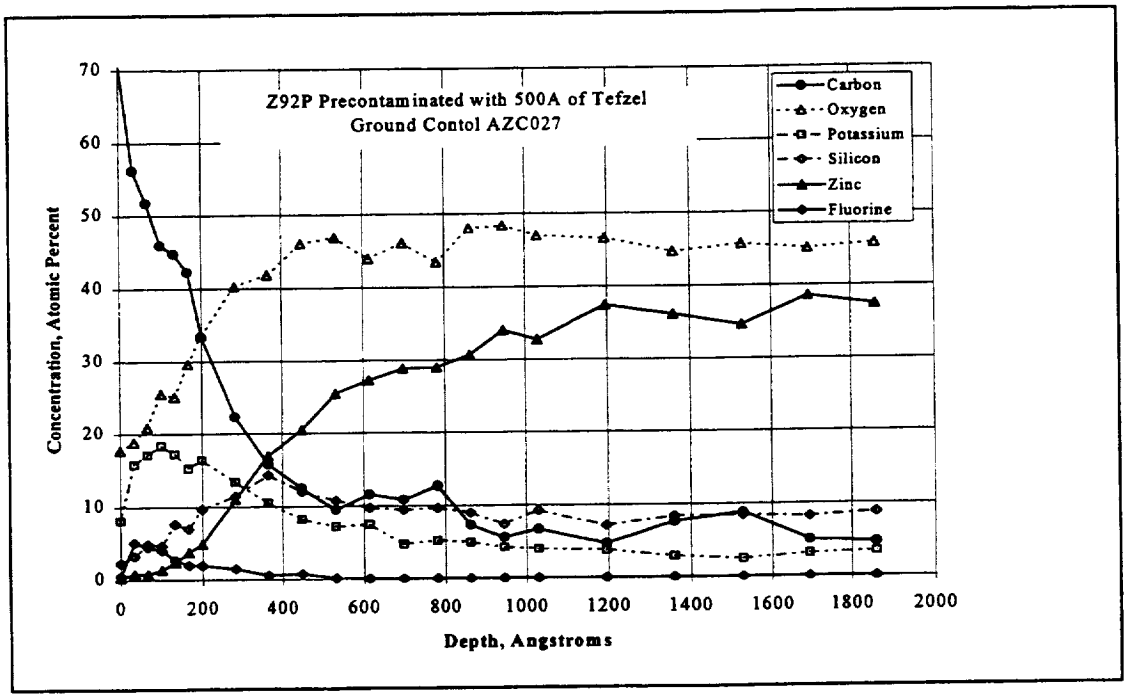

Figure F-6. Z93P Precontaminated with 500A of Tefzel; Ground Control AZC027

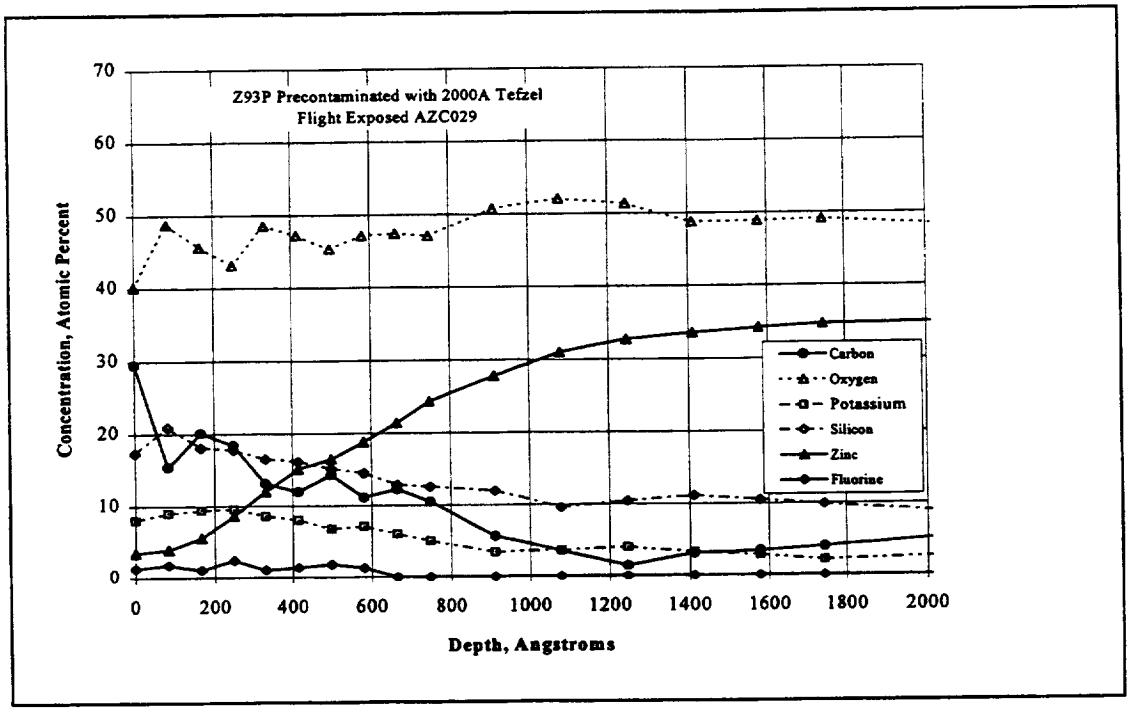

Figure F-7. Z93P Precontaminated with 2000A Tefzel; Flight Exposed AZC029

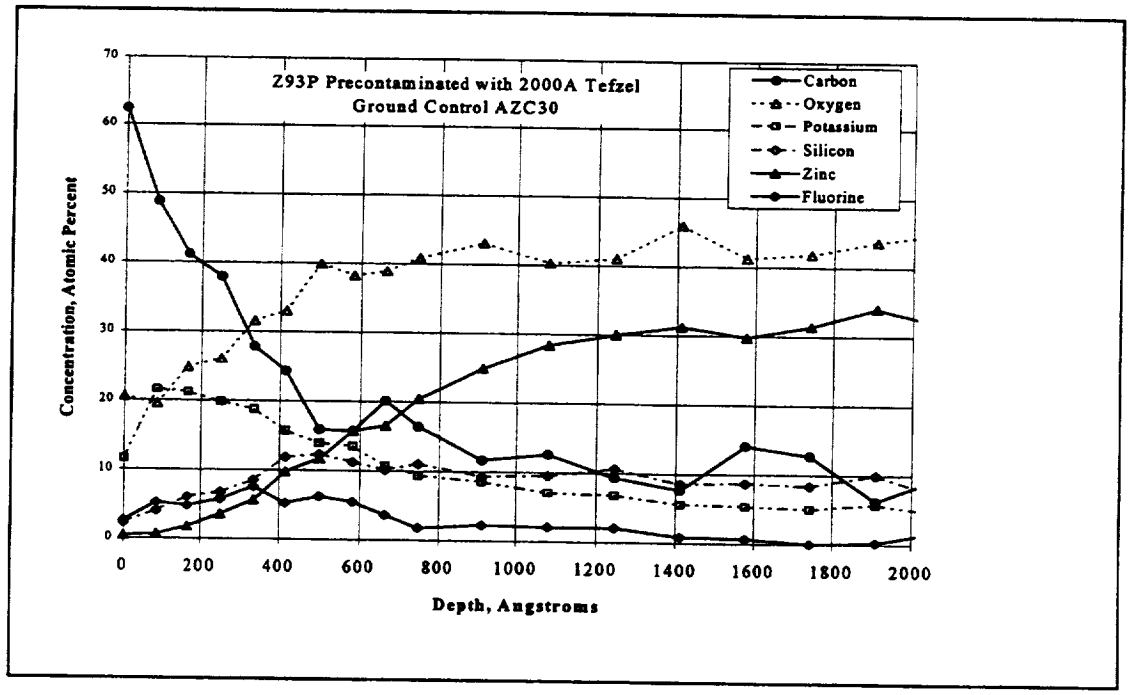

Figure F-8. Z93P Precontaminated with 2000A Tefzel; Ground Control AZC030

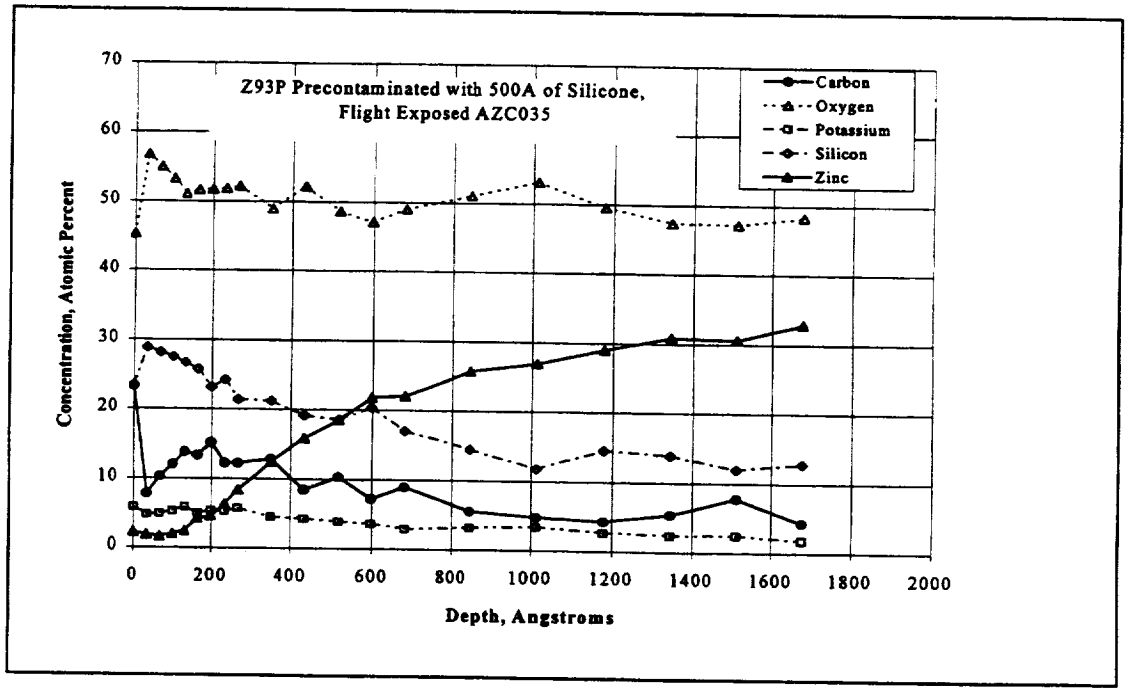

Figure F-9. Z93P Precontaminated with 500A Silicone; Flight Exposed AZC035

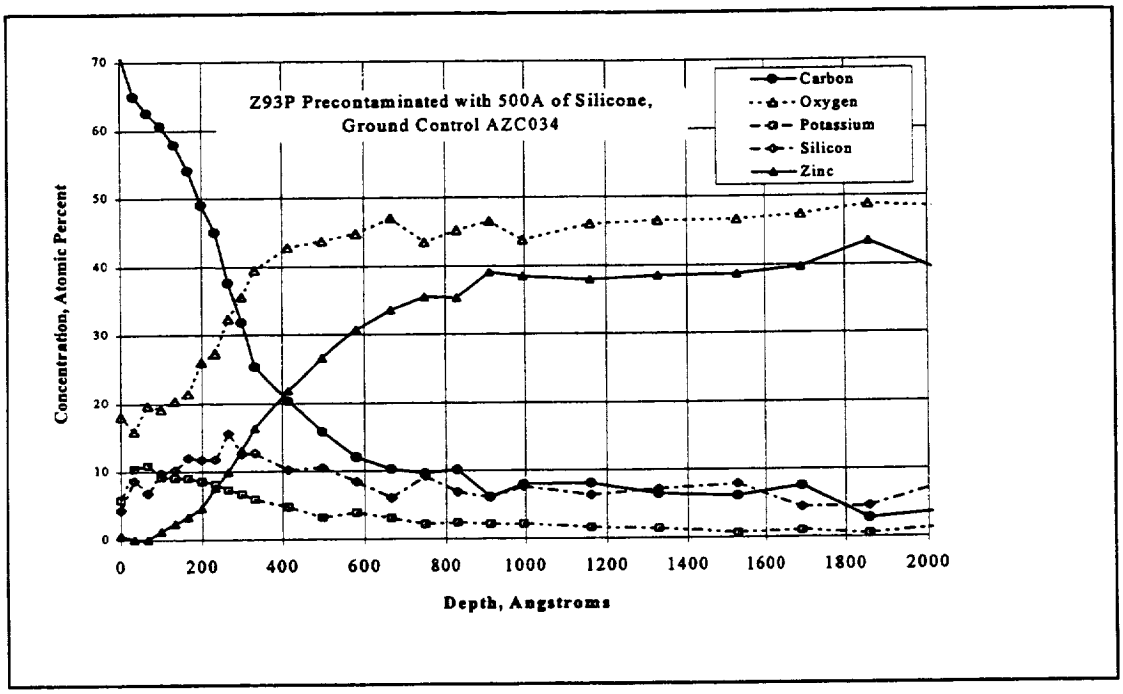

Figure F-10. Z93P Precontaminated with 500A Silicone; Ground Control AZC034

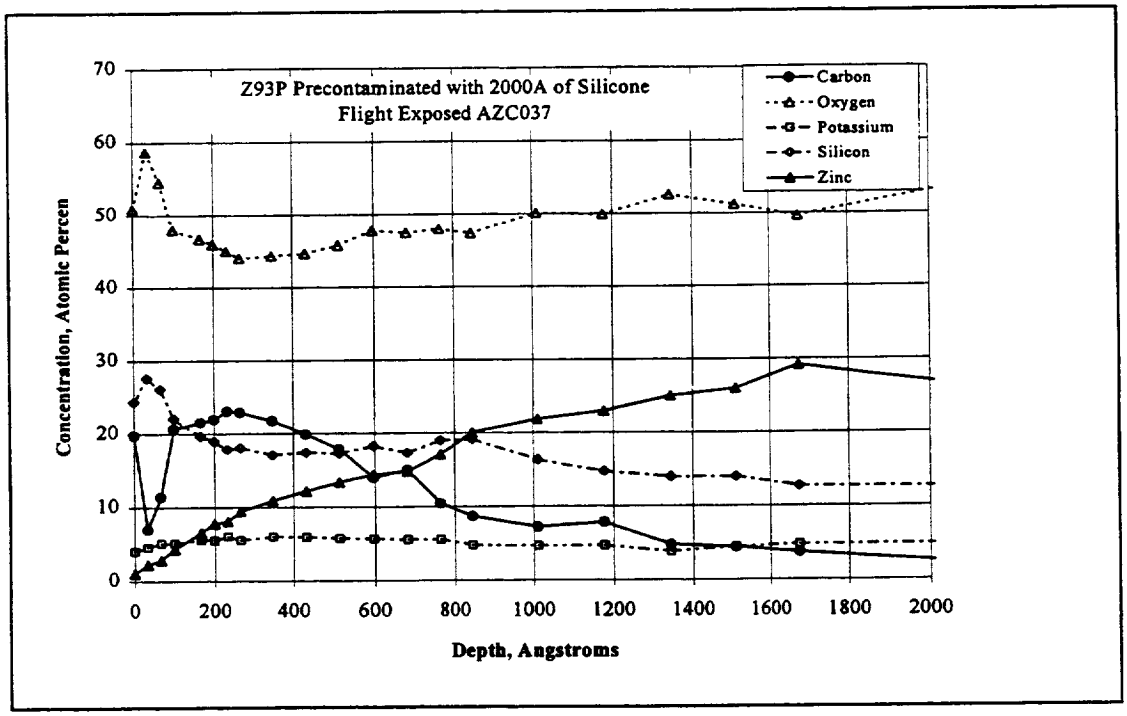

Figure F-11. Z93P Precontaminated with 2000A Silicone; Flight Exposed AZC037

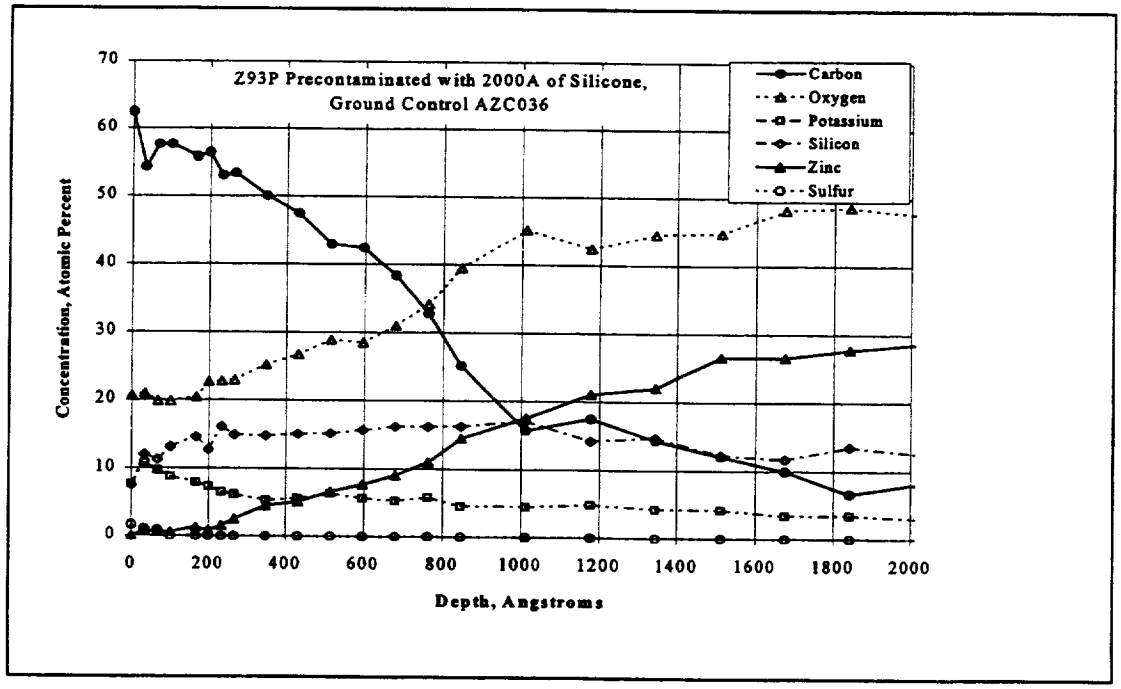

Figure F-12. Z93P Precontaminated with 2000A Silicone; Ground Control AZC036

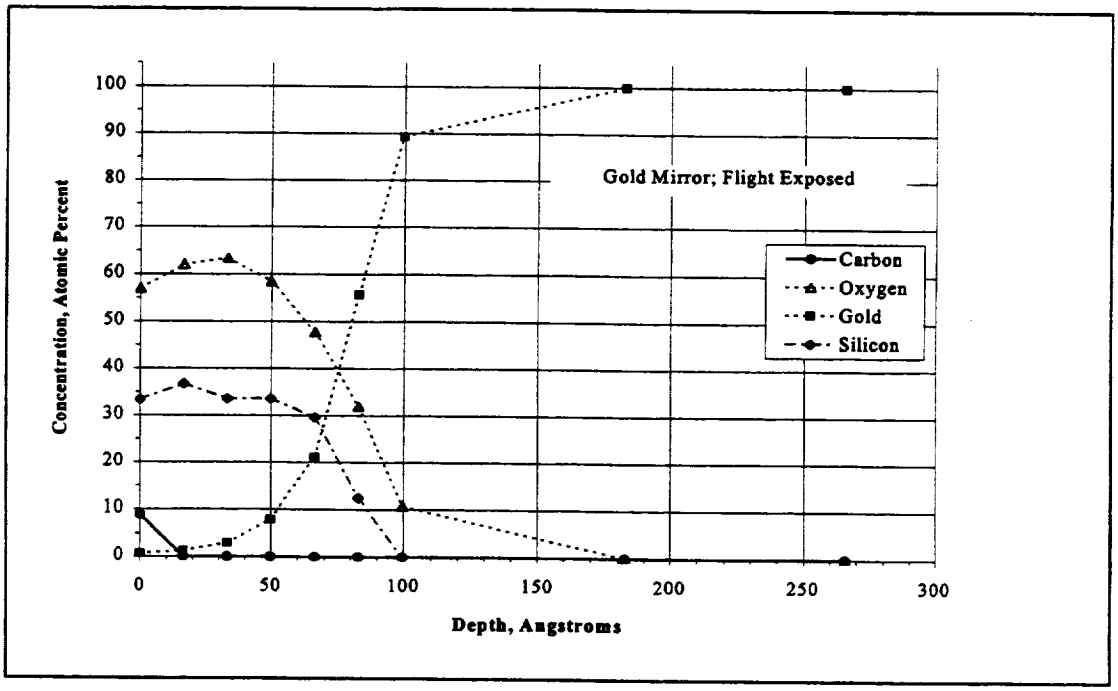

Figure F-13. Gold Mirror Exposed on OPM, Showing Silicate Contamination 100 to 180 Angstroms Thick

APPENDIX G
MATERIAL ANALYSIS DATA
XPS/ESCA SURVEY DATA

WHITE SANDS TEST FACILITY (WSTF)/JOHNSON SPACE CENTER (JSC)

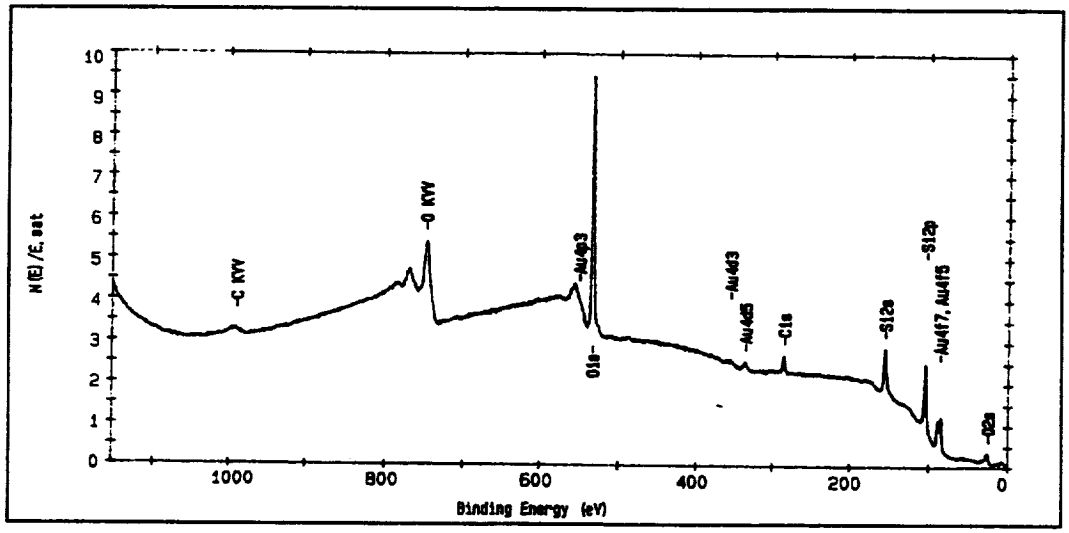

Figure G-1. Survey Spectrum of Gold Mirror on Silica Substrate

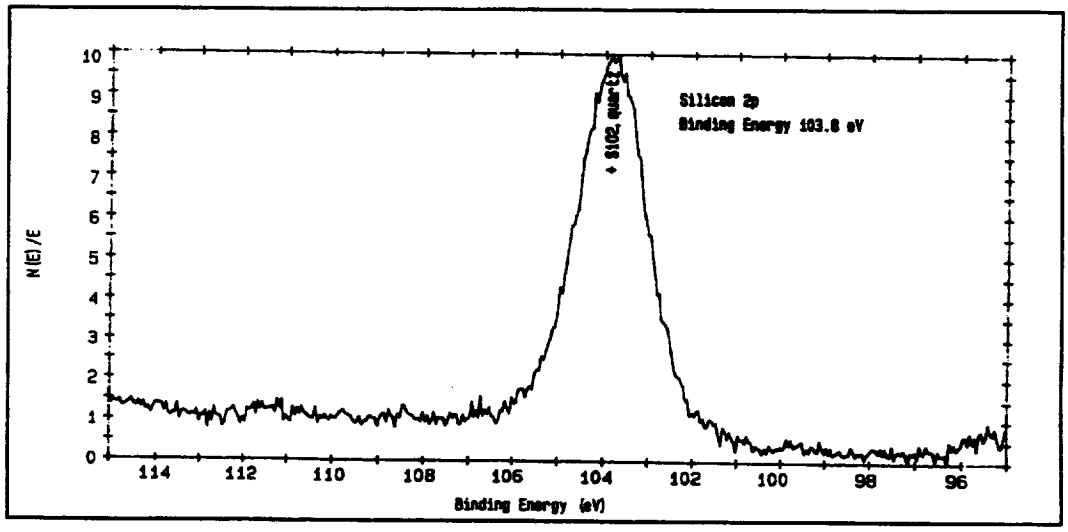

Figure G-2. Survey Spectrum of Gold Mirror on Silica Substrate, After Depth Profile.

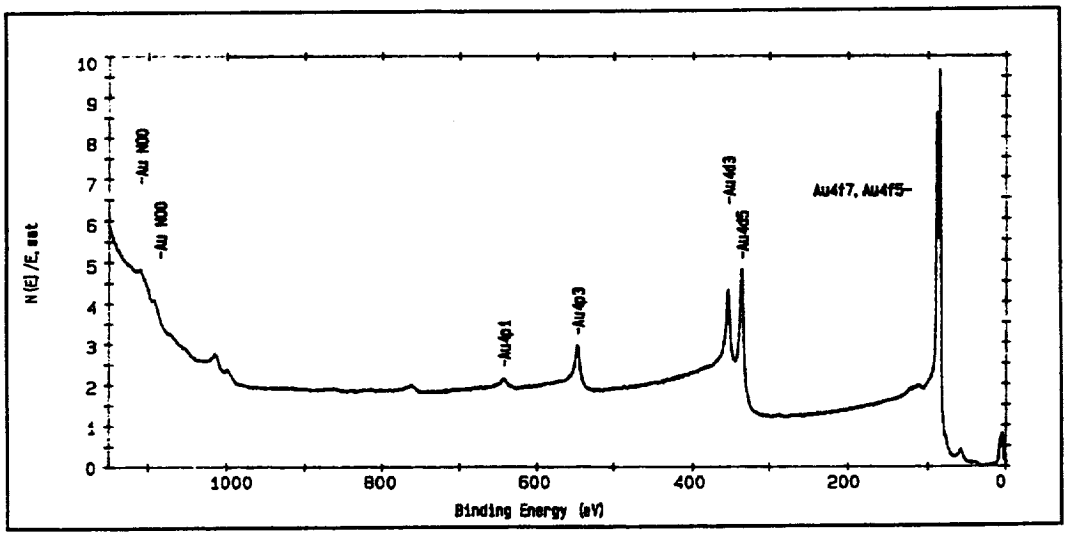

Figure G-3. High Resolution Scan on the Silicon 2p Line

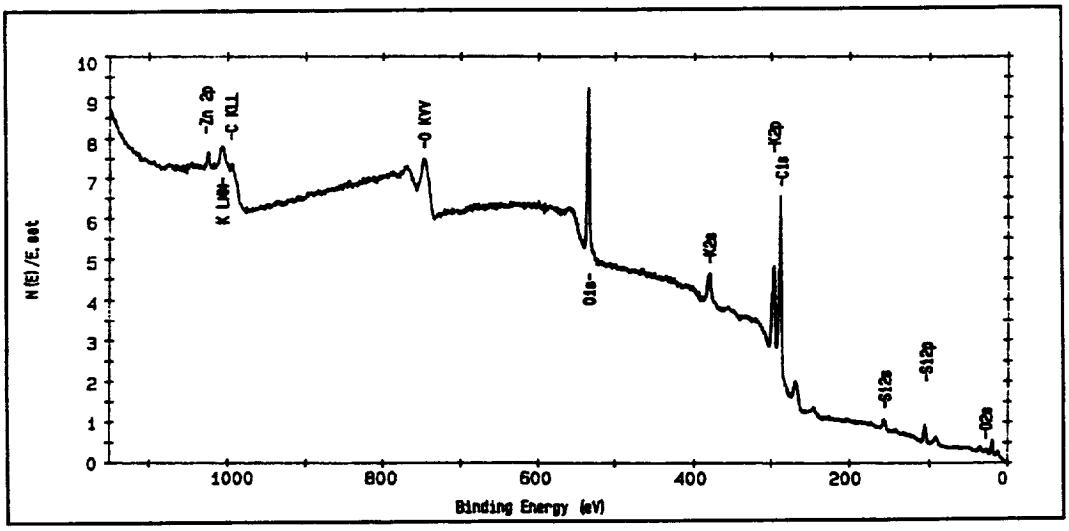

Figure G-4. Survey Spectrum of AZC033, Z93P White Ceramic Paint, Ground Control.

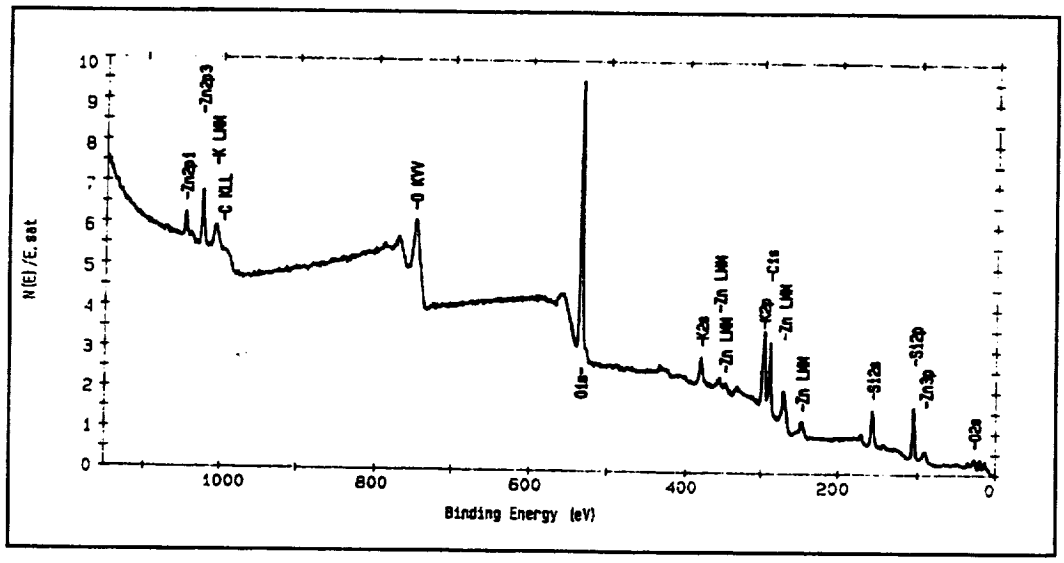

Figure G-5. Survey Spectrum of AZC032, Z93 White Ceramic Paint, Flight Exposed.

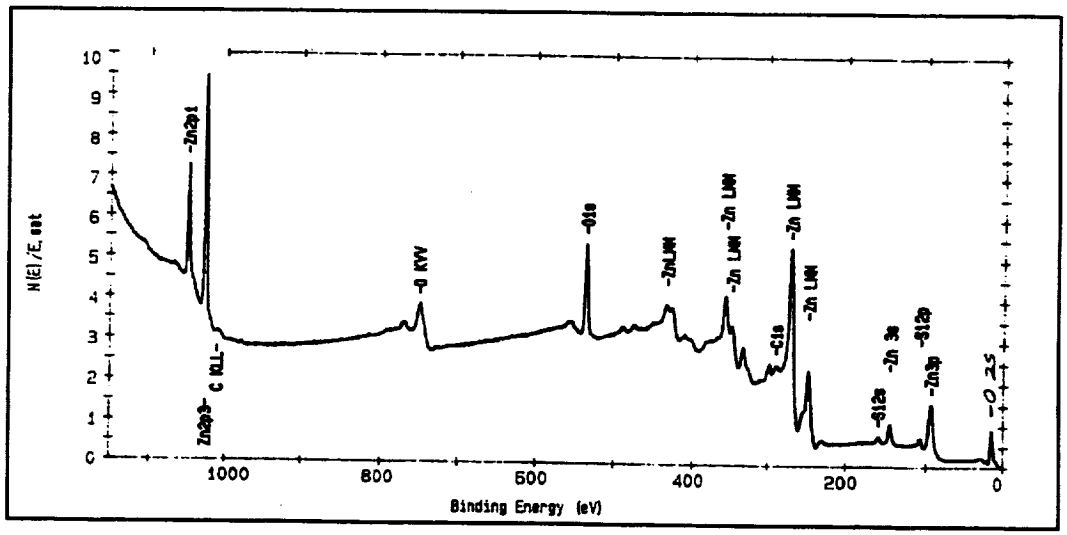

Figure G-6. Survey Spectrum of AZC033, Z93P White Ceramic Paint, Flight Exposed following Depth Profile.

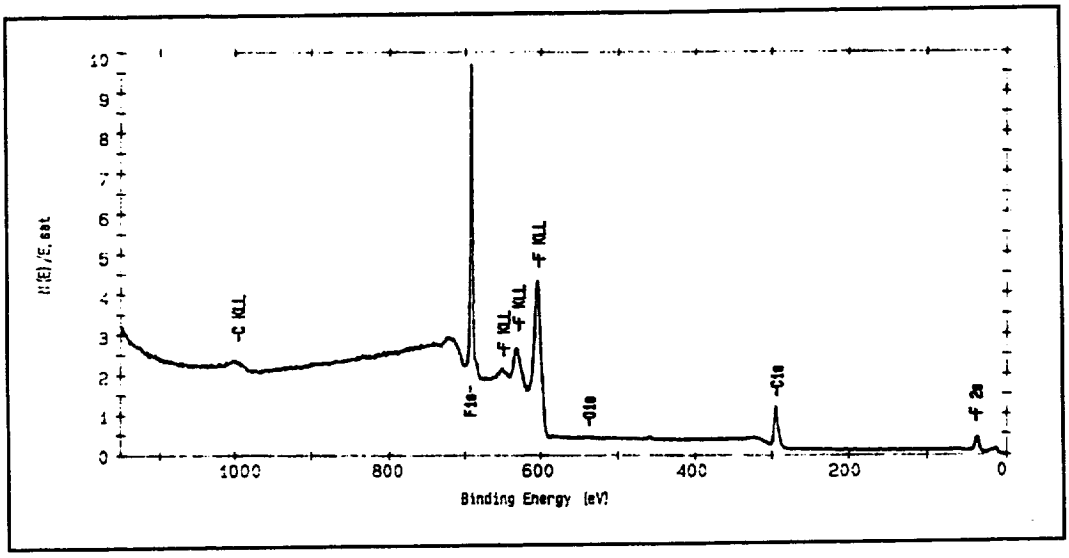

Figure G-7. Survey Spectrum of AZC017, AZ93 White Ceramic Paint with Teflon Overcoat, Ground Control.

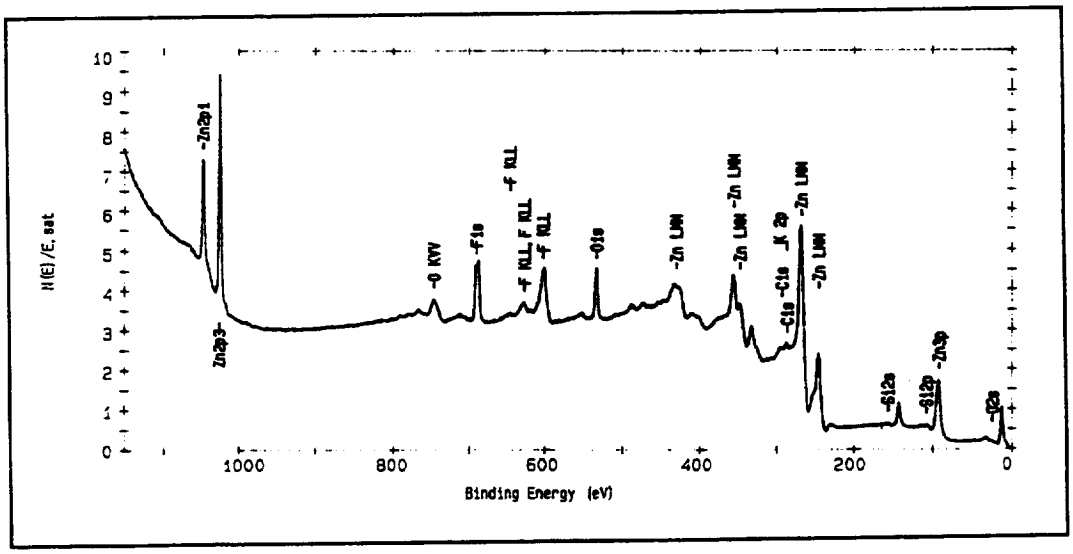

Figure G-8. Survey Spectrum of AZC017, AZ93 White Ceramic Paint with Teflon Overcoat, Ground Control, following Depth Profile.

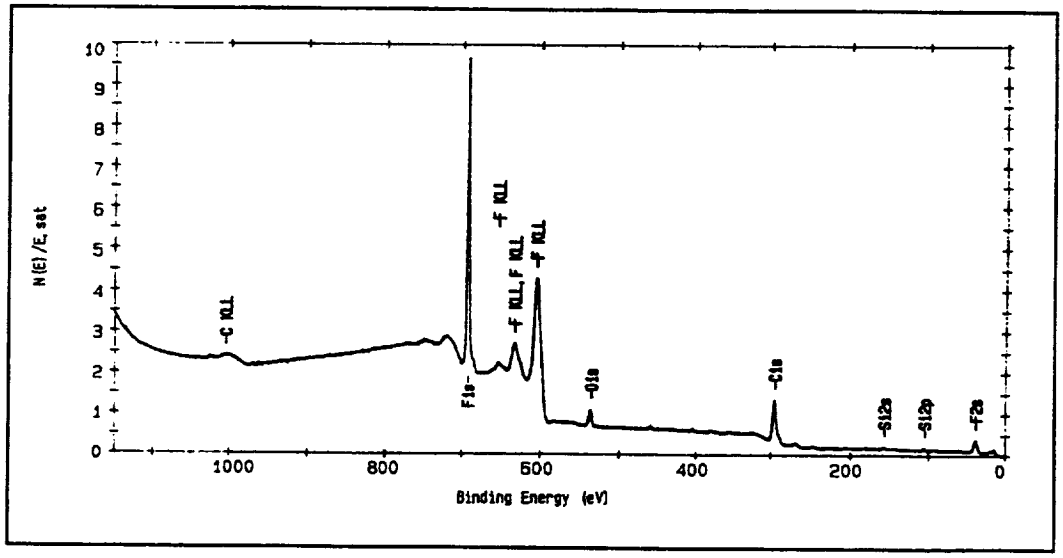

Figure G-9. Survey Spectrum of AZC018, AZ93 White Ceramic Paint with Teflon Overcoat, Flight Exposed

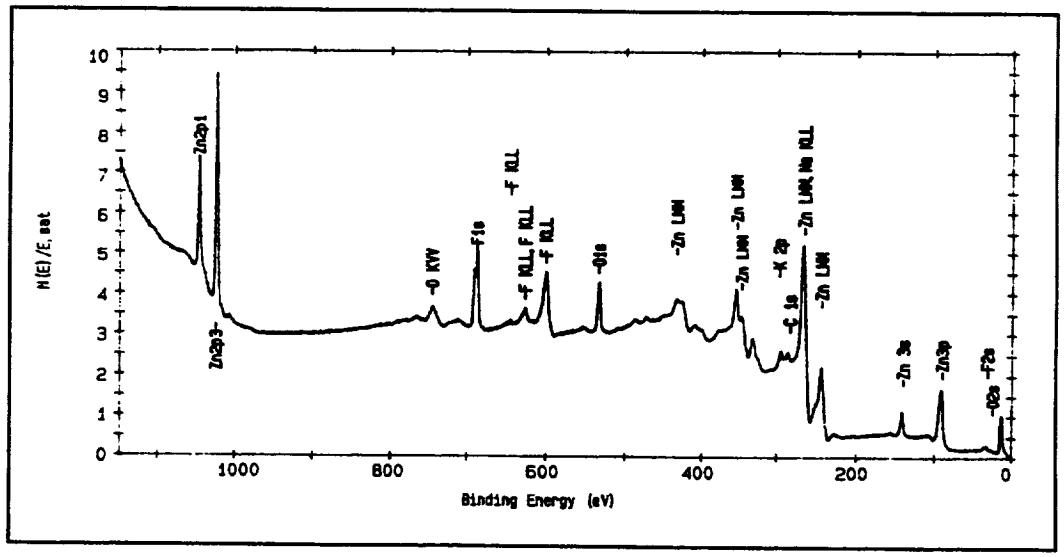

Figure G-10. Survey Spectrum of AZC018, AZ93 White Ceramic Paint with Teflon Overcoat, Flight Exposed, following Depth Profile.

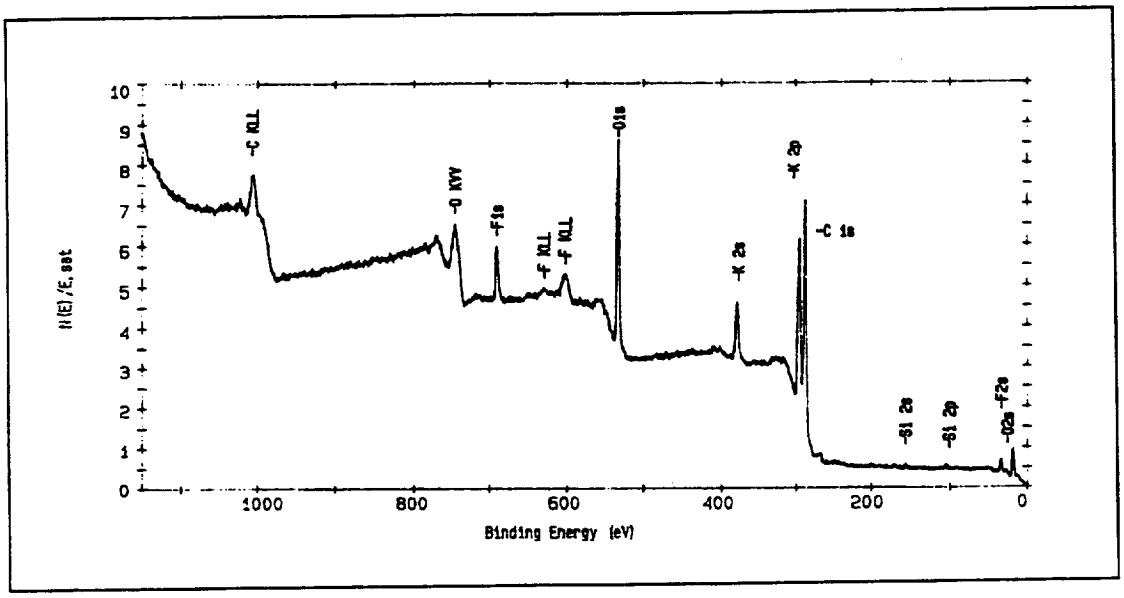

Figure G-11. Survey Spectrum for AZC030, 2000 Angstroms Tefzel on Z93 White Ceramic Paint, Ground Control

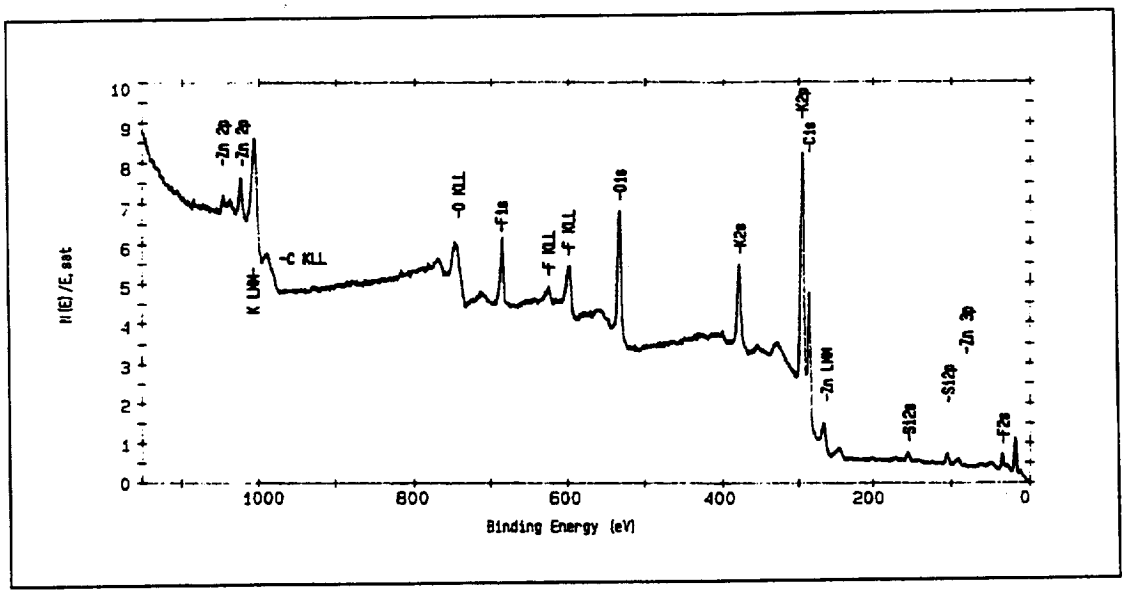

Figure G-12. Survey Spectrum for AZC030, 2000 Angstroms Tefzel on Z93 White Ceramic Paint, Ground Control, following Depth Profile.

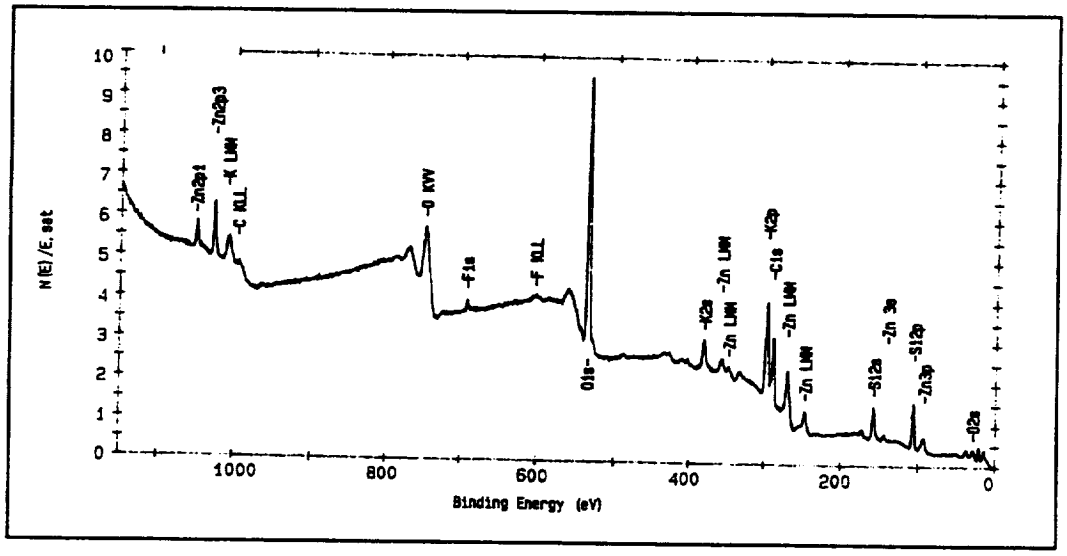

Figure G-13. Survey Spectrum for AZC029, 2000 Angstroms Tefzel on Z93 White Ceramic Paint, Flight Exposed.

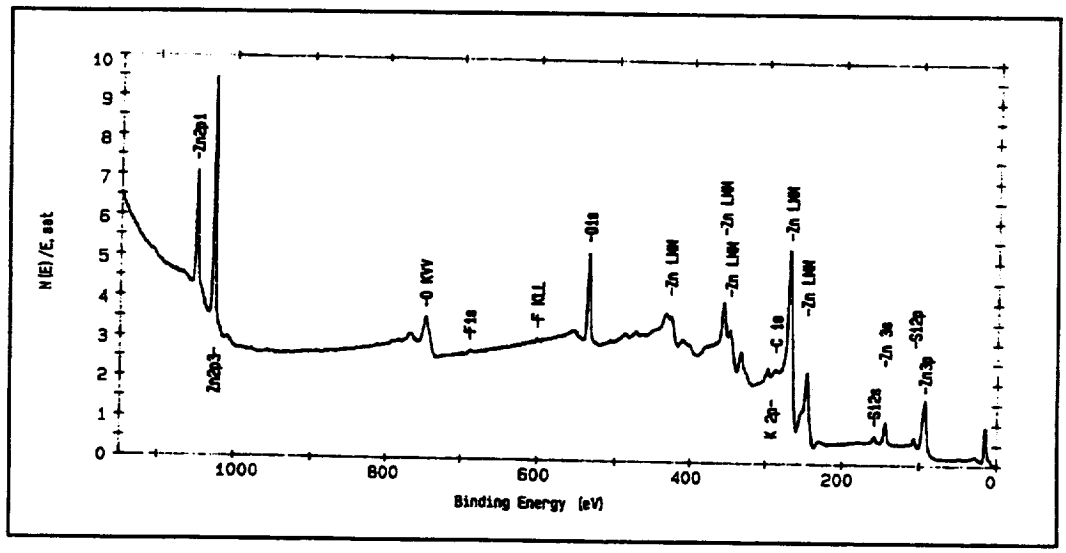

Figure G-14. Survey Spectrum for AZC029, 2000 Angstroms Tefzel on Z93 White Ceramic Paint, Flight Exposed, following Depth Profile

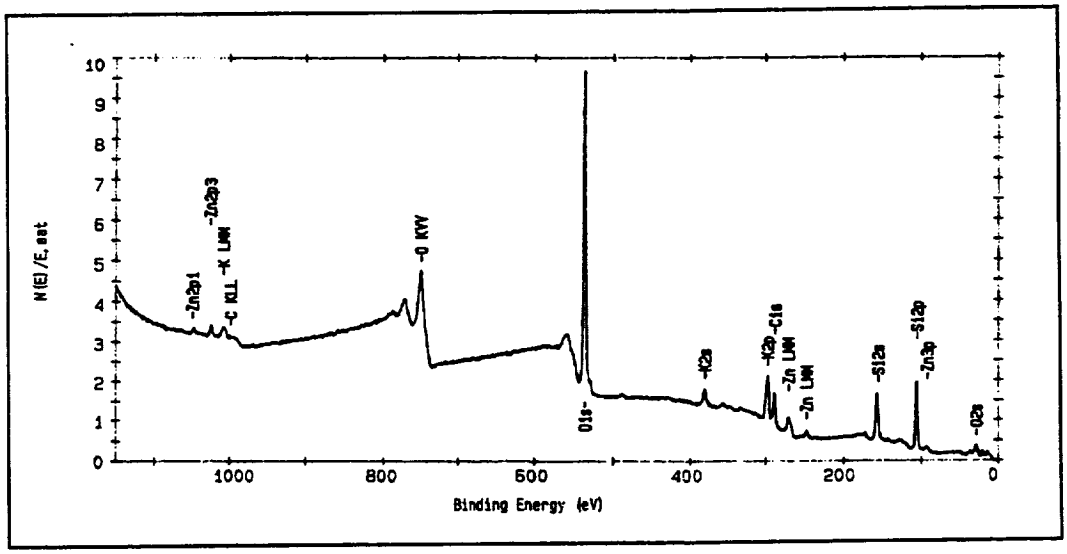

Figure G-15. Survey Spectrum for AZC037, 2000 Angstroms Silicone on Z93 White Ceramic Paint, Flight Exposed.

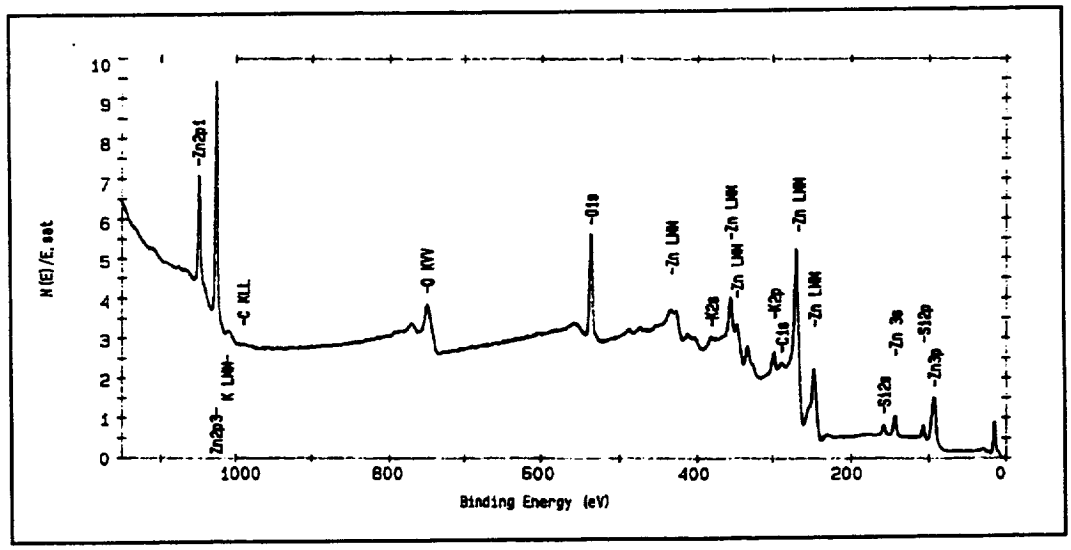

Figure G-16. Survey Spectrum for AZC037, 2000 Angstroms Silicone on Z93 White Ceramic Paint, Flight Exposed, following Depth Profile

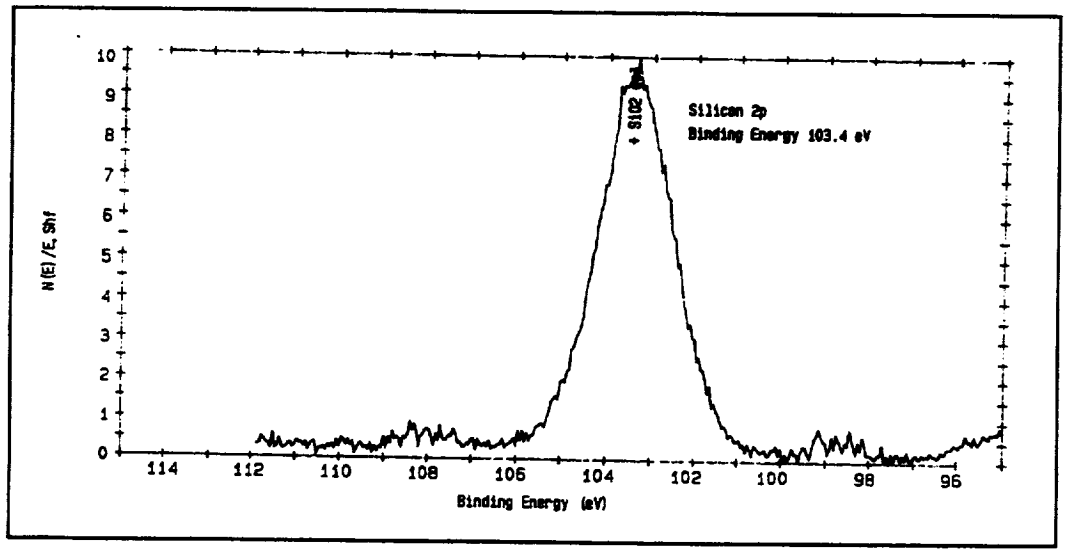

Figure G-17. High Resolution Scan of the Silicon 2p Line AZC037, 2000 Angstroms Silicone on Z93 White Ceramic Paint, Flight Exposed

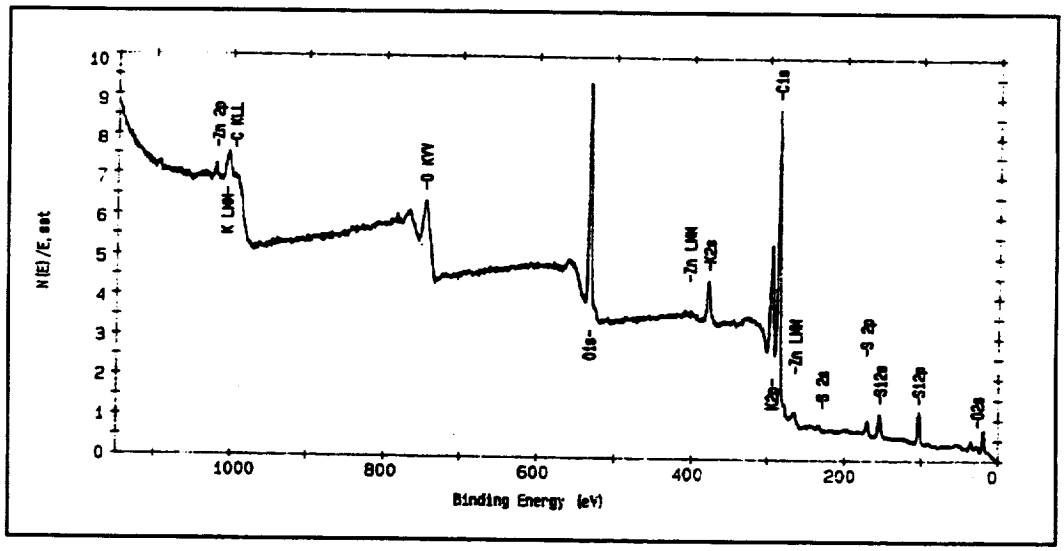

Figure G-18. Survey Spectrum for AZC036, 2000 Angstroms Silicone on Z93 White Ceramic Paint, Ground Control

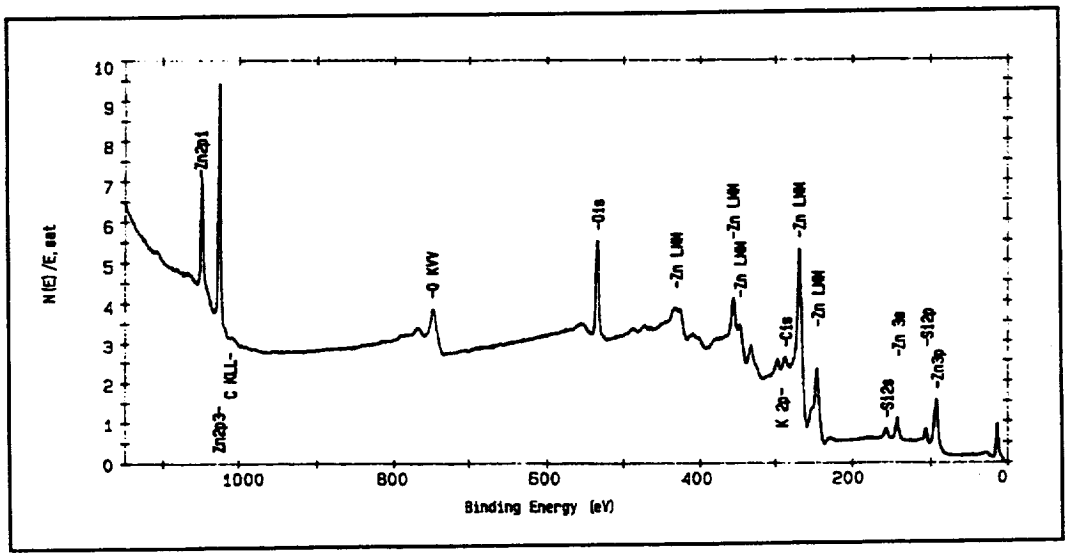

Figure G-19. Survey Spectrum for AZC036, 2000 Angstroms Silicone on Z93 White Ceramic Paint, Ground Control, Exposed, following Depth Profile

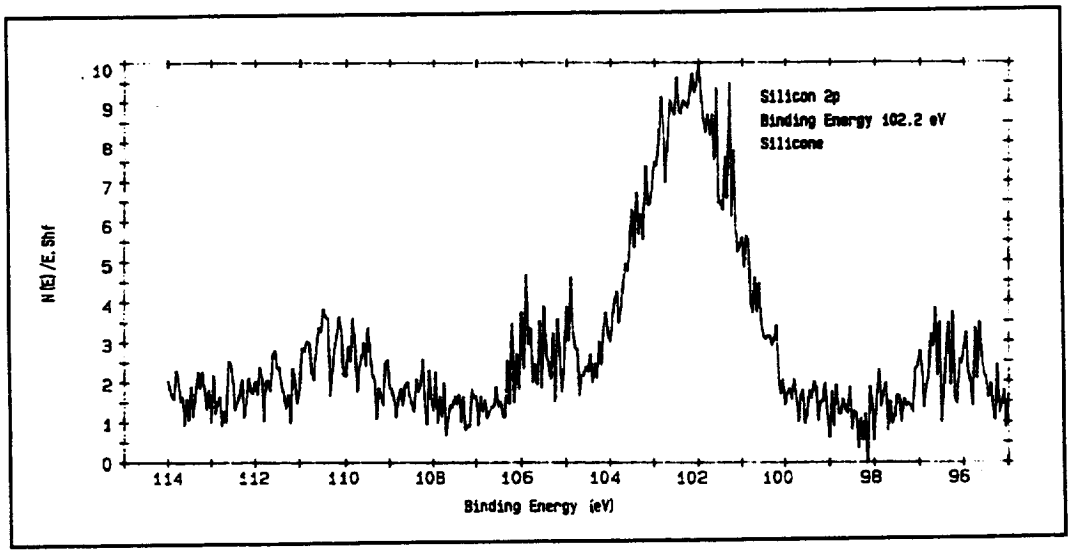

Figure G-20. High Resolution Scan of the Silicon 2p Line AZC036, 2000 Angstroms Silicone on Z93 White Ceramic Paint, Ground Control

APPENDIX H

MATERIAL ANALYSIS DATA

SEM & EDAX DATA

WHITE SANDS TEST FACILITY (WSTF)/JOHNSON SPACE CENTER (JSC)

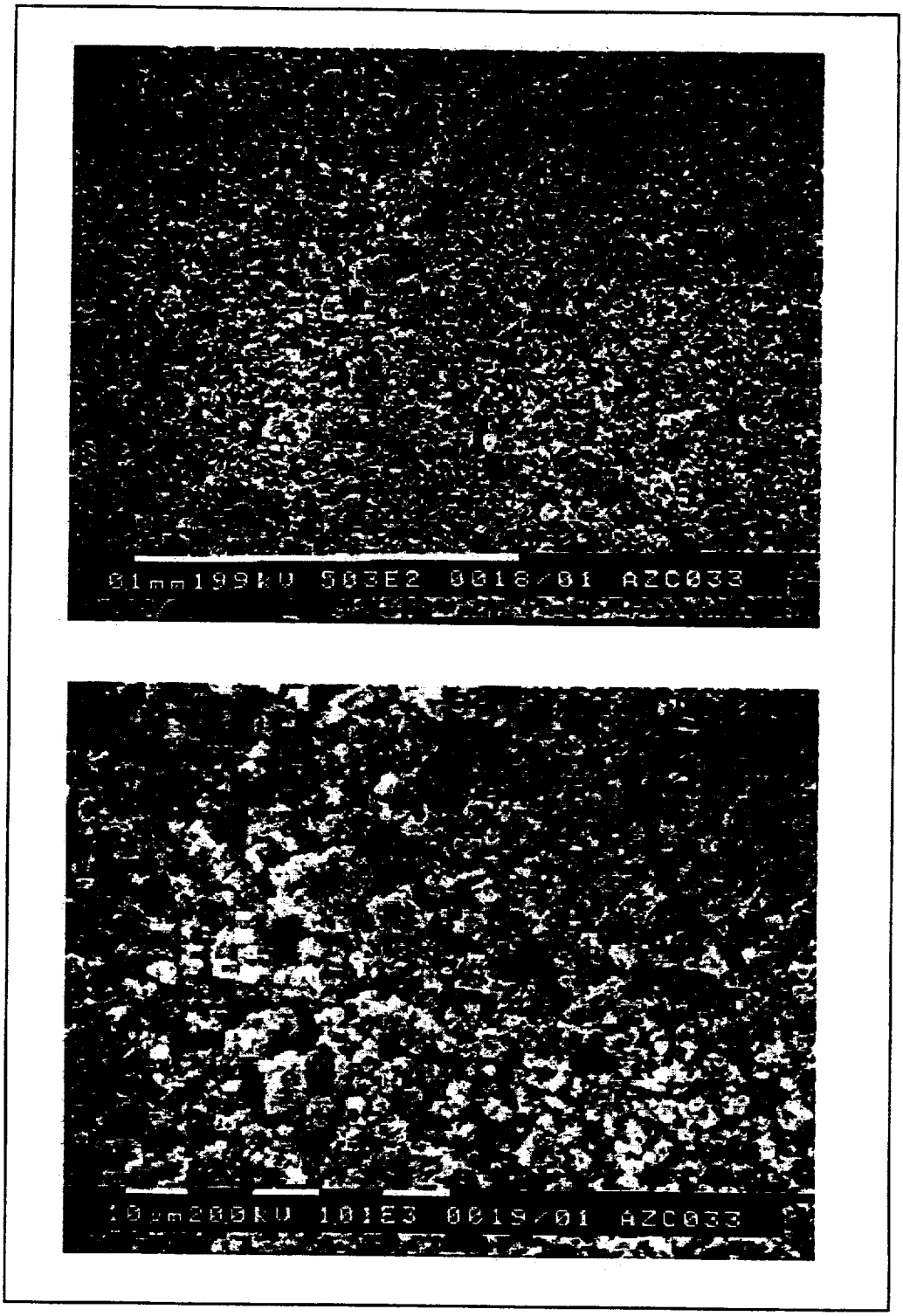

Figure H-1. 500x & 1000x SEM Image of AZC033, Z93P White Ceramic Paint, Ground Control Sample.

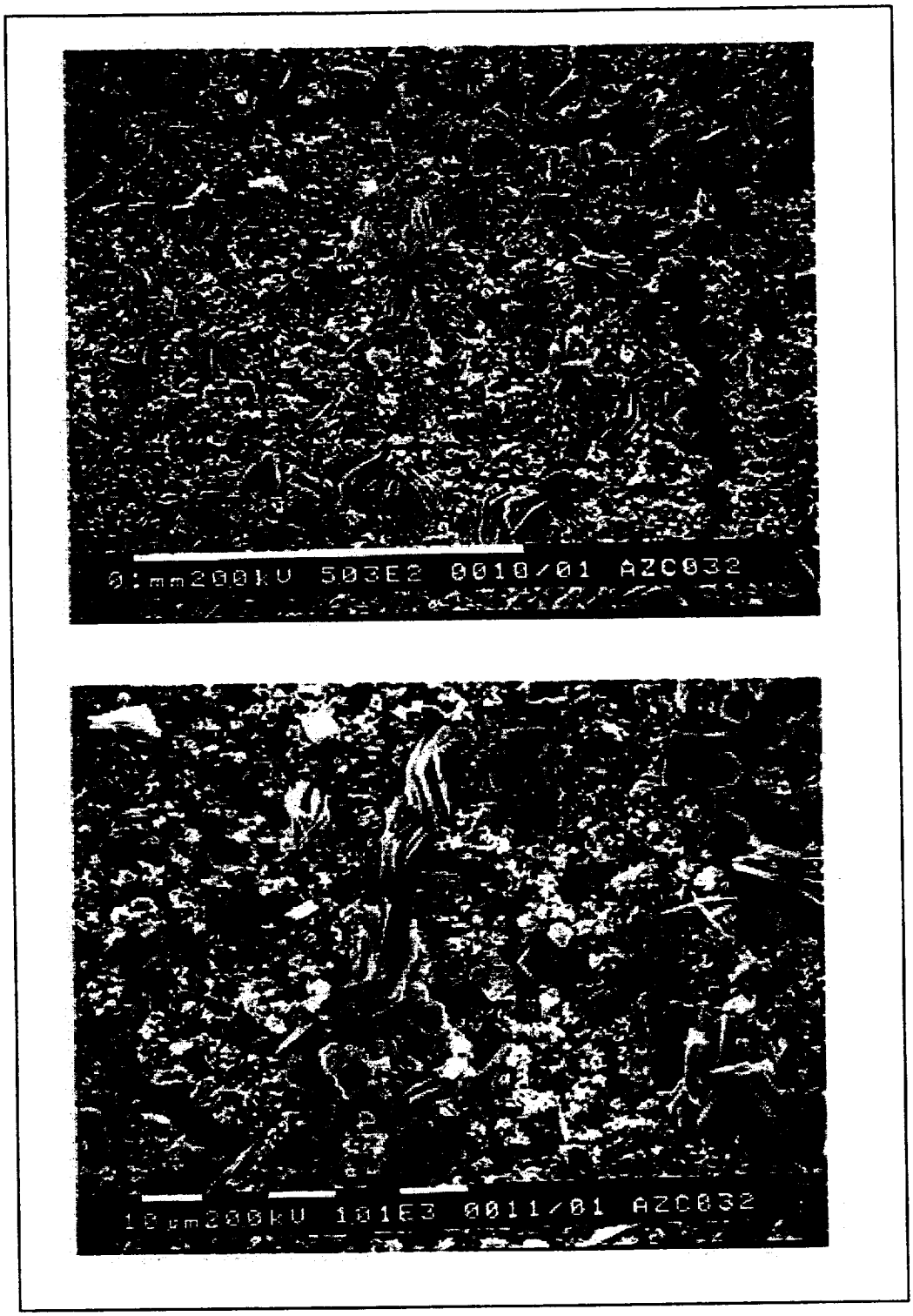

Figure H-2. 500x & 1000x SEM Image of AZC032, Z93 White Ceramic Paint, Flight Exposed Sample.

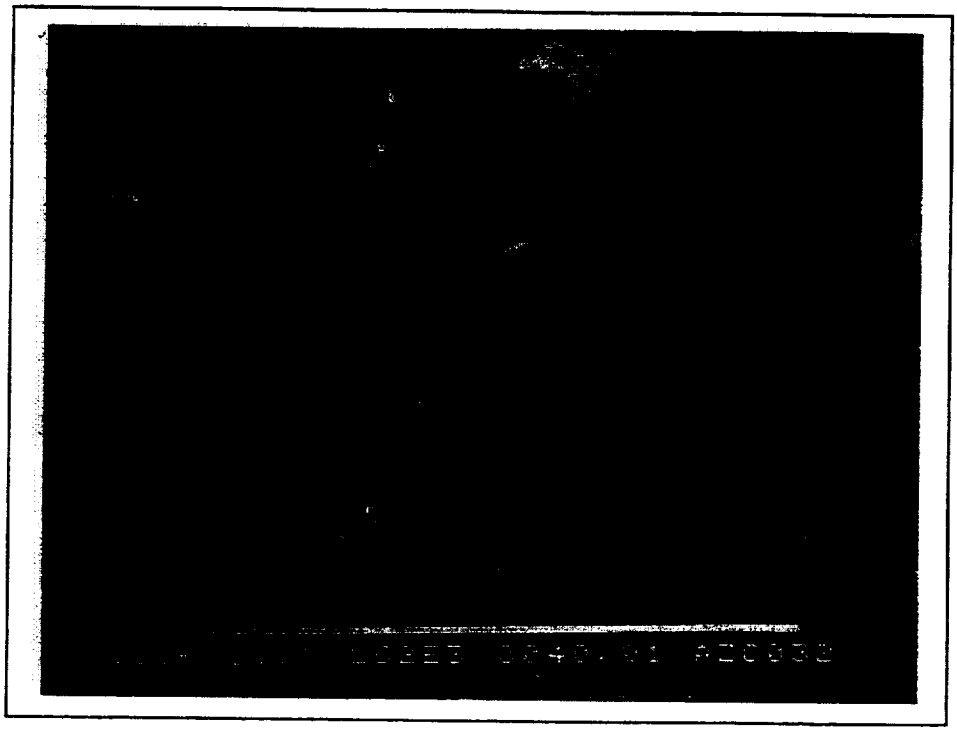

Figure H-3. Close up SEM Image of AZC032 "Crystal Type Feature," Z93 White Ceramic Paint, Flight Exposed Sample.

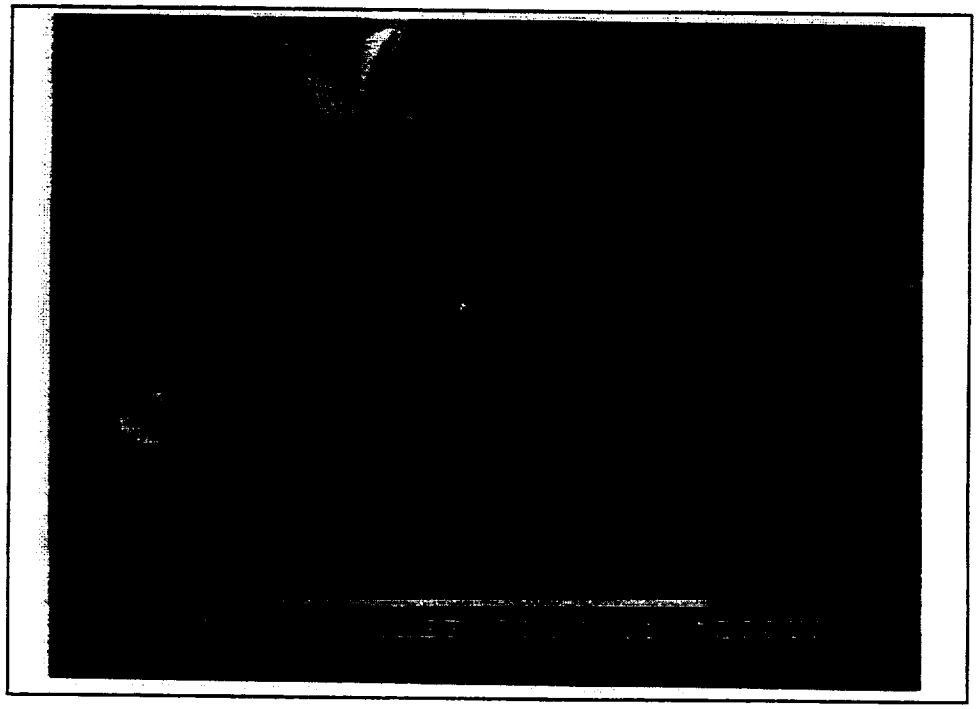

Figure H-4. Close up SEM Image of AZC032 "Mica Type Feature," Z93 White Ceramic Paint, Flight Exposed Sample.

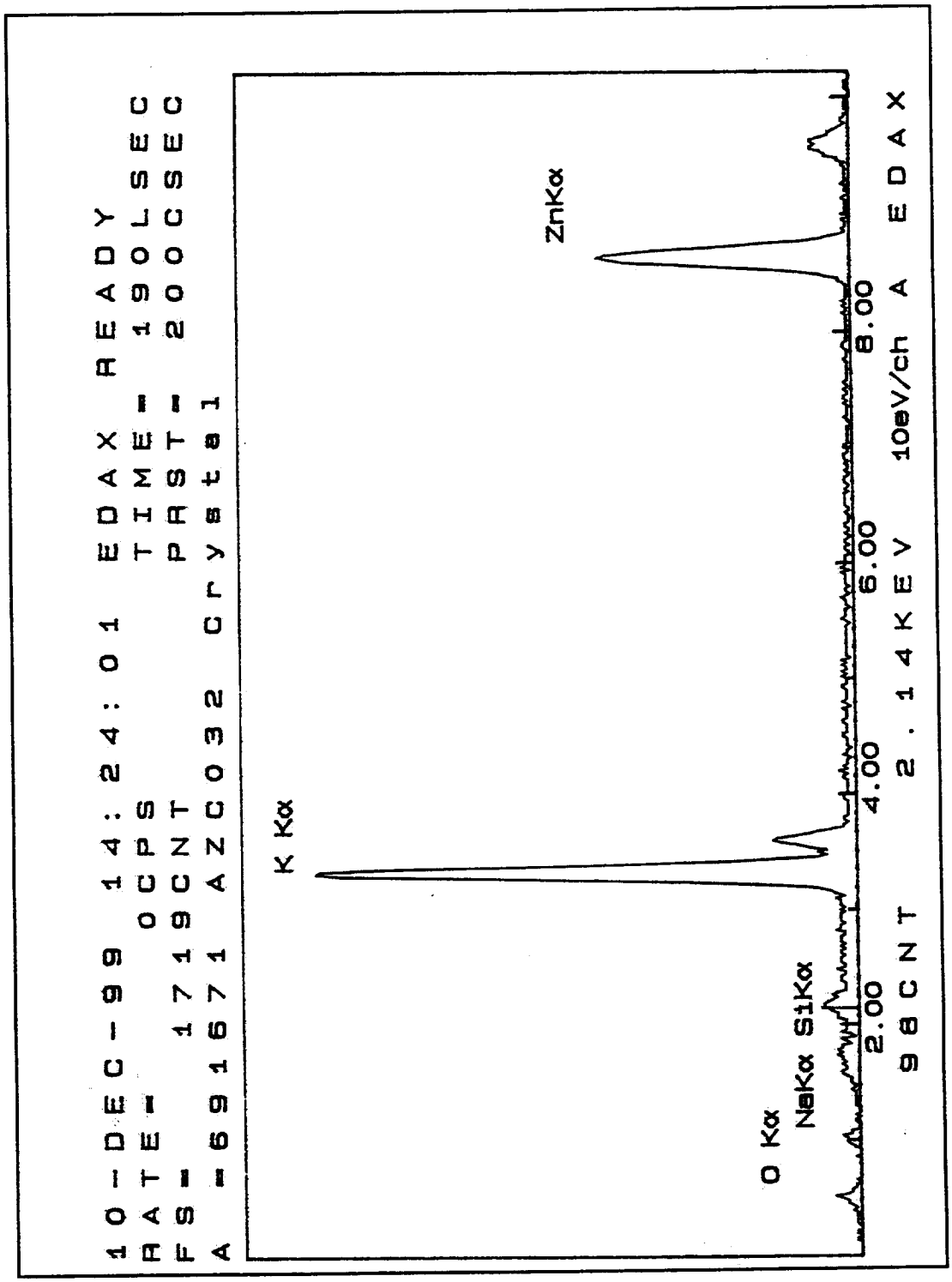

Figure H-5. EDAX Spectrum of AZC032 "Crystal Type Feature," Z93P White Ceramic Paint, Flight Exposed Sample.

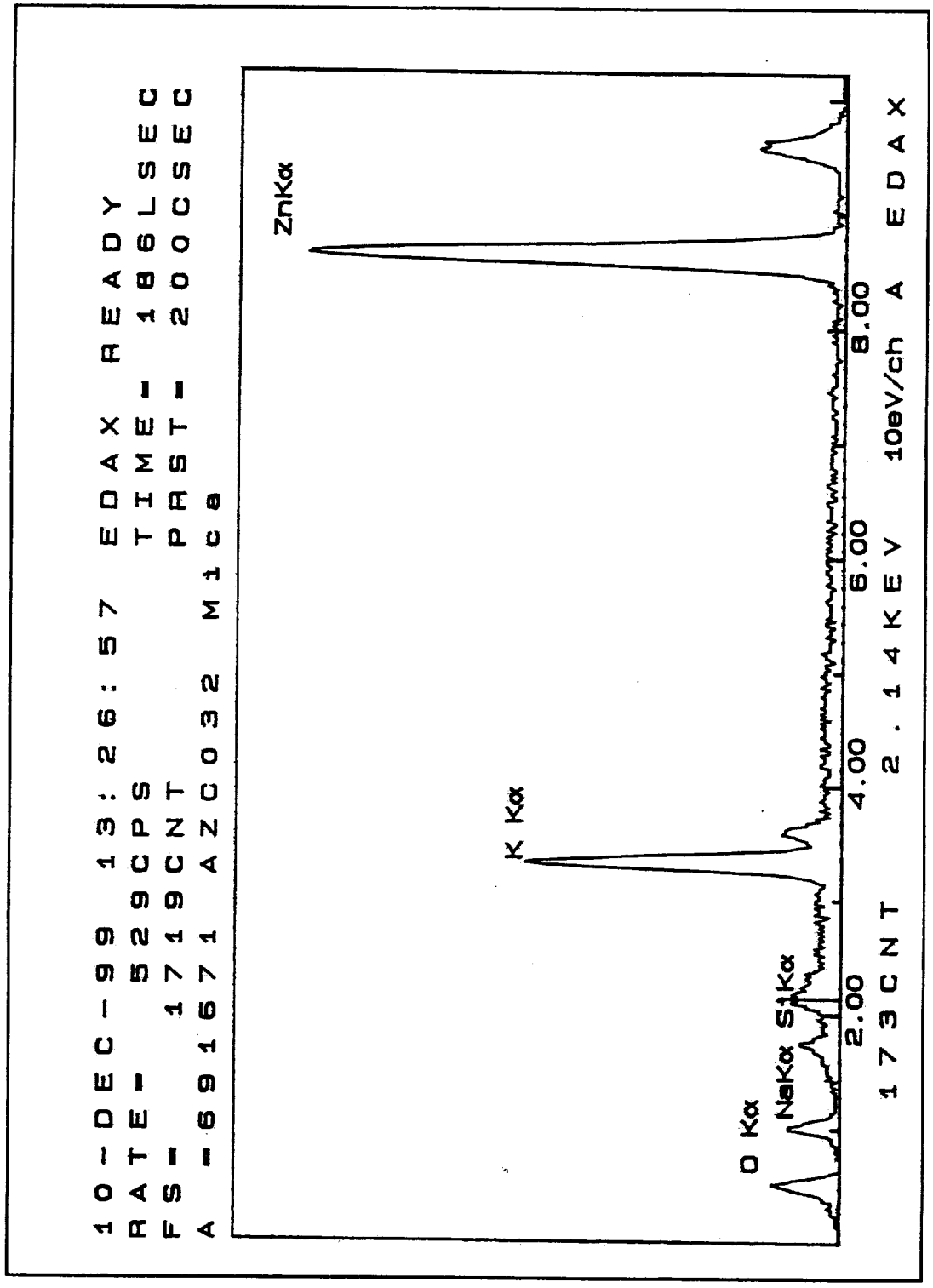

Figure H-6. EDAX Spectrum of AZC032 "Mica Type Feature," Z93P White Ceramic Paint, Flight Exposed Sample

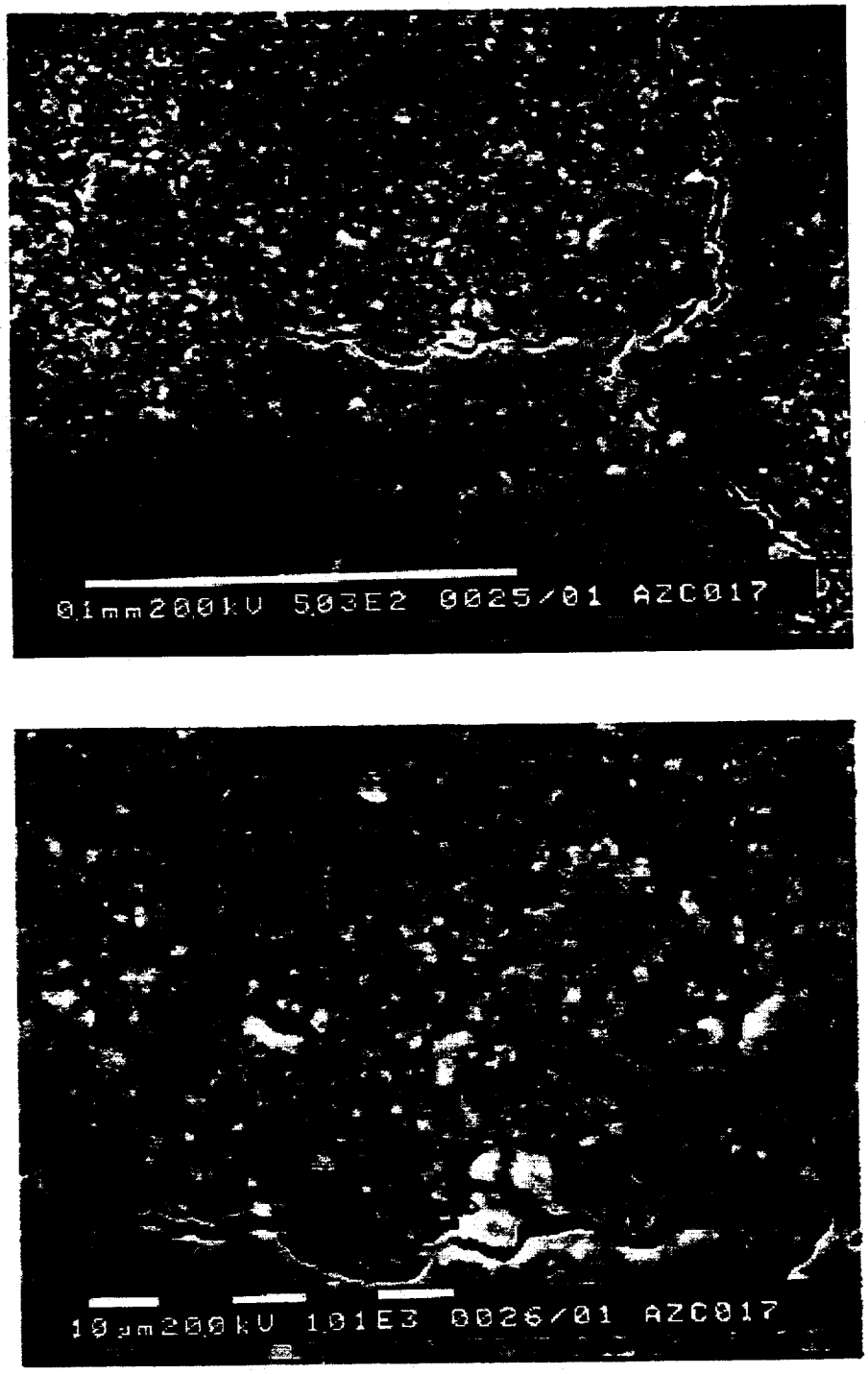

Figure H-7. 500x & 1000x SEM Image of AZC017, AZ93 White Ceramic Paint with Teflon Overcoat, Ground Control Sample

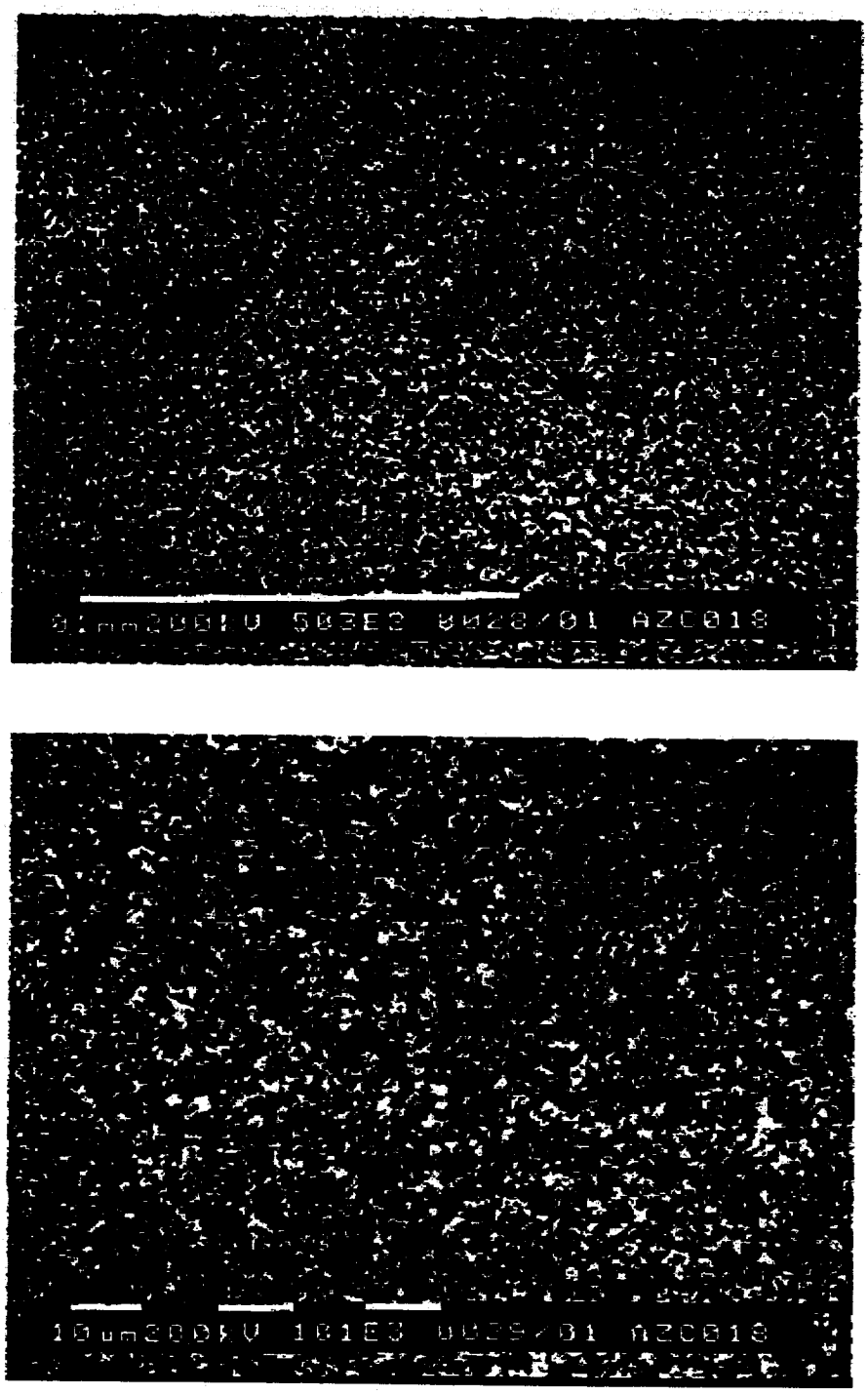

Figure H-8. 500x & 1000x SEM Image of AZC018, AZ93 White Ceramic Paint with Teflon Overcoat, Flight Exposed Sample

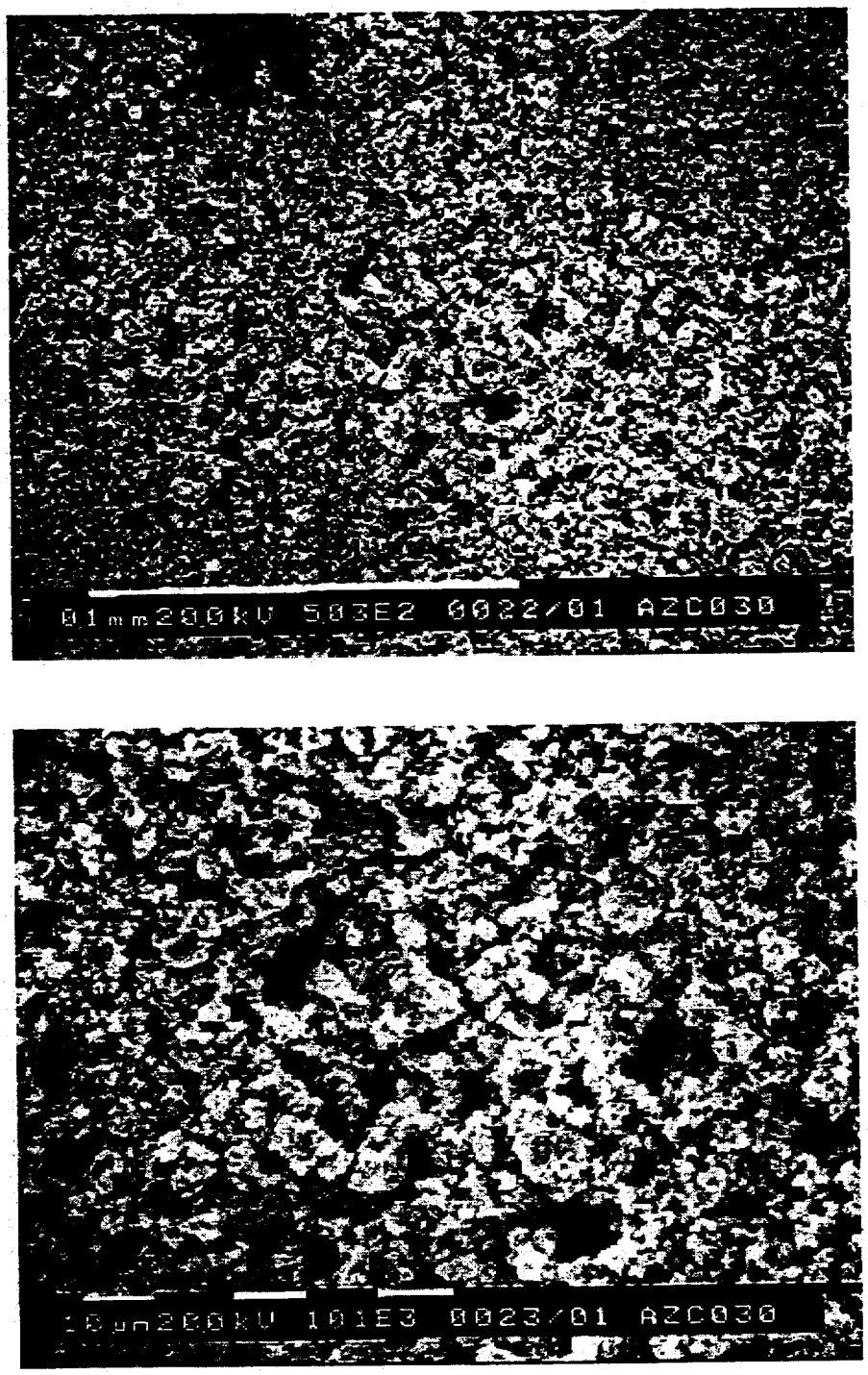

Figure H-9. 500x & 1000x SEM Image of AZC030, 2000 Angstroms Tefzel on Z93 White Ceramic Paint, Ground Control Sample

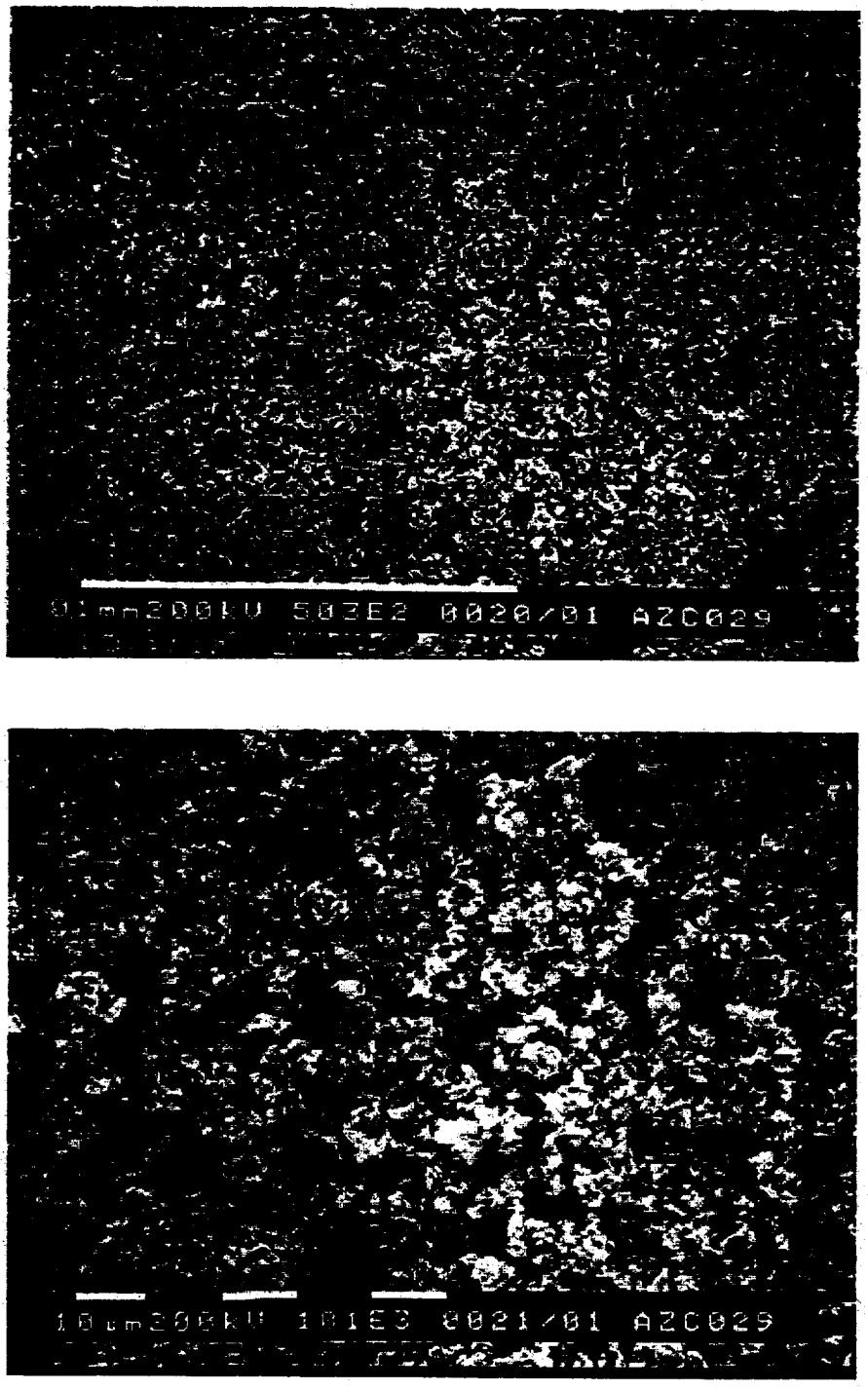

Figure H-10. 500x & 1000x SEM Image of AZC029, 2000 Angstroms Tefzel on Z93 White Ceramic Paint, Flight Exposed Sample

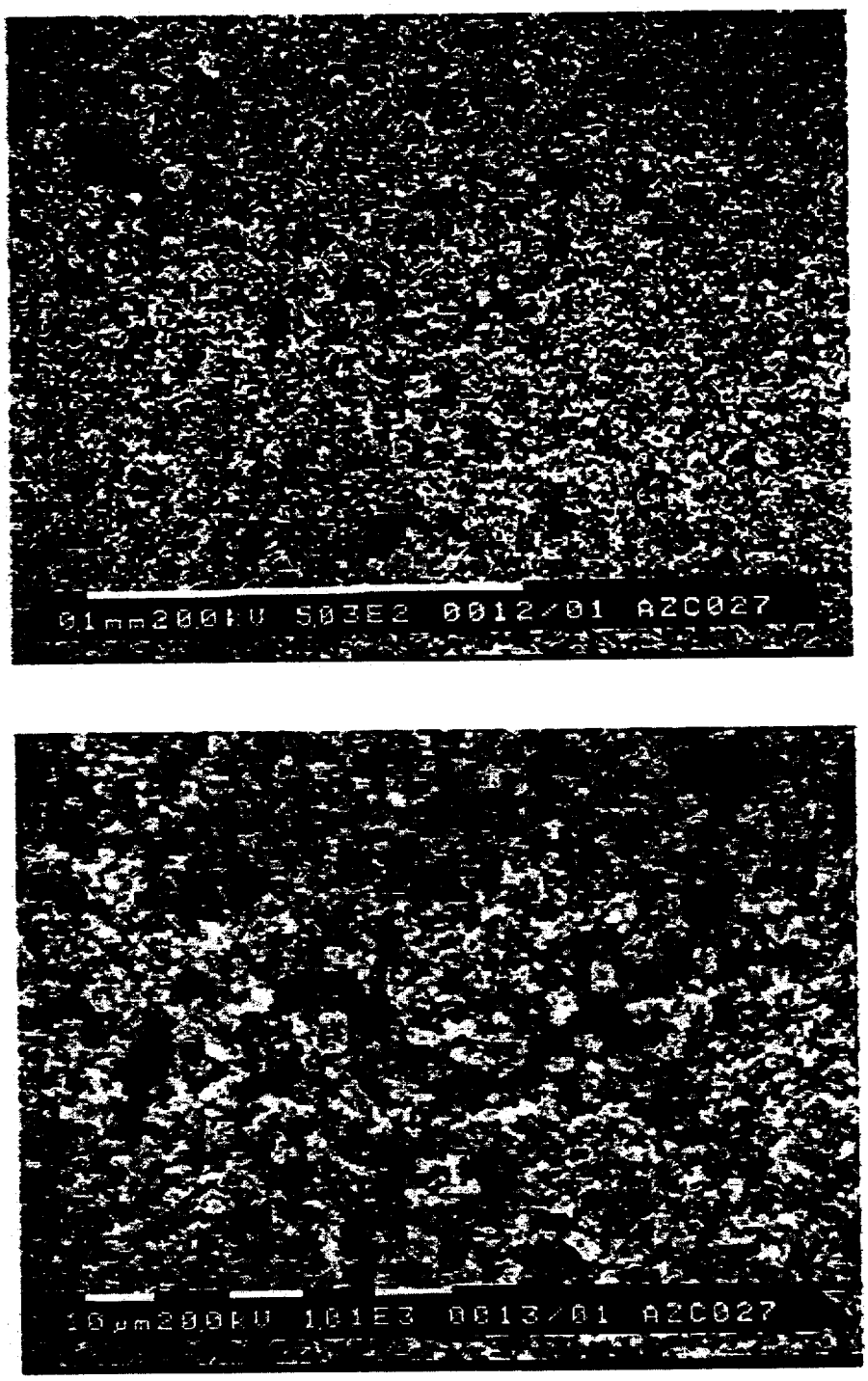

Figure H-11. 500x & 1000x SEM Image of AZC027, 500 Angstroms Tefzel on Z93 White Ceramic Paint, Ground Control Sample

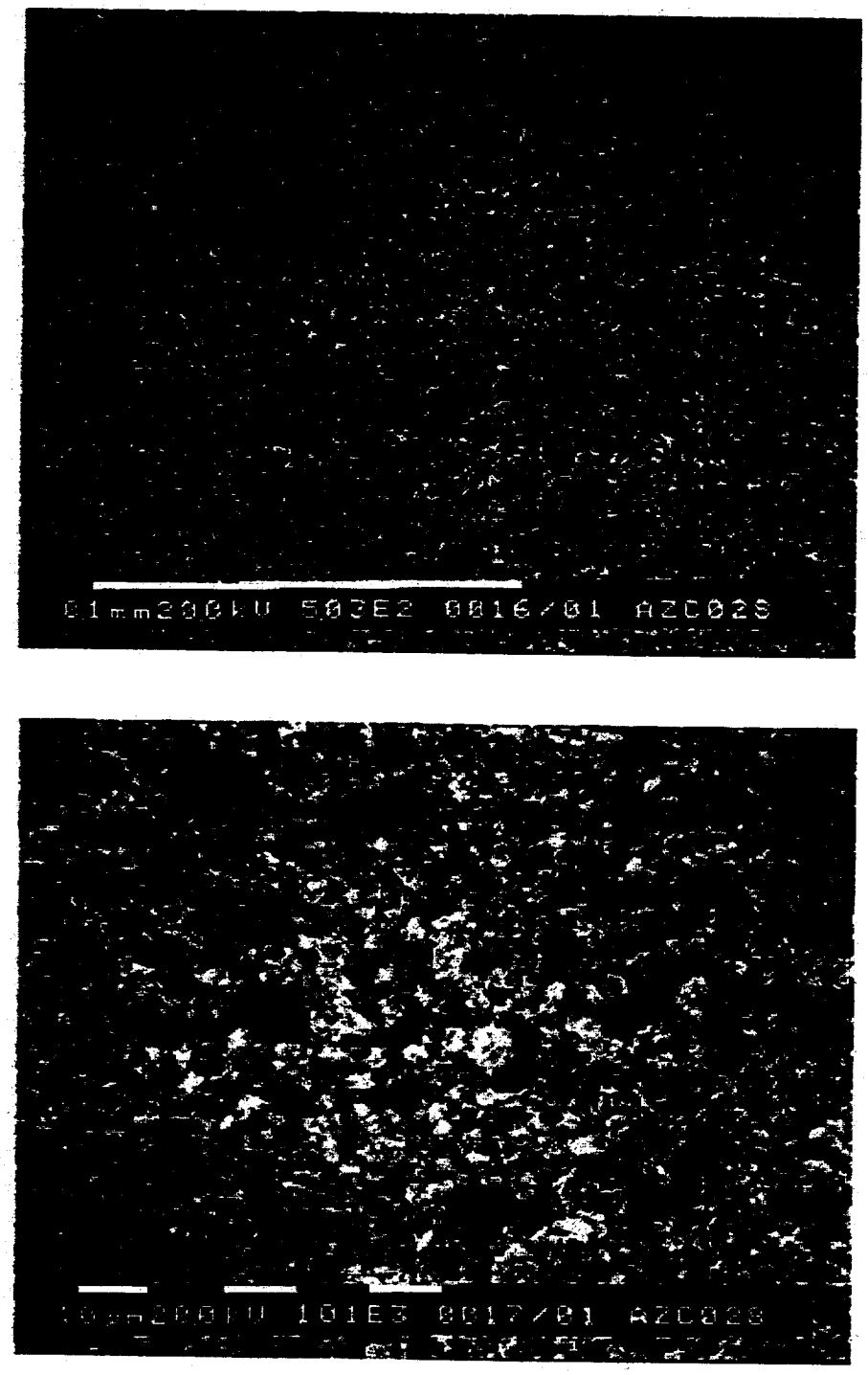

Figure H-12. 500x & 1000x SEM Image of AZC028, 500 Angstroms Tefzel on Z93 White Ceramic Paint, Flight Exposed Sample

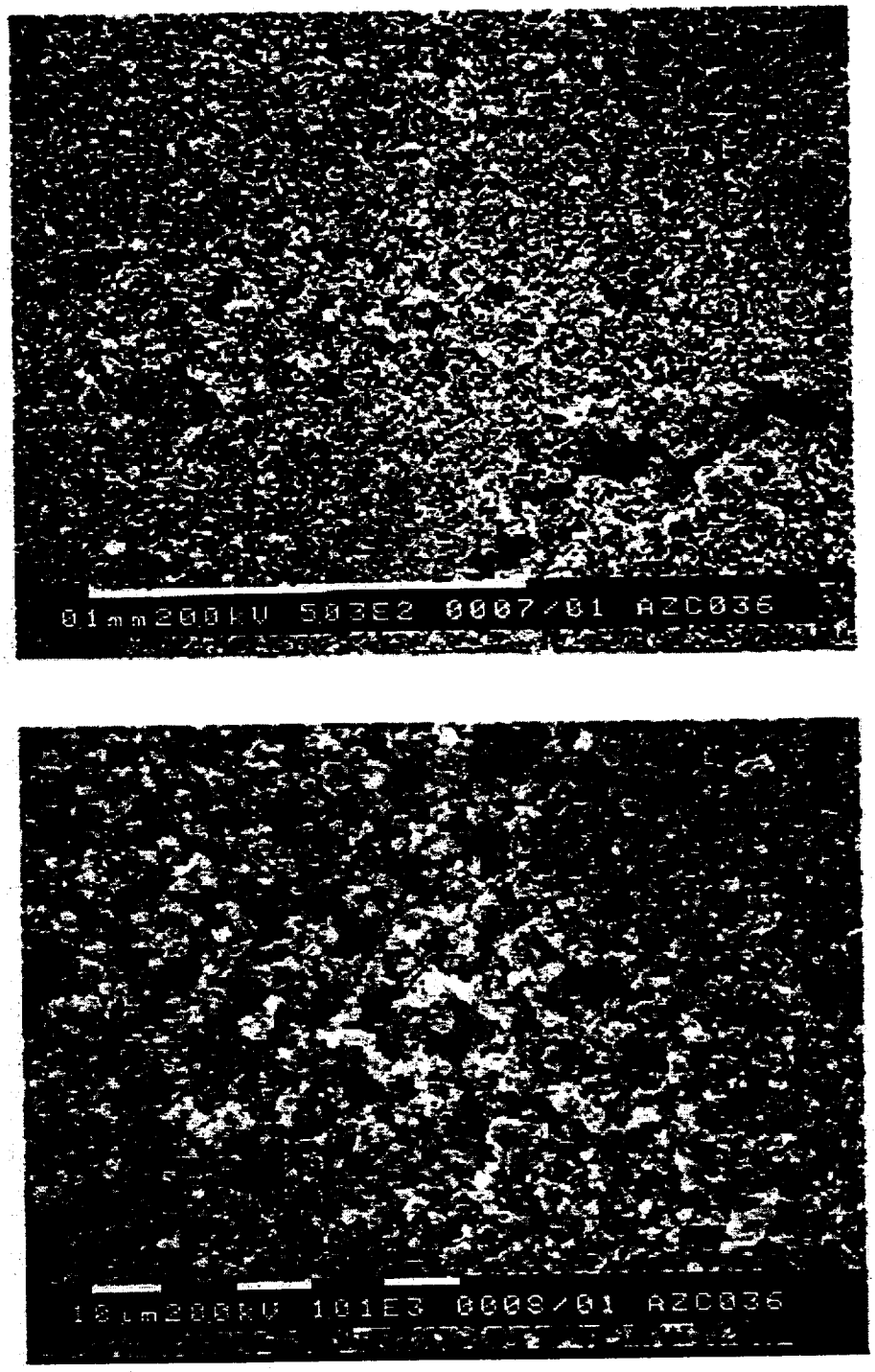

Figure H-13. 500x & 1000x SEM Image of AZC036, 2000 Angstroms Silicone on Z93 White Ceramic Paint, Ground Control Sample

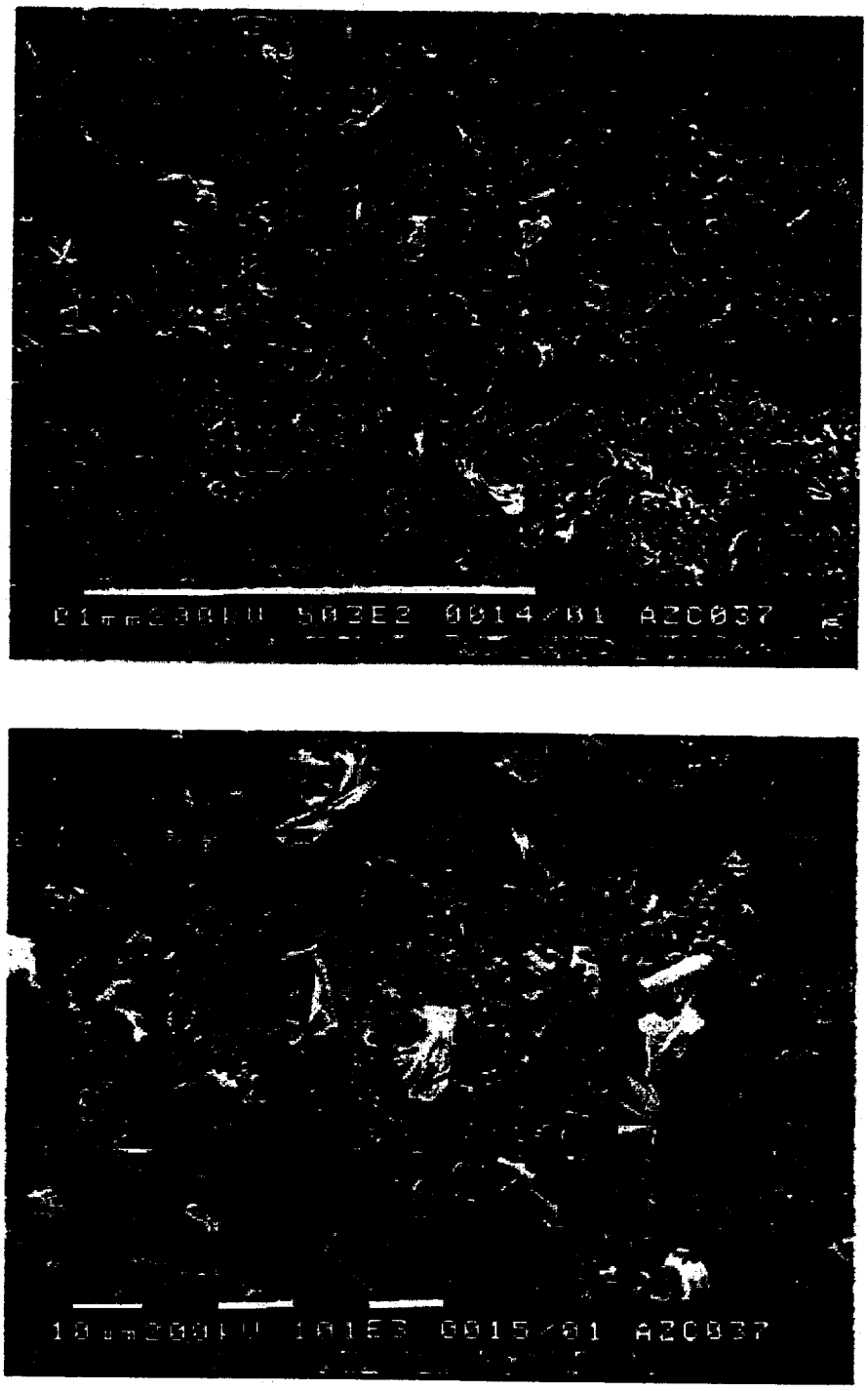

Figure H-14. 500x & 1000x SEM Image of AZC037, 2000 Angstroms Silicone on Z93 White Ceramic Paint, Flight Exposed Sample

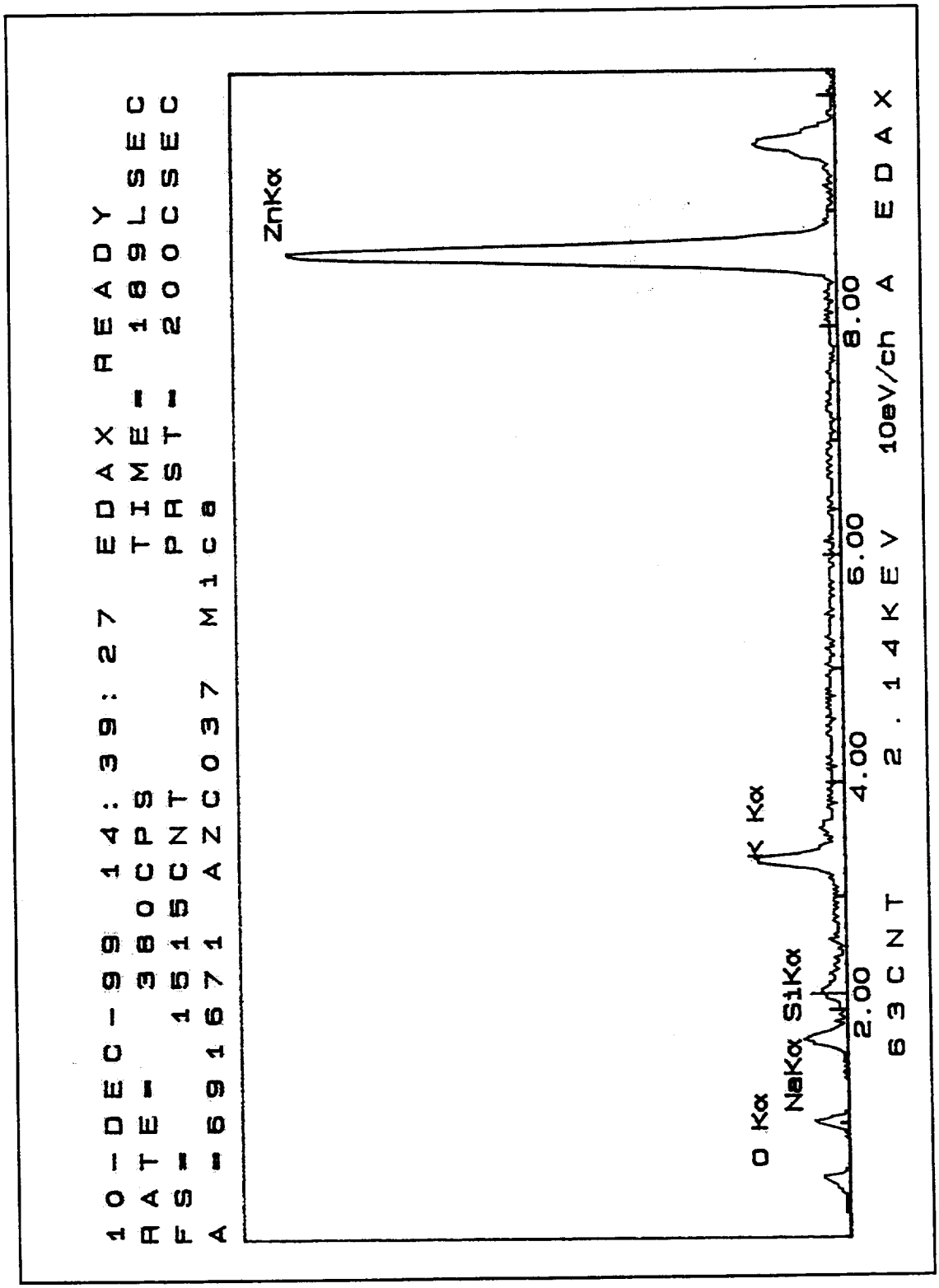

Figure H-15. EDAX Spectrum of AZC037 "Mica Type Feature," 2000 Angstroms Silicone on Z93P White Ceramic Paint, Flight Exposed Sample

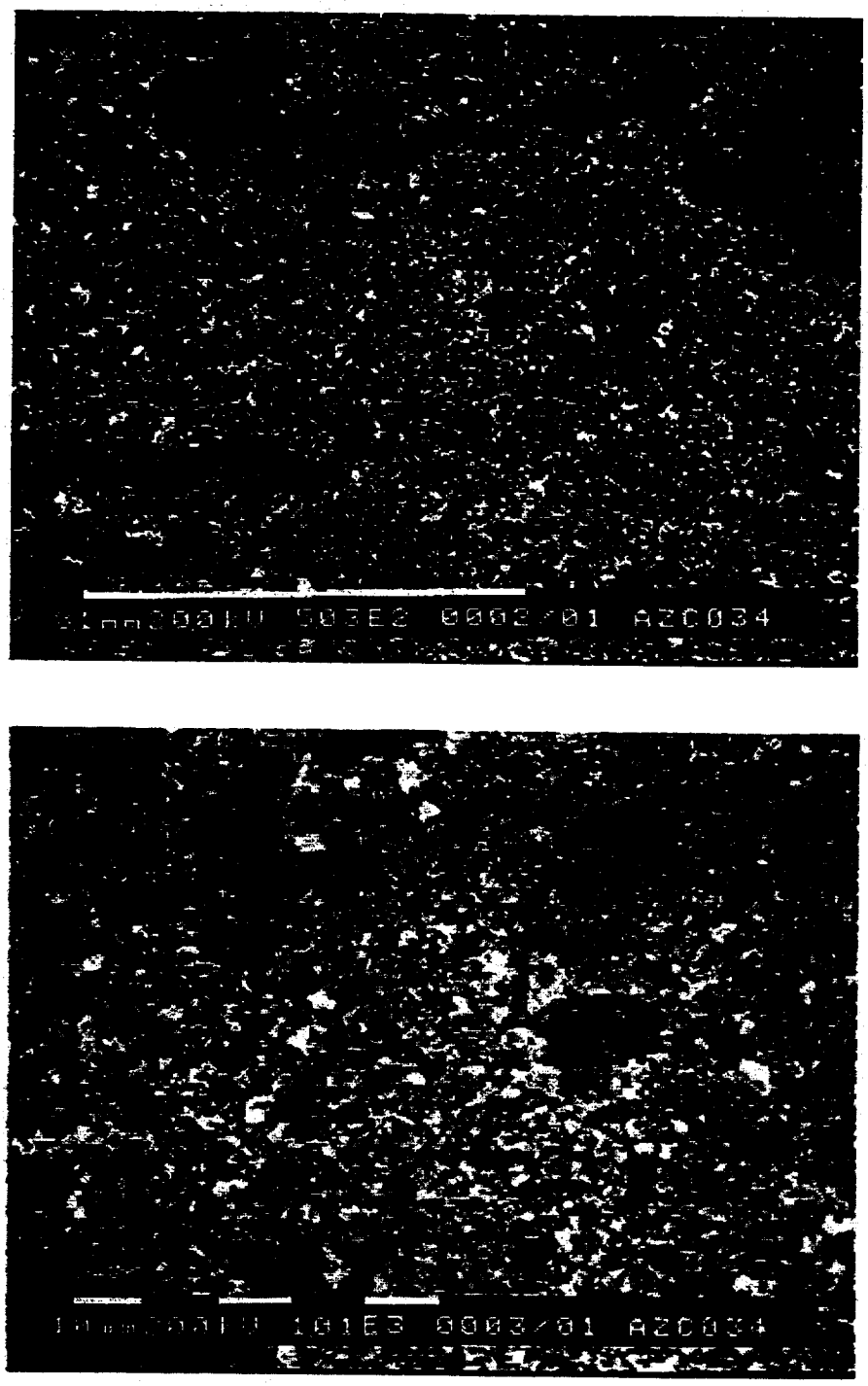

Figure H-16. 500 x & 1000 x SEM Image of AZC034, 500 Angstroms Silicone on Z93 White Ceramic Paint, Ground Control Sample

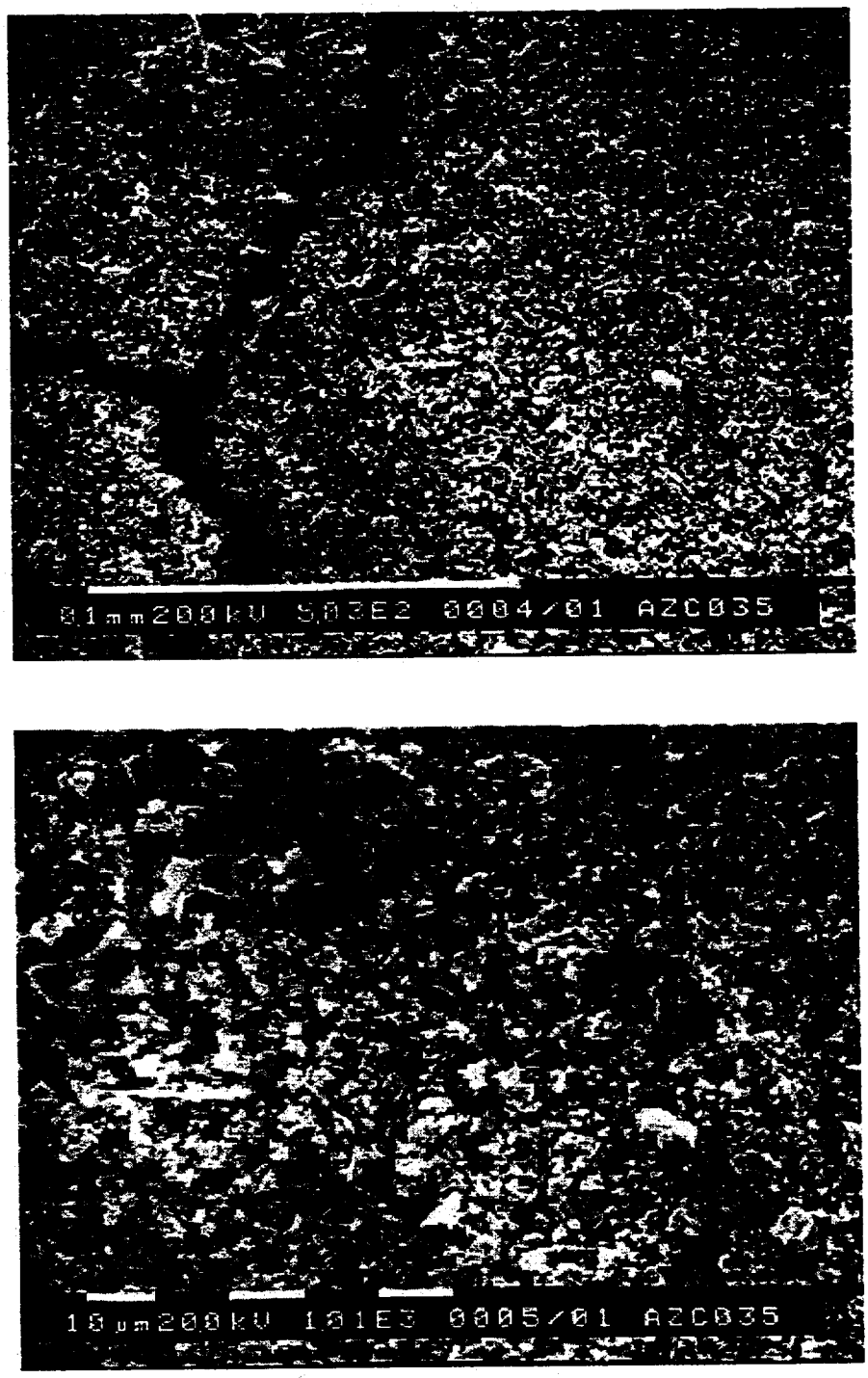

Figure H-17. 500 x & 1000 x SEM Image of AZC035, 500 Angstroms Silicone on Z93 White Ceramic Paint, Flight Exposed Sample

APPENDIX I

LISTING OF PASSIVE SAMPLES
PRE- AND POST-FLIGHT PASSIVE SAMPLE DATA

Table I-1. Listing of Passive Samples

Description	Carousel Position	Supplier Sample Number	Sample Number	Serial Number	Flight / Backup	Supplier	Contact
AO Resist. Diam.-like Nanocomp. Coatings (DYLYNTM) DLN-undoped	CP01	ZERO368a	SP01	SP1-01	F	USAF Research Laboratory	Chuck Miglionico
AO Resist. Diam.-like Nanocomp. Coatings (DYLYNTM) DLN-30% Ti doped	CP02	ZERO375a	SP02	SP2-01	F	USAF Research Laboratory	Chuck Miglionico
TCOH-COTM - "6u" glass fabric	CP18	na	SP04	SP4-01	F	RSC Energia, Moscow	S. Naumov
Beta Cloth	CP19	RB0135-044	SP05	SP5-01	F	BOEING/Rocketdyne	Pol Dano
Black marking-Metalphoto	CP20	GGP-445B	SP06	SP6-01	F	BOEING/Rocketdyne	Pol Dano
Al 1st Surface Mirror Contam Monitor	CP09	P29-ALCM7	SP10	SP10-01	F	NASA Glenn RC	Bruce Banks
Defected Al on Kapton	CP Plate 1	P30-ALK1	SP11	SP11-01	F	NASA Glenn RC	Bruce Banks
ISS Solar Array Blanket Face Sheet	CP Plate 1	P31-SKS1	SP12	SP12-01	F	NASA Glenn RC	Bruce Banks
Ir/Si Multilayer	CV31	ISRC9605B	SP14	SP14-01	F	NASA GSFC	Ritva Keski-Kuha
EIC Electrochromic Coating	CP Plate 1	na	SP15	SP15-01	F	NASA GSFC	Lonny Kauder
OCLI coating over white Tedlar	CP Plate 1	#1	SP16	SP16-01	F	NASA GSFC	Lonny Kauder
Six layer stack on Si-wafer	CP16	na	SP17	SP17-01	F	Lockheed Martin	William Saylor
YB-71P, Zn2TiO4-Potassium silicate thermal coating	CP03	na	SP19	SP19-01	F	IIT Research Institute	M.S.Deshpande
Z-93SC55	CP04	OPM	SP20	SP20-01	F	IIT Research Institute	M.S.Deshpande
S13GP/LO-1, Encapsulated ZnO in methyl silicone	CP05	na	SP21	SP21-01	F	IIT Research Institute	M.S.Deshpande
Z24P binder w/ZnO pigment + 2% Sodium Salicylate by wt	CP12	BZS-B1	SP23	SP23-01	F	Boeing (WA)	Gary Pippin
Silver Teflon 5 mil 2-1/2" x 3/4"	CP Plate 3	Sheldahl 7-G401900	SP24	SP24-01	F	Boeing (WA)	Gary Pippin
Silver Teflon 5 mil 2-1/2" x 3/4"	CP Plate 4	Sheldahl 7-G401900	SP24	SP24-02	F	Boeing (WA)	Gary Pippin
White Paint Z24P Binder w/ZnO Pigment	CP Plate 1	BZ-A1	SP25	SP25-01	F	Boeing (WA)	Gary Pippin
EVA Label - Blue	CP Plate 1	na	SP26	SP26-01	F	Boeing (TX)	John L. Golden
EVA Label - Red	CP Plate 1	na	SP27	SP27-01	F	Boeing (TX)	John L. Golden
EVA Label Decal	CP Plate 1	na	SP28	SP28-01	F	Boeing (TX)	John L. Golden
ATR Crystal-Zinc Selenide	CP Plate 2	7002-502	SP29	SP29-01	F	AZ Technology, Inc.	John Harchanko
ATR Crystal-Germanium	CP Plate 2	7002-512	SP30	SP30-01	F	AZ Technology, Inc.	John Harchanko
Kapton (1 layer)	na	P68-KH1	SP31	SP31-01s	F	NASA Glenn RC/AZ Technology, Inc.	John Harchanko
AZBEC-1	CP11	na	SP32	SP32-01	F	AZ Technology, Inc.	Rick Mell
AZWEC-2I	CP10	na	SP33	SP33-01	F	AZ Technology, Inc.	Rick Mell
AO Resist. Diam.-like Nanocomp. Coatings (DYLYNTM) DLN-undoped	na	ZERO368b	SP01	SP1-02	B	USAF Research Laboratory	Chuck Miglionico

Table I-2. Pre- and Post-Flight Passive Sample Data

Description	Carousel Position	Supplier Sample Number	Sample Number	Serial Number	Flight/ Backup	Supplier	Contact
TCOH-COTM - "6u" glass fabric	na	na	SP04	SP4-02	B	RSC Energia, Moscow	S. Naumov
Beta Cloth	na	RB0135-044	SP05	SP5-02	B	BOEING/Rocketdyne	Pol Dano
Black marking-Metalphoto	na	GGP-445B	SP06	SP6-02	B	BOEING/Rocketdyne	Pol Dano
Al 1st Surface Mirror Contam Monitor	na	P29-ALCM8	SP10	SP10-02	B	NASA Glenn RC	Bruce Banks
Defected Al on Kapton	na	P30-ALK2	SP11	SP11-02	B	NASA Glenn RC	Bruce Banks
ISS Solar Array Blanket Face Sheet	na	P31-SKS2	SP12	SP12-02	B	NASA Glenn RC	Bruce Banks
Ir/Si Multilayer	na	ISRC9605D	SP14	SP14-02	B	NASA GSFC	Ritva Keski-Kuha
OCLI coating over white Tedlar	na	#2	SP16	SP16-02	B	NASA GSFC	Lonny Kauder
Six layer stack on Si-wafer	na	na	SP17	SP17-02	B	Lockheed Martin	William Saylor
YB-71P, Zn2TiO4-Potassium silicate thermal coating	na	na	SP19	SP19-02	B	IIT Research Institute	M.S.Deshpande
Z-93SC55	na	na	SP20	SP20-02	B	IIT Research Institute	M.S.Deshpande
S13GP/LO-1, Encapsulated ZnO in methyl silicone	na	na	SP21	SP21-02	B	IIT Research Institute	M.S.Deshpande
Z24P binder w/ZnO pigment + 2% Sodium Salicylate by wt	na	BZS-B2	SP23	SP23-02	B	Boeing (WA)	Gary Pippin
Silver Teflon 5 mil 2-1/2" x 3/4"	na	Sheldahl 7-G401900	SP24	SP24-03	B	Boeing (WA)	Gary Pippin
White Paint Z24P Binder w/ZnO Pigment	na	BZ-A2	SP25	SP25-02	B	Boeing (WA)	Gary Pippin
EVA Label - Blue	na	na	SP26	SP26-02	B	Boeing (TX)	John L. Golden
EVA Label - Red	na	na	SP27	SP27-02	B	Boeing (TX)	John L. Golden
EVA Label Decal	na	na	SP28	SP28-02	B	Boeing (TX)	John L. Golden
ATR Crystal-Zinc Selenide	na	7002-502	SP29	SP29-02	B	AZ Technology, Inc.	John Harchanko
ATR Crystal-Germanium	na	7002-512	SP30	SP30-02	B	AZ Technology, Inc.	John Harchanko
Kapton (1 layer)	na	P68-KH2	SP31	SP31-02s	B	NASA Glenn RC/AZ Technology, Inc.	John Harchanko
AZBEC-1	na	na	SP32	SP32-02	B	AZ Technology, Inc.	Rick Mell
AZWEC-2I	na	na	SP33	SP33-02	B	AZ Technology, Inc.	Rick Mell

Table I-3 Pre- and Post-Flight Passive Sample Data

Description	Sample Number	Serial Number	Flight/ Back-up	Substrate	Pre-Vacuum Bakeout Data			Pre-Flight Data			Post-Flight Data		
					LPSR Solar Absorptance bbo	Hemis-pherical Total Emittance TEMP 2000, bbo	Near Normal Emittance TEMP 2000, bbo	LPSR Solar Absorptance	Hemis-pherical Total Emittance TEMP 2000	Near Normal Emittance TEMP 2000	LPSR Solar Absorptance	Hemispherical Total Emittance, TEMP 2000	Near Normal Emittance, TEMP 2000
AO Resist. Diam.-like Nanocomp. Coatings (DYLYNTM) DLN-undoped	SP01	SP1-01	F	Zerodur	na	na	na	0.874	0.842	0.884	0.887	0.841	0.898
AO Resist. Diam.-like Nanocomp. Coatings (DYLYNTM) DLN-30% Ti doped	SP02	SP2-01	F	Zerodur	na	na	na	0.762	0.711	0.748	0.795	0.744	0.793
TCOH-COTM - "6u" glass fabric	SP04	SP4-01	F	6061 Al	na	na	na	0.317	0.861	0.903	0.307	0.851	0.904
Beta Cloth	SP05	SP5-01	F	6061 Al	0.299	0.882	0.926	0.299	0.877	0.924	0.344	0.877	0.937
Black marking-Metalphoto	SP06	SP6-01	F	1100 series Al	0.832	0.830	0.873	0.832	0.825	0.870	0.834	0.825	0.885
Al 1st Surface Mirror Contam Monitor	SP10	SP10-01	F	Al2O3	na	na	na	0.079	0.015	0.031	0.083	0.017	0.047
Defected Al on Kapton	SP11	SP11-01	F	Kapton HN	0.095	0.020	0.032	0.096	0.026	0.029	0.100	0.023	na
ISS Solar Array Blanket Face Sheet	SP12	SP12-01	F	Kapton H	na	0.870	0.913	0.934	0.871	0.920	0.938	0.871	na
Ir/Si Multilayer	SP14	SP14-01	F	fused silica, Dynasil grade 4000P	na	na	na	0.410	0.172	0.180	0.438	0.182	0.217
EIC Electrochromic Coating	SP15	SP15-01	F	Corning 7059	na	na	na	0.783	0.743	0.777	na	na	na
OCLI coating over white Tedlar	SP16	SP16-01	F	6061 Al	0.330	0.798	0.840	0.328	0.796	0.836	0.335	0.799	0.855
Six layer stack on Si-wafer	SP17	SP17-01	F	6061 Al	0.459	0.721	0.765	0.463	0.727	0.768	0.486	0.723	0.778
YB-71P, Zn2TiO4-Potassium silicate thermal coating	SP19	SP19-01	F	6061 Al	na	0.889	na	0.128	0.887	0.934	0.128	0.875	0.934
Z-93SC55	SP20	SP20-01	F	6061 Al	na	0.895	na	0.136	0.895	0.944	0.135	0.889	0.950
S13GP/LO-1, Encapsulated ZnO in methyl silicone	SP21	SP21-01	F	6061 Al	na	0.903	na	0.182	0.902	0.951	0.188	0.895	0.957
Z24P binder w/ZnO pigment + 2% Sodium Salicylate by wt	SP23	SP23-01	F	6061 Al	na	0.915	0.963	0.216	0.910	0.960	0.250	0.905	0.968
Silver Teflon 5 mil 2-1/2" x 3/4"	SP24	SP24-01	F	6061 Al	na	na	na	0.074	0.709	0.743	0.092	0.727	0.777
Silver Teflon 5 mil 2-1/2" x 3/4"	SP24	SP24-02	F	6061 Al	na	na	na	0.072	0.709	0.744	0.086	0.731	0.777
White Paint Z24P Binder w/ZnO Pigment	SP25	SP25-01	F	6061 Al	0.241	0.908	0.953	0.240	0.905	0.953	0.251	0.898	0.960
EVA Label - Blue	SP26	SP26-01	F	6061 Al	0.517	0.785	0.826	0.519	0.787	0.831	0.544	0.804	0.863
EVA Label - Red	SP27	SP27-01	F	6061 Al	0.504	0.756	0.795	0.507	0.754	0.796	0.510	0.770	0.826
EVA Label Decal	SP28	SP28-01	F	1100 series Al	0.378	0.834	0.879	0.380	0.829	0.875	0.467	0.834	0.896
ATR Crystal-Zinc Selenide	SP29	SP29-01	F	ZnSe	na	na	na	0.701	0.741	0.772	0.710	0.744	0.797
ATR Crystal-Germanium	SP30	SP30-01	F	Ge	na	na	na	0.542	0.535	0.555	0.561	0.542	0.590

Description	Sample Number	Serial Number	Flight/ Back-up	Substrate	Pre-Vacuum Bakeout Data			Pre-Flight Data			Post-Flight Data		
					LPSR Solar Absorptance bbo	Hemis-pherical Total Emittance TEMP 2000, bbo	Near Normal Emittance TEMP 2000, bbo	LPSR Solar Absorptance	Hemis-pherical Total Emittance TEMP 2000	Near Normal Emittance TEMP 2000	LPSR Solar Absorptance	Hemispherical Total Emittance, TEMP 2000	Near Normal Emittance, TEMP 2000
Kapton (1 layer)	SP31	SP31-01s	F	Kapton	0.729	0.885	0.929	0.879	0.883	0.930	0.909	0.881	na
AZBEC-1	SP32	SP32-01	F	6061 Al	0.954	0.880	0.929	0.955	0.879	0.928	0.956	0.876	0.940
AZWEC-2l	SP33	SP33-01	F	6061 Al	0.170	0.912	0.962	0.171	0.911	0.962	0.168	0.901	0.966
AO Resist. Diam.-like Nanocomp. Coatings (DYLYNTM) DLN-undoped	SP01	SP1-02	B	Zerodur	na	na	na	0.874	0.845	0.888	0.879	0.841	0.900
AO Resist. Diam.-like Nanocomp. Coatings (DYLYNTM) DLN-30% Ti doped	SP02	SP2-02	B	Zerodur	na	na	na	0.758	0.713	0.752	0.769	0.721	0.777
TCOH-COTM - "6u" glass fabric	SP04	SP4-02	B	6061 Al	na	na	na	0.293	0.859	0.899	0.296	0.861	0.924
Beta Cloth	SP05	SP5-02	B	6061 Al	na	na	na	0.287	0.878	0.924	0.292	0.876	0.938
Black marking-Metalphoto	SP06	SP6-02	B	1100 series Al	na	na	na	0.841	0.833	0.878	0.840	0.836	0.895
Al 1st Surface Mirror Contam Monitor	SP10	SP10-02	B	Al2O3	na	na	na	0.078	0.016	0.029	0.078	0.012	0.045
Defected Al on Kapton	SP11	SP11-02	B	Kapton HN	na	na	na	0.115	0.023	0.036	0.114	0.023	na
ISS Solar Array Blanket Face Sheet	SP12	SP12-02	B	Kapton H	na	na	na	0.933	0.874	0.919	0.939	0.868	na
Ir/Si Multilayer	SP14	SP14-02	B	fused silica, Dynasil grade 4000P	na	na	na	0.410	0.170	0.178	0.415	0.183	0.219
OCLI coating over white Tedlar	SP16	SP16-02	B	6061 Al	na	na	na	0.329	0.797	0.840	0.329	0.801	0.854
Six layer stack on Si-wafer	SP17	SP17-02	B	6061 Al	na	na	na	0.464	0.723	0.763	0.475	0.724	0.774
YB-71P, Zn2TiO4-Potassium silicate thermal coating	SP19	SP19-02	B	6061 Al	na	na	na	0.116	0.895	0.946	0.120	0.893	0.948
Z-93SC55	SP20	SP20-02	B	6061 Al	na	na	na	0.133	0.893	0.940	0.132	0.894	0.951
S13GP/LO-1, Encapsulated ZnO in methyl silicone	SP21	SP21-02	B	6061 Al	na	na	na	0.180	0.904	0.951	0.180	0.903	0.958
Z24P binder w/ZnO pigment + 2% Sodium Salicylate by wt	SP23	SP23-02	B	6061 Al	na	na	na	0.215	0.914	0.961	0.209	0.911	0.970
Silver Teflon 5 mil 2-1/2" x 3/4"	SP24	SP24-03	B	6061 Al	na	na	na	0.073	0.704	0.741	0.067	0.711	0.767
White Paint Z24P Binder w/ZnO Pigment	SP25	SP25-02	B	6061 Al	na	na	na	0.236	0.899	0.949	0.235	0.897	0.958

Description	Sample Number	Serial Number	Flight/ Back-up	Substrate	Pre-Vacuum Bakeout Data			Pre-Flight Data			Post-Flight Data		
					LPSR Solar Absorptance bbo	Hemis-pherical Total Emittance TEMP 2000, bbo	Near Normal Emittance TEMP 2000, bbo	LPSR Solar Absorptance	Hemis-pherical Total Emittance TEMP 2000	Near Normal Emittance TEMP 2000	LPSR Solar Absorptance	Hemispher ical Total Emittance, TEMP 2000	Near Normal Emittance, TEMP 2000
EVA Label - Blue	SP26	SP26-02	B	6061 Al	na	na	na	0.518	0.786	0.826	0.520	0.791	0.848
EVA Label - Red	SP27	SP27-02	B	6061 Al	na	na	na	0.509	0.756	0.794	0.506	0.764	0.820
EVA Label Decal	SP28	SP28-02	B	1100 series Al	na	na	na	0.663	0.815	0.858	0.504	0.816	0.873
ATR Crystal-Zinc Selenide	SP29	SP29-02	B	ZnSe	na	na	na	na	na	na		#DIV/0!	#DIV/0!
ATR Crystal-Germanium	SP30	SP30-02	B	Ge	na	na	na	na	na	na	0.543	0.538	0.584
Kapton (1 layer)	SP31	SP31-02s	B	Kapton	na	na	na	0.879	0.885	0.931	0.883	0.881	na
AZBEC-1	SP32	SP32-02	B	6061 Al	na	na	na	0.954	0.880	0.927	0.961	0.876	0.940
AZWEC-21	SP33	SP33-02	B	6061 Al	na	na	na	0.174	0.913	0.961	0.172	0.910	0.968
ATR Crystal-Germanium	SP30	SP30-02	B	Ge	na	na	na	na	na	na	0.543	0.538	0.584

APPENDIX J

VUV SAMPLE DATA

Table J-1. Listing of VUV Samples

Description	Carousel Position	Proposal Number	Log Page Number	Supplier Sample Number	Flight Container Number	Sample Number	Serial Number	Flight / Backup / Control(A) / XTRA / not flown(na)	Supplier	Contact	Phone
OWS Mirrors - Gold/Fused Silica	CV14	V1	88	na	AV016	SV01	SV1-01	F	NASA MSFC	Jim Zwiener	205-544-2528
OWS Mirrors - Gold/Fused Silica	na	V1	88	na	AV___	SV01	SV1-02	B	NASA MSFC	Jim Zwiener	205-544-2528
OWS Mirrors - Iridium/Fused Silica	CV16	V2	89	na	AV010	SV02	SV2-01	F	NASA MSFC	Jim Zwiener	205-544-2528
OWS Mirrors - Iridium/Fused Silica	na	V2	89	na	AV___	SV02	SV2-02	B	NASA MSFC	Jim Zwiener	205-544-2528
OWS Mirrors - MgF2/Al/Fused Silica	CV17	V3	90	na	AV015	SV03	SV3-01	F	NASA MSFC	Jim Zwiener	205-544-2528
OWS Mirrors - MgF2/Al/Fused Silica	na	V3	90	na	AV___	SV03	SV3-02	B	NASA MSFC	Jim Zwiener	205-544-2528
OWS Mirrors - Platinum/Fused Silica	CV18	V4	91	na	AV021	SV04	SV4-01	F	NASA MSFC	Jim Zwiener	205-544-2528
OWS Mirrors - Platinum/Fused Silica	na	V4	91	na	AV___	SV04	SV4-02	B	NASA MSFC	Jim Zwiener	205-544-2528
ULTEM / 20% BTO	CV34	V12	50	U/20-4	AV037	SV13	SV13-01	F	NASA Langley/College of William & Mary	Dick Kiefer	804-221-2553
ULTEM / 20% BTO	na	V12	50	U/20-2	AV045	SV13	SV13-02	B	NASA Langley/College of William & Mary	Dick Kiefer	804-221-2553
ULTEM / 20% BTO	na	V12	50	U/20-3	na	SV13	SV13-03	A	NASA Langley/College of William & Mary	Dick Kiefer	804-221-2553
ULTEM / 10% BTO	CV33	V12	51	U/10-2	AV019	SV14	SV14-01	F	NASA Langley/College of William & Mary	Dick Kiefer	804-221-2553
ULTEM / 10% BTO	na	V12	51	U/10-3	AV013	SV14	SV14-02	B	NASA Langley/College of William & Mary	Dick Kiefer	804-221-2553
ULTEM / 10% BTO	na	V12	51	U/10-4	na	SV14	SV14-03	A	NASA Langley/College of William & Mary	Dick Kiefer	804-221-2553
ULTEM, pure	CV32	V13	52	U/0-4	AV051	SV15	SV15-01	F	NASA Langley/College of William & Mary	Dick Kiefer	804-221-2553
ULTEM, pure	na	V13	52	U/0-3	AV003	SV15	SV15-02	B	NASA Langley/College of William & Mary	Dick Kiefer	804-221-2553
ULTEM, pure	na	V13	52	U/0-1	na	SV15	SV15-03	A	NASA Langley/College of William & Mary	Dick Kiefer	804-221-2553
Ir/Si Multilayer	CV31	P34	96	ISRC9605B	AV046	SP14	SP14-01	F	NASA GSFC	Ritva Keski-Kuha	301-286-6706

Description	Carousel Position	Proposal Number	Log Page Number	Supplier Sample Number	Flight Container Number	Sample Number	Serial Number	Flight / Backup / Control(A) / XTRA / not flown(na)	Supplier	Contact	Phone
Ir/Si Multilayer	na	P34	96	ISRC9605D	AT___	SP14	SP14-02	B	NASA GSFC	Ritva Keski-Kuha	301-286-6706
Ir/Si Multilayer	na	P34	96	ISRC9605A	AT___	SP14	SP14-03	A	NASA GSFC	Ritva Keski-Kuha	301-286-6706
SiC	CV21	V10	87	SC29065F	AV036	SV05	SV5-03	F	NASA GSFC	Ritva Keski-Kuha	301-286-6706
SiC	na	V10	87	SC29065D	AV___	SV05	SV5-01	B	NASA GSFC	Ritva Keski-Kuha	301-286-6706
SiC	na	V10	87	SC29065E	AV___	SV05	SV5-02	A	NASA GSFC	Ritva Keski-Kuha	301-286-6706
Al + MgF2	CV23	V5	71	AMC9610G	AV005	SV06	SV6-01	F	NASA GSFC	Ritva Keski-Kuha	301-286-6706
Al + MgF2	na	V5	71	AMC9610I	AV___	SV06	SV6-02	B	NASA GSFC	Ritva Keski-Kuha	301-286-6706
Al + MgF2	na	V5	71	AMC9610J	AV___	SV06	SV6-03	A	NASA GSFC	Ritva Keski-Kuha	301-286-6706
Boron Carbide	CV22	V6	86	BC29602E	AV041	SV07	SV7-03	F	NASA GSFC	Ritva Keski-Kuha	301-286-6706
Boron Carbide	na	V6	86	BC29602C	AV___	SV07	SV7-01	B	NASA GSFC	Ritva Keski-Kuha	301-286-6706
Boron Carbide	na	V6	86	BC29602D	AV___	SV07	SV7-02	A	NASA GSFC	Ritva Keski-Kuha	301-286-6706
Boron Carbide	CV24	V6	86	BC29602F	AV012	SV08	SV8-01	F	NASA GSFC	Ritva Keski-Kuha	301-286-6706
Boron Carbide	na	V6	86	BC29602G	AV___	SV08	SV8-02	B	NASA GSFC	Ritva Keski-Kuha	301-286-6706
CVD Diamond	CV26	V7	69	S3	AV032	SV09	SV9-03	F	NASA GSFC	Ritva Keski-Kuha	301-286-6706
CVD Diamond	na	V7	69	S2	AV___	SV09	SV9-02	B	NASA GSFC	Ritva Keski-Kuha	301-286-6706
CVD Diamond	na	V7	69	S1	AV___	SV09	SV9-01	A	NASA GSFC	Ritva Keski-Kuha	301-286-6706
CVD-SiC	CV27	V8	70	#3	AV040	SV10	SV10-04	F	NASA GSFC	Ritva Keski-Kuha	301-286-6706

Description	Carousel Position	Proposal Number	Log Page Number	Supplier Sample Number	Flight Container Number	Sample Number	Serial Number	Flight / Backup / Control(A) / XTRA / not flown(na)	Supplier	Contact	Phone
CVD-SiC	na	V8	70	#1	AV___	SV10	SV10-02	B	NASA GSFC	Ritva Keski-Kuha	301-286-6706
CVD-SiC	na	V8	70	#4	AV___	SV10	SV10-03	A	NASA GSFC	Ritva Keski-Kuha	301-286-6706
CVD-SiC	na	V8	70	#6	AV___	SV10	SV10-01	XTRA	NASA GSFC	Ritva Keski-Kuha	301-286-6706
Iridium	CV19	V9	72	IRRC9602C	AV023	SV11	SV11-01	F	NASA GSFC	Ritva Keski-Kuha	301-286-6706
Iridium	na	V9	72	IRRC9602B	AV___	SV11	SV11-02	B	NASA GSFC	Ritva Keski-Kuha	301-286-6706
Iridium	na	V9	72	IRRC9602D	AV___	SV11	SV11-03	A	NASA GSFC	Ritva Keski-Kuha	301-286-6706
Iridium	CV28	V9	72	IRRC9602E	AV027	SV12	SV12-01	F	NASA GSFC	Ritva Keski-Kuha	301-286-6706
Iridium	na	V9	72	IRRC9602F	AV___	SV12	SV12-02	B	NASA GSFC	Ritva Keski-Kuha	301-286-6706
Window Material with MgF2 AR Coating	CV01	V16	47	na	AV001	SV17	SV17-01	F	Boeing (AL)	Gary Pippin	na
Window Material with MgF2 AR Coating	na	V16	47	na	AV___	SV17	SV17-02	B	Boeing (AL)	Gary Pippin	na
Window Material with MgF2 AR Coating	na	V16	47	na	AV___	SV17	SV17-03	A	Boeing (AL)	Gary Pippin	na
Window Material with MgF2 AR Coating	CV29	V16	47	na	AV026	SV18	SV18-01	F	Boeing (AL)	Gary Pippin	na
Window Material with MgF2 AR Coating	na	V16	47	na	AV___	SV18	SV18-02	B	Boeing (AL)	Gary Pippin	na
Window Material with MgF2 AR Coating	na	V16	47	na	AV___	SV18	SV18-03	A	Boeing (AL)	Gary Pippin	na
Alodine Baffle	CV38	V17	37	na	AV050	SV19	SV19-01	F	AZ Technology, Inc.	Rick	na
Alodine Baffle	na	V17	37	na	AV___	SV19	SV19-02	B	AZ Technology, Inc.	Rick	na
Alodine Baffle	na	V17	37	na	AV___	SV19	SV19-03	A	AZ Technology, Inc.	Rick	na
Alodine Baffle	na	V17	37	na	AV___	SV19	SV19-04	XTRA	AZ Technology, Inc.	Rick	na
Black Anodize Baffle	CV39	V18	80	na	AV034	SV20	SV20-01	F	AZ Technology, Inc.	John	na

Description	Carousel Position	Proposal Number	Log Page Number	Supplier Sample Number	Flight Container Number	Sample Number	Serial Number	Flight / Backup / Control(A) / XTRA / not flown(na)	Supplier	Contact	Phone
Black Anodize Baffle	na	V18	80	na	na	SV20	SV20-02	B	AZ Technology, Inc.	na	na
Black Anodize Baffle	na	V18	80	na	na	SV20	SV20-03	A	AZ Technology, Inc.	na	na
Crystalline Quartz Window	CV03	V19	25	13531-3/cryst.	AV047	SV21	SV21-02	F	AZ Technology, Inc.	John	na
Crystalline Quartz Window	na	V19	25	13531-3/cryst.	AV___	SV21	SV21-03	B	AZ Technology, Inc.	John	na
Crystalline Quartz Window	na	V19	25	13531-3/cryst.	AV___	SV21	SV21-01	A	AZ Technology, Inc.	John	na
Fused Silica Window	CV02	V20	22	KC4B	AV006	SV22	SV22-01	F	AZ Technology, Inc.	John	na
Fused Silica Window	na	V20	22	KC4B	AV___	SV22	SV22-02	B	AZ Technology, Inc.	John	na
Fused Silica Window	na	V20	22	KC4B	AV___	SV22	SV22-03	A	AZ Technology, Inc.	John	na
Lithium Fluoride (LiF) Window	CV04	V24	85	na	AV022	SV23	SV23-02	F	AZ Technology, Inc.	John	na
Lithium Fluoride (LiF) Window	na	V24	85	na	AV___	SV23	SV23-01	B	AZ Technology, Inc.	John	na
Lithium Fluoride (LiF) Window	na	V24	85	na	AV___	SV23	SV23-03	A	AZ Technology, Inc.	John	na
Magnesium Fluoride Window (MgF2)	CV06	V25	73	na	AV038	SV24	SV24-01	F	AZ Technology, Inc.	John	na
Magnesium Fluoride Window (MgF2)	na	V25	73	na	AV___	SV24	SV24-02	B	AZ Technology, Inc.	John	na
Magnesium Fluoride Window (MgF2)	na	V25	73	na	AV___	SV24	SV24-03	A	AZ Technology, Inc.	John	na
Magnesium Fluoride Window (MgF2)	na	V25	73	na	na	SV24	SV24-04	XTRA	AZ Technology, Inc.	na	na
MgF2 Overcoated Aluminum Mirror	CV13	V26	18	na	AV025	SV25	SV25-01	F	AZ Technology, Inc.	John	na
MgF2 Overcoated Aluminum Mirror	na	V26	18	na	AV___	SV25	SV25-02	B	AZ Technology, Inc.	John	na
MgF2 Overcoated Aluminum Mirror	na	V26	18	na	AV___	SV25	SV25-03	A	AZ Technology, Inc.	John	na
MLS85 Baffle Coating	CV37	V28	93	na	AV028	SV26	SV26-01	F	AZ Technology, Inc.	Rick	na
MLS85 Baffle Coating	na	V28	93	na	AV___	SV26	SV26-02	B	AZ Technology, Inc.	Rick	na
MLS85 Baffle Coating	na	V28	93	na	AV___	SV26	SV26-03	A	AZ Technology, Inc.	Rick	na
MLS85 Baffle Coating	na	V28	93	na	AV___	SV26	SV26-04	XTRA	AZ Technology, Inc.	Rick	na
MLS85 Baffle Coating	na	V28	93	na	AV___	SV26	SV26-05	XTRA	AZ Technology, Inc.	Rick	na

Description	Carousel Position	Proposal Number	Log Page Number	Supplier Sample Number	Flight Container Number	Sample Number	Serial Number	Flight / Backup / Control(A) / XTRA / not flown(na)	Supplier	Contact	Phone
Platinum Mirror	CV12	V29	91	na	AV018	SV27	SV27-02	F	AZ Technology, Inc.	John	na
Platinum Mirror (ST19-01)	na	V29	na	na	AV___	SV27	SV27-01	B	AZ Technology, Inc.	John	na
RM550IB Baffle Coating	CV36	V30	94	na	AV031	SV28	SV28-01	F	AZ Technology, Inc.	Rick	na
RM550IB Baffle Coating	na	V30	94	na	AV___	SV28	SV28-02	B	AZ Technology, Inc.	Rick	na
RM550IB Baffle Coating	na	V30	94	na	AV___	SV28	SV28-03	A	AZ Technology, Inc.	Rick	na
RM550IB Baffle Coating	na	V30	94	na	AV___	SV28	SV28-04	XTRA	AZ Technology, Inc.	Rick	na
RM550IB Baffle Coating	na	V30	94	na	AV___	SV28	SV28-05	XTRA	AZ Technology, Inc.	Rick	na
Sapphire Window	CV07	V31	24	na	AV007	SV29	SV29-01	F	AZ Technology, Inc.	John	na
Sapphire Window	na	V31	24	na	AV___	SV29	SV29-02	B	AZ Technology, Inc.	John	na
Sapphire Window	na	V31	24	na	na	SV29	SV29-03	A	AZ Technology, Inc.	John	na
VUV Neutral Density Filter, up	CV08	V32A	41	#2	AV033	SV30	SV30-01	F	AZ Technology, Inc.	John	na
VUV Neutral Density Filter, down	na	V32B	41	na	na	SV30	SV30-02	A	AZ Technology, Inc.	na	na
VUV Neutral Density Filter, down	CV09	V32A	41	#3	AV024	SV31	SV31-02	F	AZ Technology, Inc.	John	na
VUV Neutral Density Filter, down	na	V32B	41	#1	AV020	SV31	SV31-01	B	AZ Technology, Inc.	John	na
Gold Mirror	CV11	V33	19	na	AV043	SV32	SV32-01	F	AZ Technology, Inc.	John	na
Gold Mirror	na	V33	19	na	AV___	SV32	SV32-02	B	AZ Technology, Inc.	John	na
Gold Mirror	na	V33	19	na	AV___	SV32	SV32-03	A	AZ Technology, Inc.	John	na

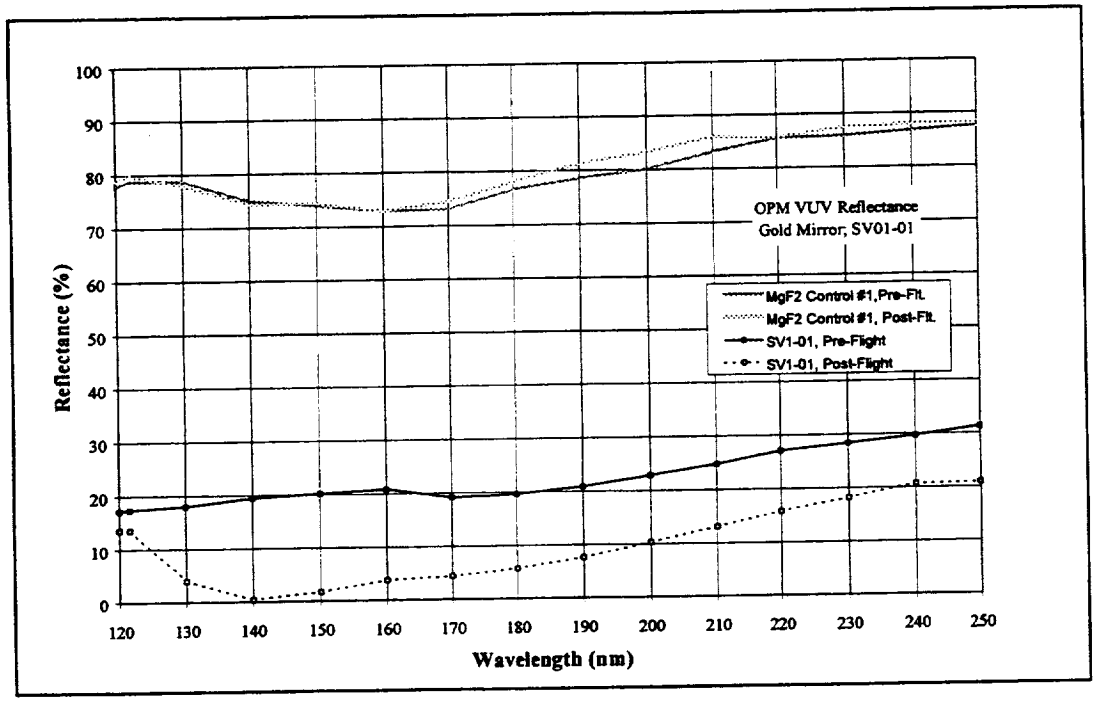

Figure J-1. Pre- & Post-Flight Reflectance of Gold Mirror SV01-01

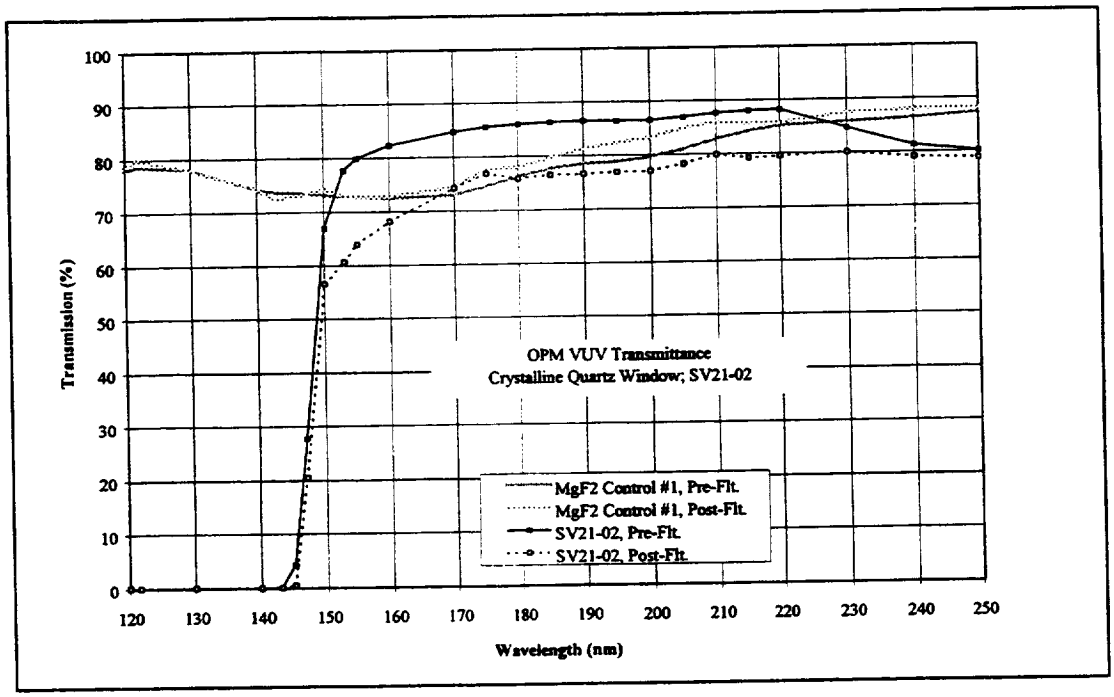

Figure J-2. Pre- & Post-Flight Transmission of Quartz Crystal Window SV21-02

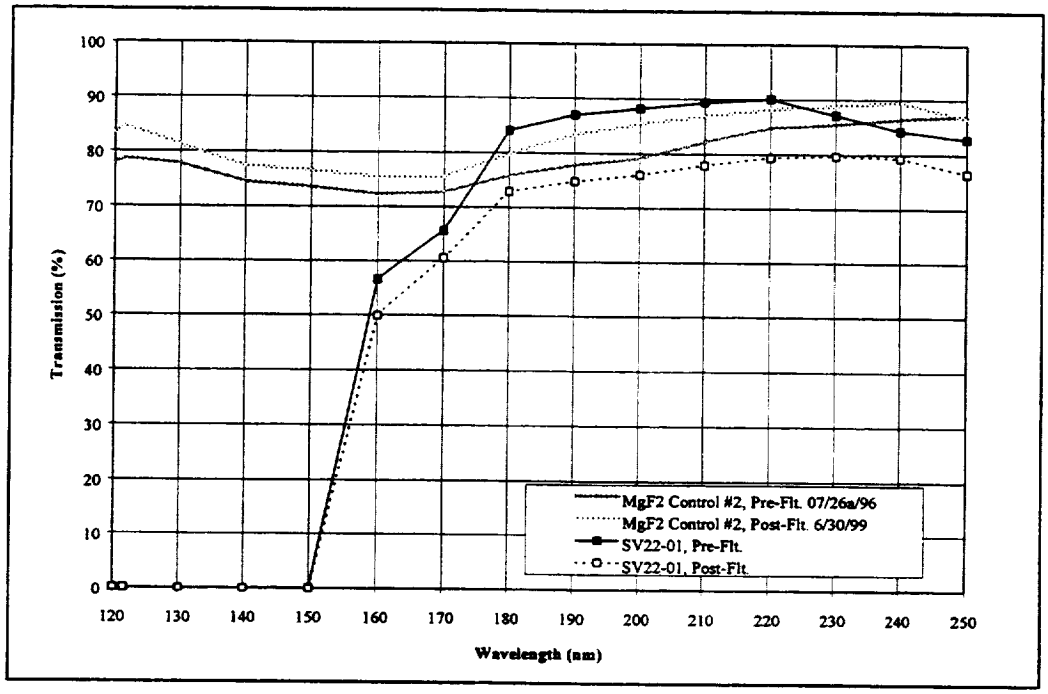

Figure J-3. Pre- & Post-Flight Transmission of Fused Silica Window SV22-01

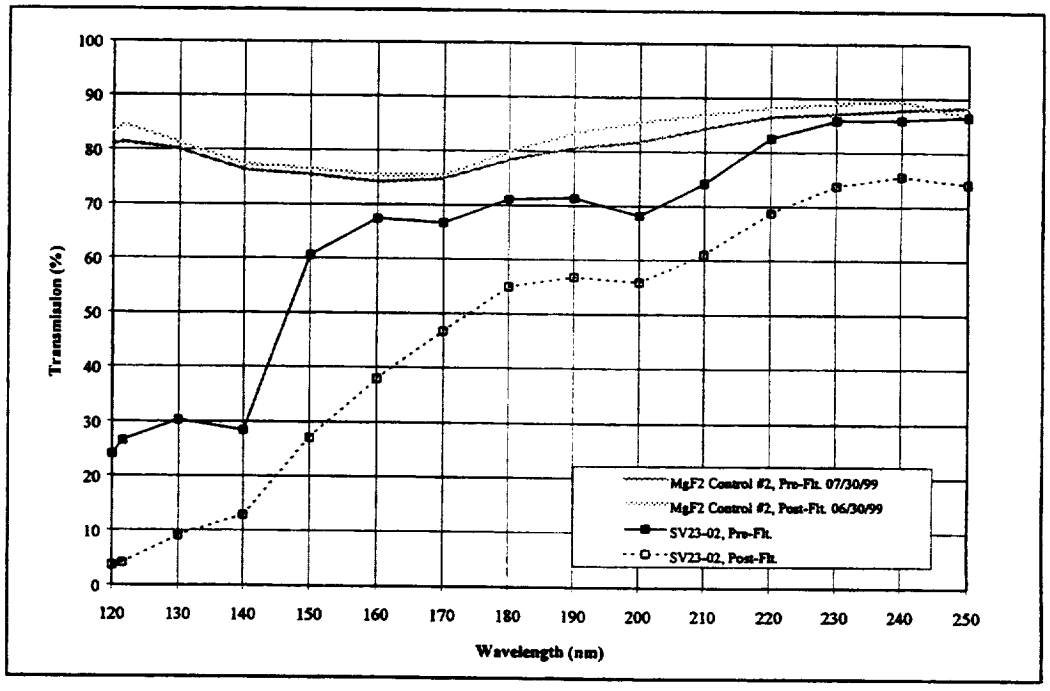

Figure J-4. Pre- & Post-Flight Transmission of Lithium Fluoride Window SV23-02

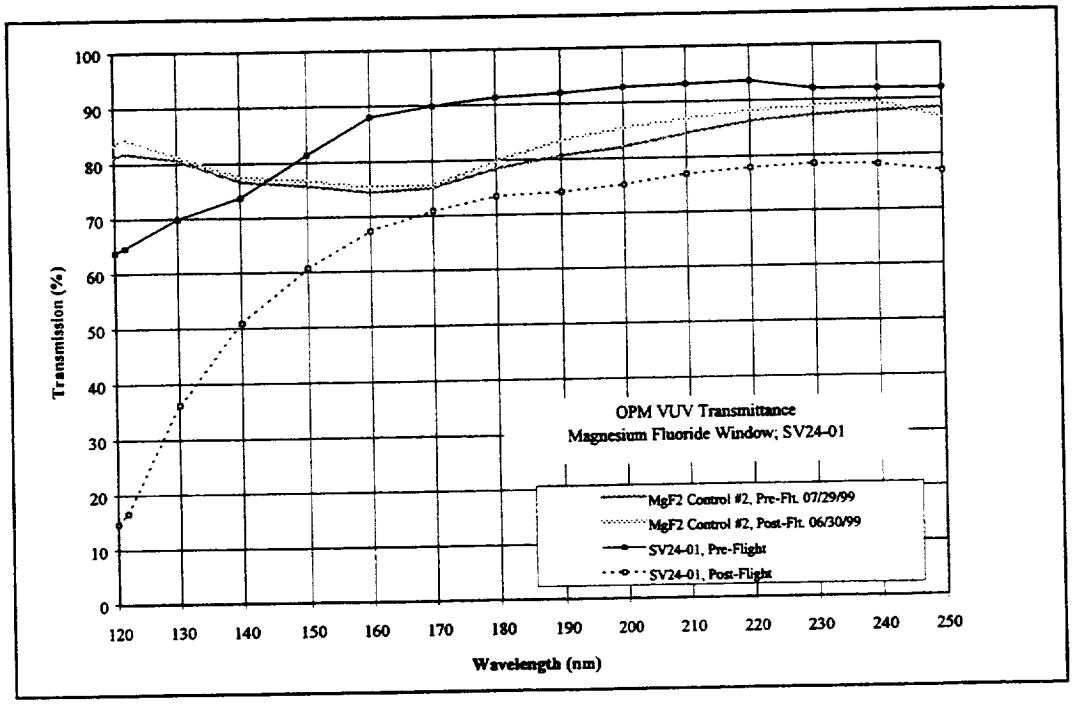

Figure J-5. Pre- & Post-Flight Transmission of Magnesium Fluoride Window SV24-01

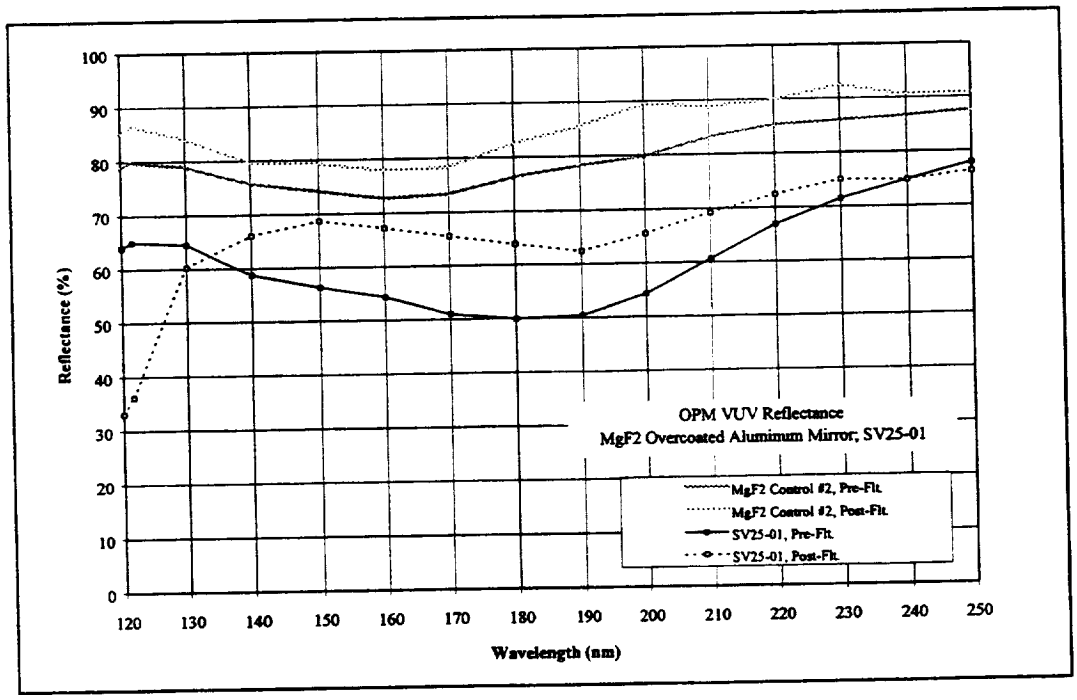

Figure J-6. Pre- & Post-Flight Reflectance of Magnesium Fluoride MgF2 Overcoated Aluminum Mirror SV25-01

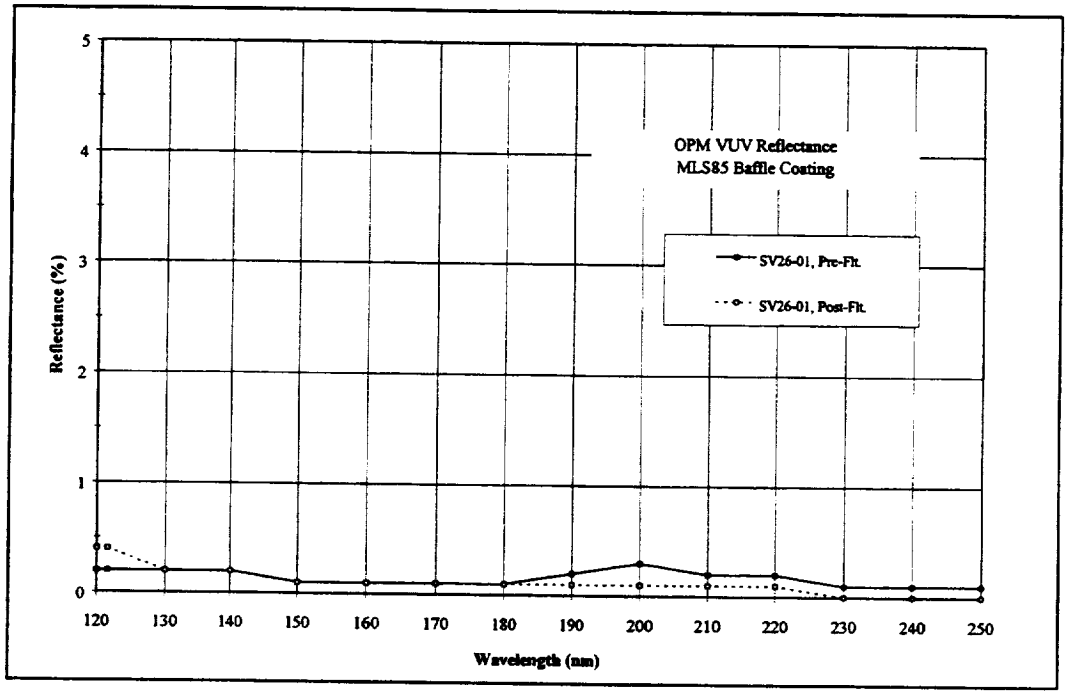

Figure J-7. Pre- & Post-Flight Reflectance of MLS85 Baffle Coating SV26-01

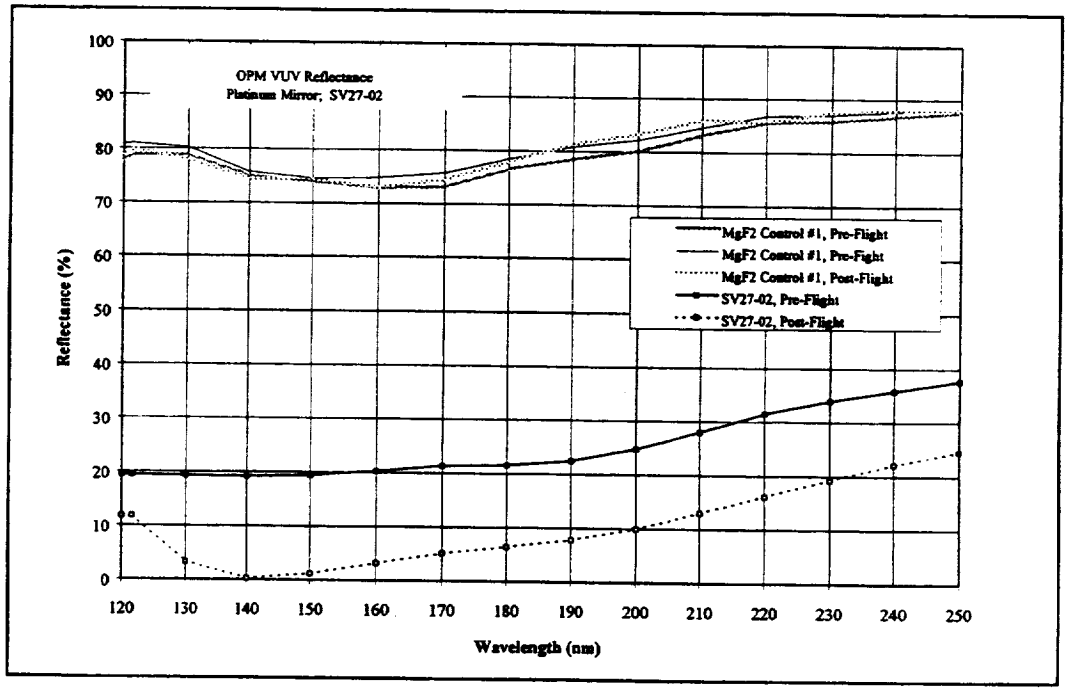

Figure J-8. Pre- & Post-Flight Reflectance of Platinum Mirror SV27-01

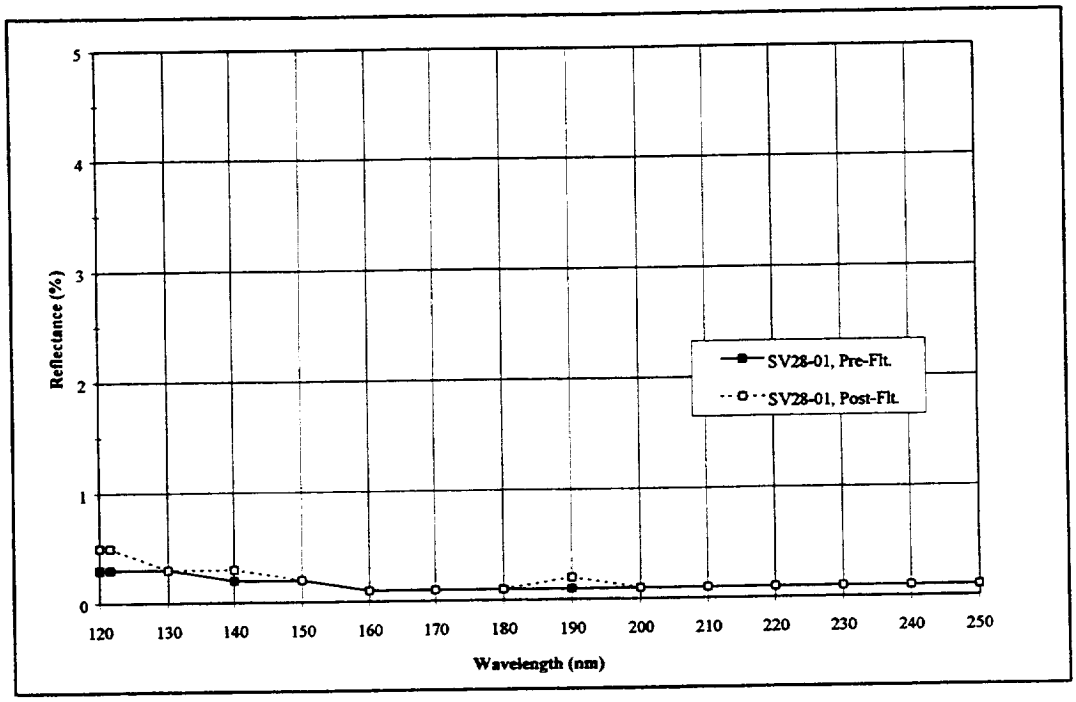

Figure J-9. Pre- & Post-Flight Reflectance of RM550B Baffle Coating SV28-01

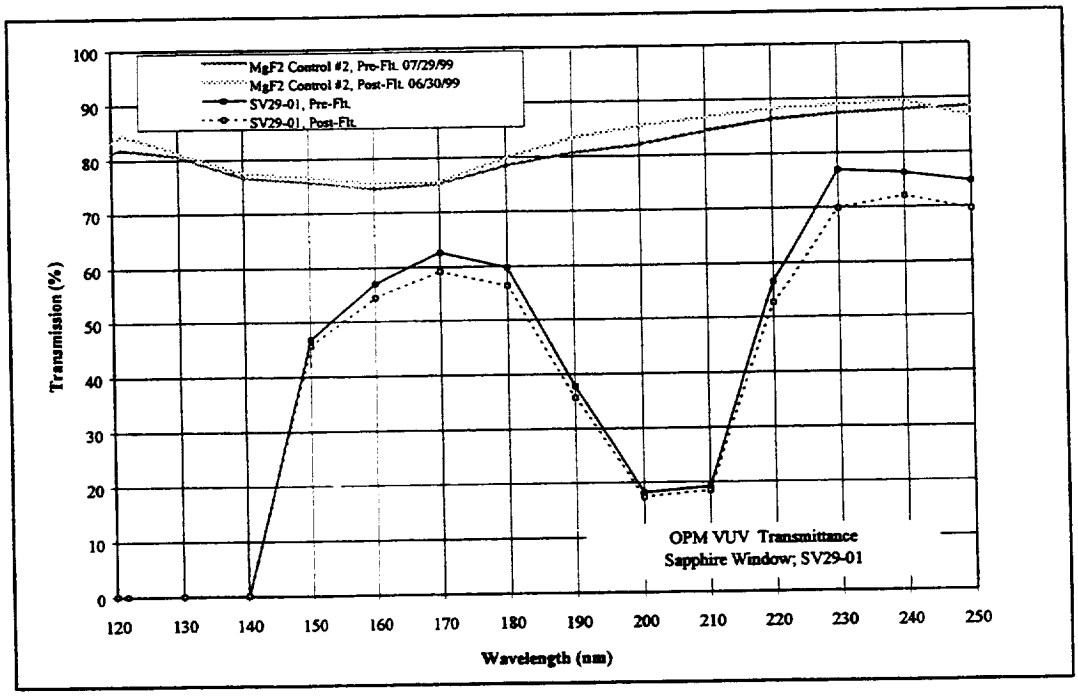

Figure J-10. Pre- & Post-Flight Transmission of Sapphire Window SV29-01

APPENDIX K

TIS SAMPLE DATA

Table K-1a. OPM TIS Sample Data

Description	Carousel Position	Supplier Sample Number	Serial Number	Category	Preflight, 532 nm	Week 1, 532 nm	Week 35, 532 nm	Post-Flight, 532 nm	Preflight, 1064 nm	Week 1, 1064 nm	Week 35, 1064 nm	Post-Flight, 1064 nm
dc Magnetron Sputtered Optical Coatings-Niobia/Silica	CT01	SS-025	ST1-01	Lowest	0.000661	0.000768	0.002194	0.002455	0.000815	0.000769	0.001391	0.002623
dc Magnetron Sputtered Optical Coatings-Zirconia/Silica	CT02	SS-021	ST2-01	Lowest	0.001444	0.001548	0.002396	0.002626	0.000652	0.000670	0.001083	0.001417
Diamond like carbon (DLC) on silicon	CT03	na	ST3-01	Low	0.002130	0.004421	0.002463	0.004321	0.001687	0.011692	0.001537	0.002584
Titanium Diboride	CT04	na	ST4-01	Lowest	0.001165	0.001775	0.002119	0.002469	0.001198	0.001172	0.001637	0.002841
Zirconium Diboride on silicon	CT05	na	ST5-01	Lowest	0.000942	0.001123	0.001935	0.001904	0.000699	0.000727	0.001374	0.001648
TixByNz film on silicon	CT06	na	ST6-01	Lowest	0.000886	0.001265	0.001617	0.002255	0.001059	0.000920	0.001324	0.002326
as-grown, undoped CVD Diamond	CT07	na	ST7-01	High	0.998164	0.997768	0.997887	0.998503	0.877207	0.869961	0.880383	0.870900
TixByOz film on silicon	CT08	na	ST8-01	Lowest 532 / Medium 1064	0.001882	0.001280	0.001987	0.003048	0.001709	0.006790	0.031255	0.090026
ZrxByNz film on silicon	CT09	na	ST9-01	Lowest	0.000829	0.001081	0.001778	0.002030	0.000875	0.000893	0.001485	0.002274
as-grown, boron-doped CVD Diamond	CT10	na	ST10-01	High	0.998371	0.997882	0.997795	0.998703	0.951499	0.951544	0.953960	0.951668
as-grown, phosphorus-doped CVD Diamond	CT11	na	ST11-01	High	0.994694	0.993815	0.994164	0.994764	0.857180	0.854909	0.862174	0.852681
Carbon nitride (CxNy) film on silicon	CT12	na	ST12-01	Low	0.009086	0.014519	0.003612	0.004320	0.001660	0.002205	0.002136	0.002289
Titanium nitride (TiN) film on silicon	CT13	na	ST13-01	Lowest	0.001820	0.002123	0.002549	0.002378	0.000946	0.000927	0.001060	0.001511
First surface aluminum-coated levelized aluminum mirror	CT17	T16-LA11	ST14-01	Low	0.008679	0.005619	0.007518	0.008942	0.005754	0.004817	0.005097	0.006550
ISS Solar Array Blanket Face Sheet	CT18	T17-SKSAL1	ST15-01	High	0.966294	0.996283	0.996364	0.998422	0.916701	0.999122	0.993817	0.999596
Gold Mirror	CT14	na	ST16-01	Lowest	0.001595	0.001663	0.002158	0.002219	0.001168	0.001235	0.001595	0.001838
Kapton H (flown as 4 layers of 5 mil)	CT19	na	ST17-01	High	0.917017	0.921228	0.987365	0.993218	0.918294	0.923330	0.942891	0.947124
MgF2 Overcoated Aluminum Mirror	CT15	na	ST18-01	Lowest	0.001314	0.001285	0.001750	0.001909	0.000824	0.000837	0.001135	0.001668
Platinum Mirror	CT16	na	ST19-02	Lowest	0.000939	0.001035	0.001484	0.001596	0.000745	0.000810	0.001153	0.002070
Silver/Teflon (5 mil)	CT20	Sheldahl 7-G401900	ST20-01	Medium	0.162412	0.178747	0.168390	0.155528	0.051435	0.052717	0.049860	0.044508

Table K-1b. OPM TIS Sample Data

Description	Carousel Position	Supplier Sample Number	Serial Number	Category	Coating thickness	Preflight, 532/1064 Ratio	Week 1, Ratio	Week 35, Ratio	Post-Flight, Ratio
dc Magnetron Sputtered Optical Coatings-Niobia/Silica	CT01	SS-025	ST1-01	Lowest	NA	0.810423	0.998714	1.577756	0.935613
dc Magnetron Sputtered Optical Coatings-Zirconia/Silica	CT02	SS-021	ST2-01	Lowest	430 Å	2.215368	2.309357	2.212620	1.853618
Diamond like carbon (DLC) on silicon	CT03	na	ST3-01	Low	~ 4500 Å	1.262496	0.378105	1.602552	1.672151
Titanium Diboride	CT04	na	ST4-01	Lowest	2000 Å	0.972751	1.514676	1.294564	0.868900
Zirconium Diboride on silicon	CT05	na	ST5-01	Lowest	4400 Å	1.347211	1.545254	1.407870	1.155546
TixByNz film on silicon	CT06	na	ST6-01	Lowest	~ 4500 Å	0.836217	1.375097	1.221436	0.969445
as-grown, undoped CVD Diamond	CT07	na	ST7-01	High	NA	1.137890	1.146911	1.133469	1.146519
TixByOz film on silicon	CT08	na	ST8-01	Lowest 532 / Medium 1064	~ 3.8 um	1.100915	0.188569	0.063585	0.033862
ZrxByNz film on silicon	CT09	na	ST9-01	Lowest	NA	0.947359	1.211554	1.197623	0.892893
as-grown, boron-doped CVD Diamond	CT10	na	ST10-01	High	5 mil FEP	1.049261	1.048698	1.045950	1.049424
as-grown, phosphorus-doped CVD Diamond	CT11	na	ST11-01	High	NA	1.160427	1.162481	1.153089	1.166631
Carbon nitride (CxNy) film on silicon	CT12	na	ST12-01	Low	NA	5.474608	6.584795	1.691098	1.887048
Titanium nitride (TiN) film on silicon	CT13	na	ST13-01	Lowest	~ 3.5 um	1.923430	2.289397	2.405926	1.573608
First surface aluminum-coated levelized aluminum mirror	CT17	T16-LA11	ST14-01	Low	1800 Å	1.508262	1.166494	1.475200	1.365336
ISS Solar Array Blanket Face Sheet	CT18	T17-SKSAL1	ST15-01	High	NA	1.054100	0.997159	1.002562	0.998825
Gold Mirror	CT14	na	ST16-01	Lowest	1500 Å	1.365363	1.347309	1.352921	1.207625
Kapton H (flown as 4 layers of 5 mil)	CT19	na	ST17-01	High	NA	0.998610	0.997724	1.047168	1.048668
MgF2 Overcoated Aluminum Mirror	CT15	na	ST18-01	Lowest	~ 2.3 um	1.595567	1.535664	1.541787	1.144519
Platinum Mirror	CT16	na	ST19-02	Lowest	1300 Å	1.260913	1.277638	1.287005	0.770770
Silver/Teflon (5 mil)	CT20	Sheldahl 7-G401900	ST20-01	Medium	NA	3.157624	3.390682	3.377282	3.494389

Table K-2. Total Hemispherical Emittance and Solar Absorptance Data for TIS Samples

Description	Sample Number	Serial Number	Flight / Backup	Preflight Hemispherical Total Emittance	Post-flight Hemispherical Total Emittance		Preflight LPSR Solar Absorptance	Post-flight LPSR Solar Absorptance	
Optical Coatings-Niobia/Silica	ST01	ST1-01	F	0.859	0.840		0.428	0.426	
Optical Coatings-Niobia/Silica	ST01	ST1-02	B	0.858	0.847		0.428	0.427	
Optical Coatings-Zirconia/Silica	ST02	ST2-01	F	0.858	0.837		0.464	0.461	
Optical Coatings-Zirconia/Silica	ST02	ST2-02	B	0.861	0.844		0.463	0.463	
Diamond like carbon (DLC) on silicon	ST03	ST3-01	F	0.751	0.616		0.848	0.598	
Titanium Diboride	ST04	ST4-01	F	0.306	0.295		0.610	0.635	
Zirconium Diboride on silicon	ST05	ST5-01	F	0.236	0.230		0.504	0.529	
TixByNz film on silicon	ST06	ST6-01	F	0.321	0.314		0.598	0.623	
as-grown, undoped CVD Diamond	ST07	ST7-01	F	0.707	0.689		0.829	0.837	
TixByOz film on silicon	ST08	ST8-01	F	0.626	0.617		0.748	0.747	
ZrxByNz film on silicon	ST09	ST9-01	F	0.251	0.251		0.504	0.529	
as-grown, boron-doped CVD Diamond	ST10	ST10-01	F	0.765	0.755		0.861	0.869	
as-grown, phosphorus-doped CVD Diamond	ST11	ST11-01	F	0.707	0.694		0.834	0.844	
Carbon nitride (CxNy) film on silicon	ST12	ST12-01	F	0.665	0.618		0.783	0.614	
Titanium nitride (TiN) film on silicon	ST13	ST13-01	F	0.217	0.219		0.619	0.660	
First surface aluminum-coated levelized aluminum mirror	ST14	ST14-01	F	0.019	0.024		0.111	0.108	
First surface aluminum-coated levelized aluminum mirror	ST14	ST14-02	B	0.020	0.021		0.112	0.111	

Description	Sample Number	Serial Number	Flight / Backup	Preflight Hemispherical Total Emittance	Post-flight Hemispherical Total Emittance	[illegible]	Preflight LPSR Solar Absorptance	Post-flight LPSR Solar Absorptance	[illegible]
ISS Solar Array Blanket Face Sheet	ST15	ST15-01	F	0.720	0.708		0.813	0.782	
ISS Solar Array Blanket Face Sheet	ST15	ST15-02	B	0.712	0.715		0.800	0.804	
Gold Mirror	ST16	ST16-01	F	0.008	0.019		0.174	0.177	
Gold Mirror	ST16	ST16-02	B	0.007	0.020		0.175	0.179	
Kapton H (flown as 4 layers of 5 mil, tested as 1 layer)	ST17	ST17-01	F	0.875	0.878		0.757	0.917	
Kapton H (see also SP31-02)	ST17	ST17-02	B	na	0.877		na	0.883	
MgF2 Overcoated Aluminum Mirror	ST18	ST18-01	F	0.016	0.014		0.092	0.095	
MgF2 Overcoated Aluminum Mirror	ST18	ST18-02	B	0.017	0.020		0.091	0.090	
Platinum Mirror	ST19	ST19-02	F	0.045	0.042		0.276	0.277	
Platinum Mirror	ST19	ST19-01	B	0.044	0.042		0.275	0.297	
Silver/Teflon (5 mil)	ST20	ST20-01	F	0.710	0.718		0.074	0.099	
Silver/Teflon (5 mil)	ST20	ST20-02	B	0.704	0.713		0.073	0.071	

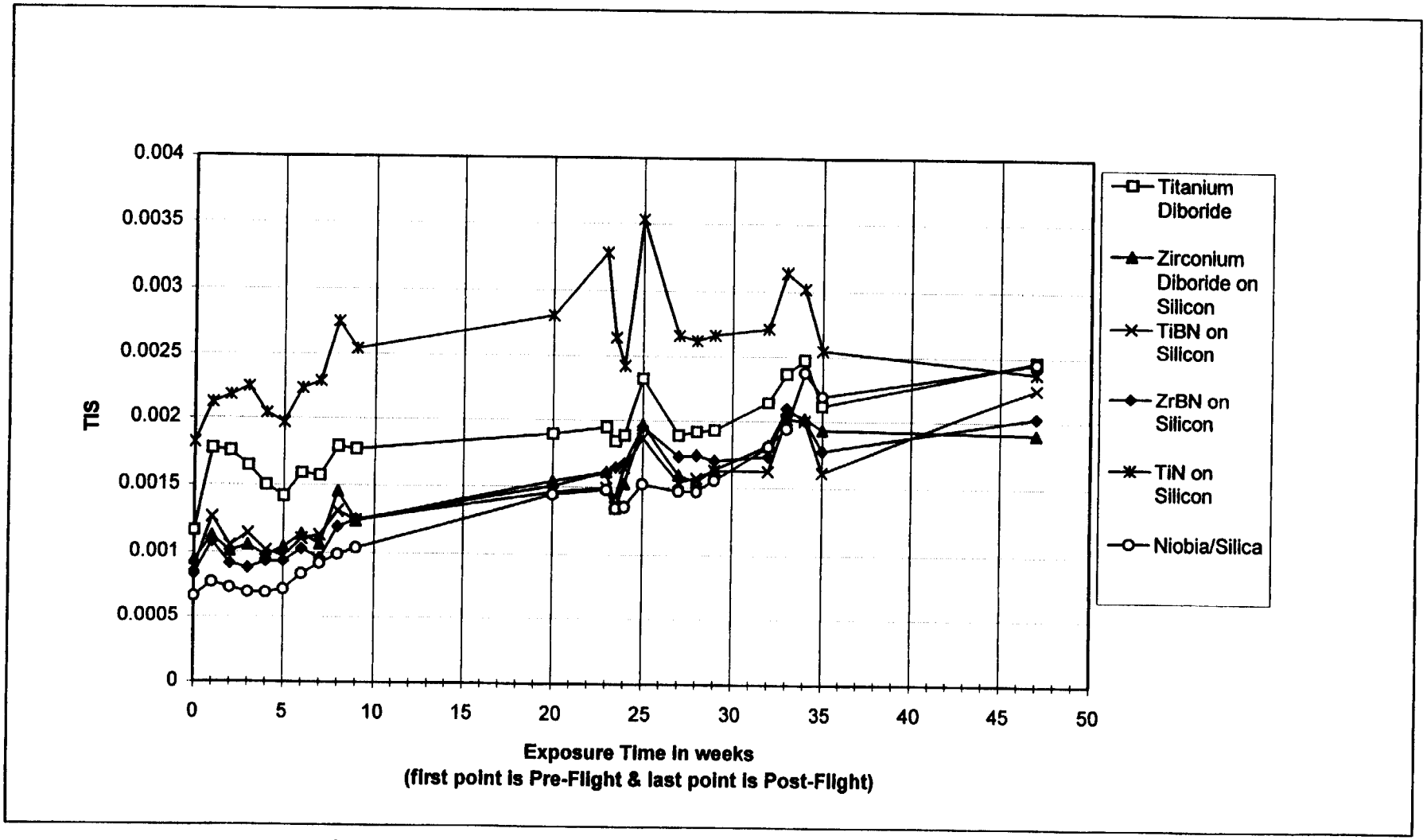

Figure K-1a. Observed Changes in TIS at532 nm (Lowest Scatter Samples)

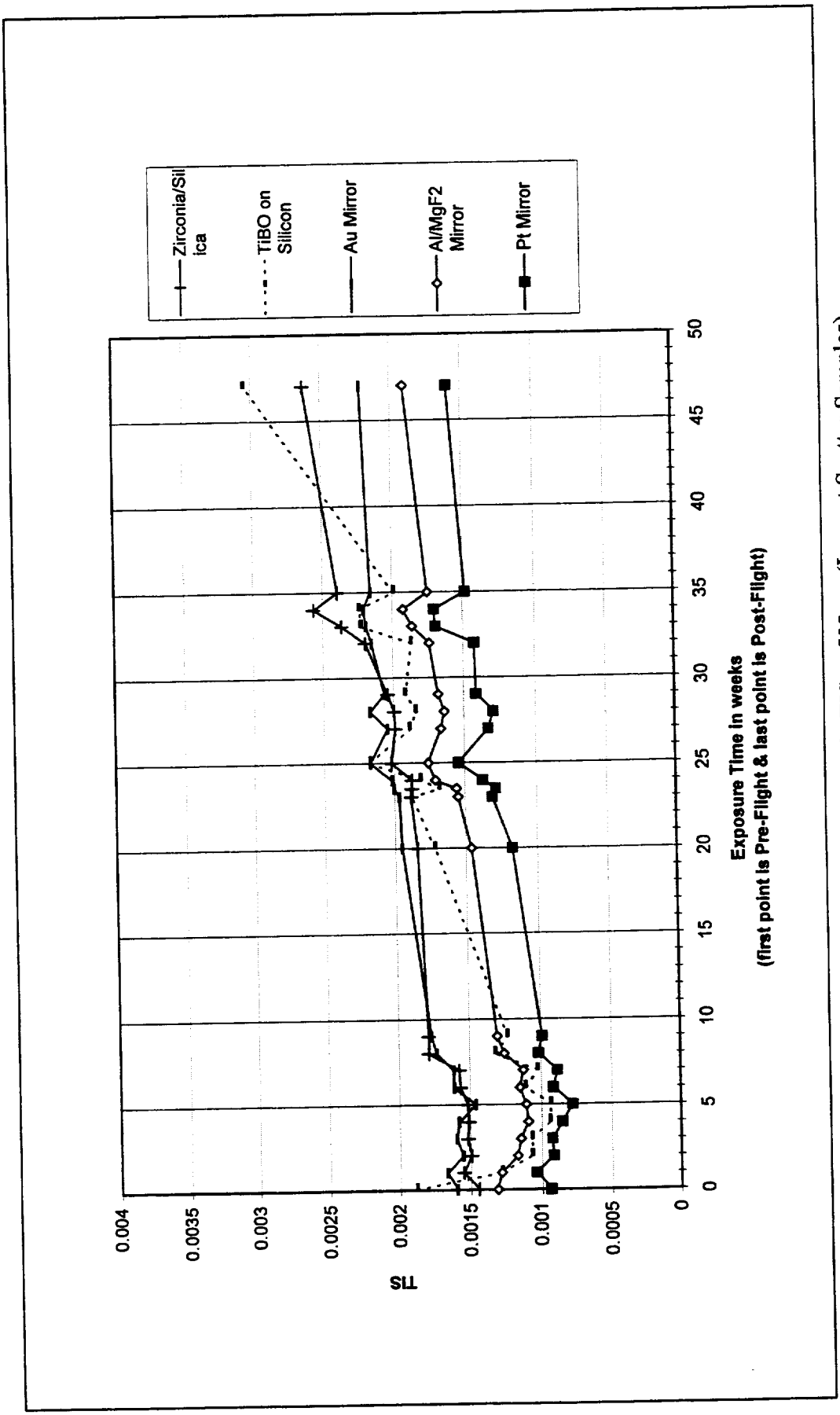

Figure K-1b. Observed Changes in TIS at 532nm (Lowest Scatter Samples)

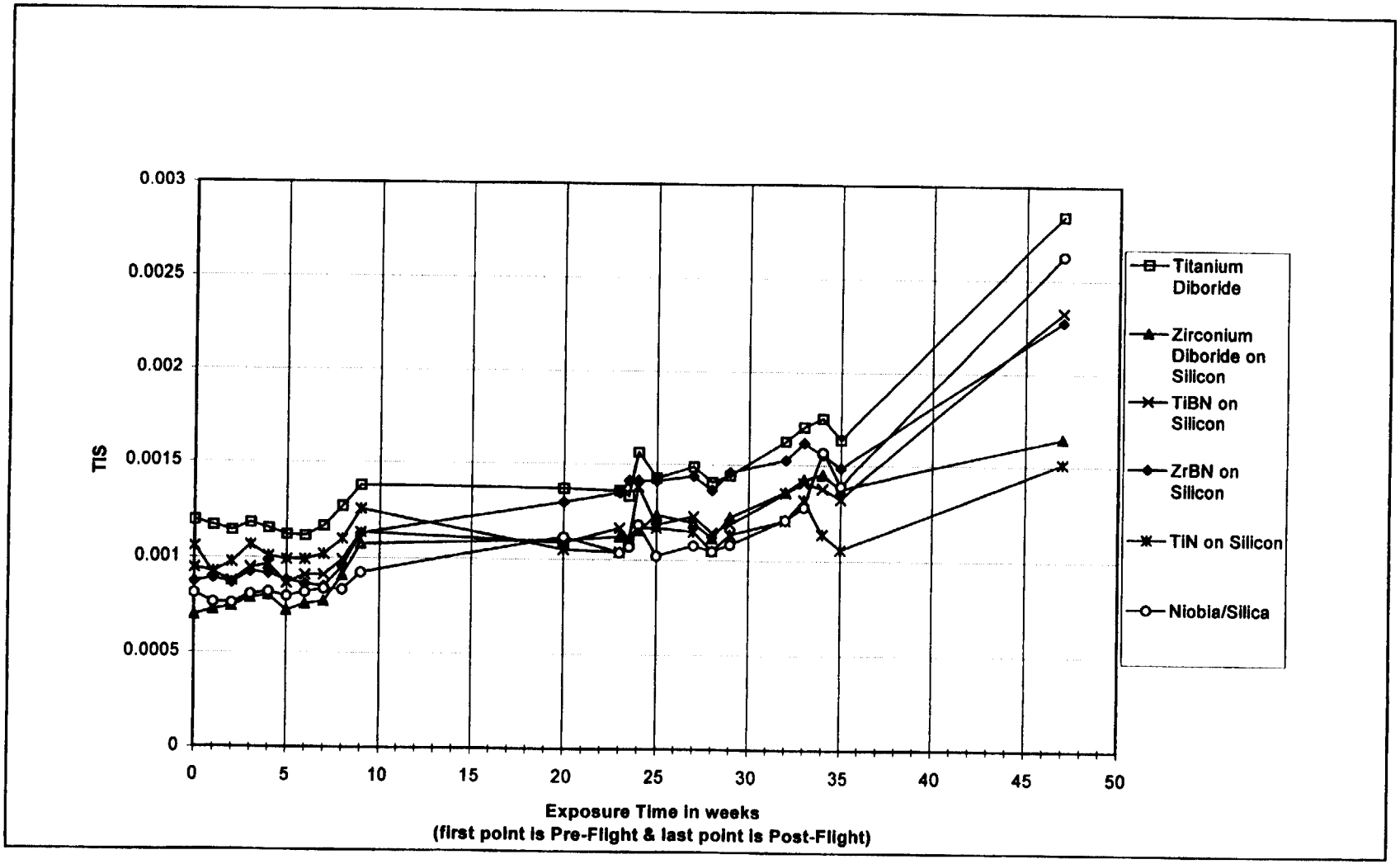

Figure K-2a. Observed Changes in TIS at 1064nm (Lowest Scatter Samples)

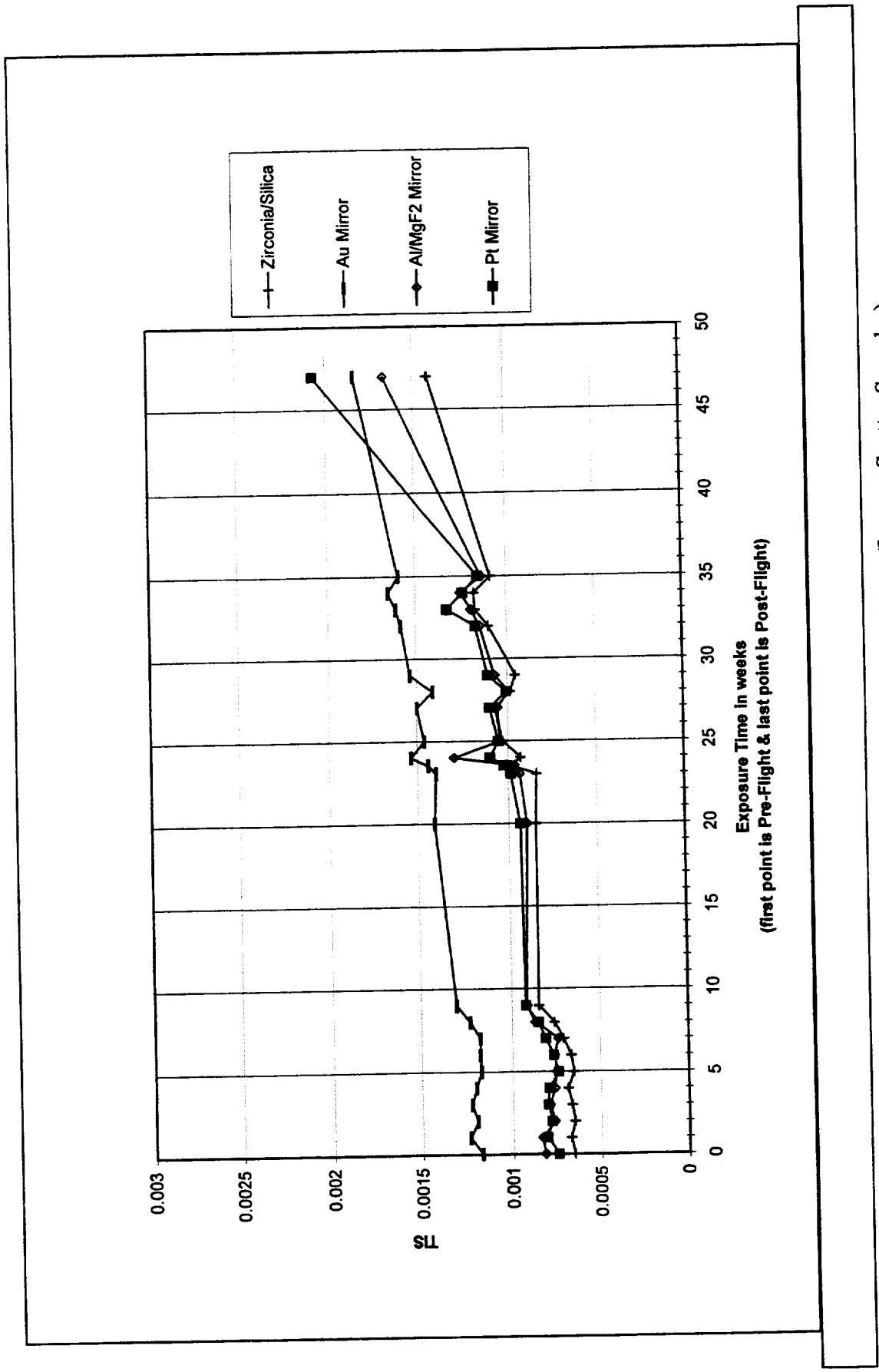

Figure K-2b. Observed Changes in TIS at 1064nm (Lowest Scatter Samples)

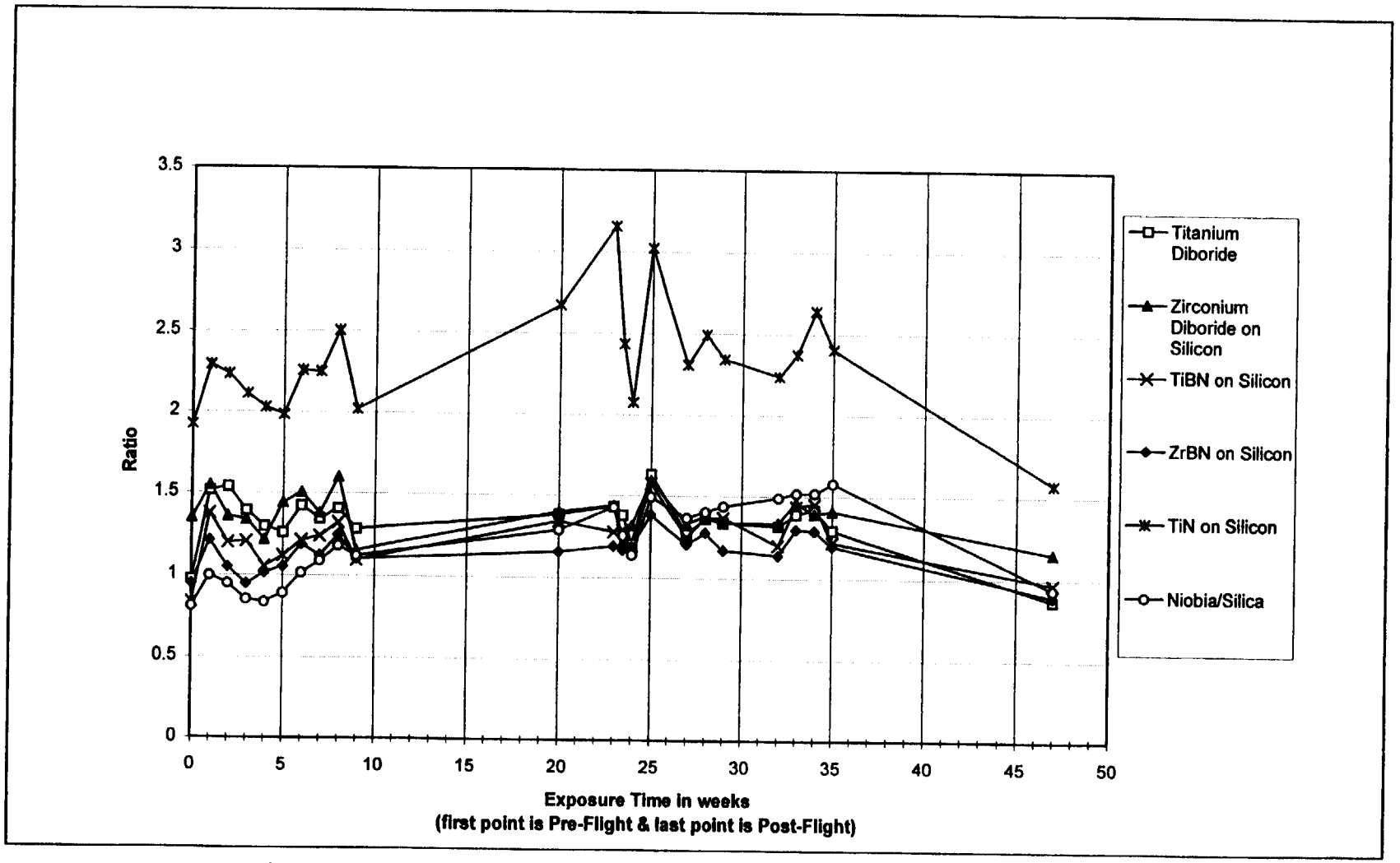

Figure K-3a. Observed Changes in 532/1064 TIS Ratios (Lowest Scatter Samples)

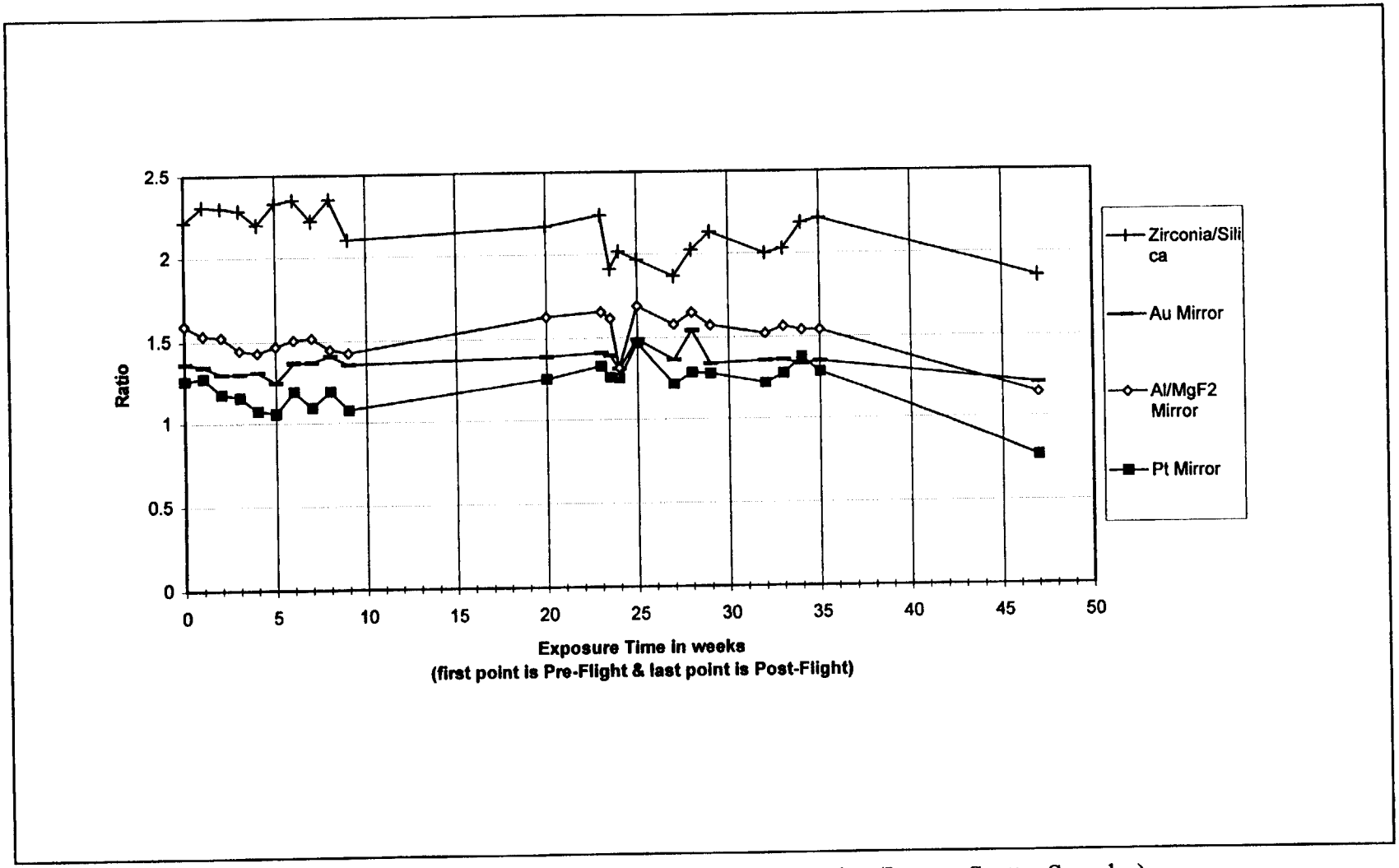

Figure K-3b. Observed Changes in 532/1064 TIS Ratios (Lowest Scatter Samples)

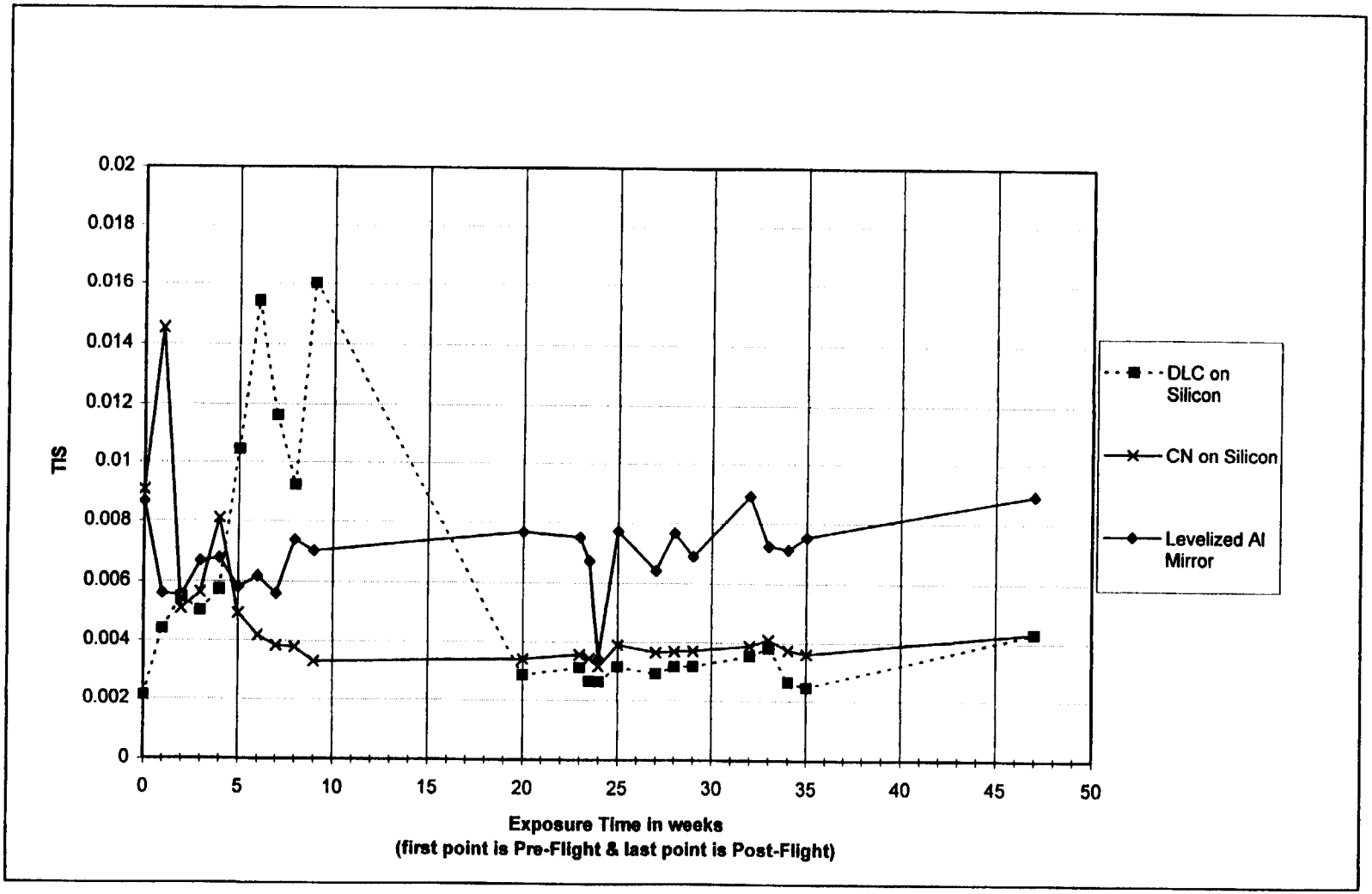

Figure K-4. Observed Changes in TIS at 532nm (Low Scatter Samples)

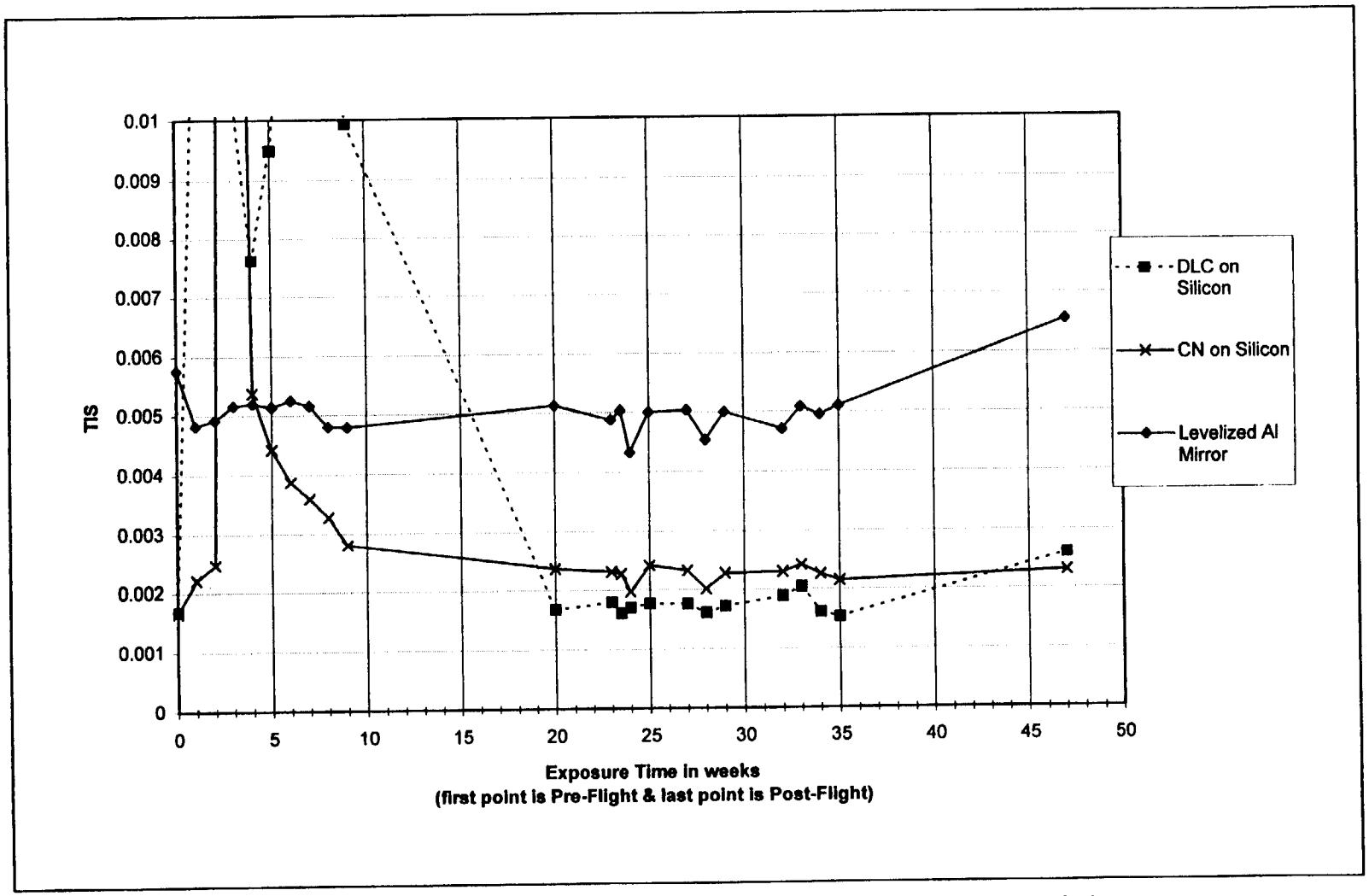

Figure K-5 Observed Changes in TIS at 1064nm (Low Scatter Samples)

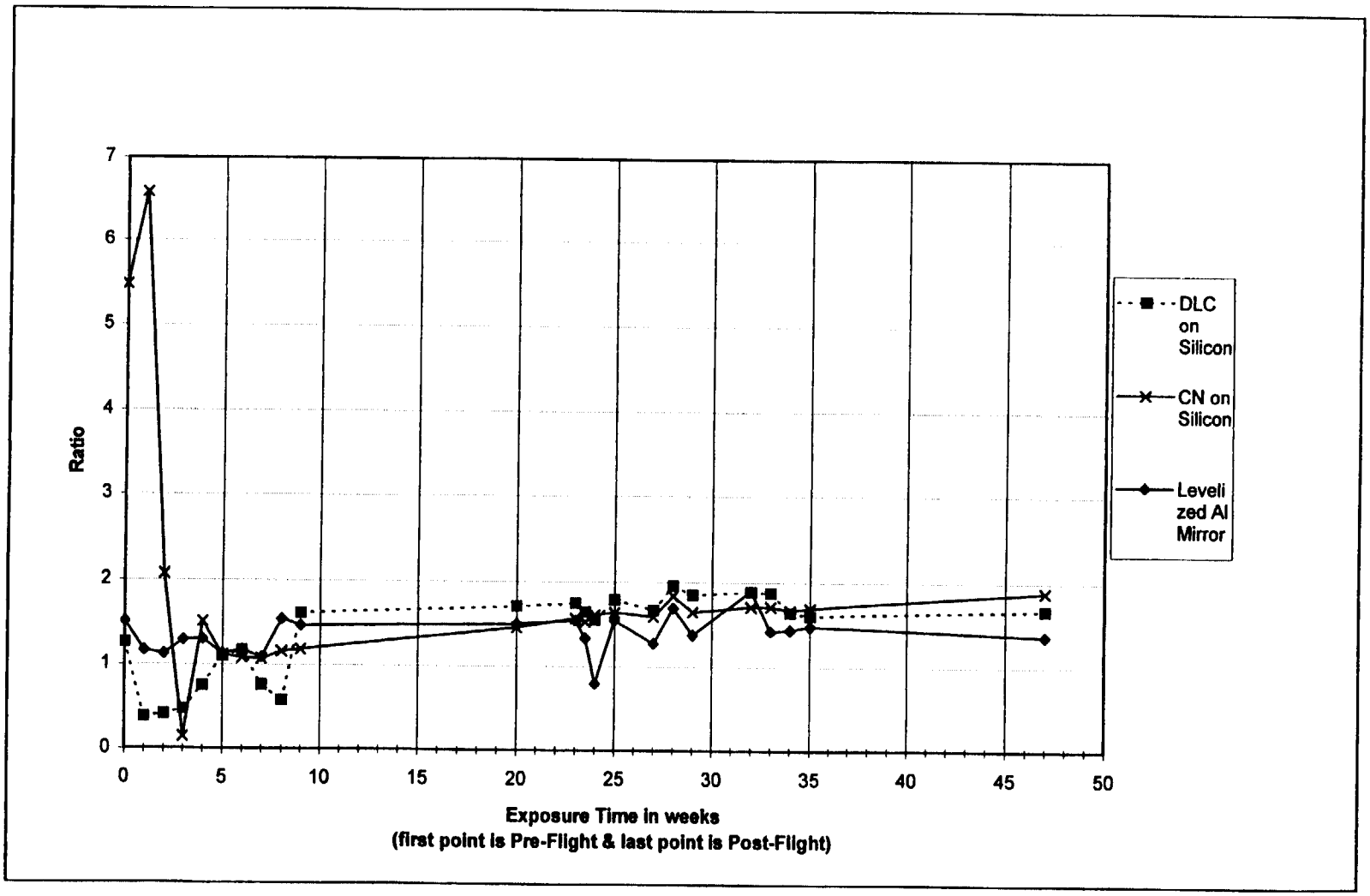

Figure K-6. Observed Changes in 532/1064 TIS Ratios (Low Scatter Samples)

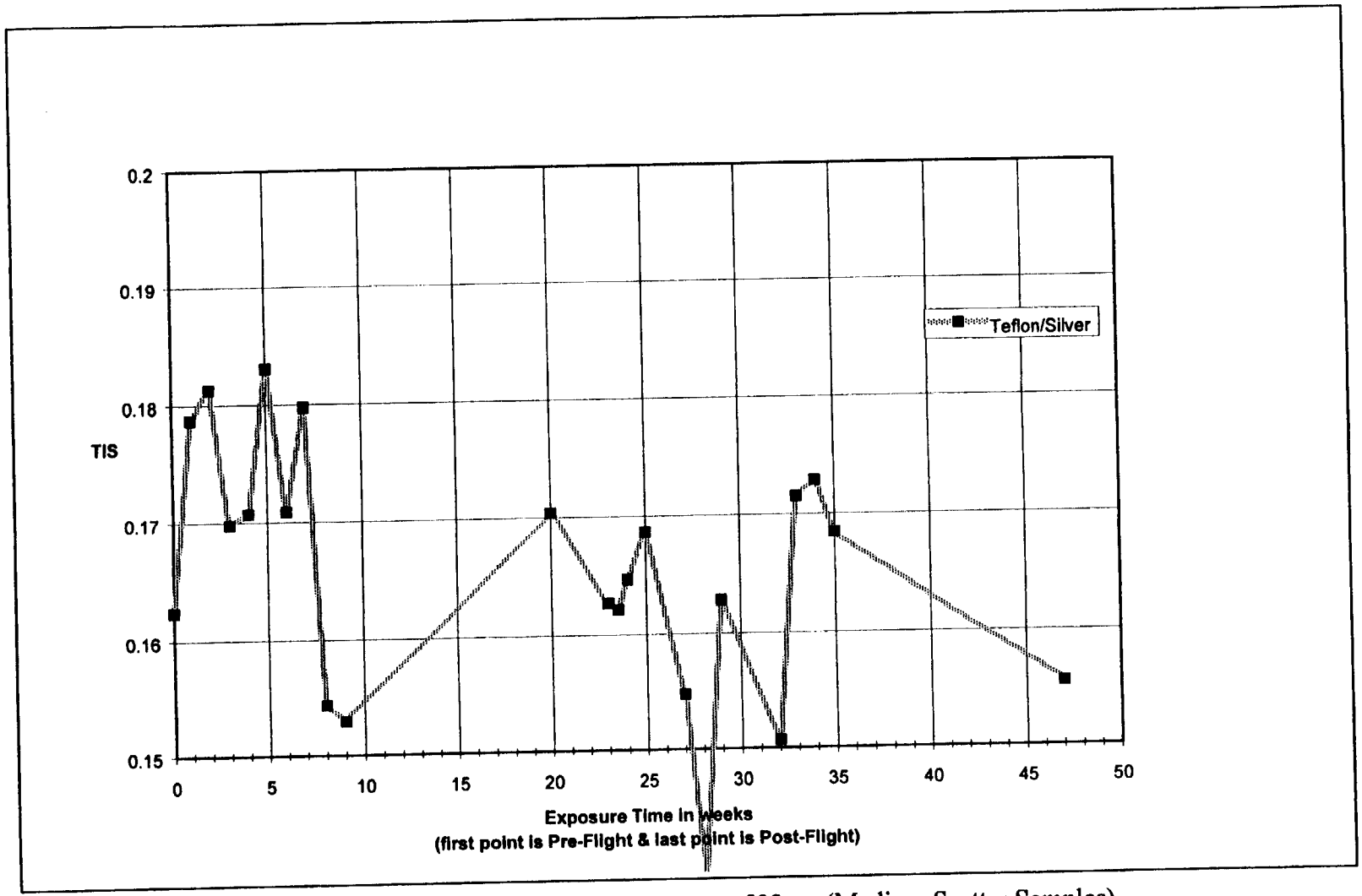

Figure K-7. Observed Changes in TIS at t532nm (Medium Scatter Samples)

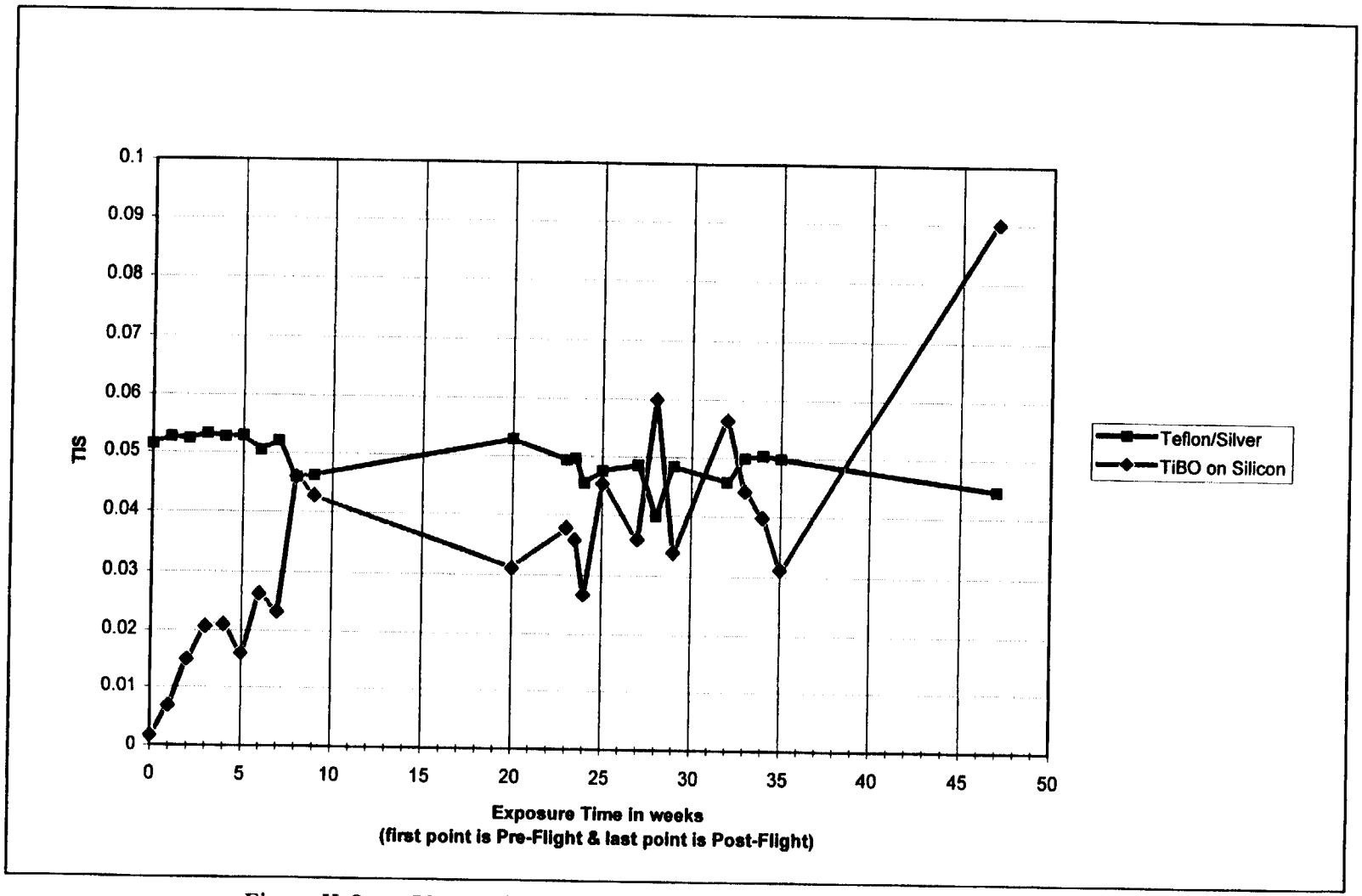

Figure K-8. Observed Changes in TIS at 1064nm (Medium Scatter Samples)

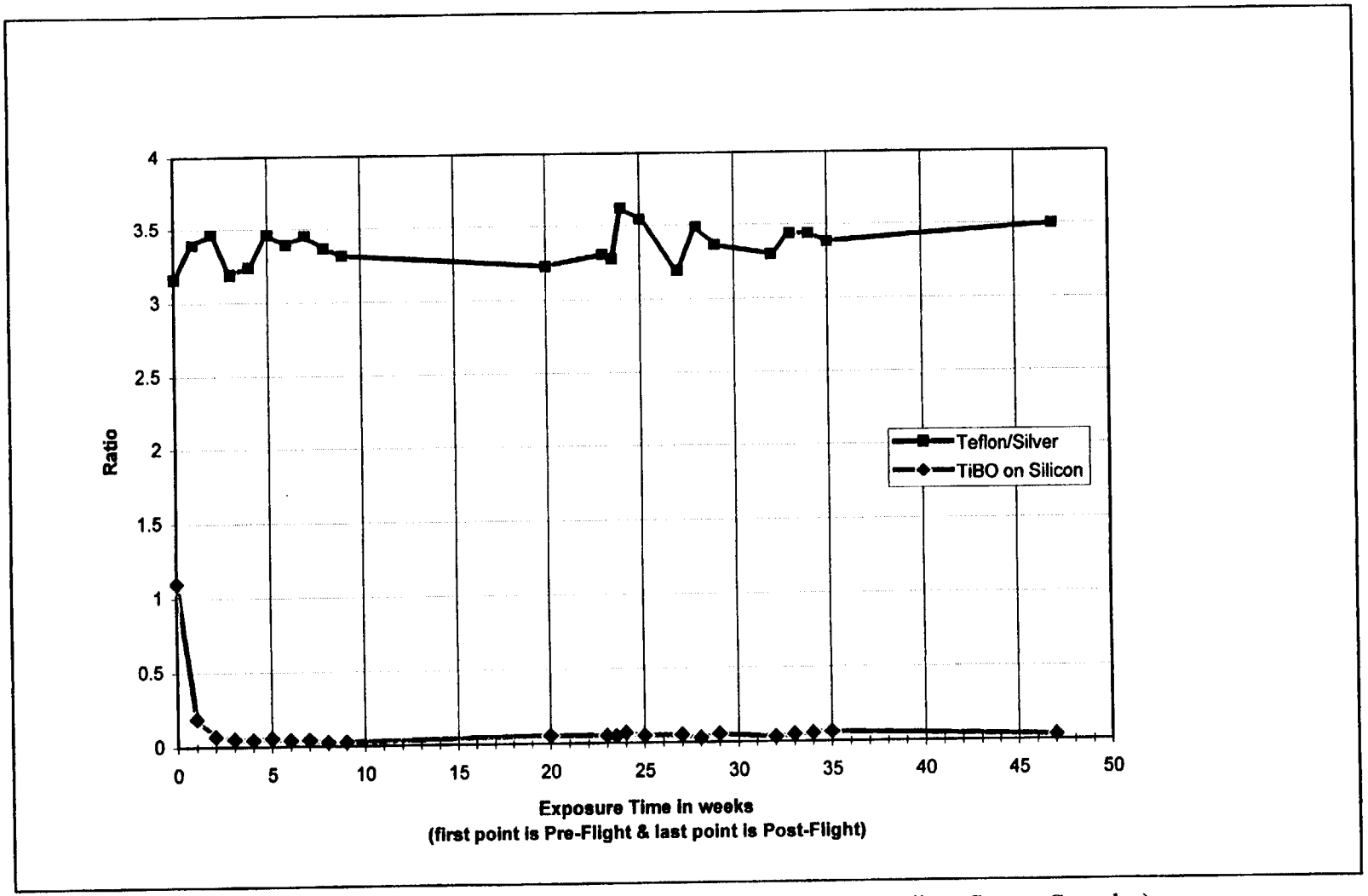

Figure K-9. Observed Changes in 532/1064 TIS Ratios (Medium Scatter Samples)

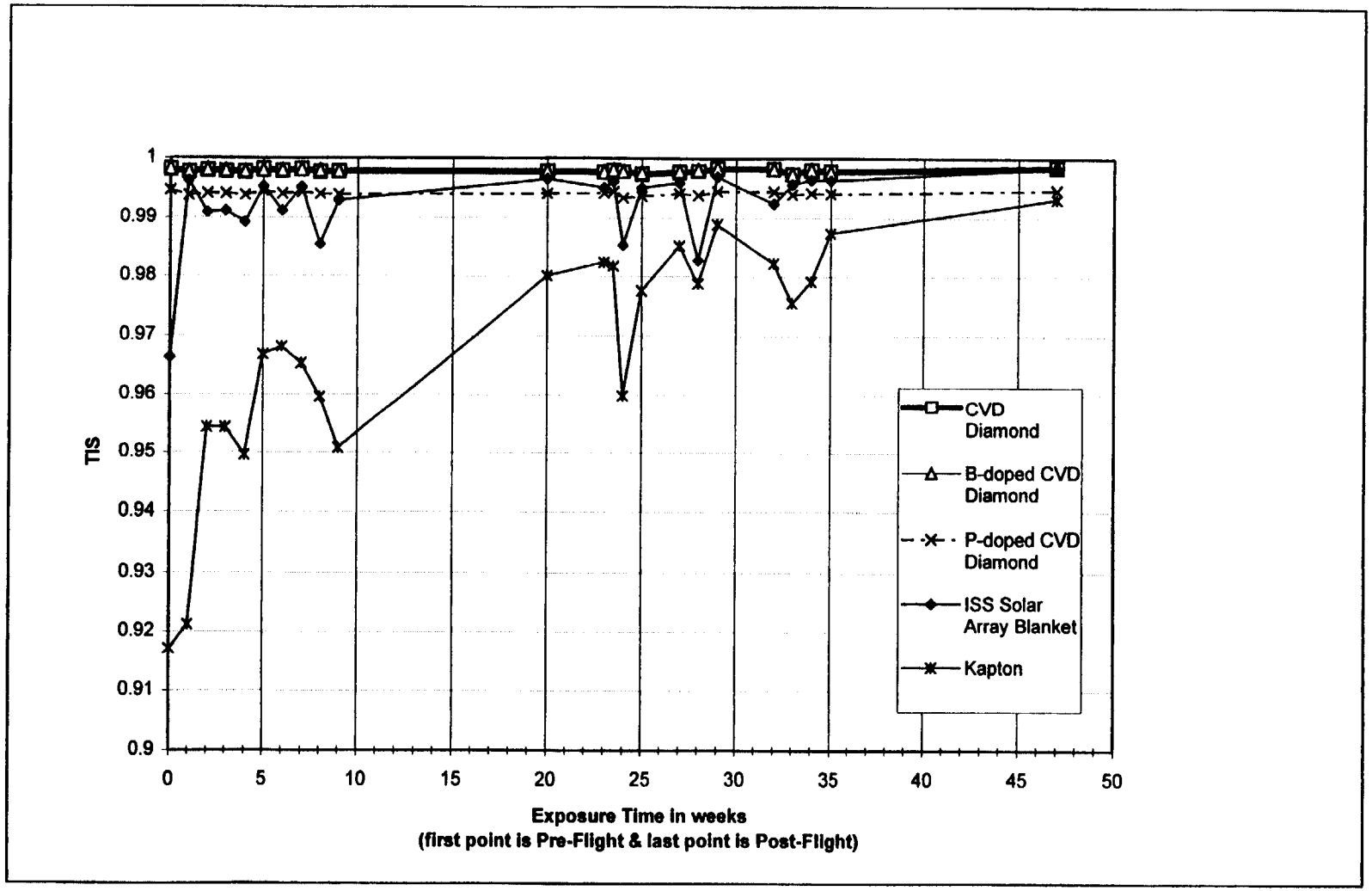

Figure K-10. Observed Changes in TIS at 532nm (High Scatter Samples)

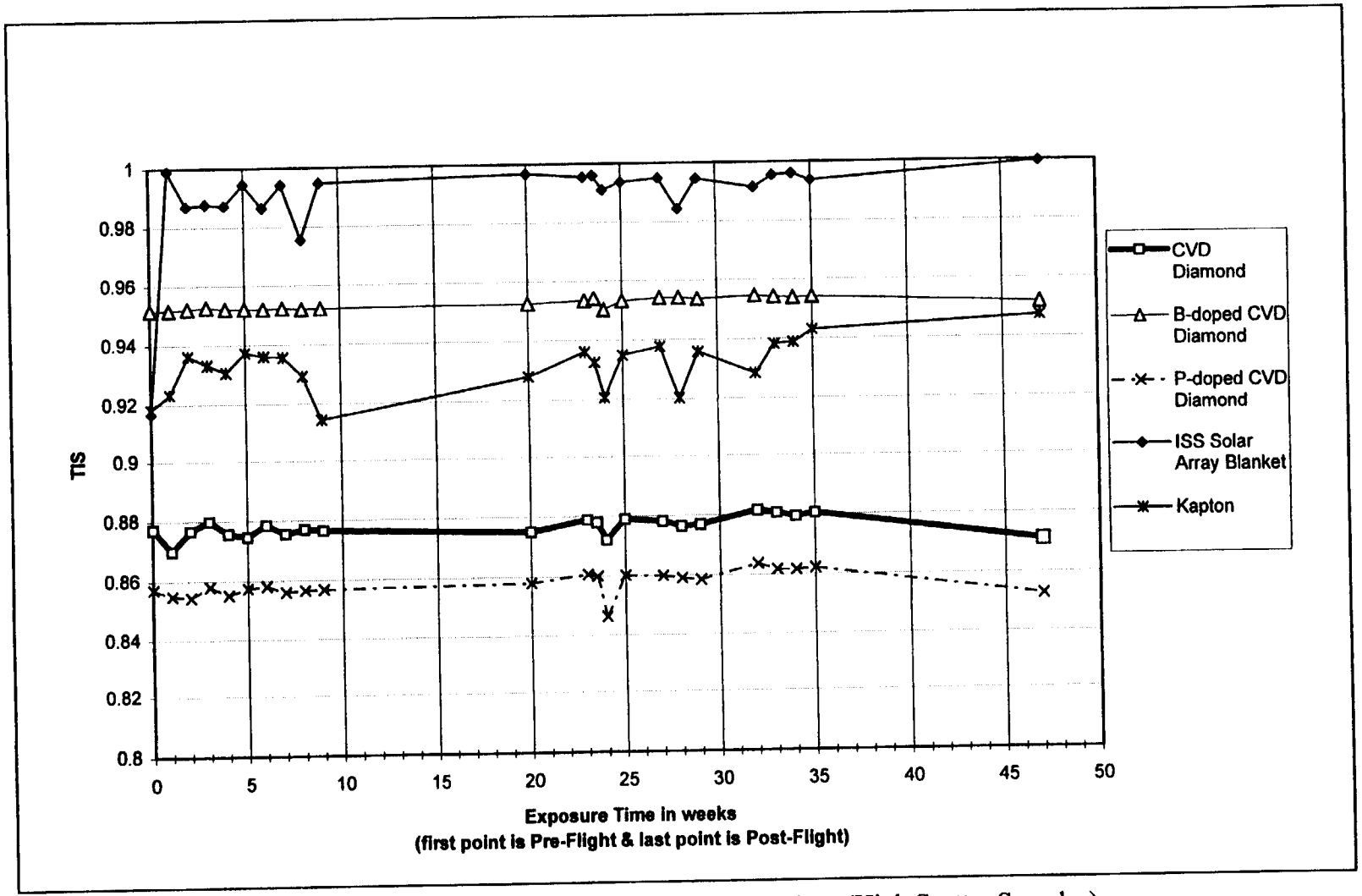

Figure K-11. Observed Changes in TIS at 1064nm (High Scatter Samples)

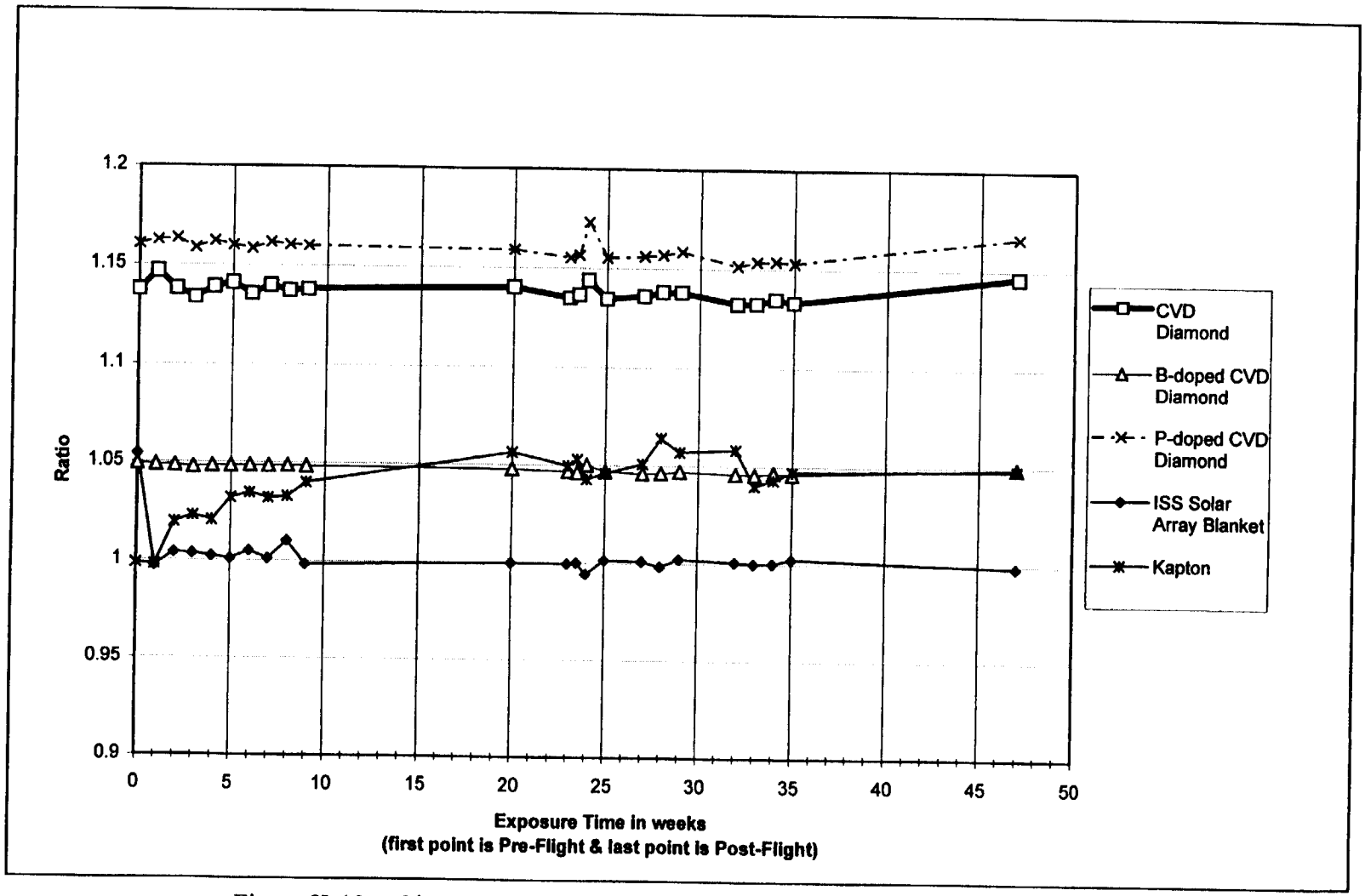

Figure K-12. Observed Changes in 532/1064 TIS Ratios (High Scatter Samples)

REPORT DOCUMENTATION PAGE

Form Approved
OMB No. 0704-0188

1. AGENCY USE ONLY *(Leave Blank)*	2. REPORT DATE	3. REPORT TYPE AND DATES COVERED
	March 2001	Contractor Report (Final)

4. TITLE AND SUBTITLE
Science Data Report for the Optical Properties Monitor (OPM) Experiment

5. FUNDING NUMBERS
NAS8–39237

6. AUTHORS
D.R. Wilkes and J.M. Zwiener

7. PERFORMING ORGANIZATION NAMES(S) AND ADDRESS(ES)
AZ Technology, Inc.
7047 Old Madison Pike, Suite 300
Huntsville, AL 35806

8. PERFORMING ORGANIZATION REPORT NUMBER
M–1007

9. SPONSORING/MONITORING AGENCY NAME(S) AND ADDRESS(ES)
George C. Marshall Space Flight Center
Marshall Space Flight Center, AL 35812

10. SPONSORING/MONITORING AGENCY REPORT NUMBER
NASA/CR—2001–210881

11. SUPPLEMENTARY NOTES
Prepared for Materials Processes and Manufacturing Department, Engineering Directorate
Technical Monitor: Ralph Carruth

12a. DISTRIBUTION/AVAILABILITY STATEMENT
Unclassified-Unlimited
Subject Category 29
Standard Distribution

12b. DISTRIBUTION CODE

13. ABSTRACT *(Maximum 200 words)*

This science data report describes the Optical Properties Monitor (OPM) experiment and the data gathered during its 9-mo exposure on the *Mir* space station. Three independent optical instruments made up OPM: an integrating sphere spectral reflectometer, vacuum ultraviolet spectrometer, and a total integrated scatter instrument. Selected materials were exposed to the low–Earth orbit, and their performance monitored in situ by the OPM instruments. Co-investigators from four NASA Centers, five *International Space Station* contractors, one university, two Department of Defense organizations, and the Russian space company, Energia, contributed samples to this experiment. These materials included a number of thermal control coatings, optical materials, polymeric films, nanocomposites, and other state-of-the-art materials. Degradation of some materials, including aluminum conversion coatings and Beta® cloth, was greater than expected.

The OPM experiment was launched aboard the Space Shuttle on mission STS–81 in January 1997 and transferred to the *Mir* space station. An extravehicular activity (EVA) was performed in April 1997 to attach the OPM experiment to the outside of the *Mir*/Shuttle Docking Module for space environment exposure. OPM was retrieved during an EVA in January 1998 and was returned to Earth on board the Space Shuttle on mission STS–89.

14. SUBJECT TERMS
materials, space environment, environmental effects, optical properties, thermal control, *Mir*, space station

15. NUMBER OF PAGES
265

16. PRICE CODE
A12

17. SECURITY CLASSIFICATION OF REPORT	18. SECURITY CLASSIFICATION OF THIS PAGE	19. SECURITY CLASSIFICATION OF ABSTRACT	20. LIMITATION OF ABSTRACT
Unclassified	Unclassified	Unclassified	Unlimited

National Aeronautics and
Space Administration
AD33
George C. Marshall Space Flight Center
Marshall Space Flight Center, Alabama
35812